Mechanistic Insights into Transition States of Sialidases

by

Fahimeh Sadat Shidmoossavee

B.Sc., Tarbiat Moallem University, 1999
M.Sc., Al-Zahra University, 2002

Thesis Submitted In Partial Fulfillment of the

Requirements for the Degree of

Doctor of Philosophy

in the

Department of Chemistry

SIMON FRASER UNIVERSITY

Summer 2013

Approval

Name: **Fahimeh Sadat Shidmoossavee**

Degree: **Doctor of Philosophy (Chemistry)**

Title of Thesis: ***Mechanistic Insights into Transition States of Sialidases***

Examining Committee: **Chair:** Firstname Surname
Position

Prof. Andrew J. Bennet
Senior Supervisor
Professor, Department of Chemistry _____

Prof. Erika Plettner
Supervisor
Professor, Department of Chemistry _____

Prof. George R. Agnes
Supervisor
Professor, Department of Chemistry _____

Prof. B. Mario Pinto
Internal Examiner
Professor
Department or Chemistry _____

Prof. John C. Vederas
External Examiner
Professor, Department of Chemistry
University of Alberta _____

Date Defended/Approved: August 14, 2013

Partial Copyright Licence

Abstract

Sialic acids, a family of nine carbon sugars, are important components of many biomolecules, and they play important roles in many biological processes. For example, they modulate cellular responses such as differentiation, proliferation and apoptosis. These critical carbohydrates are usually positioned on glycoconjugates as the terminal sugar and they are removed by a family of enzymes called sialidases. In mammals, there are several sialidases that are involved in various biological pathways; however, some human sialidases such as NEU3 have shown to be up-regulated in cancer. Also, certain viruses, bacteria, and trypanosomes have developed sialidases as part of their weaponry. Therefore, it is crucial to design selective and potent inhibitors against these enzymes, with minimal side effects. Development of such selective therapeutics involves a comprehensive understanding of the mechanism by which sialidases catalyze the removal or transfer of sialic acid moieties from glycoconjugates.

A key component when studying enzymes mechanisms involves characterization of the transition state(s) (TS) through which the enzyme:substrate complex (ES) is converted to the enzyme:product complex (EP). Hence, the focus of this thesis involves characterization of the transition states (TSs) for sialidase-catalyzed cleavage of α-sialosides (sialic acid residues covalently attached to glycoconjugates), by employing three distinct mechanistic tools. These techniques include Brønsted analysis, linear free energy relationship (LFER), and kinetic isotope effects (KIEs). Of note, chapter 4 of this thesis describes the development of a new 2D-NMR technique for measuring multiple kinetic isotope effects simultaneously as a first step in the process of solving transition state structure(s) of sialidase-catalyzed reactions.

Dedication

This thesis is dedicated to my loving husband, Davar Bajelan, who stood by me patiently during all these years.

This work is also dedicated to my respected parents, who always loved me unconditionally, and to my sister and brothers who always encouraged me in all the steps of my life.

Acknowledgements

It is with immense gratitude that I acknowledge the support and help of my senior supervisor, Professor Andrew Bennet. First of all, I deeply thank him for giving me the opportunity to be part of his research group. Also, I am especially grateful for the confidence and freedom he gave me to conduct my research projects. I would also like to thank him for sending me to numerous international and national conferences during these past years of my PhD program. As a result of presenting my research works in conferences, my presentation skills have improved tremendously. Moreover, Professor Bennet's great personality and attitude toward his students has made the work environment very pleasant. It has been a great honor to work for such a brilliant and dedicated scientist, and this thesis would not have been possible without his great support, constant encouragement and invaluable advice during these years.

I would also like to thank the members of my supervisory committee, Professors Erika Plettner and George Agnes, for all the fruitful discussions, suggestions, and constructive criticism during my committee meetings. I thank them for reading my thesis and providing valuable feedback. I would also like to thank my examining committee, Professors John Vederas and Mario Pinto for reading my thesis and providing valuable advice and feedback.

I would especially like to thank Dr. Andrew Lewis for his great help with the project discussed in the chapter 4 of this thesis. He patiently trained me in the operation of NMR spectrometers and how to run my experiments. He was always available to help whenever I encountered difficulties running my experiments. I gained a wealth of knowledge about NMR spectroscopy through one on one training and our discussions. It has been such a pleasure to collaborate with Dr. Lewis and I appreciate all of his help.

I also thank Professor Laurel Schafer at University of British Columbia for giving me the opportunity to work in her lab as a volunteer for a few months. Dr. Schafer's lab was my first immersion in an English speaking community since immigrating to Canada. There I gained much confidence and I became determined to pursue my doctorate.

I would also like to thank all my fellow lab mates past and present: Dr. Saswati Chakladar, Dr. Jefferson Chan, Lydia Cheng, Kobra Khazaie, Viviana Cerda, Saeideh Shamsi, Natalia Sannikova, Matt Courtemanche, Emilie Phillips, Michael Tran, Chloe Gerak, Dr. Sankar Mohan, Dr. Anuj Yadav, Ariel Tang, April Lu, Gurtej Sandhu, Amir Ehtemam, Mary Choi, Timothy Teoh and Hoda Shahzadeh. It was such a great pleasure to work closely with these people specially Lydia Cheng, Matt Courtemanche and Emilie Phillips who contributed to my research, and I really enjoyed working with such smart and hard working students. I wish them all the best. I would also like to thank Dr. Jacki Watson McGowan, the previous post-doc, for her contributions to my projects even though I did not get a chance to work directly with her. I also thank Dr. Deepani Indurugalla, the previous post-doc, and Dr. Ivan Hemeon, the previous PhD student, whom again I did not have a chance to work with directly but I always enjoyed meeting them and chatting with them in the annual lab events.

I would like to thank all my friends who always encouraged me and were there for me in any situations.

Finally, I would like to sincerely thank my parents, Mousa Shidmousavi and Mahin Tehrani, for their dedication and the many years of support during my education from elementary school to my master's program. My deepest gratitude and love is always with them. I would also like to deeply thank my siblings, Fatemeh, Mostafa, Morteza, and Mojtaba, for their constant encouragement in all the steps of my life. Last but not the least, I would like to thank my loving husband, Davar Bajelan, for the

constant encouragement, support, patience and love during these many years of my doctorate program. He has always stood by me through the good times and bad times, and I cannot find words to express my gratitude to him.

Table of Contents

List of Tables

List of Figures

List of Schemes

Glossary

ABI	Applied Biosystems
A_ND_N	IUPAC Nomenclature for S_N2 Reactions
BIE	Binding Isotope Effect
BSA	Bovine Serum Albumin
CAZy	Carbohydrate-Active enZYmes
CMP	Cytidine 5′-monophosphate
d	doublet
DANA	2,3-didehydro-N-acetyl-neuraminic acid
dd	doublet of doublets
ddd	doublet of doublets of doublets
dec	decomposed
23DFP-βNeuAc	2,3-difluorophenyl β-D-*N*-acetylneuraminide
25DFP-βNeuAc	2,5-difluorophenyl β-D-*N*-acetylneuraminide
26DFP-βNeuAc	2,6-difluorophenyl β-D-*N*-acetylneuraminide
2FP-βNeuAc	2-fluorophenyl β-D-*N*-acetylneuraminide
35DFP-βNeuAc	3,5-difluorophenyl β-D-*N*-acetylneuraminide
3FP-βNeuAc	3-fluorophenyl β-D-*N*-acetylneuraminide
4FP-βNeuAc	4-fluorophenyl β-D-*N*-acetylneuraminide
DMF	N, N-dimethylformamide
DNA	Deoxyribonucleic acid
dt	doublet of triplets
ES/MS	Electrospray Mass Spectrometry
FID	Free Induction Decay
F_L	Fraction of Reaction for Lighter isotopomer
GH	Glycosyl Hydrolase
HA	Hemagglutinin
HETCOR	Heteronuclear Correlation
HPLC	High-Performance Liquid Chromatography
HRMS-FAB	High-Resolution Mass Spectrometry- Fast Atom Bombardment
HSQC	Heteronuclear Single Quantum Coherence
IUPAC	International Union of Pure and Applied Chemistry
k_{cat}	Turnover number
k_{cat}/K_m	Catalytic efficiency
$k_{cat}/K_m \times 1/k_{uncat}$	Catalytic proficiency
K_i	Inhibition constant
KIE	Kinetic Isotope Effect
K_m	Michaelis constant

LC-MS	Liquid Chromatography–Mass Spectrometry
LFER	Linear Free Energy Relationship
MES	2-(N morpholino)ethanesulfonic acid
mp	melting point
MvNA	*Micromonospora viridifaciens* Neuraminidase
NA	Neuraminidase
NAD^+	Nicotinamide Adenine Dinucleotide
NADH	Nicotinamide Adenine Dinucleotide (reduced form)
NAG-thiazoline	1,2-dideoxy-2'-methyl-α-d-glucopyranoso-[2,1-d]-Δ2'-thiazoline
NANA	N-Acetylneuraminic acid also called sialic acid
Neu2en5Ac	5-Acetamido-2,6-anhydro-3,5-dideoxy-D-*glycero*-D-*galacto*-non-2-enonic acid
Neu5Ac	N-Acetylneuraminic Acid also called Sialic Acid
NeuAc	N-Acetylneuraminic Acid also called Sialic Acid
Ni-NTA	Nickel-NitriloaceTic Acid
NMR	Nuclear Magnetic Resonance
PCR	Polymerase chain reaction
Ph-βNeuAc	Phenyl β-D-*N*-acetylneuraminide
pK_a	negative base-10 logarithm of the acid dissociation constant
pNP-αNeuAc	*p*-nitrophenyl α-D-*N*-acetylneuraminide
PUGNAc	2-(acetamido-2-deoxy-D-glucopyranosylidene)amino-*N*-phenylcarbamate
QNP	Quattro Nucleus Probe
RNA	Ribonucleic acid
RPM	Revolutions per minute
SDS-PAGE	Sodium Dodecyl Sulfate Polyacrylamide Gel Electrophoresis
Sia	Sialic acid also called N-Acetylneuraminic acid
S_N1	Substitution, nucleophilic, unimolecular reaction
S_N2	Substitution, nucleophilic, bimolecular reaction
SW	Spectral Width
TcTS	Trypanosoma cruzi trans-sialidase
TMS	Tetramethylsilane
TS	Transition State
UV-Vis	Ultraviolet and Visible
^{D}V	kinetic isotope effects on the maximum velocity, for deuterium
^{T}V	kinetic isotope effects on the maximum velocity, for tritium
$^{\alpha\text{-}D}V$	α-Secondary kinetic isotope effects on the maximum velocity, for deuterium
$[\alpha]^{20}_{D}$	Specific optical rotation measured measured using Sodium light at 20 °C

^{13}V	kinetic isotope effects on the maximum velocity, for 13C
^{14}V	kinetic isotope effects on the maximum velocity, for 14C
^{15}V	kinetic isotope effects on the maximum velocity, for 15N
^{18}V	kinetic isotope effects on the maximum velocity, for 18O
V/K	V_{max}/K_m
V_{max}	Maximum reaction rate of an enzyme
Y370G	Tyrosine 370 replaced by Glycine

Preface or Executive Summary or Introductory Image

1 General Introduction

1.1 Carbohydrates

Biogenic substances, which are defined as ″substances produced by natural processes″ are classified into several groups, which include carbohydrates, proteins, nucleotides, and lipids. Carbohydrates are the most abundant compounds of the four classes and are divided into three major categories, sugars (monosaccharides, disaccharide and polyols), oligosaccharides (oligomers of 3-10 simple sugars) and polysaccharides (polymers of more than 10 sugars). Many monosaccharides have a molecular formula $C_n(H_2O)_n$ in which the same number of carbon atoms as water molecules are combined. Historically, this is how the name carbohydrate originated. For example, glucose which is the most common monosaccharide has the formula of $C_6H_{12}O_6$ **1** (Figure 1.1).

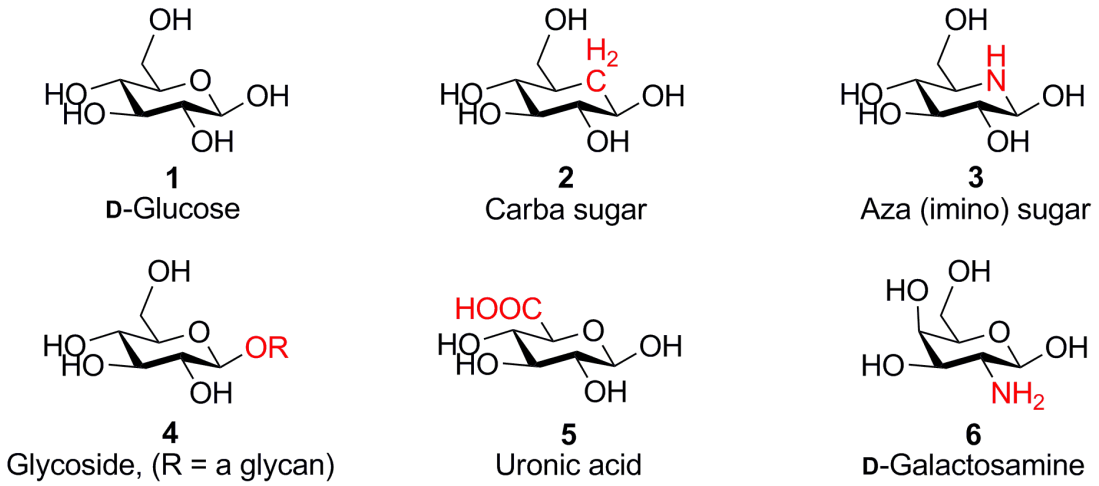

Figure 1.1. D-glucose (**1**) with the formula of $C_6H_{12}O_6$, and a few examples of other carbohydrates (**2-6**) that do not have an empirical formula of $Cn(H_2O)_n$.[1]

However, structurally modified substances that are derived from sugars are thought of as carbohydrates even though they do not have molecular formula of the type $C_n(H_2O)_n$. A few examples of these structurally modified substances (**2-6**) are shown in Figure 1.1.[1]

The biological importance of carbohydrates comes from the multitude of roles that they play in biological processes, such as: being an immediate source of energy for the body while lipids, a long-term energy resource, are used more slowly. Also, carbohydrate polymers constitute the structural components in cells and tissues ranging from the world of microbes to that of mammals.[1] For instance, cellulose and pentose-containing polysaccharides form key elements of plant cell walls. Chitin, a *N*-acetylglucosamine-containing polysaccharide, serves as a major component in the exoskeleton of insects and other arthropods.[2] In addition to their structural roles, carbohydrates when displayed on the outer surface of cells are involved in signaling events that regulate many cell-cell interactions, such as those between host and parasite. In biological systems, carbohydrates are often present in the form of glycoconjugates in which they are covalently linked to other molecules including lipids, peptides and proteins. The surface of cell membranes are covered by such glycoconjugates (Figure 1.2).[3]

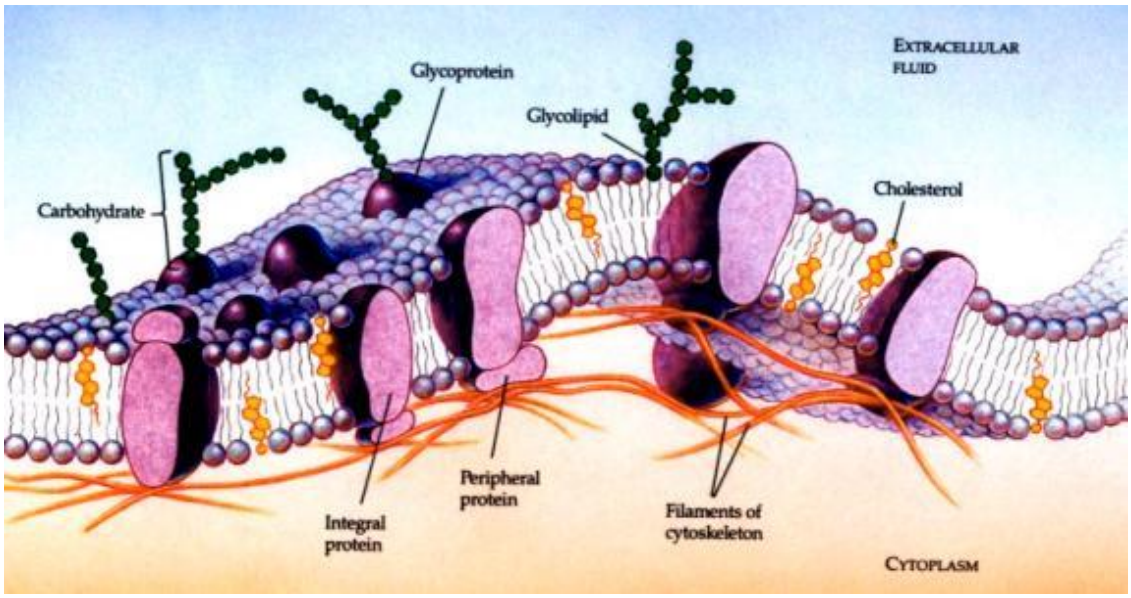

Figure 1.2. General view of a biological membrane containing the glycoconjugates

Note. Picture from Nanoscience: Nanobiotechnology and Nanobiology, 2010, Page 30.[3]

The interactions that these naturally occurring glycoconjugates undergo are often the target for the development of therapeutics against many disease states as well as viral and bacterial infections. In glycobiology, synthetic glycoconjugates are used as powerful tools to study the roles of natural glycoconjugates in various biological processes.

Carbohydrates also play significant roles in the pharmaceutical drug discovery process as they are often an essential component for activity of many natural products. That is, the carbohydrate portion in such drugs often increases water solubility by virtue of the sugar possessing multiple hydroxyl groups. Also, carbohydrate moieties can decrease toxicity and increase bioavailability of the drug.

1.2 Sialic Acids

Sialic acids are a family of keto-sugars that have a nine carbon skeleton with a carboxylate group at C-1. As a result, sialic acids are characterized as being strong organic acids (pK_a~2.2)[4] and thus they possess a negative charge at physiological pH values. The most common sialic acid is *N*-acetylneuraminic acid (5-acetamido-3,5-dideoxy-D-*glycero*-D-*galacto*-non-2-ulopyranonic acid), which is also known as Neu5Ac, NANA, NeuAc or Sia (**7**, Figure 1.3).

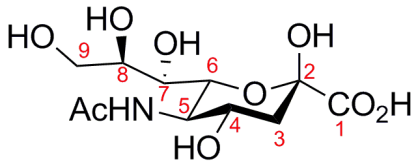

7 (Neu5Ac)

Figure 1.3. Structure of Neu5Ac (**7**), the first sialic acid discovered.

N-acetylneuraminic acid, the first sialic acid discovered was isolated from salivary mucins by Gunnar Blix in the 1930s; hence, later on in the 1950s, the generic term “sialic acid” (salavia, Greek = sialos) was adopted by Gunnar Blix and two other prominent investigators for this family of carbohydrates.[5] Recent studies have shown that sialic acids and their derivatives are indeed a large family of non-2-ulosonic acids.[6]

Sialic acids are present in all vertebrates (Mammals, Birds, Reptiles, Amphibians, and Fish); but, are rarely found in plants and lower species except for some specific pathogenic bacteria which are assumed to have obtained their sialic acids from host cells through gene transfer.[4,7]

There are more than 50 different natural sialic acids which are usually found as the terminal monosaccharide residue in glycoconjugates that are displayed on cell surfaces.[7] The diversity of sialic acids comes from modifications to the parent structure, neuraminic acid (**8**, Figure 1.4), which is not found in nature. The most widespread form of sialic acid, Neu5Ac (**7**, Figure 1.3), results from acetylation of the 5-amino group in neuraminic acid. It is believed that Neu5Ac is the biosynthetic precursor for all other natural sialic acids.[8] Hydroxylation of the *N*-acetyl methyl group; results in *N*-glycolylneuraminic acid (Neu5Gc) (**9**, Figure 1.4), which is made by most mammals; but is not made by humans and when it is found, for example, in some particular cancer tissues, it is incorporated by activation of a sialic acid salvage pathway.[9] Elimination of the gene encoding the hydroxylase (CMP-Neu5Ac hydroxylase) occurred long ago during human evolution; however, traces of Neu5Gc in humans originate from the diet (mainly from eating red meat)[10]. Another naturally occurring sialic acid is deaminated neuraminic acid which has the IUPAC name of 3-deoxy-D-*glycero*-D-*galacto*-non-2-ulosonic acid and it is known by the acronym (Kdn, keto deamino neuraminic acid) (**10**, Figure 1.4).

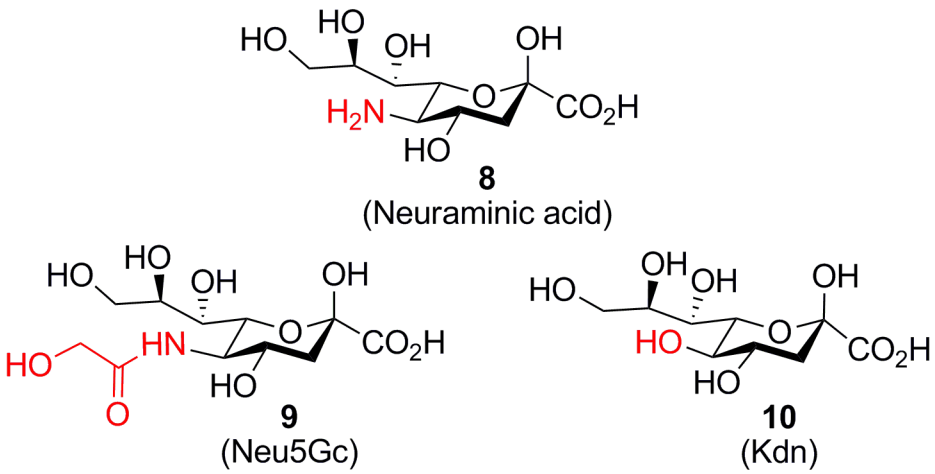

Figure 1.4. Structure of Neuraminic acid (**8**), Neu5Gc (**9**), and Kdn (**10**).

In a similar manner to Neu5Ac **8**, Kdn **9** is found in vertebrates and bacteria, but among animals, it is more abundant in lower vertebrates. The presence of high concentration of free Kdn **9** in red blood cells from umbilical cord and some malignant tumors (ovarian and breast cancer), has motivated researchers to broaden their investigations to include the world of ″Kdnology″ recently.[11] Other natural sialic acids are derived by *O*-acetylation, *O*-methylation, and *O*-sulfonation on the 4-, 7-, 8-, and 9-carbon positions of Neu5Ac **8**, Neu5Gc **9** and Kdn **10**.[4,12] Sialic acids are even more diverse with regard to the different types of α-linkages that connect them from their 2-positions to other sugars within glycoconjugates. Sialic acids are most commonly linked to the 3- or 6-position of galactose (Gal) or *N*-acetylgalactosamine (GalNAc) residues to create 2,3- or 2,6-α-linkages in sialo-glycoconjugates. In addition, 2,8- and 2,9-α-linkages are derived when another sialic acid moiety is linked from its 2-position to the 8- or 9-position of an already sialylated glycoconjugate.

Sialic acids have a variety of functions in biological systems due to their physical properties and their location within biological systems. The highly exposed location of sialic acids as the terminal residue on cell surface glycoconjugates, makes them an

important participant in molecular and cellular recognition events.

The negatively charged sialic acids play important roles in the electrostatic interactions between adjacent cells whose surfaces are covered with sialic acid.[13] These charged species create a repulsive interaction between cells to keep them apart. For example, an observed increase in concentration of sialic acid on the cell surface of some tumor cells undergoing metastasis suggests that repulsion between the cells causes them to aggregate less tightly which frees them from the primary tumor mass.[14,15]

Sialic acids also have important roles as biological masks to prevent the recognition of underlying galactose residues in glycoproteins. For instance, the half-life of some therapeutic proteins such as asparaginase[16] and erythropoietin[17] can be increased by the degree of sialylation. In these therapeutic proteins, sialic acid masks underlying galactose moieties, which in the absence of this critical sugar, are recognized as antigenic by the immune system. Therefore the unmasked protein stimulates a response that results in their removal (degradation) from the host.[18]

Another important biological consequence of sialic acids being present as the terminal sugar on a cell-surface glycoconjugate is that they are often receptors for pathogenic bacteria and viruses as well as their normal function in binding to hormones and lectins.[19] For instance, influenza virus possesses a sialic acid-recognizing protein called hemagglutinin on its surface, and this lectin interacts with the sialic acid moiety on a sialoglycoconjugate and attaches the virus to the host's cell-surface. This recognition, interaction and the following attachment event are crucial for initiation of the infection process.[19]

1.3 Glycosidases

Glycosidases which are also called glycosyl hydrolases or glycoside hydrolases (**GHs**), are a widespread group of enzymes that are found ubiquitously in nature, and they are a subgroup of glycan degrading enzymes. Glycosidases catalyze the hydrolysis of O-, N- or S-glycosidic linkages in glycosides, and they are classified in the IUPAC nomenclature system as EC.3.2.1.X, also these are divided into GH families; see the Carbohydrate-Active Enzyme database (CAZY) (http://www.cazy.org/Glycoside-Hydrolases.html). Glycosidases are commonly named based on their substrates specificity such as: galactosidase (catalyzing hydrolysis of galactoside), glucosidase (catalyzing hydrolysis of glucosides), and sialidase (catalyzing hydrolysis of sialoside). These enzymes are further divided into two categories of α- and β-glycosidases based on the stereochemistry of their substrates at the anomeric centre. α-glycosidases catalyze hydrolysis of α-glycosides, and β-glycosidases catalyze specifically the hydrolysis of β-glycosides. Glycosidases are further sub-classified as either retaining or inverting enzymes based on the stereochemical outcome of the catalyzed hydrolysis reaction. Therefore, the name of a particular glycosidase provides some basic information about its substrate, the stereochemistry of the substrate (α or β), mechanism of action (inverting or retaining), and the stereochemistry of the product (α or β). However, a more systematic classification of glycosidases can be seen in the CAZY database, which is based on structural features of the glycosidases regardless of their substrates specificity. This classification presents more than 130 families of **GHs**, and enzymes in the same family share similar amino acid sequences, protein folds and thus mechanistic features.

As discussed earlier, carbohydrates in nature exist in many forms, including simple monosaccharide, oligosaccharides, polysaccharides and glycoconjugates. The formation, degradation, and function of these biologically important compounds are catalyzed by numerous different enzyme groups. The enzymes involved in carbohydrate transfer reactions, catalyze the formation and cleavage of glycosidic linkages between the two sugars or between a sugar and another group (Figure 1.5).

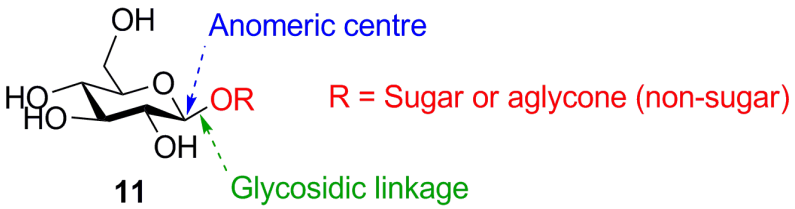

Figure 1.5. Glycosidic linkage in a β-glucoside.

The formation and cleavage of glycosidic bonds can take place with a variety of mechanisms. For example, a transglycosylation occurs to form a new glycoside bond when a glycosyltransferase enzyme catalyzes the transfer of the sugar moiety from an activated donor to an acceptor. Lyases are enzymes that degrade polysaccharides via an elimination process to form an unsaturated product, whereas, glycosidases release a free sugar by catalyzing the cleavage of a glycosidic linkage by hydrolysis (Scheme 1.1).

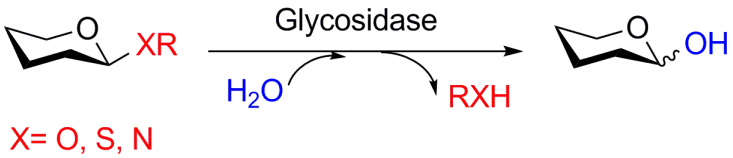

Scheme 1.1. General scheme for glycosidase catalyzed hydrolysis of glycosides.

Glycosidases are widely distributed in nature and have important biological roles. Also, they play key roles in developing therapeutic agents against a number of diseases such as pneumococcal infection[20], Alzheimer's[21] and Influenza[22]. An understanding of

the catalytic mechanisms used by glycosidases is useful for designing highly effective inhibitors as potential therapeutic agents.

1.3.1 Glycosidase Mechanisms

The catalytic mechanism of glycosidases was postulated in 1953 by Koshland[23] who categorized glycosidases into two major classes depending on whether the enzyme operates with retention or inversion of anomeric configuration (Scheme 1.2).

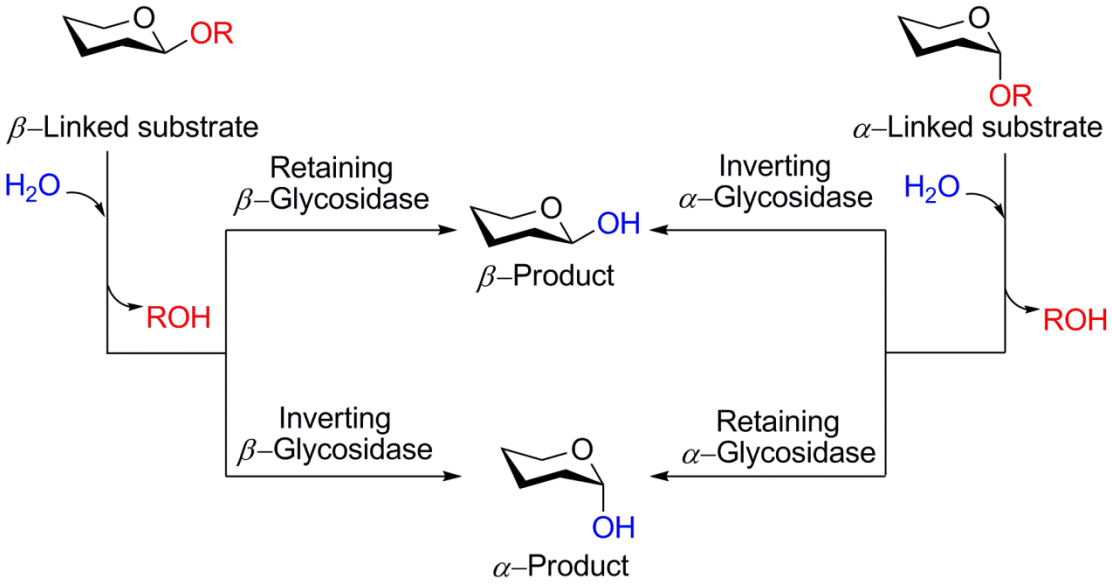

Scheme 1.2. Two major classifications for glycosidases based on the mechanism of their action (retaining and inverting).

The number of glycosidase catalyzed reactions that proceed with retention of configuration outweigh those that function by inverting the anomeric configuration.[23] Among retaining glycosidases, β–retaining glycosidases have been studied in more detail in comparison to α–retaining glycosidases, because of the easier synthesis of β–galactoside and β–glucoside substrates.

The detailed mechanisms of inverting and retaining glycosidases and the role of the catalytic residues are discussed below.

1.3.1.1 Mechanism of Inverting Glycosidases (General Features)

In the catalyzed hydrolysis of glycosides by inverting glycosidases, a single step nucleophilic displacement of the aglycone by a water molecule occurs directly at the anomeric centre (Scheme 1.3).

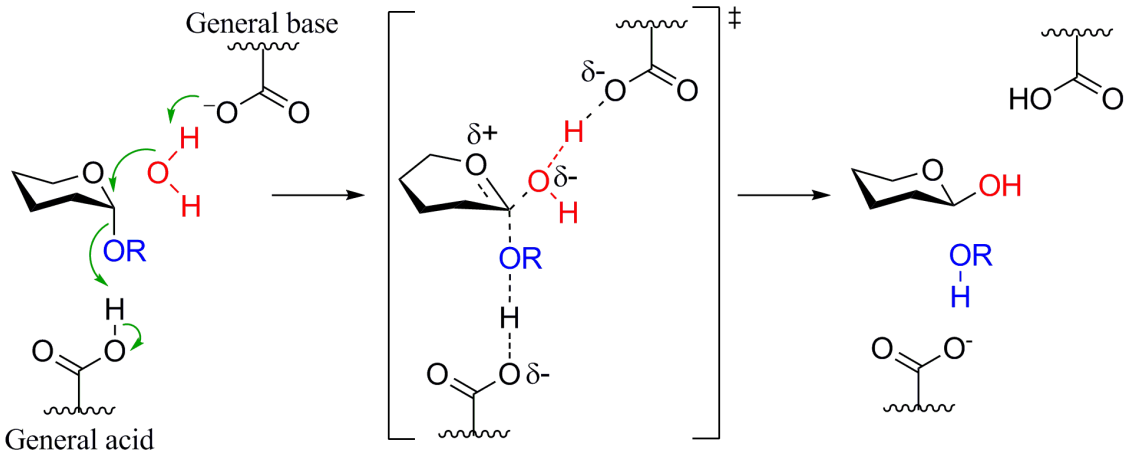

Scheme 1.3. General mechanism for inverting α–glycosidases (single displacement).

This hydrolysis is catalyzed by two key acid/base amino acid residues in the active site of the enzyme. In most of the studied glycosidases from different species,[24-27] the catalytic residues are the carboxylic acid side chains of either aspartic acid or glutamic acid residues. The general base catalytic residue deprotonates a water molecule to increase its nucleophilicity thus promoting its attack at the anomeric centre, while the acid catalytic residue protonates the glycosidic oxygen of the leaving group (OR), facilitating its departure. Mechanistic probes used by researchers including kinetic isotope effects and Bronsted relationships, have provided evidence that the hydrolysis reaction proceeds through an oxacarbenium ion-like transition state. In other words, aglycone or OR leaves prior to formation of the new C-O bond. That is, the pyranose ring adopts either a half chair or a boat conformation at the transition state, in which a planar geometry is created between C–5, O–5, C–1 and C–2. This planarity allows

efficient delocalization of the developing positive charge since the p-like lone pair of the endocyclic ring oxygen can efficiently overlap with the p-like orbital at the anomeric centre.

1.3.1.2 Mechanism of Retaining Glycosidases (General Features)

Most retaining glycosidases function through a two step mechanism involving glycosylation and deglycosylation steps (Scheme 1.4).

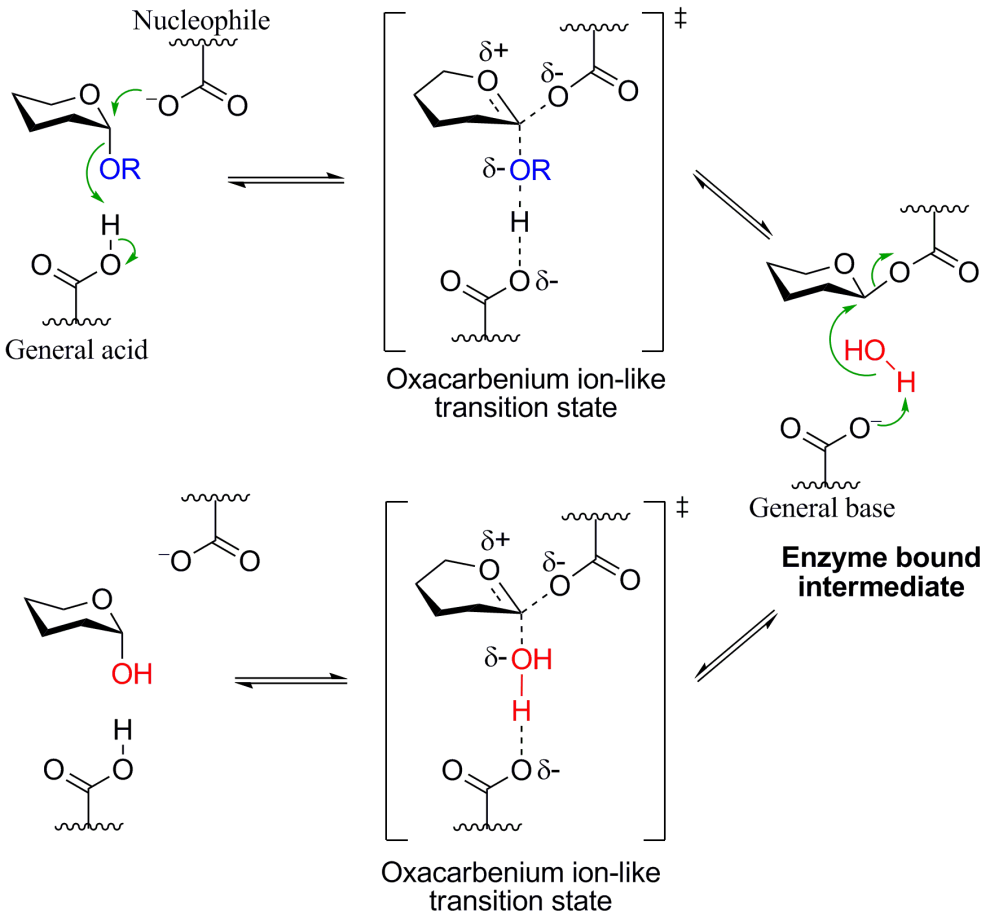

Scheme 1.4. General mechanism for retaining α–glycosidases (double displacement).

First, a general acid residue protonates the glycosidic oxygen of the leaving group (OR) as another enzymatic carboxylate side chain acts as a nucleophile and attacks the anomeric centre to afford glycosyl enzyme intermediate after going through

an oxacarbenium ion-like transition state. This step is called glycosylation because it involves formation of a glycosidic linkage between the anomeric centre and the nucleophilic residue of the enzyme. In the second step, the now deprotonated proton transfer residue acts as a general base to deprotonate a molecule of water as it attacks the anomeric centre of the glycosyl–enzyme intermediate to release the product with net retention of configuration at the anomeric centre. This step also proceeds through an oxacarbenium ion-like transition state and is called deglycosylation.

1.3.2 Mechanistic Deviances

There are some enzymes which show deviations from these two general mechanisms (direct or double displacement) used by the majority of classified glycosidases. For example, the *N*-acetyl-β-hexosaminidase enzymes that belong to GH families 18 and 20, involve anchimeric assistance (neighboring group participation) by the substrate's acetamido group to form an oxazoline intermediate.[28,29] The other glycosidases whose mechanisms are vastly different from the two general mechanisms are family 4 glycosidases. The unusual feature present in family 4 GHs is that an elimination step is involved in their mechanisms. Detailed mechanistic studies on three GH4 family members, BglT, GlvA and MelA,[30-33] have shown that this family uniquely requires NAD^+ and a divalent ion (such as Mn^{2+}, Ni^{2+}, Co^{2+}, or Fe^{2+}) to catalyze hydrolysis of a glycosidic linkage. The proposed mechanism for this family suggests that the first partially rate determining step is oxidation of C-3 to a ketone by the cofactor NAD^+. The acidic proton at C-2 is then abstracted by a suitably positioned base residue leading to 2,1-elimination of the aglycone and formation of α,β-unsaturated Michael acceptor as the intermediate. Subsequent addition of an activated water molecule to the anomeric centre of the glycal intermediate following by proton and hydride transfers

results in product formation.[34] These two unusual mechanisms are not discussed further as they are beyond the scope of this thesis.

1.4 Sialidases

Sialidases, also called neuraminidases, are categorized into four glycosyl hydrolase families which can be sub-classified into two groups in the Carbohydrate-Active Enzyme database (CAZY): i) exo-sialidases (EC 3.2.1.18) are in glycosyl hydrolases families 33, 34, and 83, while trans-sialidases (EC 2.4.1.-) are in family GH 33, ii) endo-sialidases (EC 3.2.1.129) which belong to glycosyl hydrolases family 58 (GH 58). exo-Sialidases are retaining glycosidases that catalyze hydrolysis of terminally linked sialic acids (Scheme 1.5) that are present in many sialoglycoconjugates (α-sialoside). These enzymes (exo-sialidases) are the focus of this thesis and will be referred to as sialidases throughout the remainder of this thesis.

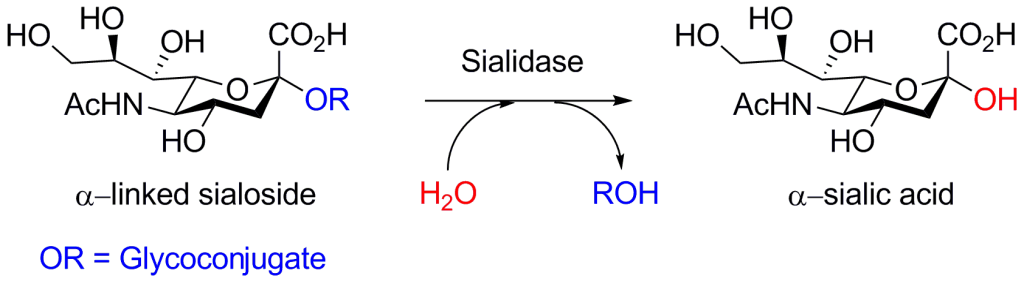

Scheme 1.5. Sialidases catalyzed hydrolysis of α-sialosides.

1.4.1 Historical Background

Sialidases were first discovered by George Hirst in 1941[35] when he was investigating the agglutination of red blood cells upon incubation with influenza virus. Since, re-agglutination of the cells was not possible after they had been infected by the influenza virus, he postulated that an enzyme on the surface of the virus destroyed the

receptors on the red blood cells. Later on in 1957, Alfred Gottschalk[36] discovered that the product released by this enzyme was *N*-acetylneuraminic acid (sialic acid); hence, the name sialidase (initially neuraminidase) was coined for these receptor destroying enzymes.

1.4.2 Biological Significance

Sialidases are widely distributed throughout nature and have been isolated from prokaryotes and eukaryotes (GH 33) as well as viruses (GH 34 and 83).

1.4.2.1 Mammalian Sialidases

Mammalian sialidases play important roles in cellular phenomena such as cell proliferation and differentiation, membrane function, lysosomal catabolism, molecular transport and antigen masking.[37] Four human enzymes are known and these are differentially localized within the cell: NEU1 (lysosome), NEU2 (cytosol), NEU3 (plasma membrane) and NEU4 (intracellular and mitochondrial membranes).[38] The human sialidase (Neu3) has been found to be over expressed in some types of cancers.[38]

1.4.2.2 Bacterial Sialidases

In contrast to mammalian sialidases, microbial sialidases mostly play roles in nutrition and disease. For example, the sialidase from *Micromonospora viridifaciens* (a soil bacterium) releases sialic acids from glycoconjugates, and the freed sugar is then used as a carbon and energy source.[39] Also, in many pathogenic microorganisms, the sialidases that are expressed by the organism are involved in disease pathogenesis.[40] There are many bacteria that express sialidases in which the biological roles of the enzyme has been elucidated and these include *Arthrobacter nicotianae*, *Arthrobacter ureafaciens*, *Clostridium perfringens*, *Pasteurella multocida*, and *Streptococcus*

pneumonia.[41] For example, 30% of otitis media (OM), a middle ear infection, is caused by *Streptococcus pneumoniae*.[41] It is believed that the sialidases expressed by S. *pneumonia* are responsible for the disease by making the host's mucus less viscous which facilitates colonization. These sialidases could also expose surface cell receptors for colonization by S. *pneumonia*. The sialidases expressed by S. *pneumonia* are also responsible for pneumococcal infection of the respiratory tract and sepsis caused by this bacterium.[42]

1.4.2.3 Viral (Influenza) Sialidases

The sialidase found on the surface of influenza virus particles has an important role for transmission of the virus. Influenza, which is an infectious and viral disease, continues to pose health problems during the yearly epidemic. Annually, around 3 to 5 million cases of severe illness and about 250,000 to 500,000 deaths worldwide are reportedly caused by influenza.[43] Belonging to the orthomyxoviridae family, influenza viruses have a single-stranded segmented RNA genome, and are subdivided in three types: A, B, and C. Of the three classes, type A virus creates the most severe disease in humans and this virus type can be further subdivided based on their two main surface glycoproteins, hemagglutinin (HA: H1-17) and sialidase (neuraminidase, NA: N1-9).[22] Among various combinations of HA and NA proteins, only a few influenza A subtypes (i.e., H1N1, H1N2, and H3N2) have circulated among humans. HA initiates the entry of the virus into the host cell by interacting with the sialic acids α-linked to glycoconjugates on the surface of the host cell (receptor-binding function) as shown in Figure 1.6.

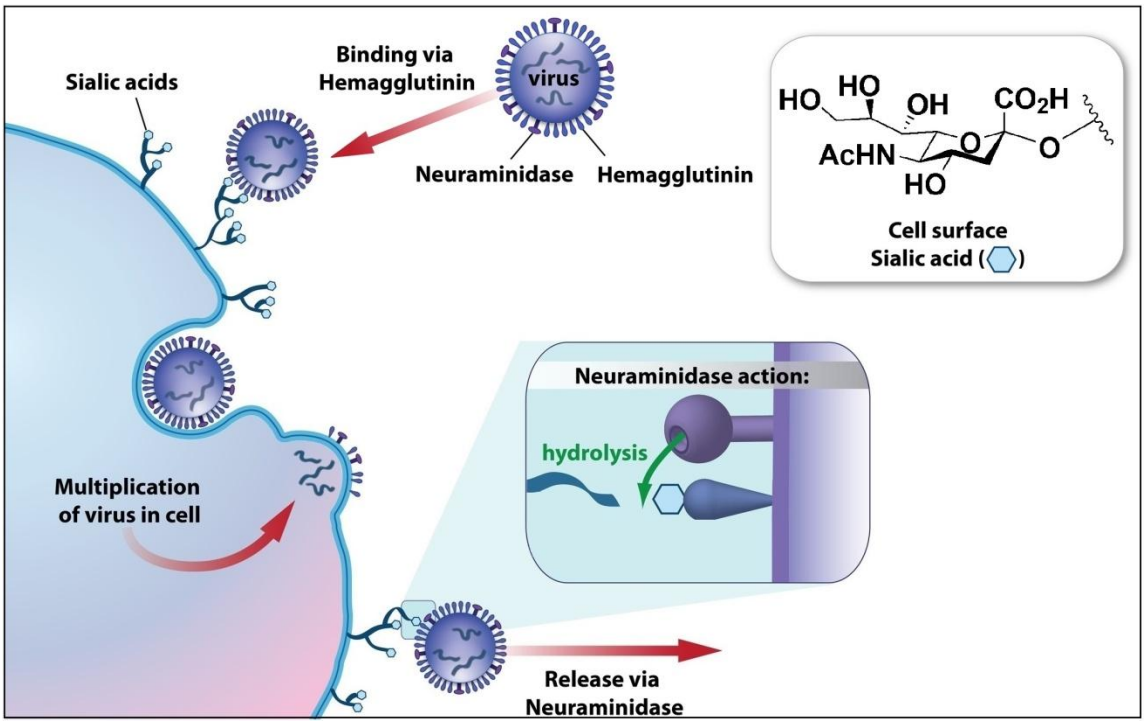

Figure 1.6. Influenza replication life cycle

Note. Modified picture from http://www.publicaffairs.ubc.ca/2013/02/21/new-flu-drug-stops-virus-in-its-tracks/. (Credit: Tom Wennekes, UBC).

Following the viral replication inside the host cell, the newly made viral particles bud through the host cell membrane. These virus particles are coated with sialic acid residues since their hemagglutinins bind to sialic acid residues on the surface of the host cell and also on the cell surface of neighboring virus particles. In order to be able to infect more cells, these aggregated viral particles use their weaponry, the cell surface sialidase (NA), to cleave the sialic acids from the host cell and from the neighboring virus (receptor-destroying function).[22]

Antiviral Drugs Against Influenza

Considering the crucial role of viral sialidase (NA) in the spread of influenza, this enzyme is a leading target for the development of therapeutic agents. Many inhibitors that have been designed to be effective against influenza viral neuraminidase have been

assumed to be transition state (TS) mimics for the neuraminidase-catalyzed hydrolysis reaction, which is an important component of the viral life cycle (oxacarbenium ion-like transition state, **11** in figure 1.7). Many inhibitors of neuraminidase are 4-substituted derivatives of Neu2en5Ac (also known as DANA **12**), such as Zanamivir (also called Relenza **13**), a current therapeutic agent for the treatment of influenza. Oseltamivir (or Tamiflu **14**) is another successful sialidase inhibitor drug used widely for combating influenza infection (Figure 1.7).

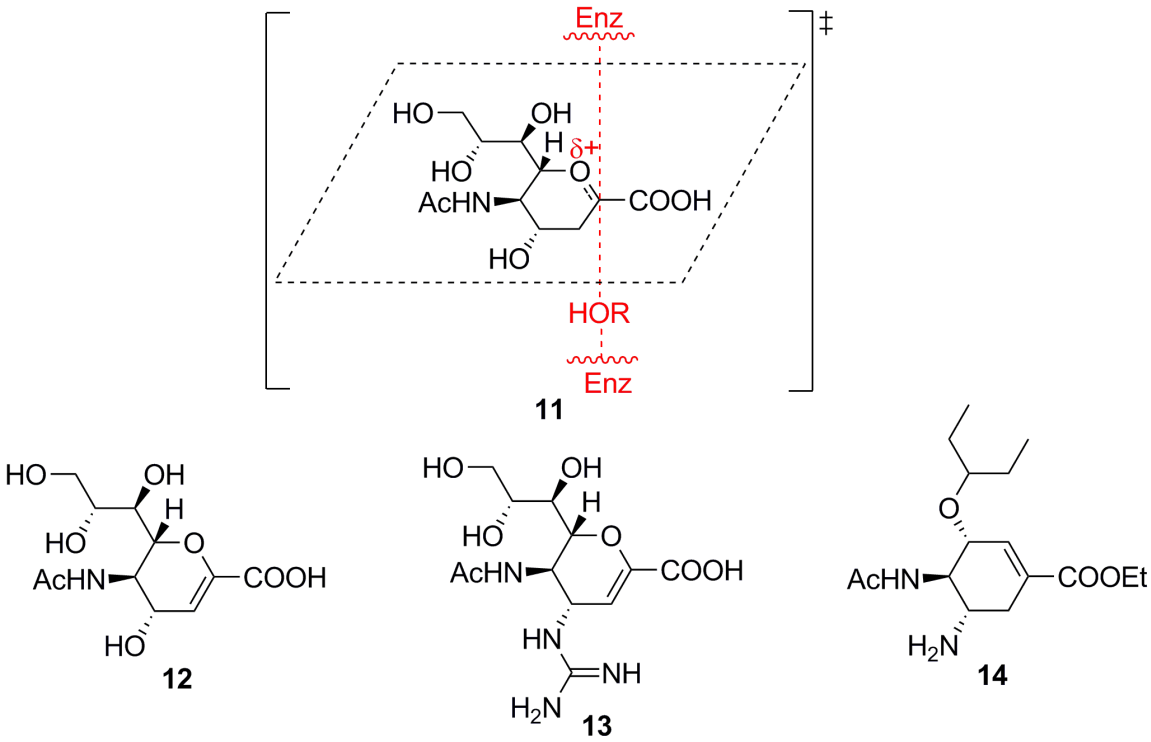

Figure 1.7. Proposed oxacarbenium ion-like transition state (**11**) formed during sialidase catalyzed-hydrolysis of sialoglycoconjugates (OR = glycoconjugates). Postulated TS analogue inhibitors: the core structure (DANA, **12**), Zanamivir (also called Relenza, **13**), Oseltamivir (or Tamiflu, **14**).

Despite numerous continuing attempts to create vaccines and chemotherapeutic agents against influenza virus, the appearance of new virus strains such as H5N1 that are resistant to antivirals (Tamiflu) can result in a major influenza pandemics. Hence,

designing selective neuraminidase inhibitors that are less prone to eliciting a viral response is an ongoing challenge. However, understanding the structures of influenza sialidases and their mechanism of action is a first step in the design of an appropriate antiviral drug for the treatment of influenza infections.

Active Site of Influenza Sialidases

Influenza virus sialidase is a tetramer composed of four identical monomers, and the enzyme has a box-shaped head atop a long slender stalk[44]. Among sialidases from influenza, A/N2 sialidase was the first whose x-ray crystal structure was successfully solved in 1970s [45,46]. Since then, x-ray structures of influenza B and many other influenza A sialidases have been solved, among which the structure of A/N1 sialidase solved in 2006[47] attracted significant attention as the authors of this paper suggested that based on the structures, new opportunities were apparent for design of influenza drugs.

The amino acid sequences of sialidases are significantly different in various strains of influenza A and B; however, there are a few amino acid residues scattered along the polypeptide chain that are conserved in all strains of influenza virus. Upon folding into its three-dimensional structure, the sialidase polypeptide brings these conserved amino acid residues together to furnish the walls and rims of the active site pocket. These invariant amino acid residues directly interact with the sialic acid moiety (terminal sugar of a sialoglycoconjugate or the product released after hydrolysis) bound into the active site. Such interactions can be seen in figure 1.8 which represents the A/N2 sialidase bound to sialic acid (α-Neu5Ac).

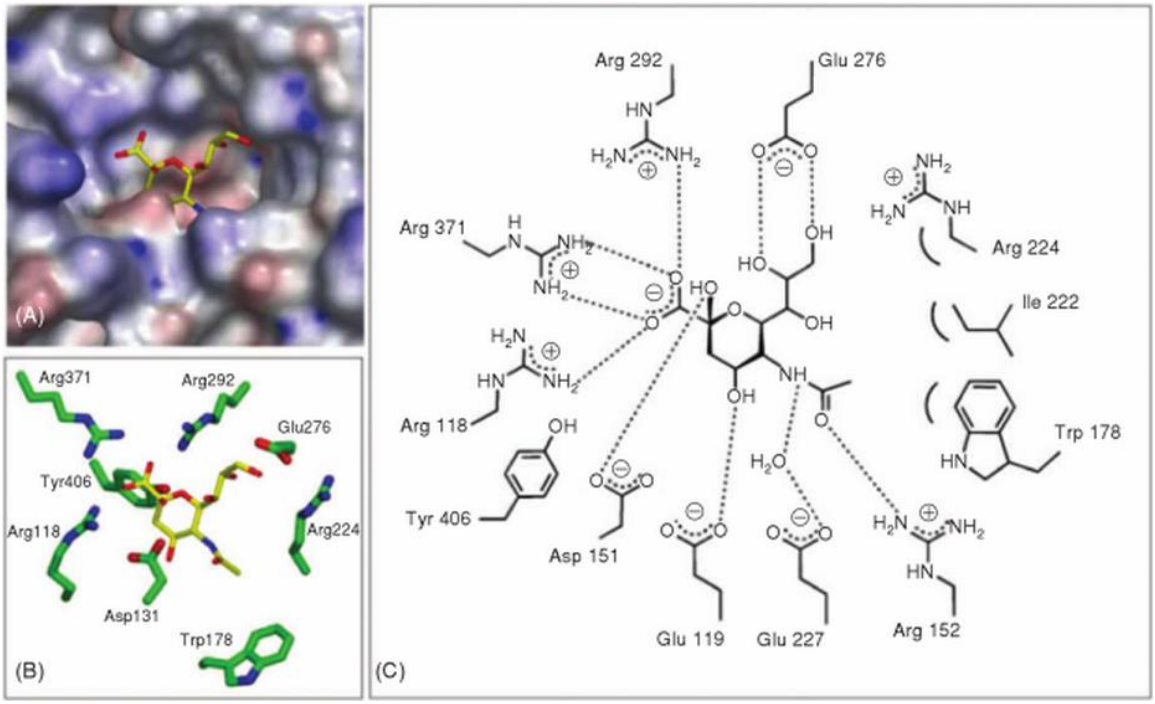

Figure 1.8. Active site of A/N2 sialidase bound to sialic acid (α-Neu5Ac). (**A**) The colored electrostatic potential map of the active site where blue and red indicate positive and negative charge distributions, respectively. (**B**) The key amino acid residues embedding sialic acid in the active site. (**C**) Key interactions between conserved amino acid residues of the active site and the bound sialic acid.

Note. Picture from Discovery and Development of Influenza Virus Sialidase Inhibitor Relenza. 2011, Page 388.[22]

Three arginine residues, Arg118, Arg292 and Arg371, interact with the carboxylate group of sialic acid (C-1). Arg152 forms a hydrogen bond with acetamido group at C-5 of sialic acid, and Glu276 interacts with hydroxyl groups of C-8 and C-9 through hydrogen bonding. The hydroxyl group at C-4 and N-H of acetamido at C-5 form hydrogen bond interactions with Glu119 and Glu227 (via a buried water molecule), respectively. Ile222 and Trp178 show hydrophobic contacts with the methyl group of the acetamido at C-5. Asp151, Glu277, and Tyr406 are involved in catalysis acting as general acid/bases and nucleophile, respectively.

1.4.3 Tyrosine as Nucleophile in Sialidases

That the active site tyrosine residue in sialidases acts as nucleophile was first shown by Withers and co-workers in 2003 when they trapped a sialyl-enzyme bound intermediate using *Trypanosoma cruzi trans*-sialidase (TcTS).[48] TcTS, a key component in Chagas' disease is cataloged as belonging to sialidase family (E.C.3.2.1.18); but, rather than catalyze hydrolysis, it catalyzes the transfer of sialic acid residues α-(2⟶3)-linked to glycoconjugates (**15**, Figure 1.9) on the host cell to the terminal galactose moiety on its cell surface of (*Trypanosoma cruzi)*, with net retention of configuration at the anomeric centre.

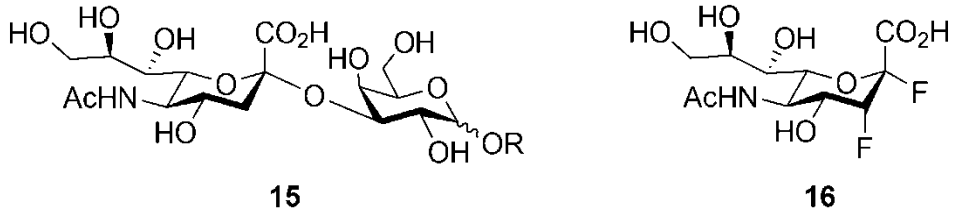

Figure 1.9. Structures of α-(2,3) sialyl-galactosyl-glycoconjugates (**15**) (OR = glycoconjugate) and 2,3-difluorosialicacid (**16**).

Withers and coworkers had previously developed fluorinated sugar analogues as trapping agents to stabilize glycosyl-enzyme intermediates, and thus enabling them to identify the carboxylate residue (Glu/Asp) that acts as a nucleophile in numerous retaining glycosidases.[49,50] With regard to identifying the nucleophile in sialidases, they used 2,3-difluorosialic acid **16** as the substrate mimic, in which the electronegative fluorine atom at C-3 destabilizes the oxacarbenium ion-like transition state, thus decelerating both glycosylation and deglycosylation steps. However, incorporation of an anomeric fluoride, a good leaving group, compensates for the rate reduction in the glycosylation step (first step) and thus results in accumulation of the enzyme-bound intermediate. ES/MS analysis of an incubated solution containing 2,3-difluorosialic acid

with TcTS showed a mass increase of 304 ± 12 Da, which is expected if 3-fluorosialyl is covalently attached to the enzyme. The attachment of the 3-fluorosialyl to active site tyrosine (Tyr342) was identified by LC-MS analysis of peptidic digestion from both labelled and unlabelled enzymes.[48]

In general, sialidases have evolved to use their active site tyrosine as a nucleophile instead of the more common aspartate or glutamate residues used in most retaining glycosidases. Watts et al[48] proposed that unfavorable electrostatic interactions between negatively charged carboxylate (C-1) of sialic acid moiety and an aspartate or glutamate residue is avoided when tyrosine acts as nucleophile. However, the negative charge on the carboxylate group of the sialic acid moiety is balanced by interacting with three active site arginine residues. Hence, Watson et al[51] rationalized that the natural selection of tyrosine arises from intrinsic reactivity differences between sialosides and glycosides. The presence of carboxylate group at the anomeric centre of the substrate and the lack of an electron-withdrawing hydroxyl group on C-3 make a sialyl-enzyme bound intermediate intrinsically more reactive than a glycosyl-enzyme bound intermediate. Therefore, in sialidases, when the intermediate is covalently bound to the poorer leaving group (tyrosine) rather than a better leaving group (glutamate/aspartate), it has a longer existence. This increase in the life time of the intermediate avoids unproductive regeneration of starting material; in other words, it gives the aglycone time to leave the active site. [51]

1.4.4 Mechanism of Sialidases

The proposed mechanism for retaining sialidases catalysing hydrolysis of α-sialosides is shown in Scheme 1.6.

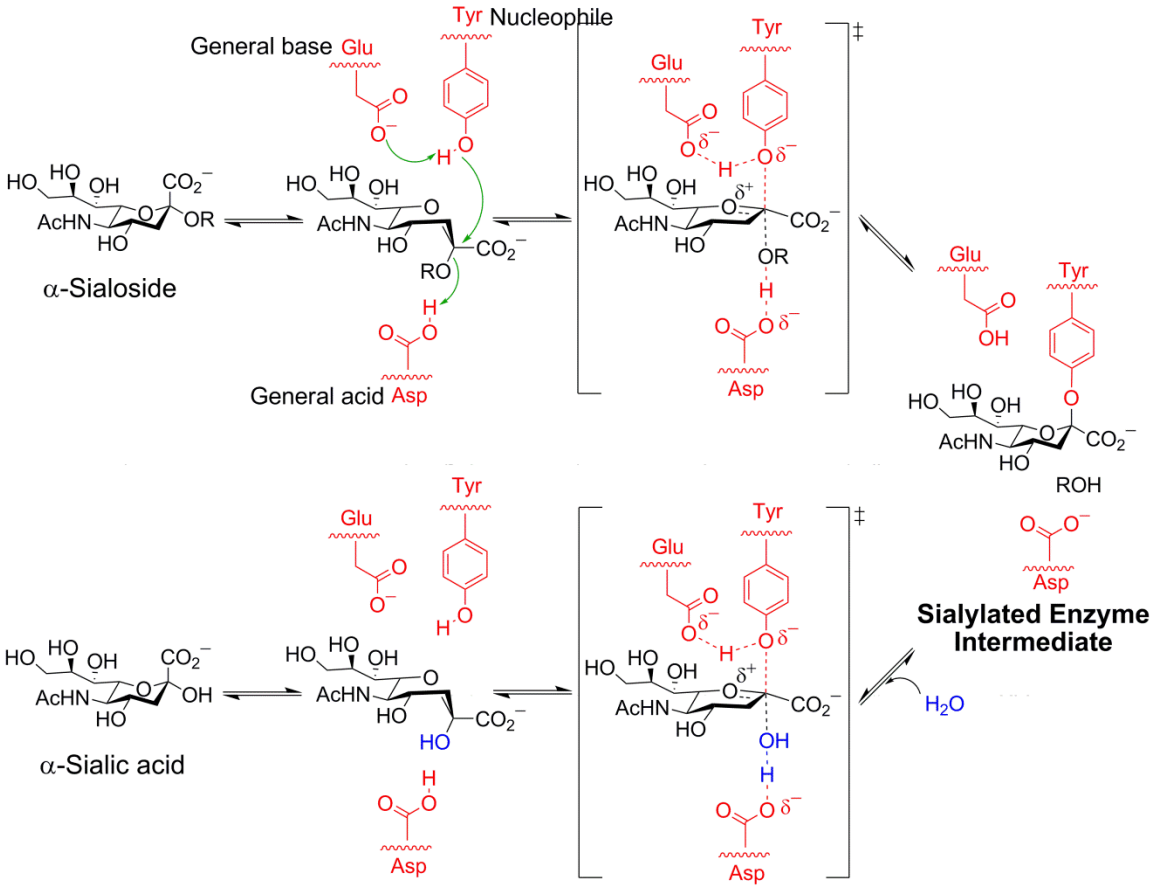

Scheme 1.6. Proposed Mechanism for sialidase catalyzed hydrolysis of α-sialosides[52]

This mechanism goes through four steps. First, the α-sialoside substrate adopts a boat conformation in the active site of the enzyme. The leaving group departs while being protonated by the active site general acid aspartic acid residue. Simultaneously, the nucleophilic tyrosine residue attacks the anomeric centre as it is deprotonated by the glutamic acid residue. This glycosylation step leads to the formation of sialosyl-enzyme bound intermediate, via either an oxacarbenium ion-like transition state or an oxocarbenium ion that is likely in a half-chair conformation. In the third step, a water molecule attacks the anomeric centre of the sialosyl-enzyme intermediate as it is being deprotonated by the aspartic acid residue and this results in cleavage of the tyrosinyl intermediate. This step forms α-sialic acid, via either an oxacarbenium ion-like transition

state, or an oxacarbenium ion in an essentially mirror process to the glycosylation reaction. In the last step, the sialic acid leaves the active site.

1.4.5 Mechanism of Mutant Sialidases Y370G, Y370A, Y370D, Y370E and Y370F

It has been observed that mutagenesis of the conserved active site tyrosine (Tyr370) of the *Micromonospora viridifaciens* sialidase to a glycine (Y370G), alanine (Y370A), aspartate (Y370D), glutamate (Y370E), or phenylalanine (Y370F) gives enzymes that function by new mechanisms.[51,52] Interestingly, Bennet & coworkers showed that these mutant sialidases had significant catalytic activities as judged by the measured k_{cat} values in comparison to that for the wild-type enzyme. Three mutant sialidases, Y370G, Y370A, and Y370D, in which tyrosine is replaced with a small amino acid residue, catalyze the hydrolysis of the activated substrate 4-methylumbelliferyl α-D-*N*-acetylneuraminide with inversion of configuration as judged by NMR spectroscopy of the products formed during the catalyzed reaction.[51] The Brønsted analysis of the mutant Y370D and wild-type sialidases on k_{cat} showed that the departure of leaving group (cleavage of glycosidic bond) is not rate limiting step for wild-type sialidase (β_{lg} = 0.02 ± 0.03); however, for the Y370D sialidase, the value of Brønsted parameter β_{lg} on k_{cat} (β_{lg} = -0.55 ± 0.03) indicates that cleavage of the glycosidic C-O bond is rate-limiting for this mutant enzyme.[51] These observations lead the authors to propose that mutation of nucleophile tyrosine to small amino acids (Y370G, Y370A, and Y370D) created a cavity inside the active site where a molecule of water can be accommodated and this then acts as a nucleophile to give inverted product (Figure 1.10).[53]

Bennet and coworkers proposed a dissociative mechanism (S_N1) for these mutants as shown in Scheme 1.7. First, a general acid/base residue (presumably

Asp92) acts as an acid to facilitate the departure of the leaving group to give a transient oxacarbenium ion that is rapidly attacked by a molecule of water, which is accommodated in the cavity created in the active site.

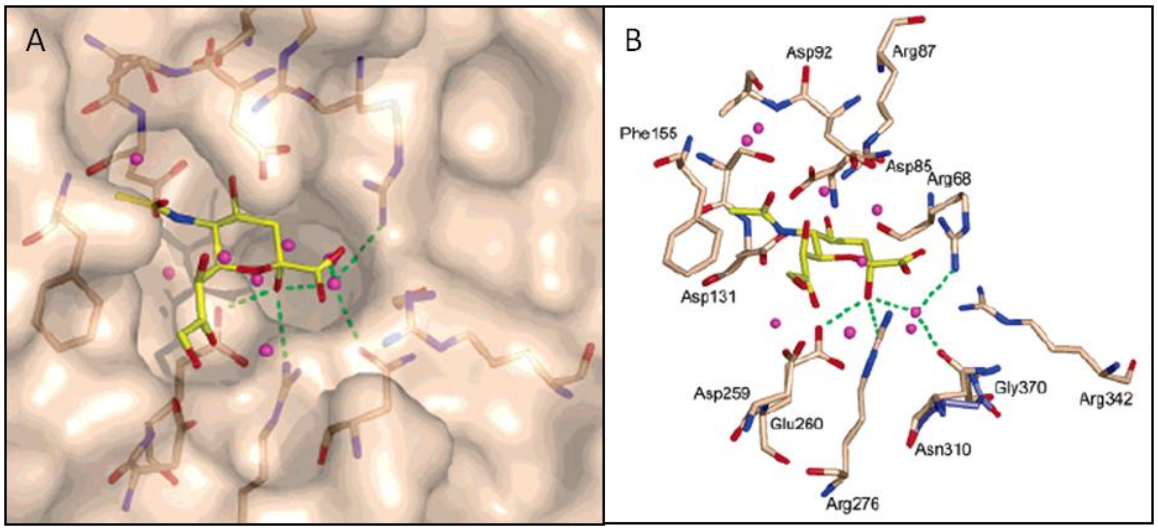

Figure 1.10. Active site of mutant Y370G sialidase from *M. viridifaciens*. (**A**) The bound sialic acid (β-Neu5Ac) is shown as yellow colored molecule and a cavity created by mutation can be seen underneath the anomeric OH group of sialic acid. Four molecules of water shown in magneta color can sit in the hole (**B**) The amino acid residues interacting with bound β-Neu5Ac in the active site

Note. Picture from Biochemistry, 2005, Page 9121.[53]

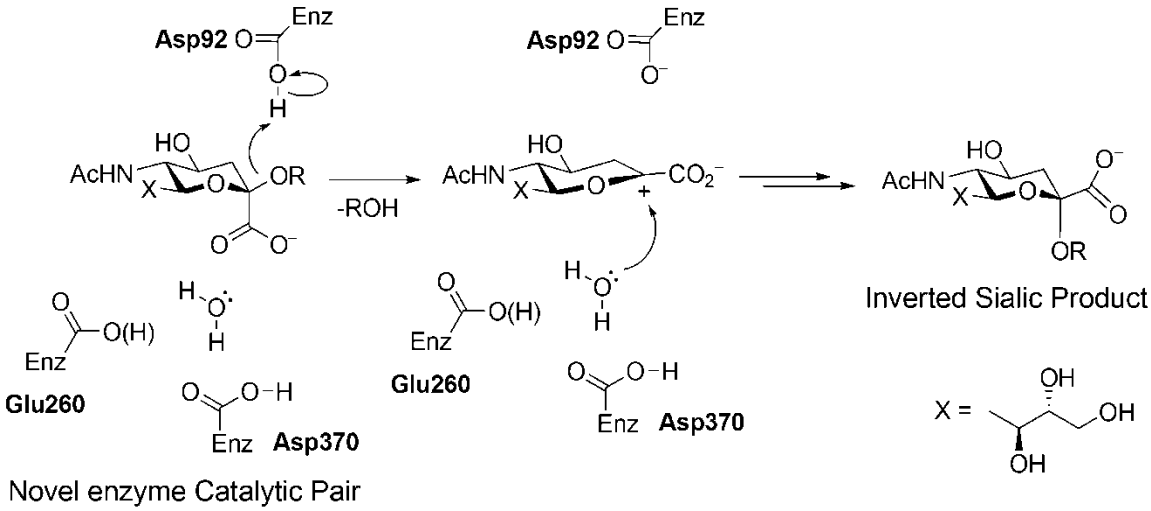

Scheme 1.7. S_N1 dissociative mechanism of mutant sialidase, Y370A, Y370G and Y370D

Note. Scheme from Biochemistry, 2003, Page 12688.[51]

Two other nucleophilic mutant sialidases (Y370E and Y370F) were active and both were retaining enzymes, in contrast to the previously mentioned mutants which catalyze hydrolysis of α-sialosides with inversion of configuration.[52] For these two mutants the Brønsted analysis showed a decrease in activities for both mutants as the leaving group became worse, thus suggesting that the rate of hydrolysis is limited by glycosidic bond cleavage. The small difference between Y370E and Y370D (an inverting enzyme) is an extra CH_2 unit (glutamate versus aspartate), which results in a change of reaction stereochemistry from retention to inversion of configuration. It is expected that the carboxylate group of glutamate residue in mutant Y370E acts as the nucleophile because the distance between glutamate and bound substrates does not allow a molecule of water to fit in the between to act as a nucleophile as observed in mutant Y370D. However, mutant Y370F in which tyrosine is replaced by phenylalanine, lacks an obvious nucleophile, but still functions with retention of configuration. Moreover, the mutant Y370E showed a much smaller value of the Bronsted parameter β_{lg} on k_{cat}/K_m (β_{lg} = –0.36 ± 0.04) compared to that of mutant Y370F (β_{lg} = –0.79 ± 0.12). These observations suggested that these two mutant enzymes function through different mechanisms. Hence, the authors proposed a concerted S_N2 (double displacement) mechanism for mutant Y370E, with the glutamate acting as a nucleophile and the retaining mutant Y370F reacting via a S_N1 mechanism (dissociative transition state), in which an oxacarbenium ion intermediate is generated that is either trapped by a nearby residue or by a solvent water molecule.[52]

1.5 Mechanistic Studies in Glycosidases

1.5.1 Enzyme Kinetics

Enzymes are efficient and specific catalysts that enhance the rate of reactions by many orders of magnitude (10^6 to 10^{20}) without themselves being consumed.

In 1913, German biochemist Leonor Michaelis and Canadian physician Maud Leonora Menten, proposed the kinetic model for enzyme catalysis and their mathematical derivation which has become known as the Michaelis-Menten equation. The Michaelis-Menten scheme in its simplest form is shown below (Scheme 1.8)

$$E + S \underset{k_{-1}}{\overset{k_1}{\rightleftharpoons}} ES \xrightarrow{k_{cat}} E + P$$

Scheme 1.8. General Michaelis-Menten (E: enzyme, S: substrate, ES: Michaelis complex which is a reversibly formed intermediate, P: product, k_1: rate constant for ES formation, k_{-1}: rate constant for conversion of ES to E+S, k_{cat}: rate constant for product formation).

The measurement of enzymatic reaction rates are traditionally made in the presence of a large excess of substrate ([S]>>[E]) under steady state conditions where the concentration of enzyme bound intermediates, such as [ES], is constant as their production and degradation occur at the same rate.[54] Under such steady state conditions, the Michaelis-Menten equation can be derived as shown in Eq 1.1:

$$v = \frac{k_{cat}[E]_0[S]}{K_m + [S]} \quad \text{where,} \quad V_{max} = k_{cat}[E]_0 \quad \text{(Eq 1.1)}$$

In order to understand the significance of the various enzymatic kinetic parameters in this equation, a more complex reaction scheme needs to be considered, such as that proposed for sialidases (Scheme 1.9).

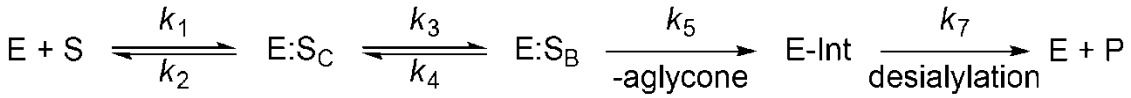

Scheme 1.9. Proposed reaction scheme for sialidases. $E:S_C$ refers to Michaelis complex in which the substrate has chair conformation whereas $E:S_B$ the substrate is in a boat conformation. E-Int is enzyme-bound intermediate whose formation is considered as the first irreversible step during the reaction; k_5 and k_7 represent the rate constants for the glycosylation (sialylation) and deglycosylation (desialylation) steps, respectively.

The catalytic constant, k_{cat}, which is also called turnover number of the enzyme is the first order rate constant for the formation of product from the Michaelis complex as expressed in Eq 1.2 for the kinetic scheme shown above. Therefore, based on this expression, for k_{cat}, the rate determining step could be either a chemical reaction, glycosylation (k_5) or deglycosylation (k_7), or the conformational change of substrate bound to the active site of enzyme (k_3) or a complex mixture of all these rate constants.

$$k_{cat} = \frac{k_3 k_5 k_7}{k_3 k_5 + k_3 k_7 + k_4 k_7 + k_5 k_7} \quad \text{(Eq 1.2)}$$

The Michaelis constant, K_m, is an apparent dissociation constant, and is defined as the substrate concentration at which the rate of the enzyme reaction is half of the maximum rate ($\nu = V_{max}/2$). The derived expression for K_m is shown in Eq 1.3.

$$K_m = \frac{k_2 k_4 k_7 + k_2 k_5 k_7 + k_3 k_5 k_7}{k_1 k_3 k_5 + k_1 k_3 k_7 + k_1 k_4 k_7 + k_1 k_5 k_7} \quad \text{(Eq 1.3)}$$

The specificity constant, k_{cat}/K_m, is an apparent second order rate constant which is also called the catalytic efficiency. The rate determining step for k_{cat}/K_m can include all steps from the enzyme encountering the substrate (diffusion) to the first irreversible step (k_5) of the reaction as shown in the expression below (Eq 1.4).

$$\frac{k_{cat}}{K_m} = \frac{k_1 k_3 k_5}{k_2 k_4 + k_2 k_5 + k_3 k_5} \quad \text{(Eq 1.4)}$$

The enzymatic catalytic proficiency is expressed as $k_{cat}/K_m \times 1/k_{uncat}$, which is the reaction rate enhancement caused by an enzyme over that of the uncatalyzed reaction.

1.5.2 Mechanistic Tools

To probe the mechanism of action for an enzyme, many different kinetic techniques can be used. For the purpose of this discussion, the three specific techniques used within this thesis are: i) Brϕnsted catalysis correlation; ii) transition state analogy; iii) kinetic isotope effect. Often, a combination of these techniques are required in order to reach conclusions concerning the mechanism of an enzyme. These techniques are discussed in detail in the following sections.

1.5.2.1 Brϕnsted Catalysis Correlation

Brϕnsted acid/base catalysis is the most common type of catalysis in organic chemistry. For general catalyzed reactions, proton transfer is occurring in the rate determining step, thus the reaction rate is increased on increasing the acid/base concentration because the acid or base is a component of the transition state. Equations **a** and **b** (Scheme 1.10) represent scenarios in which an acid or base is involved in the rate limiting-step acting as either a general-acid or a general-base catalysts.

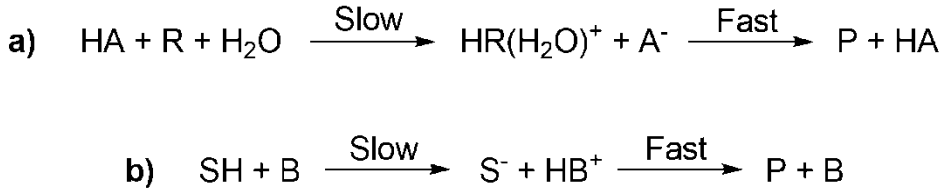

Scheme 1.10. a) A general-acid catalysis, **b)** A general-base catalysis.

Note. Scheme from Modern Physical Organic Chemistry, 2006, Page 511.[55]

In these reactions as the acid or base is involved in the rate-determining step, there should be a relationship between the rate of the reaction and the intrinsic activity of the acid or base being used as a catalyst. For example, in a general-acid catalysis, it is expected that the rate of reaction will increase when using stronger acid (low pK_a) as it can donate proton more easily during the rate-limiting step. Therefore, there exist a linear free energy relationship (LFER) in general catalysis, wherein, the changes in pK_a (thermodynamic) is reflected in logarithm of the reaction rate constant, log *k* (kinetic).[54] Such a correlation between acid strength, as expressed by its pK_a, and log(*k*) for a general acid catalysis is shown in Eq 1.5.

$$\log(k) = -\alpha\, \mathrm{p}K_a + C \quad \text{(Eq 1.5)}$$

In this equation, *k* is the reaction rate constant and α, which is the negative slope of the straight line obtained by plotting log (*k*) versus pK_a for a series of acids (Figure 1.11), represents the sensitivity parameter (a proportionality constant), and the intercept is C.

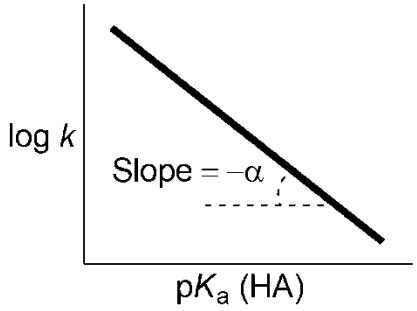

Figure 1.11. A typical Brønsted plot for a general-acid catalysis (Scheme 1.12, **a**)

A similar Brϕnsted equation can also be used for general-base catalyzed reactions (Eq 1.6)[56] where log (*k*) is linearly dependent on the pK_a of the conjugate acid

of the general base being used in the reaction and the slope of the plot is expressed as β.

$$\log(k) = \beta \, \mathrm{p}K_a + C' \quad \text{(Eq 1.6)}$$

Similar to general acid-base catalysis, the same correlations can be applied when studying nucleophilicity and nucleofugality (leaving group ability) in reactions where nucleophile attack or leaving group departure occurs during the rate-determining step. Eq 1.7 shows the correlation between nucleophilicity (as expressed by the pK_a of the conjugate acid of the nucleophile) and the reactivity (log *k*). Plotting log k versus pK_a of the conjugate acid of the nucleophile should result in a straight line with the slope of β_{Nuc} (sensitivity factor) that have a positive value. A similar correlation can be found between leaving group ability and acidity of its conjugate acid as shown in Eq 1.8. It is expected that plotting log *k* versus pK_a of the conjugate acid of the leaving group affords a straight line with the slope of β_{lg} (negative value), if the nucleofuge's leaving group ability is reflected in its basicity.

$$\log(k) = \beta_{\mathrm{Nuc}} \, \mathrm{p}K_a + C' \quad \text{(Eq 1.7)}$$

$$\log(k) = \beta_{\mathrm{lg}} \, \mathrm{p}K_a + C \quad \text{(Eq 1.8)}$$

Such Brϕnsted analyses are very common protocols for studying mechanistic features of many enzymes, including glycosidases. For example, in order to determine if the departure of a leaving group in a substrate is involved in the rate-determining step or not, a series of substrates carrying different leaving groups (phenols) are kinetically assessed. For instance, in retaining glycosidases (such as sialidases) with two step mechanisms (Scheme 1.6, page 23), the aglycone part (leaving group) is cleaved

during glycosylation. Therefore, the ease with which the leaving group departs from substrate is dictated by the reaction rate of this step. If the first step (glycosylation) is the rate-determining step, plotting the logarithm of rate constant (k_{cat} or k_{cat}/K_m) versus pK_a of the conjugate acids for different leaving groups (a range of different substituted phenols), results in a strong linear correlation. Hence, according to Eq 1.8, such a plot gives a straight line with a large negative slope (β_{lg}).

An example of Brϕnsted relationship measurement on glycosidases can be seen in the work by Sinnott et al., who measured β_{lg} for *Vibrio cholerae* sialidase, an enzyme that contributes to the severity of the disease cholera. In this work, the rate constants for *V*. *cholerae* sialidase-catalyzed hydrolysis of various aryl α-sialosides (**17a-g**, Figure 1-12) were measured.[57]

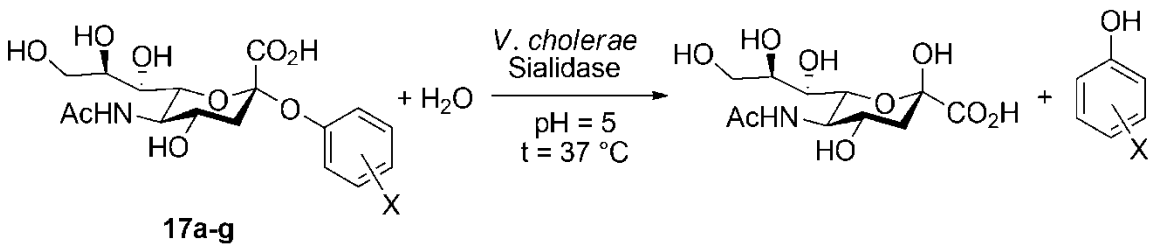

X = H (**17a**), 4-nitro (**17b**), 3-nitro (**17c**), 4-cyano (**17d**), 3,4-dichloro (**17e**), 3-chloro (**17f**), 4-chloro (**17g**)

Figure 1.12. *V*. *cholerae* sialidase catalyzed hydrolysis of various aryl α-sialosides.

A good correlation was obtained between the pK_a of the phenol leaving group and the kinetic parameters log(k_{cat}) and log(k_{cat}/K_m), resulting in straight lines with slopes, β_{lg} values on (*V*) of –0.25 (r = –0.95) and on (*V*/*K*) of –0.73 (r = –0.93). The good correlations in both cases suggest that the enzyme-catalyzed glycosylation step (cleavage of sugar-aglycone bond) is the rate limiting step, or partially so, for both k_{cat} and k_{cat}/K_m. The large negative value of β_{lg} (*V*/*K*) indicates little proton transfer to the

leaving group at the glycosylation transition state.

The spontaneous (nonenzymatic) hydrolysis of the same panel of aryl α-sialosides (**17a-g**, Figure 1.12) was also studied by Sinnott et al in 1992.[58] Brønsted plots of log k_{obs} versus the pK_a of the conjugate acid of the leaving groups were obtained at pHs 1.00, 2.69, 6.67, and 13.0 to afford β_{lg} values of 0.0, 0.01, –1.3, –0.17, respectively (Figure 1.13). The β_{lg} values for the acid-catalyzed hydrolysis of aryl α-sialosides (**17a-g**) is zero or near zero because protonation of the leaving group (resulting in the build-up of positive charge) is complete before rate-limiting cleavage of the glycosidic bond C-O, which results in little positive charge being present on the leaving group at the hydrolytic TS and thus a near zero β_{lg} value.

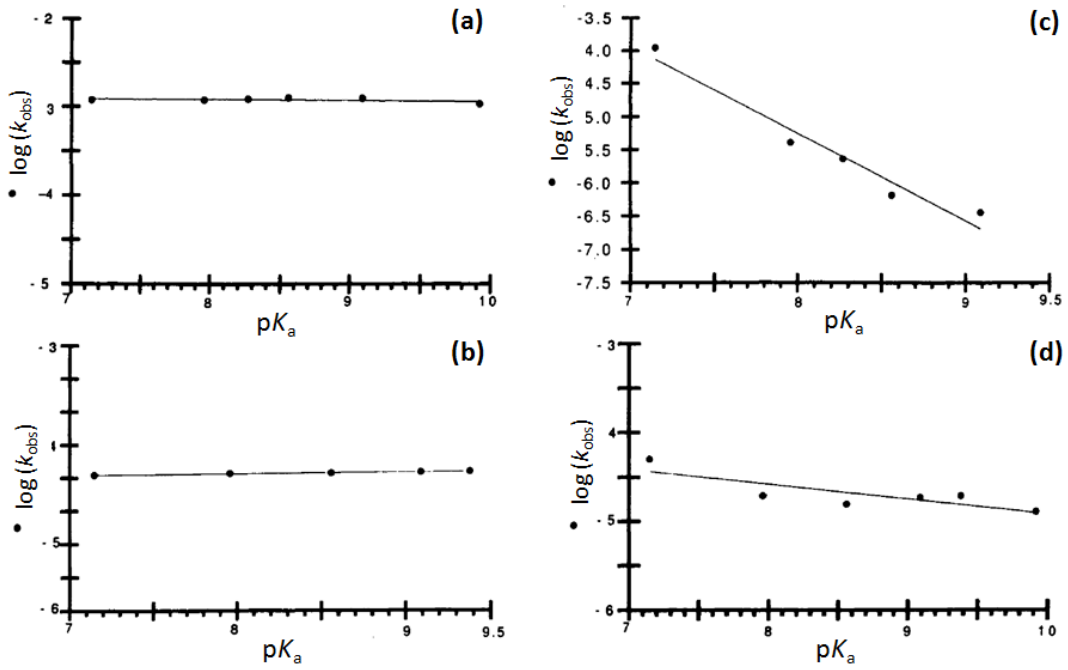

Figure 1.13. Brønsted plots obtained for spontaneous (non-enzymatic) hydrolysis of aryl-α-sialosides (**17a-f**, Figure 1.19). (**a**) pH 1.0 at 50.0 °C, (**b**) pH 2.6 at 50.0 °C, (**c**) pH 6.67 at 60.0 °C, (**d**) pH 13 at 50.0 °C

Note. Picture from J. Am. Chem. Soc, 1992, Page 10158.[58]

The small value of β_{lg} for the base reaction of aryl α-sialosides (**17a-g**) (plot **d**,

Figure 1.13, given that protonation of the leaving group is not possible at high pH values; indicates that it is unlikely that cleavage of C-OAr bond is rate-limiting.

The large negative value (β_{lg}) obtained for the uncatalyzed hydrolysis of the anion of aryl α-sialosides (**17a-g**) (plot **c**, Figure 1.13) at pH = 6.67 is an indication that glycosidic bond C-OAr cleaves in the rate limiting step and that the transition state is late with respect to C-O bond cleavage with no protonation of the leaving group.

1.5.2.2 Transition State Analogy

Transition state theory is an approach to explain how chemical reactions take place. This theory is based on the existence of a hypothetical species called the transition state, which is an activated complex, that acts as an energy barrier between reactants and products on the potential energy surface of a chemical reaction. Transition state theory rests on two basic assumptions: 1) decomposition of the activated transition-state complex controls the rate of the reaction, 2) there is an equilibrium between the transition-state complex and the reactants.[59] The rate of conversion of a transition state to product is directly dependent on the vibrational frequency of its stretching bonds that are cleaved to produce the product as shown in Eq 1.9. In this equation, *k* stands for reaction rate constant, κ is a transmission coefficient, ν is a vibrational frequency, and $K^{\ddagger}$ is a pseudo-equilibrium constant for formation of the transition state complex from starting material.[59] The virbrational frequency (ν) is dependent on k_B (Boltzman's constant), T (absolute temperature), and h (Planck's constant) as shown in Eq 1.10.

$$k = \kappa \nu K^{\neq} \quad \text{(Eq 1.9)}$$

$$\nu = \frac{k_B T}{h} \quad \text{(Eq 1.10)}$$

A theoretical relationship between transition state stabilization and enzymatic catalysis, as illustrated in the thermodynamic cycle (Scheme 1.11), was first explained by Kurz in 1963[60] and it was later elaborated by Wolfenden[61,62] and Lienhard[45].

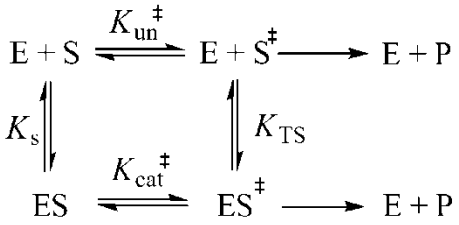

Scheme 1.11. Kurz illustration[63] of the hypothetical thermodynamic cycle relating ground-state binding and transition-state binding for an enzyme with a single substrate. *(*K_S: dissociation constant of the substrate, K_{TS}: hypothetical dissociation constant of the bound TS, $K_{un}^{\ddagger}$: pseudo equilibrium constant for formation of the activated complex in the uncatalyzed reaction, $K_{cat}^{\ddagger}$: pseudo equilibrium constant for TS formation in the catalyzed reaction)

Note. Scheme from *Chem. Rev*, 97, page 1281.[63]

The ratio of the rate constant for the enzymatic reaction (k_{cat}) to the rate constant for the same reaction in the absence of enzyme (k_{un}) can be seen in Eq 1.11.[59]

$$\frac{k_{cat}}{k_{un}} = \frac{\kappa_{cat}\nu_{cat}K_{cat}^{\neq}}{\kappa_{un}\nu_{un}K_{un}^{\neq}} \quad \text{(Eq 1.11)}$$

Because of this thermodynamic cycle, the overall free energy associated with transition from $ES^{\ddagger}$ to $S^{\ddagger}$ is independent of the pathway used; hence, the Eq 1.12 can be derived from this scheme. Large values for k_{cat}/k_{un} (10^{10}–10^{14}) are expected due to noted rate enhancements for enzymatic reactions. Assuming that values of κ and ν are comparable in both enzymatic and non enzymatic reactions, which makes it unlikely that the factor $\kappa_{cat}\nu_{cat}/\kappa_{un}\nu_{un}$ differs much from unity. Therefore, it can be approximated that K_{TS}/K_s is equal to k_{un}/k_{cat} (Eq 1.13).[59]

$$\frac{k_{cat}}{k_{un}} = \frac{\kappa_{cat}\nu_{cat}K_s}{\kappa_{un}\nu_{un}K_{TS}} \quad \text{(Eq 1.12)}$$

$$K_{TS} = \frac{k_{un}}{k_{cat}} K_s \quad \text{(Eq 1.13)}$$

Basic transition state theory states that enzymes bind their transition state ($ES^{‡}$) more tightly than they bind the substrate (ES)[59]; therefore, many enzyme inhibitors are designed to be transition state mimics. For an inhibitor which mimics the transition state ($ES^{‡}$), K_i is proportional to K_{TS} as shown in Eq 1.14 (*d* reflects the proportionality because inhibitors mimic the transition state imperfectly). Rewriting Eq 1.14 in logarithmic form gives Eq 1.15, in which the constant *d* and noncatayzed rate constant are shown as a separate term.

$$K_i = dK_{TS} = dK_m \frac{k_{un}}{k_{cat}} \quad \text{(Eq 1.14)}$$

$$\log K_i = \log \frac{K_m}{k_{cat}} + \log dk_{un} \quad \text{(Eq 1.15)}$$

Woldfenden[64] and Thompson[65] were two pioneers in utilizing this equation to evaluate if an inhibitor is a transition state analogue. If a series of alterations are made to one position of an inhibitor, and then matching alterations are also applied to the substrate, plotting log K_i versus log K_m/k_{cat} will result in a slope of one if that inhibitor is genuinely a transition state analogue.

This approach has been used with peptidases due to ease of making variations in the peptide substrates. For instance, correlations between K_i and K_m/k_{cat} have been obtained for the phosphorus-containing peptide inhibitors of thermolysin[66], carboxypeptidase A[67], and Pepsin[68].

An example of applying transition state analogy to glycosidases is the work reported by Whitworth et al in 2007[69] on human *O*-GlcNAcase. This enzyme is a member of family 84 glycosyl hydrolases, which catalyze the hydrolysis of glycosidic linkage of O-GlcNAc (2-acetamido-2-deoxy-β-D-glucopyranoside) that is *O*-linked to a serine or a threonine residue. These authors analyzed two series of known potent inhibitors, PUGNAc (O-[2-acetamido-2-deoxy-D-glucopyranosylidene]amino-*N*-phenylcarbamate) (**18a-g**, Figure 1.14) and NAG-thiazoline (1,2-dideoxy-2'-methyl-α-D-glucopyranoso-[2,1-*d*]-Δ2'-thiazoline) (**19a-g**, Figure 1.14), as transition state analogues for human *O*-GlcNAcase[69].

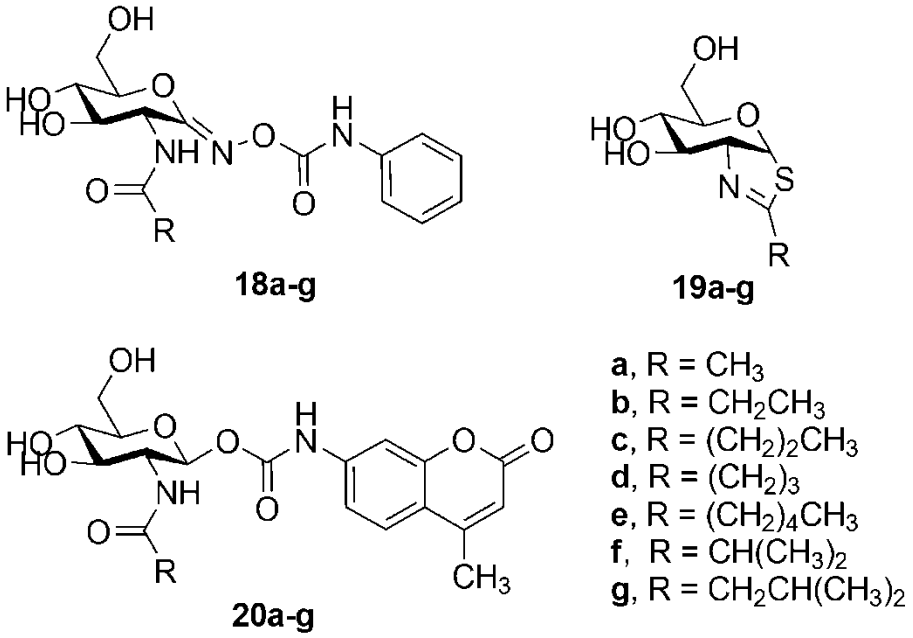

Figure 1.14. *O*-GlcNAcase inhibitor derivatives, PUGNAc (**18a-g**) and NAG-thiazoline (**19a-g**), used to study as transition analogues against a series of *O*-GlcNAcase substrates (**20a-g**).

Note. Picture from *J.Am. Chem. Soc,* 129, Page 635 (2007).[69]

Whitworth et al determined that there was strong linear correlation between log (K_i) and log (K_m/k_{cat}) for NAG-thiazoline derivatives **19a-g,** with a slope of 0.97 ± 0.06 (**A**, Figure 1.15). However, the corresponding PUGNAc derivatives **18a-g** displayed a

poor correlation (**B**, Figure 1.15). Taken together, these data suggest that NAG-thiazoline is a good transition state mimic while PUGNAc is a poor transition state mimic and thus is simply a fortuitous binder to *O*-GlcNAcase.[69]

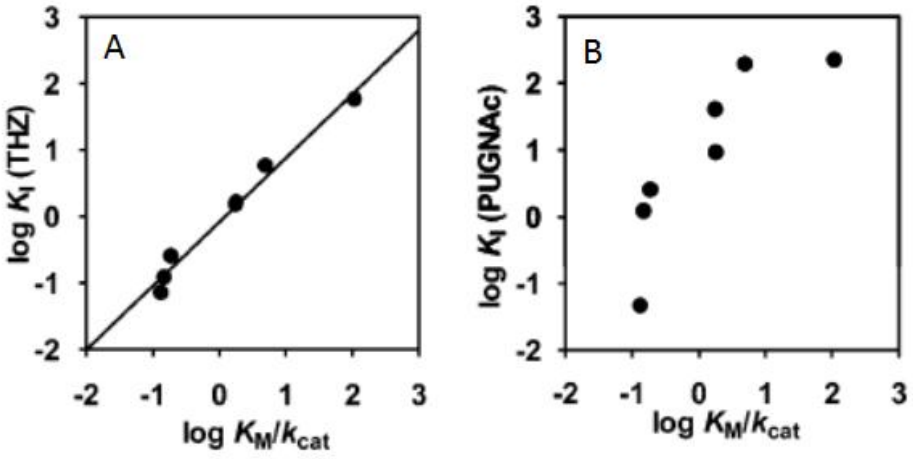

Figure 1.15. Comparison of transition state analogy free energy diagrams for NAG-thiazoline derivatives (**19a-g**) (**A**), and PUGNAc (**18a-g**) (**B**), against substrate derivatives (**20a-g**).

Note. Picture from *J.Am. Chem. Soc,* 129, Page 635 (2007).[69]

1.5.2.3 Kinetic Isotope Effects

Definition and Symbols[70,71]

The measurement of kinetic isotope effects (KIEs), which involves a comparison of rate constants for two isotopically substituted compounds, is a powerful tool for the elucidation of reaction mechanisms. KIEs provide information on which bonds are breaking, forming, and what atoms are undergoing rehybridization at the rate determining step. The isotope effect is expressed as a ratio of rate constants for that of the light isotopologue to that for the heavy isotope containing compound. For example, when studying isotope effects on reactions in which a hydrogen atom is substituted by a deuterium atom the KIE is given as k_H/k_D. When the KIE value is greater than one, this is called a normal KIE, while a value that is smaller than one is labelled as an inverse KIE.

A kinetic isotope effect that originates from isotopic substitution at a site that is undergoing bond breaking or making in the rate limiting step is called a primary KIE (1º KIE). Whereas, if the isotopic substitution is at a site that formally does not change bond order it is labelled as a secondary KIE (2º KIE). The most commonly measured KIEs are those arising from ^{2}H, ^{3}H, ^{13}C, ^{14}C, and ^{18}O substitution.

Origin of Kinetic Isotope Effect[71]

For the discussion in this thesis, the good approximation that isotope effects for organic compounds originate from differences between isotopologue zero point energies (ZPE) will be used. For instance, a comparison of C-H and C-D bonds reveals that the stretching frequency of a C-D bond is lower than that of a C-H bond because a C-D bond has a higher reduced mass (Eq 1.16). This equation is the idealized harmonic oscillator model for a diatomic molecule in which ν is the frequency of the bond, m_r refers to reduced mass of the atoms involved in the bond vibration and κ stands for the bond force constant.[71]

$$\nu = \frac{1}{2\pi}\sqrt{\frac{\kappa}{m_r}} \quad \textit{where} \quad m_r = \frac{m_1 m_2}{m_1 + m_2} \quad \text{(Eq 1.16)}$$

The zero point energy is also related to the frequency of the bond as shown in equation 1.17:

$$E = \frac{1}{2}h\nu \quad \text{(Eq 1.17)}$$

Therefore, the zero point energy of C-D is lower than C-H, which results in a higher activation energy for homolysis of a C-D bond relative to a C-H bond, as shown below in the Morse potential diagram (Figure 1.16).

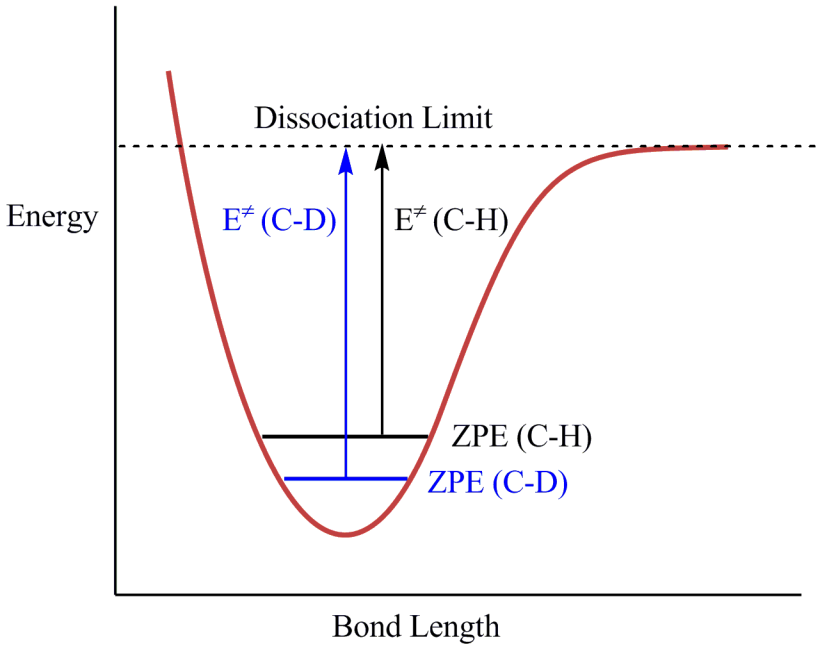

Figure 1.16. Morse potential for a C-H bond. $E^{\neq}$ refers to activation energy

Note. Picture from *Modern Physical Organic Chemistry* , Page 421 (2006).[71]

Given that a rate constant and activation energy for a reaction are related to each other as shown in Eq 1.18, a normal KIE (k_H/k_D >1) is usually observed for primary kinetic isotope effects. However; secondary kinetic isotope effects can be either normal or inverse.

$$\text{KIE} = \frac{k_H}{k_D} = e^{\left[\frac{-(E_H^{\neq} - E_D^{\neq})}{RT}\right]} \quad \text{(Eq 1.18)}$$

Isotope Effects in Enzyme Kinetics

In enzymatic reactions, the magnitude of a kinetic isotope effect (KIE) can be used to provide insight into the geometric structure of the transition state. In an enzymatic reaction, a kinetic isotope effect can be measured on the two kinetic parameters: k_{cat} (maximal first order rate constant); and k_{cat}/K_m (apparent second order rate constant at low substrate concentration). By convention, the symbols that designate

KIEs measurements are *V* (KIE on k_{cat}) and *V*/*K* (KIE on k_{cat}/K_m) with a superscript prefix that designates the isotopic substitution, for example ^{D}V, ^{T}V, ^{13}V, ^{14}V, ^{15}V, and ^{18}V stand for kinetic isotope effects on the maximum velocity, for deuterium, tritium, ^{13}C, ^{14}C, ^{15}N, and ^{18}O, respectively.

With regard to glycosidases, the measurement of kinetic isotope effects goes back to the pioneering work of Sinnott and Souchard[72] who measured α-secondary deuterium kinetic isotope effects on *a retaining* β-galactosidase from *E.coli*. The mechanism of action involves glycosylation and deglycosylation steps (see Scheme 1.4 on page 12). This seminal study by Sinnott and Souchard provided the first evidence for the existence of a covalent glycosyl-enzyme intermediate in retaining β-glycosidases. That is, they observed large normal values ($k_H/k_D>1$) for both glycosylation and deglycosylation steps, indicating a decrease in coordination number ($sp^3 \longrightarrow sp^2$) at the anomeric centre (C-1) for both steps. Specifically for the deglycosylation step, the measured kinetic isotope effect of greater than 1 ($^{\alpha-D}V$ = 1.25) strongly supported the existence of a covalent intermediate (a tetrahedral species carrying sp^3 hybridized centre at the anomeric carbon), which is flanked by a transition state with trigonal sp^2-hybridized centre (C-1). An inverse KIE ($^{\alpha-D}V$ <1) would have been obtained if the intermediate was an oxacarbenium ion paired with an anion. [37]

1.6 Thesis Overview

This thesis work is compromised of four chapters starting with Chapter 1, a general introduction, followed by Chapter 2 that is a published journal article, Chapter 3 presents a submitted manuscript as a communication, Chapter 4 is a progress report on a method development, and Chapter 5 describes the conclusions and future work.

Chapter 2. This chapter presents the published manuscript in *Biochemistry* (F. S. Shidmoossavee, L. Cheng, J. N. Watson and A.J. Bennet, Brønsted Analysis of a Pseudo-Deglycosylation Reaction: Mechanism of Desialylation in Sialidases, *Biochemistry*, **2010**, *49*, 6473-6484.). In this study, the first mechanistic tool discussed in the introduction (Brϕnsted catalysis correlation) is applied in order to get more insight into the deglycosylation step during the *Micromonospora viridifaciens* sialidase (wild-type) catalyzed hydrolysis of sialosides. A mutant sialidase (Y370G from *M. viridifaciens*) and a series of non-natural substrates were used as mimics of deglycosylation step in wild-type sialidase. Specifically, the author of this thesis performed the two main parts of this project. First, a reagent panel of 7 mono- and di-fluorophenyl *β*-D-sialosides (**1a-h**, Figure 2.1) was synthesized, and then these compounds were used, in conjunction with the parent phenyl *β*-D-sialoside, to probe the mechanism for *M. viridifaciens* Y370G mutant sialidase-catalyzed hydrolyses through extensive kinetics experiments.

Chapter 3. This chapter titled as “Chemical Insight into the Emergence of Influenza Virus Strains that are Resistant to Relenza” presents the manuscript written in the template for communications in Journal of American Chemical Society (JACS), and it has been submitted to JACS for publication. In this study, the second mechanistic tool described in the introduction (transition state analogy) is used to examine if 4-substituted derivatives of Neu2en5Ac (**12**, Figure 1.7) including the well known Relenza (**13**, Figure 1.7), a current therapeutic agent for the treatment of influenza, are transition state analogues. In other words, it is examined if the interactions between the influenza sialidase and its substrate are similar to that of enzyme and the corresponding modified inhibitor. To test the hypothesis of transition state mimicry the author of this thesis synthesized, single handed; a series of 4-subsitituted Neu2en5Ac derivatives (**2a-j**,

Figure 3.2) and the corresponding 4-substituted *p*-nitrophenyl α-sialosides (**1a-j**, Figure 3.2) and performed the required extensive kinetics experiments. Results reported include those for the sialidases from influenza and the highly-evolved soil bacterium *Micromonospora Viridifaciens*.

Chapter 4. This chapter titled as "Simultaneous Measurements of Multiple Kinetic Isotope Effects by NMR Spectroscopy" presents the last, but the most powerful, mechanistic tool discussed in the introduction (kinetic isotope effects). This work involves developing a two dimensional nuclear magnetic resonance (NMR) spectroscopic method for the simultaneous measurement of several KIEs on sialidase-catalyzed reactions. The technique is developed by performing the experiments on sialidase from *M. viridifaciens* whose TS structure resembles the already solved TS structure for *V. cholerae* sialidase. The developed technique will be then applied to solve the TS structure for influenza and human sialidases. The author of this thesis synthesized a panel of six singly and doubly labeled α-sialyl- (2$\rightarrow$6)-β-1-thiophenyllactosides (**7a-f**, Figure 4.3) which are natural substrate analogues of sialidases, and performed the kinetic isotope effect measurements using both one dimensional (1D, ^{13}C) and two dimensional (2D, HETCOR and HSQC) NMR spectroscopic methods. The results of the KIEs measurements using 1D NMR spectroscopy are presented; however, the two dimensional (2D, HETCOR and HSQC) technique is still under investigation even though the preliminarily 2D experiments are very promising and are also presented in this chapter.

Chapter 5. This chapter presents discussion and future work related to this thesis.

1.7 References

[1] Lindhorst, T. K. *Essentials of Carbohydrate Chemistry and Biochemistry*; 3rd ed.; WILLEY-VCH, 2007.

[2] Cao, H.; Hwang, J.; Chen, X. In *Opportunity, Challenge and Scope of Natural Products in Medicinal Chemistry*; Research Signpost: 2011, p 411.

[3] Girard-Egrot, A.; Blum, L.; Richter, R.; Brisson, A. In *Nanoscience: Nanobiotechnology and Nanobiology*; Patrick Boisseau, P. H., Marcel Lahmani, Ed. 2010, p 30.

[4] Traving, C.; Schauer, R. *Cell Mol Life Sci* **1998**, *54*, 1330.

[5] Blix, F. G.; Gottschalk, A.; Klenk, E. *Nature* **1957**, *179*, 1088.

[6] Chen, X.; Varki, A. *ACS Chem Biol* **2010**, *5*, 163.

[7] Varki, A. *Glycobiology* **1992**, *2*, 25.

[8] Rosenberg, A.; Schengrund, C. L. In *Biological Roles of Sialic Acid*; Rosenberg, A., Schengrundand, C. L., Eds.; Plenum Press: New York, 1976, p 294.

[9] Schauer, R.; Kelm, S.; Reuter, G.; Roggentin, P.; Shaw, L. In *Biology of the Sialic Acids*; Rosenberg, A., Ed.; Plenium Press: New York, 1995, p 7.

[10] Varki, A. *Proc Natl Acad Sci U S A* **2010**, *107 Suppl 2*, 8939.

[11] Inoue, S.; Kitajima, K. *Glycoconj J* **2006**, *23*, 277.

[12] Angata, T.; Varki, A. *Chem Rev* **2002**, *102*, 439.

[13] Wieser, R. J.; Baumann, C. E.; Oesch, F. *Glycoconj J* **1995**, *12*, 672.

[14] Troy, F. A. In *Biology of the Sialic Acids* Rosenberg, A., Ed.; Plenum Press: New York, 1995, p 95.

[15] Thomas, P. *Cancer J* **1996**, *9*, 32.

[16] Fernandes, A. I.; Gregoriadis, G. *Int J Pharm* **2001**, *217*, 215.

[17] Egrie, J. C.; Browne, J. K. *Br J Cancer* **2001**, *84 Suppl 1*, 3.

[18] Byrne, B.; Donohoe, G. G.; O'Kennedy, R. *Drug Discov Today* **2007**, *12*, 319.

[19] Paulson, J. C.; Rogers, G. N.; Carroll, S. M.; Higa, H. H.; Pritchett, T.; Milks, G.; Sabesan, S. *Pure Appl Chem* **1984**, *56*, 797.

[20] Abbott, D. W.; Macauley, M. S.; Vocadlo, D. J.; Boraston, A. B. *J Biol Chem* **2009**, *284*, 11676.

[21] Yuzwa, S. A.; Macauley, M. S.; Heinonen, J. E.; Shan, X.; Dennis, R. J.; He, Y.; Whitworth, G. E.; Stubbs, K. A.; McEachern, E. J.; Davies, G. J.; Vocadlo, D. J. *Nat Chem Biol* **2008**, *4*, 483.

[22] Thomason, R.; Itzstein, M. V. In *Antiviral Drugs: From Basic Discovery Through Clinical Trials.*; Kazmierski, W. M., Ed.; John Wiley & Sons, Inc. : Hoboken, New Jersey (published simultaneously in Canada), 2011, p 385.

[23] Koshland, D. E. *Biol Rev* **1953**, *28*, 416.

[24] Rouvinen, J.; Bergfors, T.; Teeri, T.; Knowles, J. K.; Jones, T. A. *Science* **1990**, *249*, 380.

[25] Spezio, M.; Wilson, D. B.; Karplus, P. A. *Biochemistry* **1993**, *32*, 9906.

[26] Aleshin, A. E.; Firsov, L. M.; Honzatko, R. B. *J Biol Chem* **1994**, *269*, 15631.

[27] Aleshin, A. E.; Hoffman, C.; Firsov, L. M.; Honzatko, R. B. *J Mol Biol* **1994**, *238*, 575.

[28] Piszkiewicz, D.; Bruice, T. C. *J Am Chem Soc* **1968**, *90*, 2156.

[29] Rye, C. S.; Withers, S. G. *Curr Opin Chem Biol* **2000**, *4*, 573.

[30] Yip, V. L.; Withers, S. G. *Biochemistry* **2006**, *45*, 571.

[31] Yip, V. L.; Thompson, J.; Withers, S. G. *Biochemistry* **2007**, *46*, 9840.

[32] Yip, V. L.; Varrot, A.; Davies, G. J.; Rajan, S. S.; Yang, X.; Thompson, J.; Anderson, W. F.; Withers, S. G. *J Am Chem Soc* **2004**, *126*, 8354.

[33] Chakladar, S.; Cheng, L.; Choi, M.; Liu, J.; Bennet, A. J. *Biochemistry* **2011**, *50*, 4298.

[34] Yip, V. L.; Withers, S. G. *Org Biomol Chem* **2004**, *2*, 2707.

[35] Hirst, G. K. *Science* **1941**, *94*, 22.

[36] Gottschalk, A. *Biochim Biophys Acta* **1957**, *23*, 645.

[37] Monti, E.; Preti, A.; Venerando, B.; Borsani, G. *Neurochem Res* **2002**, *27*, 649.

[38] Albohy, A.; Li, M. D.; Zheng, R. B.; Zou, C.; Cairo, C. W. *Glycobiology* **2010**, *20*, 1127.

[39] Gaskell, A.; Crennell, S.; Taylor, G. *Structure* **1995**, *3*, 1197.

[40] Vimr, E.; Lichtensteiger, C. *Trends Microbiol* **2002**, *10*, 254.

[41] Tong, H. H.; Blue, L. E.; James, M. A.; DeMaria, T. F. *Infect Immun* **2000**, *68*,

921.

[42] Manco, S.; Hernon, F.; Yesilkaya, H.; Paton, J. C.; Andrew, P. W.; Kadioglu, A. *Infect Immun* **2006**, *74*, 4014.

[43] *http://wwwwhoint/mediacentre/factsheets/fs211/en/* **2009**.

[44] Garman, E.; Laver, G. In *Viral Membrane Proteins: Structure, Function, and Drug Design*; Fischer, W., B, Ed.; Springer US: New York, 2005; Vol. 1, p 247.

[45] Colman, P. M.; Varghese, J. N.; Laver, W. G. *Nature* **1983**, *303*, 41.

[46] Varghese, J. N.; Laver, W. G.; Colman, P. M. *Nature* **1983**, *303*, 35.

[47] Russell, R. J.; Haire, L. F.; Stevens, D. J.; Collins, P. J.; Lin, Y. P.; Blackburn, G. M.; Hay, A. J.; Gamblin, S. J.; Skehel, J. J. *Nature* **2006**, *443*, 45.

[48] Watts, A. G.; Damager, I.; Amaya, M. L.; Buschiazzo, A.; Alzari, P.; Frasch, A. C.; Withers, S. G. *J Am Chem Soc* **2003**, *125*, 7532.

[49] Wicki, J.; Rose, D. R.; Withers, S. G. *Methods Enzymol* **2002**, *354*, 84.

[50] Zechel, D. L.; Withers, S. G. *Acc Chem Res* **2000**, *33*, 11.

[51] Watson, J. N.; Dookhun, V.; Borgford, T. J.; Bennet, A. J. *Biochemistry* **2003**, *42*, 12682.

[52] Watson, J. N.; Newstead, S.; Narine, A. A.; Taylor, G.; Bennet, A. J. *Chembiochem* **2005**, *6*, 1999.

[53] Newstead, S.; Watson, J. N.; Knoll, T. L.; Bennet, A. J.; Taylor, G. *Biochemistry* **2005**, *44*, 9117.

[54] Fersht, A. *Enzyme Structure and Mechanism*; W. H. Freeman and Company: New York, 1985.

[55] Anslyn, E. V.; Dougherty, D. A. In *Modern Physical Organic Chemistry*; Murdzek, J., Ed.; University Science Books: United State of America, 2006, p 489.

[56] Williams, A. In *The Chemistry of Enzyme Action*; Page, M. I., Ed.; Elsevier Science Publishers B. V: New York, 1984.

[57] Guo, X.; Sinnott, M. L. *Biochem J* **1993**, *294 (Pt 3)*, 653.

[58] Ashwell, M.; Xumin, G.; Sinnott, M. L. *J Am Chem Soc* **1992**, *114*, 10158.

[59] Kraut, J. *Science* **1988**, *242*, 533.

[60] Kurz, J. L. *J Am Chem Soc* **1963**, *85*, 987.

[61] Wolfenden, R. *Nature* **1969**, *223*, 704.

[62] Lienhard, G. E. *Science* **1973**, *180*, 149.

[63] Mader, M. M.; Bartlett, P. A. *Chem Rev* **1997**, *97*, 1281.

[64] Westerik, J. O.; Wolfenden, R. *J Biol Chem* **1972**, *247*, 8195.

[65] Thompson, R. C. *Biochemistry* **1973**, *12*, 47.

[66] Bartlett, P. A.; Marlowe, C. K. *Biochemistry* **1983**, *22*, 4618.

[67] Hanson, J. E.; Kaplan, A. P.; Bartlett, P. A. *Biochemistry* **1989**, *28*, 6294.

[68] Bartlett, P. A. G., Mark A. *J Org Chem* **1996**, *61*, 3433.

[69] Whitworth, G. E.; Macauley, M. S.; Stubbs, K. A.; Dennis, R. J.; Taylor, E. J.; Davies, G. J.; Greig, I. R.; Vocadlo, D. J. *J Am Chem Soc* **2007**, *129*, 635.

[70] Frey, P. A.; Hegeman, A. D. In *Enzymatic Reaction Mechanisms*; Oxford University Press, Inc: New York, 2007, p 91.

[71] Anslyn, E. V.; Dougherty, D. A. In *Modern Physical Organic Chemistry*; University Science Books: Sausalito, 2006, p 421.

[72] Sinnott, M. L.; Souchard, I. J. *Biochem J* **1973**, *133*, 89.

2 Brønsted Analysis of an Enzyme-Catalyzed Pseudo-Deglycosylation Reaction: Mechanism of Desialylation in Sialidases†

† Funded by the Natural Science and Engineering Research Council of Canada

Fahimeh S. Shidmoossavee[a], *Lydia Cheng*[b], *Jacqueline N. Watson*[b] *And Andrew J. Bennet*[a]

[a]Departments of Chemistry, Simon Fraser University, 8888 University Drive, Burnaby, British Columbia, V5A 1S6, Canada
[b]Departments of Molecular Biology and Biochemistry, Simon Fraser University, 8888 University Drive, Burnaby, British Columbia, V5A 1S6, Canada

This Chapter comprises the manuscript ″Brønsted Analysis of an Enzyme-Catalyzed Pseudo-Deglycosylation Reaction: Mechanism of Desialylation in Sialidases″ which was published in Biochemistry (2010, *30*, 6473-6484).

Authors Contributions:

This project was designed by Prof. Andrew J. Bennet and the author of this thesis performed all the experimental synthetic work of the compounds and the kinetic measurements. Dr. Jacqueline N. Watson cloned the genes and Lydia Cheng expressed the proteins.

2.1 Abstract

The *Micromonospora viridifaciens* Y370G inverting mutant sialidase has been found to possess β-sialidase activity with various fluoro-substituted phenyl β-sialosides. A reagent panel of seven mono- and di-fluorophenyl β-D-sialosides was synthesized and these compounds were used, in conjunction with the parent phenyl β-D-sialoside, to probe the mechanism of *M. viridifaciens* Y370G mutant sialidase-catalyzed hydrolyses. These hydrolysis reactions mimic the deglycosylation reaction step of the crucial tyrosinyl enzyme-bound intermediate that is formed during the corresponding wild-type sialidase reactions. The derived Brønsted parameter (β_{lg}) on k_{cat}/K_m is –0.46 ± 0.02 for the four substrates that display significant activity, and these span a range of leaving group abilities (as judged by the pK_a of their conjugate acids being between 7.09 and 9.87). The 4-fluoro, 2,3- and 2,5-difluorosubstrates display a diminished activity, whereas, the 3,5-difluoro compound undergoes catalyzed hydrolysis exceedingly slowly. These observations, taken with solvent deuterium kinetic isotope effects (k_{H_2O}/k_{D_2O}) on the catalyzed hydrolysis of the 2-fluorophenyl substrate of 0.88 ± 0.24 (k_{cat}/K_m) and 1.16 ± 0.12 (k_{cat}) and the poor inhibition shown by phenol (IC_{50} > 1 mM) are consistent with glycosidic C–O cleavage being rate determining for both k_{cat}/K_m and k_{cat} with little or no protonation of the departing aryloxide leaving group. The kinetic data reported herein are consistent with rate-limiting glycoside hydrolysis occurring via two distinct transition states that incorporates a nonproductive binding component for the tighter binding substrates.

2.2 Introduction

Glycosyl transferring enzymes are found ubiquitously in all kingdoms of life and

moreover around 1-3% of the proteins encoded by a typical genome possess such activity[1]. Glycosyl hydrolases (glycosidases) can be initially sub-divided into two families: those in which the product of hydrolysis has either the same (retaining) or the opposite (inverting) configuration at the anomeric center[2]. With regard to retaining glycosidases, three different mechanisms of action have been reported, and these involve: (i) NAD^+ dependent oxidation-elimination[3]; (ii) intramolecular neighboring group assisted catalysis from an acetamido group[4]; and (iii) nucleophilic catalysis from an enzyme active site residue[2]. For the latter mechanism the nucleophile is normally either a glutamate or an aspartate residue[5]. However, the *exo*-sialidases[6,7] and *trans*-sialidases[8,9] use a tyrosine residue as the nucleophile during transfer of a sialic acid moiety from an α-sialoside onto either a water molecule or a carbohydrate acceptor, respectively. Scheme 2.1 shows the mechanism by which these two classes of enzymes catalyze the transfer reaction via a covalently linked α-sialosyl tyrosine intermediate (α-NeuAc-OTyr), a species that is subsequently attacked by an incoming ROH molecule to give the product, αNeuAc-OR (ROH being water for the hydrolases)[6,7,10].

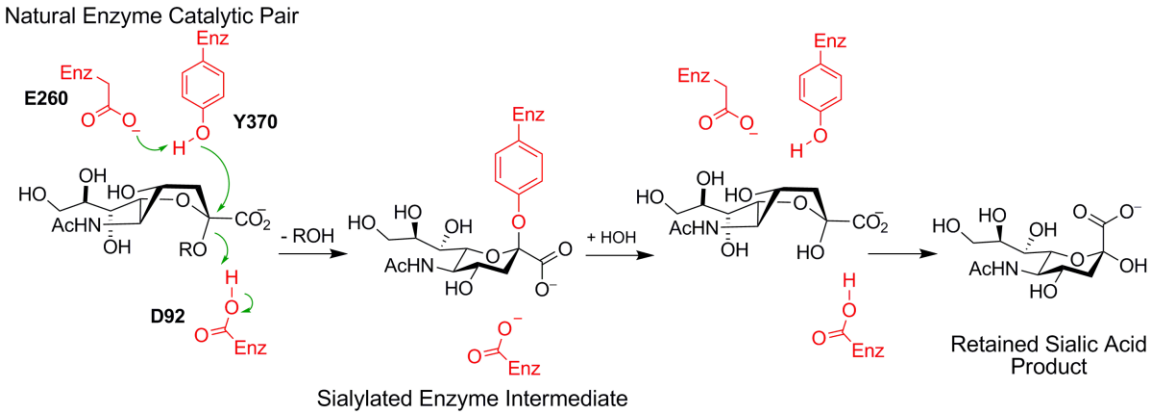

Scheme 2.1. Mechanism of wild-type sialidase-catalyzed hydrolysis of α-sialosides

Many of the traditional tools developed by physical organic chemists[11] have been adapted for use in probing the mechanisms of enzyme-catalyzed reactions[12]. One

of the more commonly used protocols for glycosidases, and many other enzyme families, involves measuring the changes in the enzymatic rate constants as the leaving group ability of the aglycone is varied. Usually, such experiments involve making a series of aryl glycosides and plotting the logarithm of the measured rate constant against the pK_a of the conjugate acid of the leaving group; the slope of such a graph (Brønsted parameter: β_{lg}) can give mechanistic information on the enzymatic glycosylation step. The complementary protocol that involves measuring rate constant changes as the nucleophilicity of the attacking group (Swain-Scott parameter *n*) is varied, an approach that has been used in physical organic studies on glycoside hydrolyses in solution as a means to probe for concerted (S_N2, A_ND_N)[13] or sequential (S_N1; D_N * A_N)[14] reactions, cannot be used for those enzyme-catalyzed reactions where the nucleophile is an enzymatic active site residue because of the limited number of substitutions that are possible with the current technology. A recent report detailed an in-depth study on a glycosidase that operates by the substrate-assisted mechanism, in this case the intramolecular acetamido group's nucleophilicity was attenuated by the incorporation of fluorine atoms [15]

In theory, a second Brønsted-type analysis is possible for the deglycosylation reaction if one could vary the leaving group ability of the enzymatic nucleophile, however, to date this approach has not been possible due to the same factors mentioned above for varying the nucleophilicity of an enzymatic group to probe the mechanism of the glycosylation reaction. Previously, it has been reported that mutation of the active site nucleophilic tyrosine in the *M. viridifaciens* sialidase to small amino acid residues, such as glycine, aspartic acid, and serine, causes a change in mechanism from one that occurs with retention of configuration to one where the first-formed product has an inverted anomeric center[6,16,17]. The Y370G mutant *M. viridifaciens* sialidase has

been shown to be able to hydrolyze the non-natural phenyl β-D-sialoside[18], a reaction in which the Michaelis complex mimics the enzymatic tyrosinyl-bound intermediate that is formed in wild-type sialidase-catalyzed reactions (Scheme 2.2).

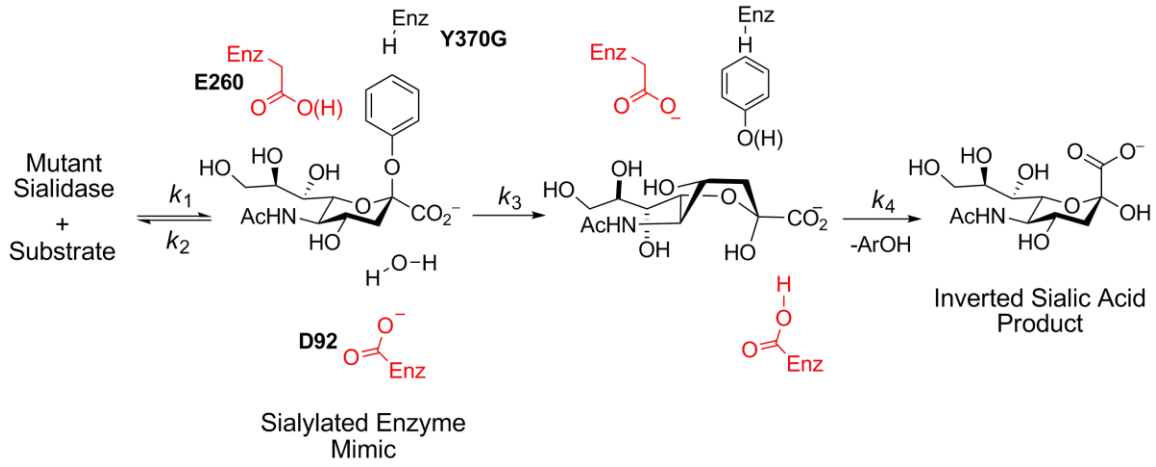

Scheme 2.2. Proposed mechanism of Y370G mutant sialidase-catalyzed hydrolysis of aryl β-sialosides.

The present study details a Brønsted-type mechanistic investigation into the Y370G mutant enzyme-catalyzed hydrolysis of fluoro-substituted aryl β-sialosides (**1a–h**, Figure 2.1), a reaction that mimics deglycosylation of the wild-type sialidase tyrosinyl enzyme intermediate.

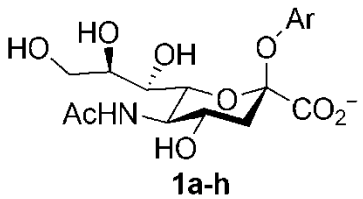

1a-h

Ar = phenyl (**1a**), 2-fluorophenyl (**1b**), 3-fluorophenyl (**1c**), 4-fluorophenyl (**1d**), 2,3-difluorophenyl (**1e**), 2,5-difluorophenyl (**1f**), 2,6-difluorophenyl (**1g**), 3,5-difluorophenyl (**1h**)

Figure 2.1. Synthesized fluoro-substituted aryl β-sialosides (**1a–h**).

2.3 Materials and Methods

Materials. All chemicals were of analytical grade or better and were purchased from Sigma-Aldrich unless noted otherwise.

2.3.1 Substrate Synthesis

Ph-βNeuAc[1] and fully protected β-sialosyl fluoride **4** were made according to literature procedures[19,20]. NMR spectra were acquired on either a Bruker 600 MHz or 400 MHz spectrometer. Chemical shifts are reported in parts per million downfield from the signal for TMS. The residual signal from deuterated chloroform and that from external TMS-salt (D_2O) were used as ^1H NMR references; for ^{13}C NMR spectra, natural abundance signals from $CDCl_3$ and external TMS-salt (D_2O) were used as references. Coupling constants (*J*) are given in hertz. Melting points were determined on a Gallenkamp melting-point apparatus and are not corrected. Optical rotations were measured on a Perkin-Elmer 341 polarimeter and are reported in units of deg cm^2 g^{-1} (concentrations reported in units of g per 100 mL).

Methyl [2-fluorophenyl (5-acetamido-4,7,8,9-tetra-*O*-acetyl-3,5-dideoxy-D-*glycero*-*β*-D-*galacto*-non-2-ulopyranosyl)]onate (2b)

To activated 3 Å molecular sieves (5 g) was added peracetylated sialosyl fluoride **4** (400 mg, 0.81 mmol), and the mixture was dried under vacuum for 30 min. To this

[1]**Abbreviations:** 23DFP-βNeuAc, 2,3-difluorophenyl β-D-*N*-acetylneuraminide; 25DFP-βNeuAc, 2,5-difluorophenyl β-D-*N*-acetylneuraminide; 26DFP-βNeuAc, 2,6-difluorophenyl β-D-*N*-acetylneuraminide; 35DFP-βNeuAc, 3,5-difluorophenyl β-D-*N*-acetylneuraminide; 2FP-βNeuAc, 2-fluorophenyl β-D-*N*-acetylneuraminide; 3FP-βNeuAc, 3-fluorophenyl β-D-*N*-acetylneuraminide; 4FP-βNeuAc, 4-fluorophenyl β-D-*N*-acetylneuraminide; KIE, kinetic isotope effect; MvNA, *Micromonospora viridifaciens* neuraminidase; Neu2en5Ac, 5-Acetamido-2,6-anhydro-3,5-dideoxy-D-*glycero*-D-*galacto*-non-2-enonic acid; Neu5Ac, *N*-acetylneuraminic acid; Ph-βNeuAc, phenyl β-D-*N*-acetylneuraminide; pNP-αNeuAc, *p*-nitrophenyl α-D-*N*-acetylneuraminide.

mixture a solution of 2-fluorophenol (482 mg, 4.30 mmol) in dry CH_2Cl_2 (30 ml) was added under a N_2 atmosphere, and the resultant mixture was then stirred for 1 h. Following which a solution of $BF_3.OEt_2$ (0.7 ml, 5.8 mmol) in CH_2Cl_2 (4 ml) was added and the resultant mixture was stirred overnight under a N_2 atmosphere at room temperature. The resultant mixture was filtered through celite, and washed thoroughly with CH_2Cl_2. The combined filtrates were washed with saturated $NaHCO_3$ (150 ml), water (150 ml) and brine (150 ml), and the resulting solution was dried over anhydrous Na_2SO_4. After evaporating the solvent under reduced pressure, a yellow syrup was obtained, which crystallized from diethyl ether to give a white powder (187 mg, 40% yield). mp 167−168 °C; $[\alpha]^{20}_D$ = −57.6 (0.17, CH_2Cl_2); ^{1}H NMR (600 MHz, $CDCl_3$) δ: 1.79, 1.87, 2.02, 2.02, 2.13 (5 × s, 15 H, CH_3), 2.02 (m, H-3a), 2.71 (dd, 1 H, $J_{3e,3a}$ = 13.0, $J_{3e,4}$ = 5.0, H-3e), 3.70 (s, 3 H, OCH_3), 4.10 (dd, 1 H, $J_{9a,9b}$ = 12.4, $J_{9a,8}$ = 6.6, H-9a), 4.14 (dd, 1 H, $J_{6,5}$ = 10.7, $J_{6,7}$ = 2.3, H-6), 4.22 (q, 1 H, $J_{5,4}$ + $J_{5,6}$ + $J_{5,NH}$ = 31.1, H-5), 4.61 (dd, 1 H, $J_{9b,9a}$ = 12.5, $J_{9b,8}$ = 2.3, H-9b), 4.92 (m, 1 H, H-8), 5.27 (d, 1 H, $J_{NH,5}$ = 10.5, NH), 5.36 (dd, 1 H, $J_{7,8}$ = 4.8, $J_{6,7}$ = 2.3, H-7), 5.45 (td, 1 H, $J_{4,3a}$ = $J_{4,5}$ = 11.1, $J_{3e,4}$ = 4.9, H-4), 6.91−7.01 (m, 3 H, H-4', H-5', H-6'), 7.08 (m, 1 H, H-3'). ^{13}C NMR (150 MHz, $CDCl_3$) δ: 20.80, 20.82 (2C), 20.90, 23.21 (5 × C, CH_3), 37.97 (C-3), 49.21 (C-5), 53.22 (OCH_3), 62.09 (C-9), 67.92 (C-7), 68.42 (C-4), 71.67 (C-8), 72.72 (C-6), 100.02 (C-2), 116.85 (d, $J_{C,F}$ = 18.5, C-3'), 118.47 (C-5'), 124.02 (d, $J_{C,F}$ = 7.0, C-4'), 124.54 (d, $J_{C,F}$ = 3.9, C-6'), 141.65 (d, $J_{C,F}$ = 10.7, C-1'), 152.99 (d, $J_{C,F}$ = 247.4, C-2'), 166.85 (C-1), 170.07, 170.34, 170.45, 170.53, 170.99 (5 × C=O). Anal Calcd for $C_{26}H_{32}FNO_{13}$: C, 53.33; H, 5.51; N, 2.39. Found: C, 53.06; H, 5.45; N, 2.22.

Methyl [3-fluorophenyl (5-acetamido-4,7,8,9-tetra-*O*-acetyl-3,5-dideoxy-D-*glycero*-*β*-D-*galacto*-non-2-ulopyranosyl)]onate (2c)

A mixture of activated 3 Å molecular sieves (5 g) and peracetylated sialosyl

fluoride **4** (400 mg, 0.81 mmol) was dried under vacuum for 30 min. To the resultant solid 3-fluorophenol (482 mg, 4.30 mmol) and dry CH_2Cl_2 (30 ml) were added under a N_2 atmosphere, and the mixture was then stirred for 1 h at rt. Then, $BF_3.OEt_2$ (0.7 ml, 5.80 mmol) in CH_2Cl_2 (4 ml) was added and the mixture was stirred overnight under a N_2 atmosphere at room temperature. The resultant mixture was filtered through celite, and washed thoroughly with CH_2Cl_2. The combined filtrates were washed with saturated $NaHCO_3$ (150 ml), water (150 ml) and brine (150 ml), and the resulting solution was dried over anhydrous Na_2SO_4. After evaporating the solvent under reduced pressure, a yellow syrup was obtained, which crystallized from diethyl ether to give a white powder (280 mg, 60% yield). mp 194−195 °C; $[\alpha]^{20}_D$ = −38.5 (0.12, CH_2Cl_2); ^{1}H NMR (600 MHz, $CDCl_3$) δ: 1.77, 1.87, 2.03 , 2.04, 2.14 (5 × s, 15 H, CH_3), 1.98 (t, 1 H, $J_{3a,3e} = J_{3a,4}$ = 11.7, H-3a), 2.62 (dd, 1 H, $J_{3e,3a}$ = 13.0, $J_{3e,4}$ = 5.0, H-3e), 3.73 (s, 3 H, OCH_3), 4.04 (dd, 1 H, $J_{6,5}$ = 10.7, $J_{6,7}$ = 2.4, H-6), 4.12 (dd, 1 H, $J_{9a,9b}$ = 12.5, $J_{9a,8}$ = 6.6, H-9a), 4.20 (q, 1 H, $J_{5,4} + J_{5,6} + J_{5,NH}$ = 31.4, H-5), 4.66 (dd, 1 H, $J_{9b,9a}$ = 12.6, $J_{9b,8}$ = 2.4, H-9b), 4.90 (m, H-8), 5.23 (d, 1 H, $J_{NH,5}$ = 10.2, NH), 5.34 (dd, 1 H, $J_{7,8}$ = 4.6, $J_{6,7}$ = 2.3, H-7), 5.44 (td, 1 H, $J_{4,3a} = J_{4,5}$ =11.1, $J_{4,3e}$ = 4.9, H-4), 6.66−6.77 (m, 3 H, H-2', H-4', H-6'), 7.18 (m, 1 H, H-5'). ^{13}C NMR (150 MHz, $CDCl_3$) δ: 20.66, 20.70, 20.76, 20.87, 23.17 (5 × C, CH_3), 38.44 (C-3), 49.16 (C-5), 53.28 (OCH_3), 62.01 (C-9), 67.93 (C-7), 68.30 (C-4), 71.88 (C-8), 72.59 (C-6), 99.22 (C-2), 104.50 (d, $J_{C,F}$ = 25.4, C-2'), 109.99 (d, $J_{C,F}$ = 21.1, C-4'), 112.34 (d, $J_{C,F}$ = 2.9, C-6'), 130.79 (d, $J_{C,F}$ = 9.8, C-5'), 154.90 (d, $J_{C,F}$ = 10.8, C-1'), 163.16 (d, $J_{C,F}$ = 247.7, C-3''), 167.00 (C-1), 170.07, 170.23, 170.45, 170.65, 171.98 (5 × C=O). Anal Calcd for $C_{26}H_{32}FNO_{13}$: C, 53.33; H, 5.51; N, 2.39. Found: C, 53.26; H, 5.66; N, 2.17.

Methyl [4-fluorophenyl (5-acetamido-4,7,8,9-tetra-*O*-acetyl-3,5-dideoxy-D-*glycero*-*β*-D-*galacto*-non-2-ulopyranosyl)]onate (2d)

To activated 3 Å molecular sieves (5 g) was added peracetylated sialosyl fluoride **4** (400 mg, 0.81 mmol), and the mixture was dried under vacuum for 30 min. To the resultant mixture was added 4-fluorophenol (482 mg, 4.3 mmol) and dry CH_2Cl_2 (30 ml) under N_2 atmosphere, and the mixture was then stirred for 1 hour. Then, $BF_3.OEt_2$ (0.7 ml, 5.8 mmol) in CH_2Cl_2 (4 ml) was added and the mixture was stirred overnight under N_2 atmosphere at room temperature. The resultant mixture was filtered through celite, and washed thoroughly with CH_2Cl_2. The combined filtrates were washed with saturated $NaHCO_3$ (150 ml), water (150 ml) and brine (150 ml), and the resulting solution was dried over anhydrous Na_2SO_4. After evaporating the solvent under reduced pressure, a yellow syrup was obtained, which crystallized from diethyl ether to give a white powder (234 mg , 50% yield). mp 202-203 °C; $[\alpha]^{20}_D$ = –45.2 (0.22, CH_2Cl_2); ^{1}H NMR (600 MHz, $CDCl_3$) δ: 1.77, 1.87, 1.96, 2.03, 2.14 (5 × s, 15 H, CH_3), 1.96 (dd, 1 H, $J_{3a,3e}$ = 13.0, $J_{3a,4}$ = 11.5, H-3a), 2.63 (dd, 1 H, $J_{3e,3a}$ = 13.0, $J_{3e,4}$ = 4.9, H-3e), 3.68 (s, 3 H, OCH_3), 4.08 (dd, 1 H, $J_{6,5}$ = 10.7, $J_{6,7}$ = 2.3, H-6), 4.12 (dd, 1 H, $J_{9a,9b}$ = 12.6, $J_{9a,8}$ = 6.4, H-9a), 4.18 (q, 1 H, $J_{5,4}$ + $J_{5,6}$ + $J_{5,NH}$ = 31.1, H-5), 4.62 (dd, 1 H, $J_{9b,9a}$ = 12.5, $J_{9b,8}$ = 2.4, H-9b), 4.94 (ddd, 1 H, $J_{8,9a}$ = 6.4, $J_{8,7}$ = 5.0, $J_{8,9b}$ = 2.4, H-8), 5.22 (d, 1 H, $J_{NH,5}$ = 10.1, NH), 5.36 (dd, 1 H, $J_{7,8}$ = 5.0, $J_{6,7}$ = 2.3, H-7), 5.45 (m, 1 H, H-4), 6.85 (m, 2 H, H-2', H-6'), 6.87 (m, 2 H, H-3', H-5'). ^{13}C NMR (150 MHz, $CDCl_3$) δ: 20.94, 21.00, 21.01, 21.12, 23.43 (5 × C, CH_3), 38.67 (C-3), 49.49 (C-5), 53.37 (OCH_3), 62.15 (C-9), 68.10 (C-7), 68.61 (C-4), 71.80 (C-8), 72.51 (C-6), 99.63 (C-2), 116.49 (d, $J_{C,F}$ = 22.9, C-3', C-5'), 118.40 (d, $J_{C,F}$ = 8.2, C-2', C-6'), 150.14 (s, C-1'), 158.66 (d, $J_{C,F}$ = 242.1, C-4') 167.30 (C-1), 170.27, 170.45, 170.71, 171.23 (5 × C=O). Anal Calcd for $C_{26}H_{32}FNO_{13}$: C, 53.33; H, 5.51; N, 2.39. Found: C, 53.09; H, 5.49; N, 2.24.

Methyl [2,5-difluorophenyl (5-acetamido-4,7,8,9-tetra-*O*-acetyl-3,5-dideoxy-D-*glycero*-*β*-D-*galacto*-non-2-ulopyranosyl)]onate (2f)

To activated 3 Å molecular sieves (5 g) was added peracetylated sialosyl fluoride **4** (400 mg, 0.81 mmol), and the resulting solid mixture was dried under vacuum for 30 min. To this mixture was a solution of 2,5-difluorophenol (482 mg, 4.30 mmol) in dry CH_2Cl_2 (30 ml) was added under a N_2 atmosphere, and the mixture was then stirred for 1 h. Then, $BF_3{\cdot}OEt_2$ (0.7 ml, 5.8 mmol) in CH_2Cl_2 (4 ml) was added and the mixture was stirred overnight under a N_2 atmosphere at room temperature. The resultant mixture was filtered through celite, and washed thoroughly with CH_2Cl_2. The combined filtrates were washed with saturated $NaHCO_3$ (150 ml), water (150 ml) and brine (150 ml), and this solution was dried over anhydrous Na_2SO_4. After evaporating the solvent under reduced pressure, a yellow syrup was obtained, which crystallized from diethyl ether to give a white powder (157 mg , 33% yield). mp 167–168 °C; $[\alpha]^{20}_D$ = –44.0 (0.10, CH_2Cl_2); ^{1}H NMR (600 MHz, $CDCl_3$) δ: 1.86, 1.92, 2.02, 2.03, 2.14 (5 × s, 15 H, CH_3), 2.03 (dd, 1 H, $J_{3a,3e}$ = 13.1, $J_{3a,4}$ = 11.5, H-3a), 2.71 (dd, 1 H, $J_{3e,3a}$ = 13.3, $J_{3e,4}$ = 5.0, H-3e), 3.77 (s, 3 H, OCH_3), 4.07 (m, 2 H, H-6 and H-9a), 4.24 (q, 1 H, $J_{5,4}$ + $J_{5,6}$ + $J_{5,NH}$ = 31.3, H-5), 4.67 (dd, 1 H, $J_{9b,9a}$ = 12.5, $J_{9b,8}$ = 2.3, H-9b), 4.84 (m, 1 H, H-8), 5.31 (d, 1 H, $J_{NH,5}$ = 10.3, NH), 5.32 (dd, 1 H, $J_{7,8}$ = 6.1, $J_{6,7}$ = 2.5, H-7), 5.45 (td, 1 H, $J_{4,3e}$ = 5.0, $J_{4,3a}$ = $J_{4,5}$ = 11.3, H-4), 6.70 (m, 1 H, H-4'), 6.77 (m, 1 H, H-6'), 7.06 (m, 1 H, H-3'). ^{13}C NMR (150 MHz, $CDCl_3$) δ: 21.08, 21.17, 21.20, 21.27, 23.55 (5 × C, CH_3), 38.29 (C-3), 49.46 (C-5), 53.87 (OCH_3), 62.36 (C-9), 68.55 (C-7), 68.70 (C-4), 72.87 (C-8), 73.81 (C-6), 100.47 (C-2), 106.45 (d, $J_{C,F}$ = 25.1, C-6'), 110.10 (dd, $J_{C,F}$ = 24.4 and 7.1, C-4'), 117.50 (dd, $J_{C,F}$ = 21.1, $J_{C,F}$ = 9.8, C-3'), 142.24 (m, C-1'), 149.65 (dd, $J_{C,F}$ = 243.9 and 3.2, C-2'), 158.45 (dd, $J_{C,F}$ = 244.3 and 2.3, C-5'), 166.91 (C-1), 170.53, 170.76, 171.14, 171.16, 171.35 (5

× C=O). Anal Calcd for $C_{26}H_{31}F_2NO_{13}$: C, 51.74; H, 5.18; N, 2.32. Found: C, 51.56; H, 5.13; N, 2.09.

Methyl [3,5-difluorophenyl (5-acetamido-4,7,8,9-tetra-*O*-acetyl-3,5-dideoxy-D-*glycero*-*β*-D-*galacto*-non-2-ulopyranosyl)]onate (2h)

To activated 3 Å molecular sieves (5 g) was added peracetylated sialosyl fluoride **4** (400 mg, 0.81 mmol), and the mixture was dried under vacuum for 30 min. To the resulting mixture 3,5-difluorophenol (560 mg, 4.30 mmol) and dry CH_2Cl_2 (30 ml) were added under a N_2 atmosphere, and the mixture was then stirred for 1 h. Subsequently a solution of $BF_3.OEt_2$ (0.7 ml, 5.81 mmol) in CH_2Cl_2 (4 ml) was added and the mixture was stirred overnight under N_2 atmosphere at room temperature. The resultant mixture was filtered through celite, and washed thoroughly with CH_2Cl_2. The combined filtrates were washed with saturated $NaHCO_3$ (150 ml), water (150 ml) and brine (150 ml), and the resulting solution was dried over anhydrous Na_2SO_4. After removal of the solvent under reduced pressure, a yellow syrup was obtained and this material was crystallized from diethyl ether to give a white powder (241 mg, 50% yield). mp 196–197 °C; $[\alpha]^{20}_D$ = –44.2 (0.13, CH_2Cl_2); ^{1}H NMR (600 MHz, $CDCl_3$) δ: 1.87, 1.88, 2.03, 2.04, 2.14 (5 × s, 15 H, CH_3), 1.98 (dd, 1 H, $J_{3a,3e}$ = 13.0, $J_{3a,4}$ = 11.5, H-3a), 2.62 (dd, 1H, $J_{3e,3a}$ = 13.1, $J_{3e,4}$ = 5.0, H-3e), 3.76 (s, 3 H, OCH_3), 4.02 (dd, 1 H, $J_{6,5}$ = 10.6, $J_{6,7}$ = 2.4, H-6), 4.10 (dd, 1 H, $J_{9a,9b}$ = 12.5, $J_{9a,8}$ = 7.3, H-9a), 4.20 (q, 1 H, $J_{5,4}$ + $J_{5,6}$ + $J_{5,NH}$ = 31.4, H-5), 4.69 (dd, 1 H, $J_{9b,9a}$ = 12.6, $J_{9b,8}$ = 2.3, H-9b), 4.88 (m, 1 H, H-8), 5.24 (d, 1 H, $J_{NH,5}$ = 10.2, NH), 5.33 (dd, 1 H, $J_{7,8}$ = 3.6, $J_{6,7}$ = 2.4, H-7), 5.39 (td, 1 H, $J_{4,3a}$ = $J_{4,5}$ = 11.2, $J_{4,3e}$ = 4.9, H-4), 6.48–6.56 (m, 3 H, Ar-H). ^{13}C NMR (150 MHz, $CDCl_3$) δ: 20.87, 20.93, 20.97, 21.08, 23.39 (5 × C, CH_3), 38.54 (C-3), 49.31 (C-5), 53.70 (OCH_3), 62.43 (C-9), 68.27 (C-7), 68.39 (C-4), 72.60 (C-8), 73.32 (C-6), 99.08 (t, $J_{C,F}$ = 25.2, C-4'), 99.70 (C-2), 100.86 (m, C-2' and C-6'), 155.58 (C-1'), 163.32 (dd, $J_{C,F}$ = 248.6 and 15.7, C-3' and C-5'), 166.84

(C-1), 170.32, 170.45, 170.82, 170.96, 171.16 (5 × C=O). Anal Calcd for $C_{26}H_{31}F_2NO_{13}$: C, 51.74; H, 5.18; N, 2.32. Found: C, 51.38; H, 5.36; N, 2.33.

Methyl [2,3-difluorophenyl (5-acetamido-3,5-dideoxy-D-*glycero*-*β*-D-*galacto*-non-2-ulopyranosyl)]onate (3e)

A mixture of activated 3 Å molecular sieves (12 g) and peracetylated sialosyl fluoride **4** (1.0 g, 2.02 mmol) was dried under vacuum for 30 min. To the resulting solid, 2,3-difluorophenol (1.398 g, 10.75 mmol) and dry CH_2Cl_2 (75 ml) were added under a N_2 atmosphere, and the mixture was then stirred for 1 h at rt. Then, $BF_3.OEt_2$ (1.75 ml, 14.5 mmol) in CH_2Cl_2 (10 ml) was added and the mixture was stirred overnight under a N_2 atmosphere at room temperature. The resultant mixture was filtered through celite, and washed thoroughly with CH_2Cl_2. The combined filtrates were washed with saturated $NaHCO_3$ (375 ml), water (375 ml) and brine (375 ml), and the resulting solution was dried over anhydrous Na_2SO_4. After evaporating the solvent under reduced pressure, a yellow syrup containing 26% of Neu2en5Ac was obtained. The syrup was dissolved in dry methanol (60 ml), and a methanolic sodium methoxide solution (22 ml, 11 mmol) was then added at 0 °C. The resulting solution was stirred at 0 °C for 30 min. Subsequently, the solution was then neutralized by the addition of Amberlite IR-120 resin (H^+ form). After removal of the resin, which was washed several times with methanol, the combined solutions were concentrated under reduced pressure to give a yellow syrup that was purified by flash-column chromatography using ethyl acetate/methanol/water (10:3:1 v/v/v). The fractions containing the product were combined and concentrated to give a solid residue (371 mg, 42% yield); mp 71–72 °C; $[\alpha]^{20}_D$ = −41.7 (*c* 0.29, H_2O); ^{1}H NMR (400 MHz, D_2O) δ: 1.85 (dd, 1 H, $J_{3a,3e}$ = 13.2 $J_{3a,4}$ = 11.4, H-3a), 2.07 (s, 3 H, CH_3), 2.73 (dd, 1 H, $J_{3e,3a}$ = 13.3, $J_{3e,4}$ = 4.9, H-3e), 3.55 (d, 1 H, $J_{7,8}$ = 9.2, H-7), 3.67 (m, 2 H, H-9a and H-8), 3.77 (dd, 1 H, $J_{9b,9a}$ = 11.51, $J_{9b,8}$ = 2.13

H-9b.), 3.82 (s, 3 H, OCH_3), 3.93 (d, 1 H, $J_{5,6}$ = 10.64, H-6), 4.06 (t, 1 H, $J_{5,6}$ = $J_{5,4}$ = 10.33, H-5), 4.34 (td, 1 H, $J_{4,3e}$ = 4.89, $J_{4,3a}$ = $J_{4,5}$ = 11.1, H-4), 7.02 (m, 3 H, H-4', H-5', H-6'). ^{13}C NMR (100 MHz, D_2O) δ: 22.09 (CH_3), 39.87 (C-3), 51.48 (C-5), 54.03 (OCH3), 63.02 (C-9), 65.96 (C-4), 67.77 (C-7), 69.81 (C-8), 71.92 (C-6), 100.37 (C-2), 100.14 (d, $J_{C,F}$ = 17.46, C-6'), 113.35 (d, $J_{C,F}$ = 3.33, C-5′), 123.35 (dd, $J_{C,F}$ = 8.4 and 5.10, C-4'), 141.52 (dd, $J_{C,F}$ = 244.16 and $J_{C,F}$ = 14.69 , C-2'), 142.55 (dd, $J_{C,F}$ = 7.87 and $J_{C,F}$ = 2.86, C-1'), 151.04 (dd, $J_{C,F}$ = 245.37 and $J_{C,F}$ = 10.92, C-3'), 169.57, 174.89 (C=O, C-1). HRMS-FAB (*m*/*z*): [M+H$^+$] calcd for $C_{18}H_{24}NO_9F_2$, 436.1419; found, 436.1410.

Methyl [2,6-difluorophenyl (5-acetamido-3,5-dideoxy-D-*glycero*-*β*-D-*galacto*-non-2-ulopyranosyl)]onate (3h)

To activated 3 Å molecular sieves (12 g), peracetylated sialosyl fluoride **4** (1.0 g, 2.02 mmol) was added, and the resulting mixture was dried under vacuum for 30 min. To this mixture, 2,6-difluorophenol (1.4 g, 10.76 mmol) and dry CH_2Cl_2 (75 ml) were added under a N_2 atmosphere, and the mixture was then stirred for 1 h at rt. Then, $BF_3.OEt_2$ (1.75 ml, 14.5 mmol) in CH_2Cl_2 (10 ml) was added and the mixture was stirred overnight under a N_2 atmosphere at room temperature. The resultant mixture was filtered through celite, and washed thoroughly with CH_2Cl_2. The combined filtrates were washed with saturated $NaHCO_3$ (375 ml), water (375 ml) and brine (375 ml), and the resulting solution was dried over anhydrous Na_2SO_4. After evaporating the solvent under reduced pressure, a yellow syrup containing 54% Neu2en5Ac was obtained. The syrup was dissolved in dry methanol (50 ml), and a methanolic sodium methoxide solution (22 ml, 11 mmol) was then added at 0 °C. The resulting solution was stirred at 0 °C for 30 min. Subsequently the solution was then neutralized by the addition of Amberlite IR-120 resin (H^+ form). After filtration of the resin, which was washed several times with methanol, the filtrate was concentrated under reduced pressure to give a yellow syrup that was purified

by flash-column chromatography using ethyl acetate/methanol/water (10:3:1 v/v/v). The fractions containing the product were combined and concentrated to give a solid residue (120 mg, 14% yield); mp 68–69 °C; $[\alpha]^{20}_{D}$ = −15.6 (*c* 0.29, H_2O); ^{1}H NMR (400 MHz, $CDCl_3$) δ: 2.0 (dd, 1 H, $J_{3a,3e}$ = 14.13 $J_{3a,4}$ = 11.19, H-3a), 2.06 (s, 3 H, CH_3), 2.76 (dd, 1 H, $J_{3e,3a}$ = 13.83, $J_{3e,4}$ = 4.97, H-3e), 3.48 (m, 3 H, H-9a, H-8 and H-7), 3.67 (dd, 1 H, $J_{9b,9a}$ = 121.01, $J_{9b,8}$ = 2.36 H-9b.), 3.84 (d, 1 H, $J_{5,6}$ = 10.62, H-6), 3.89 (s, 3 H, OCH3), 4.02 (t, 1 H, $J_{5,6}$ = $J_{5,4\ 5}$= 10.42, H-5), 4.32 (td, 1 H, $J_{4,3e}$ = 4.74, $J_{4,3a}$ = $J_{4,5}$ = 11, H-4), 7.07 (m, 2 H, H-3', H-5'), 7.19 (m, 2 H, H-4'). ^{13}C NMR (100 MHz, D_2O) δ: 22.06 (CH_3), 39.27 (C-3), 51.99 (C-5), 53.86 (OCH3), 62.88 (C-9), 65.67 (C-4), 67.84 (C-7), 70.01 (C-8), 73.25 (C-6), 100.99 (C-2), 112.56 (dd, 2×C, $J_{C,F}$ = 17.21, $J_{C,F}$ = 5.44, C-3' and C-3'), 125.12 (t, $J_{C,F}$ =9.58, C-4'), 128.17 (t, $J_{C,F}$ = 14.62, C-1'), 155.10 (dd, 2×C, $J_{C,F}$ = 245.78 and $J_{C,F}$ = 4.79 , C-2' and C-6'), 169.70, 174.94 (C=O, C-1). HRMS-FAB (*m*/*z*): [M+H$^+$] calcd for $C_{18}H_{24}NO_9F_2$, 436.1419; found, 436.1409.

2-Fluorophenyl (5-acetamido-3,5-dideoxy-D-*glycero*-*β*-D-*galacto*-non-2-ulopyranosylonic acid) (1b)

Peracetylated sialoside **2b** (153 mg, 0.26 mmol) was dissolved in dry methanol (7.6 ml), and a methanolic sodium methoxide solution (2.7 ml, 1.30 mmol) was then added at 0 °C. The resulting solution was stirred at 0 °C for 30 min and the solution was then neutralized by adding Amberlite IR-120 resin (H^+ form). After filtering and washing the resin several times with methanol the combined filtrate was concentrated under reduced pressure, and the resulting residue was dissolved in a 3:1 v/v THF/H_2O solution (3 ml). After adding LiOH.H_2O (55 mg, 1.31 mmol), the mixture was stirred at 0 °C for 30 min. Then, the solution was neutralized using Amberlite IR-120 resin (H^+ form) and the resin was then filtered and washed thoroughly with methanol. The filtrate was concentrated under reduced pressure to give a solid residue that was purified by flash-

column chromatography using ethyl acetate/methanol/water (10:2:1 v/v/v). The fractions that contained the product were combined and evaporated to give a colorless solution (~ 5 mL). This aqueous solution was then lyophilized to give a white solid (63 mg, 60% yield); mp 182 °C (dec); $[\alpha]^{20}_{D}$ = –64.4 (*c* 0.477, H_2O). ^{1}H NMR (600 MHz, D_2O) δ: 1.84 (t, 1 H, $J_{3a,3e}$ = $J_{3a,4}$ = 12.9, H-3a), 2.05 (s, 3 H, CH_3), 2.63 (dd, 1 H, $J_{3e,3a}$ = 13.2, $J_{3e,4}$ = 5.0, H-3e), 3.45 (d, 1 H, $J_{7,8}$ = 9.3, H-7), 3.59 (dd, 1 H, $J_{9a,9b}$ = 11.9, $J_{9a,8}$ = 5.3, H-9a), 3.65 (m, 1 H, H-8), 3.72 (m, 2 H, H-6, H-9b), 4.02 (t, 1 H, $J_{5,6}$ = $J_{5,4}$ = 10.3, H-5), 4.30 (td, 1 H, $J_{4,3e}$ = 4.9, $J_{4,3a}$ = $J_{4,5}$ = 10.6, H-4), 7.03 (m, 1 H, H-4'), 7.08 (m, 1 H, H-6'), 7.2 (m, 2 H, H-3' and H-5'). ^{13}C NMR (150 MHz, D_2O) δ: 22.05 (CH_3), 40.39 (C-3), 51.72 (C-5), 63.04 (C-9), 66.67 (C-4), 68.13 (C-7), 70.02 (C-8), 72.28 (C-6), 100.71 (C-2), 116.33 (d, $J_{C,F}$ = 18.2, C-3'), 117.32 (C-5'), 122.50 (d, $J_{C,F}$ = 6.8, C-4'), 124.12 (d, $J_{C,F}$ = 3.6, C-6'), 141.75 (d, $J_{C,F}$ = 10.2, C-1'), 151.99 (d, $J_{C,F}$ = 243.0, C-2'), 174.45, 174.73 (C=O, C-1). HRMS-FAB (*m*/*z*): [M+H$^+$] calcd for $C_{17}H_{23}NO_9F$, 404.1357; found, 404.1352.

3-Fluorophenyl (5-acetamido-3,5-dideoxy-D-*glycero*-*β*-D-*galacto*-non-2-ulopyranosylonic acid) (1c)

Peracetylated sialoside **2c** (168 mg, 0.29 mmol) was dissolved in dry methanol (8.5 ml), and a methanolic sodium methoxide solution (3 ml, 1.50 mmol) was then added at 0 °C. The resulting solution was stirred at 0 °C for 30 min. Subsequently the solution was then neutralized by the addition of Amberlite IR-120 resin (H^+ form). After filtration of the resin, which was washed several times with methanol, the filtrate was concentrated under reduced pressure. The resultant residue was dissolved in a 3:1 v/v THF/H_2O solution (3.4 ml). After adding $LiOH.H_2O$ (60 mg, 1.42 mmol) the mixture was stirred at 0 °C for 30 min. Then, the solution was neutralized using Amberlite IR-120 resin (H^+ form) and then filtered. The resin was then washed thoroughly with methanol, and the combined solution was concentrated under reduced pressure to give a solid residue that

was purified by flash-column chromatography using ethyl acetate/methanol/water (10:2:1 v/v/v). The fractions containing the product were combined and concentrated to a volume of approximately 5 mL. This aqueous solution was lyophilized to give a white solid (70 mg, 60% yield); mp 195 °C (dec); $[\alpha]^{20}_{D}$ = −42.3 (*c* 0.354, H_2O). ^{1}H NMR (600 MHz, D_2O) δ: 1.8 (t, 1 H, $J_{3a,3e} = J_{3a,4}$ = 12.3, H-3a), 2.03 (s, 3 H, CH_3), 2.54 (dd, 1 H, $J_{3e,3a}$ = 13.2, $J_{3e,4}$ = 5.0, H-3e), 3.46 (d, 1 H, $J_{7,8}$ = 9.8, H-7), 3.59 (dd, 1 H, $J_{9a,9b}$ = 12.6, $J_{9a,8}$ = 5.9, H-9a), 3.67–3.76 (m, 3 H, H-6, H-8, H-9b), 3.99 (t, 1 H, $J_{5,6} = J_{5,4}$ = 10.3, H-5), 4.24 (td, 1 H, $J_{4,3a} = J_{4,5}$ = 10.7, $J_{4,3e}$ = 4.9, H-4), 6.75–6.89 (m, 3 H, H-2', H-4', H-6'), 7.28 (m, 1 H, H-5'). ^{13}C NMR (150 MHz, D_2O) δ: 22.06 (CH_3), 40.51 (C-3), 51.76 (C-5), 63.01 (C-9), 66.69 (C-4), 68.09 (C-7), 70.12 (C-8), 71.18 (C-6), 100.57 (C-2), 104.28 (d, $J_{C,F}$ = 25.4, C-2'), 108.70 (d, $J_{C,F}$ = 21.4, C-4'), 112.37 (d, $J_{C,F}$ = 2.4, C-6'), 130.33 (d, $J_{C,F}$ = 9.9, C-5'), 155.44 (d, $J_{C,F}$ = 11.4, C-1'), 162.84 (d, $J_{C,F}$ = 242.5, C-3'), 174.54, 174.72 (C=O, C-1). HRMS-FAB (*m*/*z*): [M+H^+] calcd for $C_{17}H_{23}NO_9F$, 404.1357; found, 404.1365.

4-Fluorophenyl (5-acetamido-3,5-dideoxy-D-*glycero*-*β*-D-*galacto*-non-2-ulopyranosylonic acid) (1d)

To a solution of protected sialoside **2d** (150 mg, 0.26 mmol) in dry methanol (7.5 ml) a methanolic sodium methoxide solution (2.7 ml, 1.30 mmol) was added at 0 °C. After the resulting solution was stirred at 0 °C for 30 min, it was neutralized by the addition of Amberlite IR-120 resin (H^+ form). After removing and washing the resin with methanol, the combined filtrate was concentrated under reduced pressure. The resulting solid residue was dissolved in a 3:1 v/v THF/H_2O solution (3 ml) to which LiOH.H_2O (54 mg, 1.28 mmol) was added and, the mixture was stirred at 0 °C for 30 min. Then, the solution was neutralized using Amberlite IR-120 resin (H^+ form) and filtered. The resin was then washed thoroughly with methanol, and the filtrate was concentrated under reduced pressure to give a solid residue that was purified by flash-column

chromatography using ethyl acetate/methanol/water (10:2:1 v/v/v). The fractions containing the product were combined and concentrated. The remaining aqueous residue was then lyophilized to give a white solid (53 mg, 50% yield); mp 188 °C (dec); $[\alpha]^{20}_{D}$ = –42.9 (*c* 0.933, H_2O). ^{1}H NMR (600 MHz, D_2O) δ: 1.80 (t, 1 H, $J_{3a,3e} = J_{3a,4} = 12.5$, H-3a), 2.05 (s, 3 H, CH_3), 2.56 (dd, 1 H, $J_{3e,3a}$ = 13.2, $J_{3e,4}$ = 4.9, H-3e), 3.46 (d, 1 H, $J_{7,6}$ = 9.3, H-7), 3.61 (dd, 1 H, $J_{9a,9b}$ = 11.8, $J_{9a,8}$ = 5.3, H-9a), 3.69 (m, 1 H, H-8), 3.75 (m, 2H, H-6, H-9b), 4.00 (t, 1 H, $J_{5,6} = J_{5,4}$ = 10.3, H-5), 4.26 (td, 1 H, $J_{4,3e}$ = 5.0, $J_{4,3a} = J_{4,5}$ = 10.8, H-4), 7.05 (m, 4 H, Ar-H). ^{13}C NMR (150 MHz, D_2O) δ: 24.60 (CH_3), 43.13 (C-3), 54.36 (C-5), 65.61 (C-9), 69.31 (C-4), 70.72 (C-7), 72.60 (C-8), 73.56 (C-6), 102.95 (C-2), 118.15 (d, $J_{C,F}$ = 23.3, C-3', C-5'), 120.32 (d, $J_{C,F}$ = 8.1, C-2', C-6'), 152.83 (d, $J_{C,F}$ = 2.0, C-1'), 160.13 (d, $J_{C,F}$ = 237.0, C-4'), 177.25, 177.33 (C=O, C-1). HRMS-FAB (*m*/*z*): [M+H$^+$] calcd for $C_{17}H_{23}NO_9F$, 404.1357; found, 404.1356.

2,3-Difluorophenyl (5-acetamido-3,5-dideoxy-D-*glycero*-*β*-D-*galacto*-non-2-ulopyranosylonic acid) (1e)

Methyl ester **3e** (371 mg, 0.852 mmol) was dissolved in a 3:1 v/v THF/H_2O solution (11 ml). After adding LiOH.H_2O (194.3 mg, 4.57 mmol) to the solution, the resultant mixture was stirred at 0 °C for 30 min. Then, the solution was neutralized using Amberlite IR-120 resin (H^+ form) and filtered. The resin was then washed thoroughly with methanol, and the combined filtrate was concentrated under reduced pressure to give a solid residue. Purification was accomplished using flash-column chromatography with ethyl acetate/methanol/water (10:3:1 v/v/v) as the eluent. The fractions containing the product were combined and evaporated. The remaining aqueous residue lyophilized to give a white solid (250 mg, 70%); mp 176–177 °C. $[\alpha]^{20}_{D}$ = −54.1 (*c* 0.59, H_2O). ^{1}H NMR (400 MHz, D_2O) δ: 1.86 (dd, 1 H, $J_{3a,3e}$ = 13.08, $J_{3a,4}$ = 11.52, H-3a), 2.06 (s, 3 H, CH_3), 2.64 (dd, 1 H, $J_{3e,3a}$ = 13.24, $J_{3e,4}$ = 4.96, H-3e), 3.49 (d, 1 H, $J_{7,8}$ = 9, H-7), 3.59 (dd, 1 H,

$J_{9a,9b}$ = 11.48, $J_{9a,8}$ = 4.94, H-9a), 3.69 (m, 2 H, H-9b and H-8), 3.77 (d, 1 H, $J_{5,6}$ = 10.59, H-6), 4.03 (t, 1 H, $J_{5,6}$ = $J_{5,4}$ = 10.33, H-5), 4.34 (td, 1 H, $J_{4,3e}$ = 4.95, $J_{4,3a}$ = $J_{4,5}$ = 11.1, H-4), 6.99 (m, 3 H, H-4', H-5', H-6'). ^{13}C NMR (100 MHz, D_2O) δ: 22.11 (CH_3), 40.33 (C-3), 51.72 (C-5), 63.04 (C-9), 66.58 (C-4), 68.04 (C-7), 70.11 (C-8), 71.49 (C-6), 101.21 (C-2), 110.20 (d, $J_{C,F}$ = 17.29, C-6'), 112.61 (d, $J_{C,F}$ = 3.02, C-5′), 123.23 (dd, $J_{C,F}$ = 8.32 and 4.99, C-4'), 141.05 (dd, $J_{C,F}$ = 244.90 and $J_{C,F}$ = 14.56 , C-2'), 143.48 (dd, $J_{C,F}$ = 7.65 and $J_{C,F}$ = 3.01, C-1'), 151.02 (dd, $J_{C,F}$ = 244.46 and $J_{C,F}$ = 11, C-3'), 174.08, 174.79 (C=O, C-1). HRMS-FAB (*m*/*z*): [M+H$^+$] calcd for $C_{17}H_{22}NO_9F_2$, 422.1263; found, 422.1251.

2,5-Difluorophenyl (5-acetamido-3,5-dideoxy-D-*glycero*-*β*-D-*galacto*-non-2-ulopyranosylonic acid) (1f)

To a solution of peracetylated sialoside **2f** (61 mg, 0.10 mmol) in dry methanol (2.7 ml) a methanolic sodium methoxide solution (1 ml, 0.50 mmol) was added at 0 °C. The resulting solution was stirred at 0 °C for 30 min, after which the solution was neutralized by adding Amberlite IR-120 resin (H^+ form). Following removal of the resin, which was washed several times with methanol, the resulting filtrates were combined and concentrated under reduced pressure to give a solid. This material was dissolved in a 3:1 v/v THF/H_2O solution (1 ml). After adding LiOH.H_2O (20 mg, 0.47 mmol) to the solution, the resultant mixture was stirred at 0 °C for 30 min. Then, the solution was neutralized using Amberlite IR-120 resin (H^+ form) and filtered. The resin was then washed thoroughly with methanol, and the combined filtrate was concentrated under reduced pressure to give a solid residue. Purification was accomplished using flash-column chromatography with ethyl acetate/methanol/water (10:3:1 v/v/v) as the eluent. The fractions containing the product were combined and evaporated. The remaining aqueous residue lyophilized to give a white solid (24 mg, 58% yield); mp 161 °C (dec); $[\alpha]^{20}_D$ = −62.8 (*c* 0.17, H_2O). ^{1}H NMR (600 MHz, D_2O) δ: 1.85 (t, 1 H, $J_{3a,3e}$ = $J_{3a,4}$ = 12.2,

H-3a), 2.05 (s, 3 H, CH_3), 2.63 (dd, 1 H, $J_{3e,3a}$ = 13.4, $J_{3e,4}$ = 4.6, H-3e), 3.49 (d, 1 H, $J_{7,8}$ = 9.5, H-7), 3.64 (dd, 1 H, $J_{9a,9b}$ = 12.0, $J_{9a,8}$ = 4.9, H-9a), 3.69 (m, 1 H, H-8), 3.76 (m, 2 H, H-6 and H-9b), 4.03 (t, 1 H, $J_{5,6}$ = $J_{5,4}$ = 10.2, H-5), 4.29 (td, 1 H, $J_{4,3a}$ = $J_{4,5}$ = 10.5, $J_{4,3e}$ = 4.9, H-4), 6.76 (m, 1 H, H-4'), 6.97 (m, 1 H, H-6'), 7.17 (m, 1 H, H-3'). ^{13}C NMR (150 MHz, D_2O) δ: 22.06 (CH_3), 40.25 (C-3), 51.66 (C-5), 63.01 (C-9), 66.52 (C-4), 67.94 (C-7), 70.01 (C-6), 71.43 (C-8), 101.21 (C-2), 105.11 (d, $J_{C,F}$ = 28.7, C-6'), 108.20 (dd, $J_{C,F}$ = 25.2 and 7.5, C-4'), 116.46 (dd, $J_{C,F}$ = 21.1 and 10.9, C-3'), 142.29 (t, $J_{C,F}$ = 11.4, C-1'), 148.38 (d, $J_{C,F}$ = 237.9, C-2'), 157.77 (d, $J_{C,F}$ = 157.8, C-5'), 173.89, 174.75 (C=O, C-1). HRMS-FAB (*m*/*z*): [M+H^+] calcd for $C_{17}H_{22}NO_9F_2$, 422.1263; found, 422.1256.

2,6-Difluorophenyl (5-acetamido-3,5-dideoxy-D-*glycero*-*β*-D-*galacto*-non-2-ulopyranosylonic acid) (1g)

Methyl ester **3g** (120 mg, 0.275 mmol) was dissolved in a 3:1 v/v THF/H_2O solution (4 ml). After adding LiOH.H_2O (62.8 mg, 1.47 mmol) to the solution, the resultant mixture was stirred at 0 °C for 30 min. Then, the solution was neutralized using Amberlite IR-120 resin (H^+ form) and filtered. The resin was then washed thoroughly with methanol, and the combined filtrate was concentrated under reduced pressure to give a solid residue. Purification was accomplished using flash-column chromatography with ethyl acetate/methanol/water (10:3:1 v/v/v) as the eluent. The fractions containing the product were combined and evaporated. The remaining aqueous residue lyophilized to give a white solid (48 mg, 41%. mp 141-142 °C. $[\alpha]^{20}_D$ = −28.47 (*c* 0.28, H_2O). ^{1}H NMR (400 MHz, $CDCl_3$) δ: 1.88 (dd, 1 H, $J_{3a,3e}$ = 13.30 $J_{3a,4}$ = 11.45, H-3a), 2.05 (s, 3 H, CH_3), 2.69 (dd, 1 H, $J_{3e,3a}$ = 13.39, $J_{3e,4}$ = 4.86, H-3e), 3.48 (d, 1 H, H-7), 3.40 (m, 2 H, H-9a, H-8), 3.64 (m, 2 H, H-6, H-9b), 3.99 (t, 1 H, $J_{5,6}$ = $J_{5,4}$ = 10.42, H-5), 4.31 (td, 1 H, $J_{4,3e}$ = 4.83, $J_{4,3a}$ = $J_{4,5}$ = 11, H-4), 7.07 (m, 3 H, H-3', H-4', H-5'). ^{13}C NMR (100 MHz, D_2O) δ: 22.09 (CH_3), 40.22 (C-3), 51.67 (C-5), 62.98 (C-9), 66.40 (C-4), 68.13 (C-7), 70.22 (C-8),

72.81 (C-6), 102.32 (C-2), 112.40 (dd, 2×C, $J_{C,F}$ = 16.94, $J_{C,F}$ = 5.58, C-3' and C-3'), 123.41 (t, $J_{C,F}$ =9.73, C-4'), 129.21 (t, $J_{C,F}$ = 14.25, C-1'), 154.72 (dd, 2×C, $J_{C,F}$ = 245.22 and $J_{C,F}$ = 5.81 , C-2' and C-6'), 174.61, 174.82 (C=O, C-1). HRMS-FAB (*m*/*z*): [M+H$^+$] calcd for $C_{17}H_{22}NO_9F_2$, 422.1263; found, 422.1253.

3,5-Difluorophenyl (5-acetamido-3,5-dideoxy-D-*glycero*-*β*-D-*galacto*-non-2-ulopyranosylonic acid) (1h)

Protected sialoside **2h** (206 mg, 0.34 mmol) was dissolved in dry methanol (9.5 ml), and a methanolic sodium methoxide solution (3.5 ml, 1.70 mmol) was then added at 0 °C. The resulting solution was stirred at 0 °C for 30 min. Then, the solution was neutralized by the addition of Amberlite IR-120 resin (H^+ form) and the resin, which was removed by filtration, was then washed several times with methanol. The combined filtrate was concentrated under reduced pressure, and the resulting residue was dissolved in a 3:1 v/v THF/H_2O solution (3.8 ml). After adding LiOH.H_2O (68 mg, 1.60 mmol), the mixture was stirred at 0 °C for 30 min. Then, the solution was neutralized using Amberlite IR-120 resin (H^+ form) and filtered. The resin was then washed thoroughly with methanol, and filtrate was concentrated under reduced pressure to give a solid residue which was purified by flash-column chromatography using ethyl acetate/methanol/water (10:2:1 v/v/v). The fractions containing the product were combined and concentrated. The remaining aqueous residue was then lyophilized to give a white solid (70 mg, 60% yield); mp 180 °C (dec); $[\alpha]^{20}_D$ = –88.7 (*c* 0.248, H_2O). ^{1}H NMR (150 MHz, D_2O) δ: 1.82 (t, 1 H, $J_{3a,3e}$ = $J_{3a,4}$ = 12.3, H-3a), 2.05 (s, 3 H, CH_3), 2.56 (dd, 1 H, $J_{3e,3a}$ = 13.2, $J_{3e,4}$ = 4.9, H-3e), 3.49 (d, 1 H, $J_{7,8}$ = 9.3, H-7), 3.65 (dd, 1 H, $J_{9a,9b}$ = 12.1, $J_{9a,8}$ = 4.9, H-9a), 3.73 (m, 1 H, H-8), 3.77 (m, 2 H, H-6, H-9b), 4.00 (t, 1 H, $J_{5,6}$ = $J_{5,4}$ = 10.2, H-5), 4.24 (td, 1 H, $J_{4,3a}$ = $J_{4,5}$ = 10.7, $J_{4,3e}$ = 4.8, H-4), 6.62 (m, 1 H, H-4'), 6.68 (m, 2 H, H-2' and H-6'). ^{13}C NMR (150 MHz, D_2O) δ: 22.07 (CH_3), 40.41 (C-3),

51.70 (C-5), 63.06 (C-9), 66.59 (C-4), 68.03 (C-7), 69.95 (C-8), 71.25 (C-6), 97.38 (t, $J_{C,F}$ = 27.2, C-4'), 100.42 (m, C-2' and C-6'), 100.95 (C-2), 156.04 (t, $J_{C,F}$ = 14.1, C-1'), 162.90 (dd, $J_{C,F}$ = 244.3 and 15.1, C-3' and C-5'), 174.27, 174.91 (C=O, C-1). HRMS-FAB (*m*/*z*): [M+H$^+$] calcd for $C_{17}H_{22}NO_9F_2$, 422.1263; found, 422.1253.

2.3.2 MvNA Active Site Construct

Plasmid pJW-OSH-Y370g, encoding the full-length Y370G mutant sialidase[17,18], was used as the template DNA. A portion of the sialidase gene encoding the MvNA active site domain (up to amino acid residue G401;[21]) was amplified by PCR, incorporating a new Hind III site to allow read through for the expression of a C-terminal linker and His_6-tag. The amplification reaction was carried out in 10% DMSO, using the forward primer, Eco*'[17], and the reverse primer, GGHin-R' (5'-CCC AAG CTT CAG CCA GGC GAG GTT G-3') to produce a 1,205 bp fragment. The isolated fragment was purified, digested with EcoR I and Hind III, and then ligated into similarly digested and dephosphorylated pJW-OSH vector and propagated in *Escherichia coli*. Plasmid DNA was isolated from a single colony and the resultant 6,526 bp plasmid,designated as pJWβ-Y370g, was verified by restriction digests, and DNA sequencing using primer MV1396R' (5'-CCA GCC CGG GTC CGG GG-3') and the T7 Terminator primer (Novagen) to ensure that spurious mutations had not occurred during DNA manipulations.

2.3.3 Y370G Expression and Purification

Expression was performed as reported previously[6]. At 41 h post-induction, the 35 ml culture was harvested by setting on ice for 20 min prior to removing the cells by centrifugation at 3,700 × *g* for 15 min. The sialidase active site-His_6 protein was purified

using agarose Ni-NTA resin (2 ml, Qiagen), $(NH_4)SO_4$ precipitation, and dialysis, as described in a previous report[17]. Purity was assessed by SDS-PAGE with Coomassie staining and total protein concentration was determined by Bradford assay using bovine serum albumin as the standard. Aliquots of the purified enzyme were stored at –80 °C. *N*-terminal Edman sequencing was performed on an ABI Procise 494 sequencer (Alphalyse Inc.).

2.3.4 Product Studies

^{1}H NMR spectroscopy (600 MHz) was employed to identify the products of the enzyme-catalyzed reactions[6]. Reactions were carried out in 0.6 mL (25 °C, 10 mM tartrate buffer pD 5.5) and ^{1}H NMR spectra were recorded at various time intervals. Also, a solution of each substrate (1 mM), buffered to a pH value of 5.25, was incubated with enzyme for either 24 hr (substrates **1b**, **1c**, **1e**, **1f** and **1g**) or 48 hr (substrates **1d** and **1h**), and then an aliquot was diluted (10–fold) and the UV-vis spectrum (250–400 nm) was recorded and compared to a spectrum of the appropriate phenol at the same pH and concentration. Of note, even after 48 hr substrate **1h** had not been completely hydrolyzed.

2.3.5 Enzyme Kinetics

The enzyme-catalyzed hydrolysis reactions were monitored using a HPLC protocol. Specifically, each 0.5 ml reaction was performed at 37 °C by equilibrating the buffer, substrate and internal standard (4-nitrophenyl *β*-D-glucopyranoside, 0.01 mM) for 1 min before the addition of enzyme stock solution containing BSA (final concentration of BSA in the reaction mixture = 0.01% w/v). Reactions were terminated at five different time points by adding an aliquot of the reaction mixture (100 µl) to ethanol (300 µl).

Protein precipitation occurred when the ethanolic solutions were cooled to –20 °C for 20 min. Following centrifugation (20 min) the supernatants were evaporated to dryness. The resultant residues were dissolved in "milli-Q" water (100 µl) and, HPLC analysis was performed on a gradient pump system from Agilent Technologies using a Phenomenex C18 column 150 × 60 mm (3 µm particle size). The two mobile phase solutions were water containing 0.1 % formic acid (solvent A), and acetonitrile (solvent B). Isocratic mobile phases were delivered at 1.0 ml/min, 10 µl sample aliquots were injected onto the column, and the column temperature was 25 °C. The decrease in substrate concentration was monitored as a function of reaction time using a standard integration protocol. Substrate and internal standard retention times were 2.73 min for Ph-βNeuAc (eluting with 20% B and followed at λ = 270 nm); 3.50 min for 2FP-βNeuAc (15% B, λ = 270 nm); 2.87 min for 3FP-βNeuAc (20% B, λ = 270 nm); 3.02 min for 4FP-βNeuAc (20% B, λ = 270 nm); 2.35 min for 23DFP-βNeuAc (30% B, λ = 254 nm); 2.81 min for 25DFP-βNeuAc (20% B, λ = 270 nm); 2.52 min for 26DFP-βNeuAc (20% B, λ = 260 nm); 3.15 min for 35DFP-βNeuAc (20% B, λ = 270 nm); and 6.20, 4.00 and 3.00 min for 4-nitrophenyl *β*-D-glucopyranoside eluting with 15% B, 20% B or 30% B, respectively. Michaelis–Menten parameters were calculated by non-linear least squares fitting of a minimum of five initial rate data, which spanned a substrate concentration of at least $K_m/4$ to $4K_m$, to the standard Michaelis-Menten equation (Prism). Estimates of k_{cat} for the two slowest substrates, 4FP-βNeuAc and 35DFP-βNeuAc, were made using ^{1}H NMR spectroscopy. Specifically, under identical conditions where substrate concentration (~5 mM) was much greater than K_d the hydrolysis of 2FP-βNeu5Ac, 4FP-βNeu5Ac and 35DFP-βNeu5Ac were monitored by ^{1}H NMR spectroscopy. Solvent deuterium KIEs were measured using identical ratios of buffer components in both H_2O and D_2O.

2.3.6 Measurement of Phenol pK_a Values

During neutralization of a solution of the appropriate phenol (0.01 M, 50 mL, I = 0.05 M NaCl), by the addition of aliquots of a NaOH solution (0.5 mL; 0.05 M), pH values were automatically recorded using a standard pH titrator assembly. The phenolic pK_a values were calculated by fitting the measured pH versus addition data to a standard titration curve (Prism).

2.3.7 Measurement of pH-Rate Profiles

To determine the effect of pH on catalysis, kinetics parameters were measured over a pH range of 3.8–6.6. The buffers used were NaOAc-HOAc (pH range 3.8–5.7), 2-(N morpholino)ethanesulfonic acid (MES-NaOH) (pH range 5.6–6.6). The substrate for this experiment was 2FP-βNeuAc. Separate Michaelis-Menten plots were obtained for each of the five buffers according to the HPLC procedure described above.

2.3.8 Measurement of Dissociation Constants

To determine the dissociation constants for the slow substrates (4FP-βNeuAc and 35DFP-βNeuAc) and a known neuraminidase inhibitor (Neu2en5Ac) standard IC_{50} assays were performed using pNP-αNeu5Ac at a single concentration and the IC_{50} value was corrected to give K_d values[22]. For the reaction product phenol three separate assays were performed: i) an IC_{50} experiment with 2FP-βNeu5Ac as substrate; ii) a time-dependent inhibition assay with 2FP-βNeu5Ac as substrate; and iii) an activation assay with pNP-αNeu5Ac to probe whether bound phenol could accelerate the production of 4-nitrophenol. This last experiment was also performed with 4-fluorophenol and 3,5-difluorophenol.

2.4 Results

2.4.1 Synthesis

The panel of fluorinated phenyl β-sialosides were synthesized by following the literature procedure as reported by Dookhun et al[19] (Scheme 2.3).

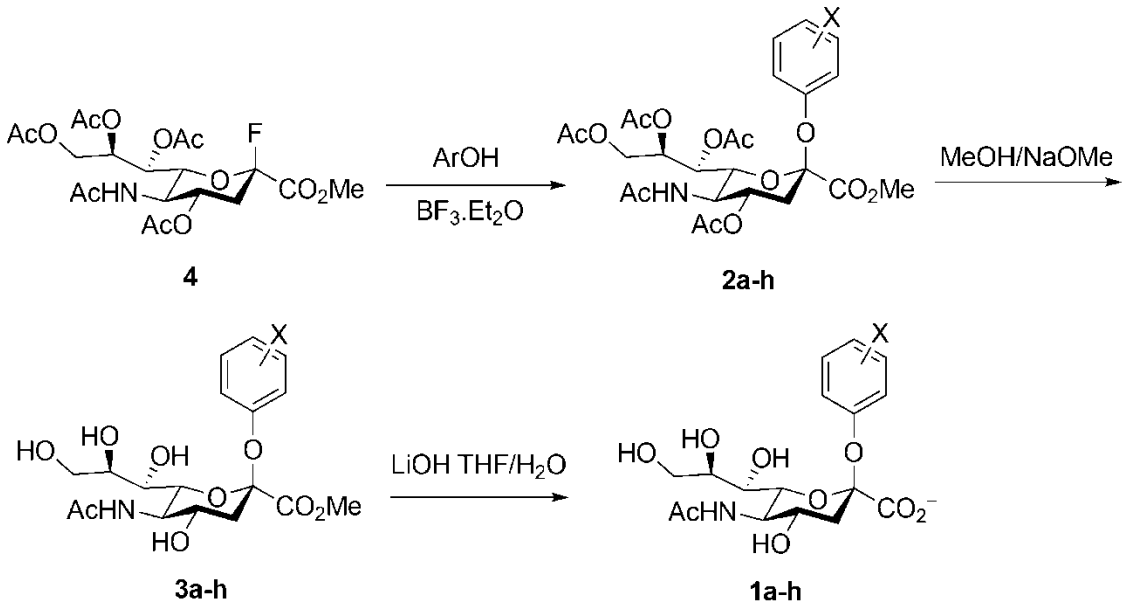

Scheme 2.3. Synthetic route to make aryl β-sialoside substrates

In order to ensure that measured kinetic parameters are as accurate as possible it is essential to ensure that the synthetic substrates are free of contaminating inhibitors. Thus, fully protected Neu2en5Ac, which is invariably produced during glycosylation, was removed from the majority of protected sialosides by recrystallization from diethyl ether. However, for the syntheses of 23DFP-β-NeuAc and 26DFP-β-NeuAc the methyl ester of Neu2en5Ac was separated from the methyl esters of 23DFP-βNeuAc and 26DFP-βNeuAc by flash column chromatography. Presented in the supporting information section are the ^{1}H and ^{13}C NMR spectra of all new substrates (**1b**–**1h**).

2.4.2 Cloning, Expression & Purification of Y370G Mutant Sialidase.

The full-sized Y370G mutant *M. viridifaciens* sialidase, which comprises three separate domains[16,21], has been shown previously to hydrolyze phenyl β-sialoside, a process that occurs with an inversion of anomeric configuration[18]. In order to eliminate any possibility of kinetic complications being caused by binding of either substrate or reaction products to the hydrophobic surface of the lectin domain in the full-sized sialidase[21], it was decided to express the active site domain only, and to measure kinetic parameters on this single domain protein. Successful plasmid construction was confirmed by DNA sequencing. The expression profile showed sialidase activity similar to that of the full-size Y370G sialidase reported previously[16]. The protein was purified by Ni-NTA affinity chromatography in a manner similar to that used to purify the full-size enzyme with a C-terminal His_6-tag. SDS-PAGE analysis revealed that the purified product actually contained two closely running bands, the lower molecular weight band had higher intensity, corresponding to the predicted size of the active site with the C-terminal His_6-tag. The bands were submitted for *N*-terminal Edman sequencing with the major band having an identical processing site as that of the full-length wild-type sialidase[6], and the minor product showed an *N*-terminal cleavage pattern that had not been observed in this system when the expression construct included the latter two *C*-terminal domains of the sialidase. These two bands could not be resolved to isolate a single sialidase species, so the kinetic parameters were evaluated using an enzyme stock containing both bands under the assumption that slight changes at the *N*-terminus would not affect the catalytic activity between these two expression products. Shown in Figure 2.5 (supporting information) is a picture of the SDS-PAGE gel for the recombinant active site domain Y370G mutant sialidase, and listed in Table S1 are the two Edman N-terminal sequences.

2.4.3 Enzyme Kinetics and Product Studies

The reaction products from the active site Y370G mutant sialidase-catalyzed hydrolysis of aryl β-sialosides were shown to be sialic acid and phenol by NMR spectroscopic analysis. Also, the phenol absorption band in the UV-vis spectrum of product mixture was of equal intensity, within experimental error, to that of an identical concentration of free phenol. Due to the generally small absorbance changes that occur during the catalyzed hydrolyses of these β-sialosides, resulting from the absence of an auxochromic group in the fluoroaryl substrates, a HPLC analytical method had to be developed in order to monitor the reaction progress. For the two slowest substrates (4FP-βNeu5Ac and 35DFP-βNeu5A) full Michaelis-Menten curves could not be obtained because of the difficulty of measuring hydrolysis rates at low substrate concentration. Therefore, an estimate for k_{cat} was made by noting the fraction of reaction for 2FP-βNeu5Ac, 4FP-βNeu5Ac and 35DFP-βNeu5Ac at single time points under saturating conditions. Using identical, high, concentrations of enzyme 33% of 2FP-βNeu5Ac (4.77 mM) had reacted after 3 min, while 6 hr was needed for 25% hydrolysis of 4FP-βNeu5Ac (4.90 mM) and after 3 days 16% of 35DFP-βNeu5Ac (4.90 mM) had hydrolyzed. Michaelis-Menten kinetic parameters for the active site Y370G mutant sialidase with the eight aryl β-sialosides are listed in Table 2.1. The variations of the kinetic parameters k_{cat}/K_m and k_{cat} for the Y370G-catalyzed hydrolysis of 2-fluorophenyl β-sialoside as a function of pH are listed in Table 2.2.

Table 2.1. Michaelis-Menten Kinetic Parameters of the Y370G Mutant Sialidase Catalyzed Hydrolysis of Fluoro-substituted Ph-βNeuAc at 37 °C and pH 5.25.

Substrate	pK_a (ArOH)[a]	k_{cat} (s^{-1})	k_{cat}/K_m (M^{-1} s^{-1})	K_m (μM)
Ph-βNeuAc[b]	9.87	0.110 ± 0.004	(3.3 ± 0.5) × 10^3	33 ± 5
4FP-βNeuAc	9.72	0.018[c]	4.6 × 10^2[c]	39 ± 3[d]
3FP-βNeuAc	9.03	1.58 ± 0.17	(7.2 ± 2.1) × 10^3	220 ± 60
2FP-βNeuAc	8.49	2.77 ± 0.09	(1.51 ± 0.21) × 10^4	182 ± 18
35DFP-βNeuAc	8.26	9.6 × 10^{-5}[c]	0.36[c]	270 ± 70[d]
23DFP-βNeuAc	7.65	0.965 ± 0.037	(4.90 ± 0.54) × 10^3	200 ± 20
25DFP-βNeuAc	7.63	0.284 ± 0.011	(4.4 ± 0.7) × 10^3	61 ± 9
26DFP-βNeuAc	7.09	2.31 ± 0.09	(6.1 ± 0.9) × 10^4	38 ± 5

[a] Ionic strength = 0.05 M (NaCl). [b] Reported values for the full-sized *M. viridifaciens* Y370G mutant sialidase are k_{cat} = 13.3 ± 0.3 s^{-1} and k_{cat}/K_m = (2.9 ± 0.3) × 10^5 M^{-1} s^{-1} [18]. [c] Value estimated using NMR spectroscopy, see experimental details (T = 25 °C): estimated error ± 10%. [d] Calculated according to reference[22] using the measured IC_{50} value for the inhibition Y370G-catalyzed hydrolysis of pNP-αNeuAc (expt conc = 50 μM; K_m = 65.8 μM).

Table 2.2. Michaelis-Menten Kinetic Parameters of the Y370G Mutant Sialidase Catalyzed Hydrolysis of 2-Fluorophenyl β-Sialoside as a Function of pH at 37 °C.

pH	k_{cat} (s^{-1})	k_{cat}/K_m (M^{-1} s^{-1})
3.83	13.1 ± 0.4	(5.25 ± 0.49) × 10^4
4.25	4.02 ± 0.37	(1.78 ± 0.46) × 10^4
5.25	2.77 ± 0.09	(1.51 ± 0.16) × 10^4
6.08	2.37 ± 0.04	(1.05 ± 0.06) × 10^4
6.59	1.85 ± 0.09	(1.05 ± 0.17) × 10^4

Shown in Figures 2.2 and 2.3 are Brønsted plots for the two catalytic constants k_{cat}/K_m and k_{cat}. Substitution at the para position with fluorine (4FP-βNeuAc) results in a lower enzymatic activity, while all difluorinated substrates with the exception of the 2,6-

isomer also display low activities (Table 2.1).

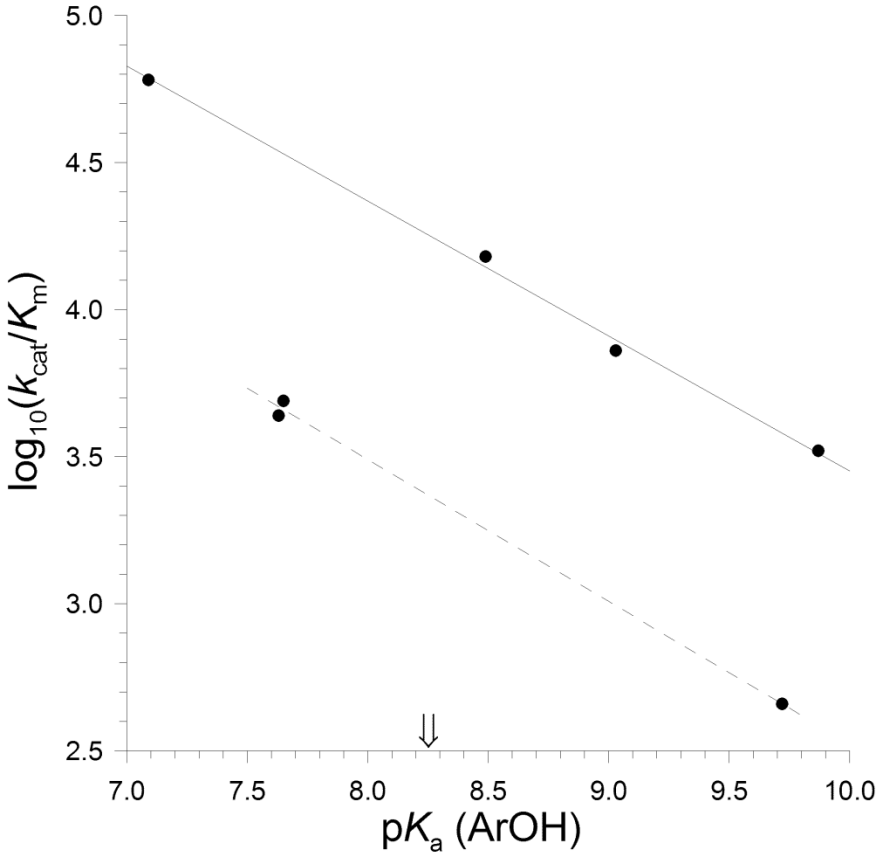

Figure 2.2. Effect of leaving group ability on k_{cat}/K_m for the Y370G mutant sialidase. Leaving group ability represented as pK_a (ArOH) as follows: 2,6-difluorophenol (7.09); 2,5-difluorophenol (7.63); 2,3-difluorophenol (7.65); 3,5-difluorophenol (8.26); 2-fluorophenol (8.49); 3-fluorophenol (9.03); 2-fluorophenol (9.72); and phenol (9.87). The lines shown are the best linear fits to two data subsets (see discussion). The point for 3,5-difluorophenyl β-sialoside is not shown because of the extremely low activity of this substrate with the mutant sialidase, rather the pK_a of 3,5-difluorophenol is indicated on the x-axes by an arrow.

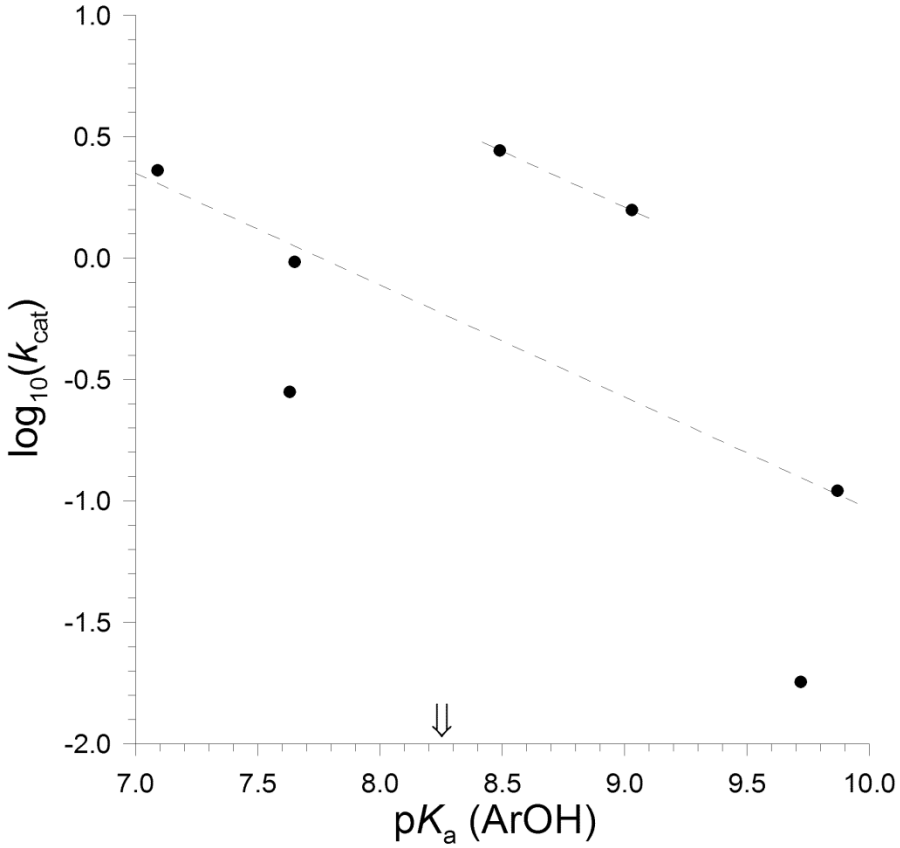

Figure 2.3. Effect of leaving group ability on k_{cat} for the Y370G mutant sialidase. Leaving group ability represented as pK_a (ArOH) as follows: 2,6-difluorophenol (7.09); 2,5-difluorophenol (7.63); 2,3-difluorophenol (7.65); 3,5-difluorophenol (8.26); 2-fluorophenol (8.49); 3-fluorophenol (9.03); 2-fluorophenol (9.72); and phenol (9.87). The drawn lines have β_{lg} values of –0.46 (see discussion). The point for 3,5-difluorophenyl β-sialoside is not shown because of the extremely low activity of this substrate with the mutant sialidase, rather the pK_a of 3,5-difluorophenol is indicated on the x-axes by an arrow.

The solvent deuterium kinetic isotope effects on the Y370G mutant-catalyzed hydrolysis of 2FP-βNeuAc were measured by maintaining identical ratios of the two buffer components in H_2O and D_2O as suggested by Schowen[23]. Thus, at an acetate to acetic acid ratio of 3.46 and with a total buffer concentration of 0.1 M, the following kinetic parameters were measured: k_{cat} (H_2O) = 2.29 ± 0.19 s^{-1} and k_{cat} (D_2O) = 2.23 ± 0.26 s^{-1}, so k_{H2O}/k_{D2O} = 1.03 ± 0.15, while k_{cat}/K_m (H_2O) = (1.42 ± 0.30) × 10^4 M^{-1} s^{-1} and k_{cat}/K_m (D_2O) = (1.60 ± 0.54) × 10^4 M^{-1} s^{-1} so that k_{H2O}/k_{D2O} = 0.89 ± 0.35. A second independent set of measurements using a different batch of enzyme gave the following

values for the solvent deuterium KIE: k_{H2O}/k_{D2O} = 1.36 ± 0.19 (k_{cat}) and 0.88 ± 0.33 (k_{cat}/K_m). The weighted averages for these solvent KIE values are: k_{H2O}/k_{D2O} = 1.16 ± 0.12 (k_{cat}) and 0.88 ± 0.24 (k_{cat}/K_m)[24].

The binding of phenol to the Y370G mutant was probed using a standard IC_{50} inhibition assay with 2FP-βNeu5Ac as the substrate. At a phenol concentration of 1 mM the rate for the mutant sialidase-catalyzed hydrolysis of 2FP-βNeu5Ac (100 μM ≈ K_m/2) decreased by approximately 35%. Also, it was shown that this inhibition is not time dependent (slow binding of phenol to the active site pocket) by measuring the inhibition of 2FP-βNeu5Ac (50 μM) hydrolysis after incubation of up to 30 min with phenol (100 μM). The dissociation constants for the two slowest substrates (4FP-βNeuAc and 35DFP-βNeuAc) and the unsaturated acid Neu2en5Ac were estimated, by using a similar inhibition protocol with pNP-αNeu5Ac as the substrate, to be 39, 270 and 13 μM, respectively. The Y370G mutant-catalyzed rate of hydrolysis for pNP-αNeu5Ac did not display any significant deviation as a function of added phenol, 4-fluorophenol or 3,5-difluorophenol.In addition, during the Y370G mutant-catalyzed hydrolysis of pNP-αNeu5Ac (10.3 mM), which was monitored by ^{1}H NMR spectroscopy, in the presence of 4-fluorophenol (10.0 mM) no visible sign (< 2%) of transfer product (4FP-βNeuAc) could be seen in the final spectrum.

2.5 Discussion

2.5.1 β-Sialidase Activity of Mutant Y370G.

As reported earlier for phenyl β-sialoside with the full-sized Y370G mutant sialidase[18], the initial product formed in the reactions catalyzed by the active site

domain Y370G mutant sialidase of all fluorinated aryl β-sialoside substrates, which undergo rapid reaction, is α-NeuAc and this material undergoes a subsequently facile water-catalyzed mutarotation to give predominantly the β-anomer at equilibrium (data not shown)[25]. Thus, the minimal mechanism for the Y370G mutant sialidase-catalyzed hydrolysis of aryl β-sialosides is shown in Scheme 2.2. Here, the first formed Michaelis complex, in which the aryl ring is bound into the active site "hole" [16], undergoes glycosidic bond cleavage (k_3) to give a ternary complex from which dissociation of the α-sialic acid and phenol(ate) products (k_4), presumably in a stepwise manner, results in the regeneration of active inverting enzyme that is ready to perform another catalytic cycle.

The reported catalytic constants for the full-sized Y370G mutant sialidase[18] are about a hundred times larger than those measured with the truncated enzyme, which was used in this study in order to avoid kinetic complications that might arise from binding of the unnatural β-substrates to the lectin domain of the full length enzyme. The size of the sialidase naturally produced by *M. viridifaciens* depends on the sialoside source that induces expression, where columinic acid gives rise to the single domain enzyme and milk casein results in production of the three domain protein[26]. When expressed in *S. lividans* the single domain *M. viridifaciens* sialidase displays about 55-60% of the activity of the full-length enzyme[26,27]. Of note, the absolute magnitude of all kinetic parameters reported in the current study and in earlier investigations[18,27] relies on the assumption that all of the purified, expressed protein is catalytically active. Thus at the present time, it is impossible, given the lack of sensitive sialidase active site titrants, to discern the main cause for the lower activity of the current enzyme. That being said, the hydrolytic activity of the current Y370G mutant on six out of the eight substrates studied ($k_{cat}/K_m \geq 3 \times 10^3$ M^{-1} s^{-1}), a value which is greater than that for the *V.*

cholerae sialidase-catalyzed hydrolysis of phenyl α-sialoside[28], suggests that its mechanism of action is a valid model for the deglycoslyation reaction of sialidase enzymes.

The hole created by mutation of the active site tyrosine residue in the single domain construct is able to accommodate a number of pK_a perturbing fluorine for hydrogen atom substitutions, which are often considered to be approximately sterically neutral (Table 1). However, such replacements can result in a catastrophic loss of catalytic activity as observed for the 3,5-difluorophenyl substrate (35DFP-βNeu5Ac) which reacts about three orders of magnitude more slowly than the parent compound (Ph-βNeu5Ac) despite possessing a better leaving group.

It is important to remember, that unlike other reported Brønsted correlation studies on wild-type glycosidases the current Y370G mutant enzyme possesses a specific pocket in which the substrate's aryl group binds. However, given that this inverting enzyme has not been subject to evolutionary pressure it seems prudent to postulate the simplest possible kinetic scheme (Scheme 2.2, page 52). Thus, the plausible rate determining steps for k_{cat}/K_m are either binding (k_1) or glycosidic cleavage (k_3), while k_{cat} might be limited by k_3 or product release (k_4).

2.5.2 Effect of Leaving Group on the Catalytic Activity.

The magnitude of k_{cat}/K_m values measured for the mutant enzyme-catalyzed hydrolysis of the non-natural aryl β-sialoside substrates, which are several orders of magnitude below the diffusion limit[12], suggests that k_3 is the likely rate determining step. Indeed, the data displayed in Figure 2.2 suggests two separate Brønsted correlations with the calculated β_{lg} value on k_{cat}/K_m for the four most active substrates of –0.46 ± 0.02

and that for the three other active substrates being –0.48 ± 0.02 (Figure 2.2 solid and dashed lines, respectively). Even though fitting three data points to a line is not optimal, the identical β_{lg} values for both fits suggests that the degree of productive binding is important in this system [29]. With regard to binding, K_m (Scheme 2.2: k_2/k_1) values for the catalyzed hydrolysis reactions can be grouped into two subsets, $K_m \approx 40$ and 200 μM. These binding interactions between the Y370G mutant sialidase pocket and the aryl groups of the substrates may be productive, and if expressed at both the Michaelis complex and the transition state for the catalyzed cleavage of **1a–h** then an increase in k_{cat}/K_m will result[29]. That is, the k_{cat}/K_m data is consistent with two separate transition states, which have similar degrees of glycosidic bond cleavage, that likely have different productive binding modes, for the variously substituted aromatic rings, in the active site pocket. The β_{lg} values when taken with the measured solvent kinetic isotope effect for 2FP-βNeuAc catalyzed hydrolysis, a value that is indistinguishable from unity (0.88 ± 0.24), and the β_{lg} value of –1.24 for the spontaneous hydrolysis of aryl β-sialosides (pH = 8.1, T = 100 °C)[19] suggests that the rate-determining step for the Y370G mutant-catalyzed reaction is glycosidic bond cleavage that occurs with no significant general-acid catalysis. Also, the flatness of the k_{cat}/K_m pH-rate profiles for the catalyzed hydrolyses of 2FP-βNeuAc (this work) between pH values of 4.2–6.6 (Table 2) and that reported for Ph-βNeuAc (full-sized Y370G mutant enzyme[18]) suggest that no catalytically important protonation change occurs over this pH range.

With regard to the Brønsted plot for k_{cat} (Figure 2.3), given that sialic acid only weakly binds to wild-type sialidases, a mimic for the initial ternary product complex, and phenol is only a weak inhibitor of the Y370G variant sialidase (35% inhibition at 1 mM) it appears implausible that product release (Scheme 2.2: k_4) limits k_{cat} because combining

the k_{cat} value (0.11 s^{-1}) with the estimated K_i value for phenol binding (1.2 mM[22]) would require an exceptionally slow "on" rate for phenol binding of ~10^2 M^{-1} s^{-1} (= k_{cat}/K_i). Thus, it can be concluded that both k_{cat} and k_{cat}/K_m are limited by glycosidic bond cleavage (k_3) and that the Brønsted plot for k_{cat} should show similar β_{lg} correlations to those measured on k_{cat}/K_m (two such lines of slope –0.46 are drawn on Figure 2.3). The apparent scatter in kcat values likely arises from nonproductive binding, which is expressed at the Michaelis complex but not the transition state[29]. That is, the requisite loss of binding energy on progressing from the Michaelis complex to transition state results in decreasing k_{cat} values but does not affect k_{cat}/K_m [29]. As noted above for Michaelis complex formation, K_m values can be sub-divided into two groups and that, based on the kinetic data, the tight binders, such as Ph-βNeuAc and 26DFP-βNeuAc (**1a** and **1g**), likely exhibit a nonproductive binding component during catalysis.

Indeed, with the exception of the worst substrate (35DFP-βNeuAc), which surely binds unproductively to the mutant sialidase, all k_{cat}/K_m and k_{cat} data are consistent with rate-limiting glycoside hydrolysis occurring via two energetically distinct transition states that may incorporate a nonproductive binding component.

2.5.3 Mechanism of Action

Based on the solvent KIE on k_{cat}/K_m (k_{H2O}/k_{D2O} = 0.88 ± 0.24) and the pH-rate profile data (pH values ≥ 4.25) it is likely that at the transition state, for the desialylation mimic reaction, the phenolate leaving group is departing with little or no general-acid catalyzed assistance from either of the two residues that are within H-bonding distance to its oxygen atom (Scheme 2.4).

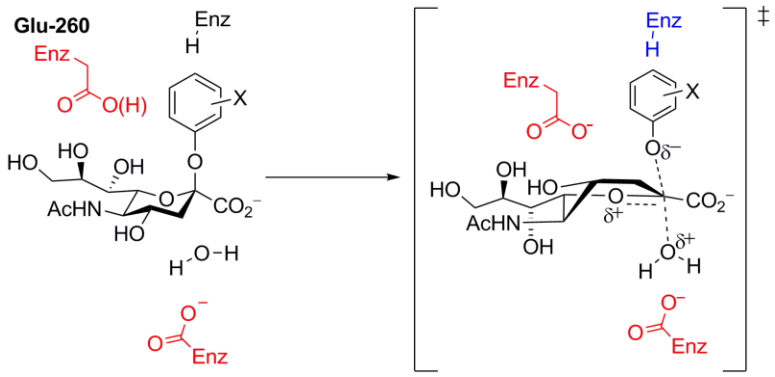

Scheme 2.4. Proposed mechanism for the Y370G mutant-catalyzed hydrolysis of aryl β-sialosides.

These two residues are the active site Glu-260 and Arg-276. Figure 2.4 shows this diad, and the various close O–O and N–O contacts to the tyrosinyl oxygen atom in the wild-type sialidase structure that contains the presumed transition state analogue inhibitor Neu2en5Ac [21].

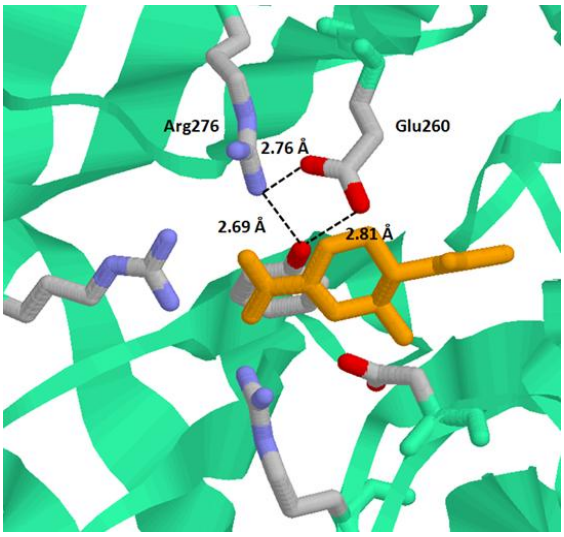

Figure 2.4. Illustration of a possible product complex formed during the Y370G mutant sialidase-catalyzed reactions of aryl β-sialosides. Wild-type MvNA structure (blue-green ribbon) with Neu2en5Ac (orange) bound (PDB code 1EUS), both the methylene carbon of the wild-type Y370 residue (to show a bound phenol) and the glycerol side chain of Neu2en5Ac have been removed for clarity. Also, shown are the short O–O and O–N distances taken from the wild-type MvNA structure. The three arginine residues shown make up the strictly conserved triad that is found in all known *exo*-sialidases.

If this wild-type structure reasonably mimics the transition state for the Y370G mutant-catalyzed hydrolysis of aryl β-sialosides (Scheme 2.4) then the close proximity of the nascent phenolate and glutamate residues may result in the deprotonation of arginine-276. At the moment, it is impossible to conclude whether this catalyzed hydrolysis reaction proceeds either via a discrete oxacarbenium ion (D_N * A_N; S_N1) or by direct displacement (A_ND_N; S_N2). However, if the water nucleophile has started to form a bond to the anomeric carbon center then this attack must be occurring with no general-base catalysis (k_{H_2O}/k_{D_2O} = 0.88 ± 0.24). Of note, an inverse solvent deuterium KIE would be consistent with an uncatalyzed water attack at the reaction transition state[30]. Unfortunately, the precision of the HPLC monitored substrate depletion kinetics is inadequate to allow such a conclusion to be made.

Listed in Table 2.3 are a catalog of reported Brønsted β_{lg} values on k_{cat} and k_{cat}/K_m for a series of sialidases.

Table 2.3. Brønsted β_{lg} Values for Sialidase-Catalyzed Reactions

Enzyme Source	β_{lg} value (k_{cat}/K_m)	β_{lg} value (k_{cat})	pK_a (ROH)[a]	Reference
Vibrio Cholerae	–0.73 (r = –0.93)	–0.25 (r = –0.95)	7.2–9.9	[28]
Influenza A[b]	–0.45 (r = –0.93)	–0.11 (r = –0.81)	7.2–9.9	[31]
Salmonella typhimurium	–0.80 (r = +0.96)	–0.53 (r = –0.95)	7.2–9.9	[31]
Micromonospora viridifaciens	–0.30 ± 0.04	+0.02 ± 0.03	7.2–13.8	[6]
M. viridifaciens – Y370G mutant[c]	–0.80 ± 0.08	–0.63 ± 0.05	7.2–13.6	[16]
M. viridifaciens – Y370G mutant[d]	**–0.46 ± 0.02**	**–**	**7.1–9.9**	**This study**

[a] Range of pK_a values for the conjugate acids of the leaving groups used in the correlation. [b] Subtype N2. [c] Catalyzed hydrolysis of α-sialosides with inversion of configuration. [d] Catalyzed hydrolysis of aryl β-sialosides with inversion of configuration.

Although the current study involves an artificial catalyst, which hydrolyzes unnatural β-sialosidic linkages, some of the mechanistic conclusions are remarkably similar to those from studies on natural sialidases: an observation that in itself that suggests the multi-dimensional free energy surface for sialyl transfer reactions is intrinsically flat in the vicinity of the enzymatic transition state(s). For example, the Y370G mutant *M. viridifaciens* enzyme does not need proton catalysis to hydrolyze aryl β-sialosides and the Vibrio cholerae sialidase-catalyzed reactions of α-sialosides also occur with little or no protonation of the leaving group, even for carbohydrate-based aglycones[32]. Such a conclusion may be a consequence of the active sites of sialidases containing a large number of acid/base residues, which likely results in substantial electrostatic stabilization of the various enzymatic transition states. For example, within 7.5 Å of the nucleophilic oxygen (Tyr-370) in the *M. viridifaciens* enzyme there are 5 acidic (3 Asp + 2 Glu), 4 basic (4 Arg), 3 hydroxylic (2 Ser + 1 Thr), 2 amidic (2 Asn) and 2 hydrophobic (1 Ile + 1 Phe) residues[21].

2.6 Conclusion

The Y370G inverting mutant enzyme possesses β-sialidase activity with several fluorophenyl sialosides. The rate-determining step on k_{cat}/K_m and k_{cat} involves glycosidic bond cleavage that occurs with little or no general-acid catalysis. The enzyme-catalyzed transfer reactions of sialosides, and presumably those of other ketoaldonic acid-based carbohydrates, appear to be mechanistically distinct from the majority of aldopyranoside processing enzymes that involve nucleophilic reactions at the anomeric center in that glycosidic bond cleavage, even with natural, unactivated, leaving groups, occurs in advance of rather than concerted with the associated general-acid catalytic event.

2.7 Acknowledgement

The authors thank two anonymous referees for their many helpful comments concerning this manuscript.

2.8 Supporting Information:

Brønsted Analysis of an Enzyme-Catalyzed Pseudo-Deglycosylation Reaction: Mechanism of Desialylation in Sialidases

Fahimah Shidmoossavee[a], Lydia Cheng[b], Jacqueline N. Watson[b] And Andrew J. Bennet[a]

[a]Departments of Chemistry, Simon Fraser University, 8888 University Drive, Burnaby, British Columbia, V5A 1S6, Canada
[b]Departments of Molecular Biology and Biochemistry, Simon Fraser University, 8888 University Drive, Burnaby, British Columbia, V5A 1S6, Canada

A SDS-PAGE gel for the recombinant active site domain Y370G mutant sialidase, a listing of the two Edman N-terminal sequences, and ^{1}H and ^{13}C NMR spectra for all new aryl β-D-sialosides (**1b**–**1h**). This material is available free of charge via the Internet at http://pubs.acs.org.

2.8.1 Supporting Figures

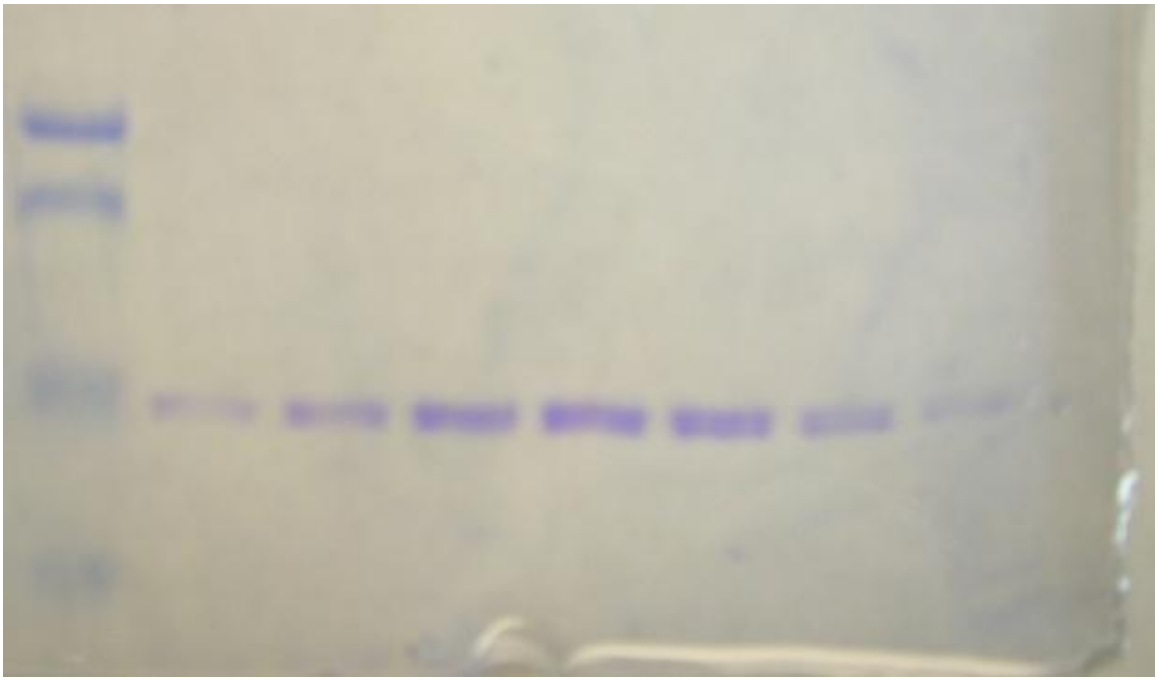

Figure 2.5. 10% SDS-PAGE Denaturing Gel Fractions after Size Exclusion Column were loaded. Left-hand channel, top to bottom, contains molecular weight markers of 104, 83, 49 and 37 KDa.

2.8.2 NMR Spectra

2-fluorophenyl β-D-*N*-acetylneuraminide (2FP-βNeuAc) (1b)

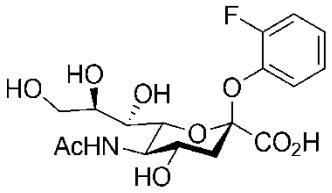

1b

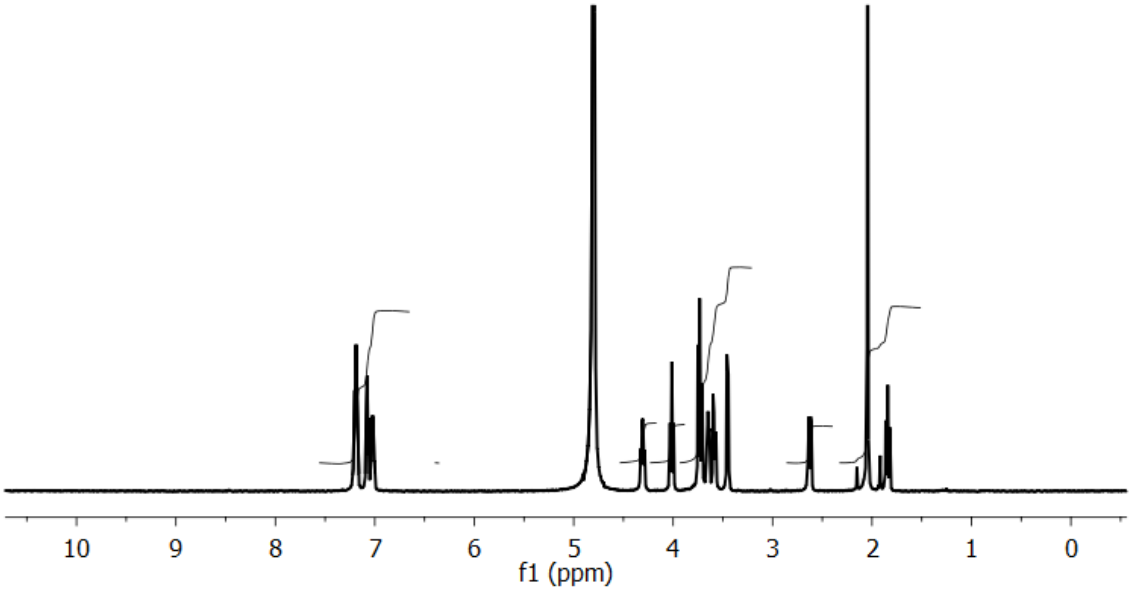

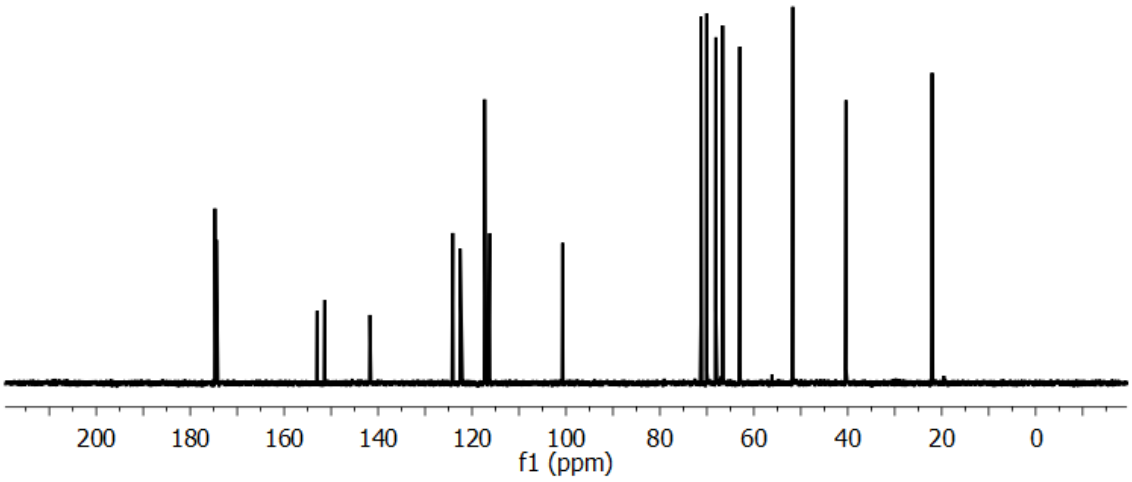

3-fluorophenyl β-D-*N*-acetylneuraminide (3FP-βNeuAc) (1c)

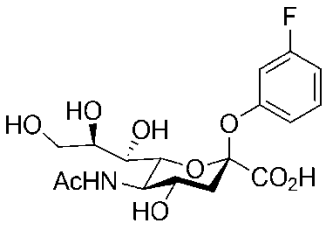

1c

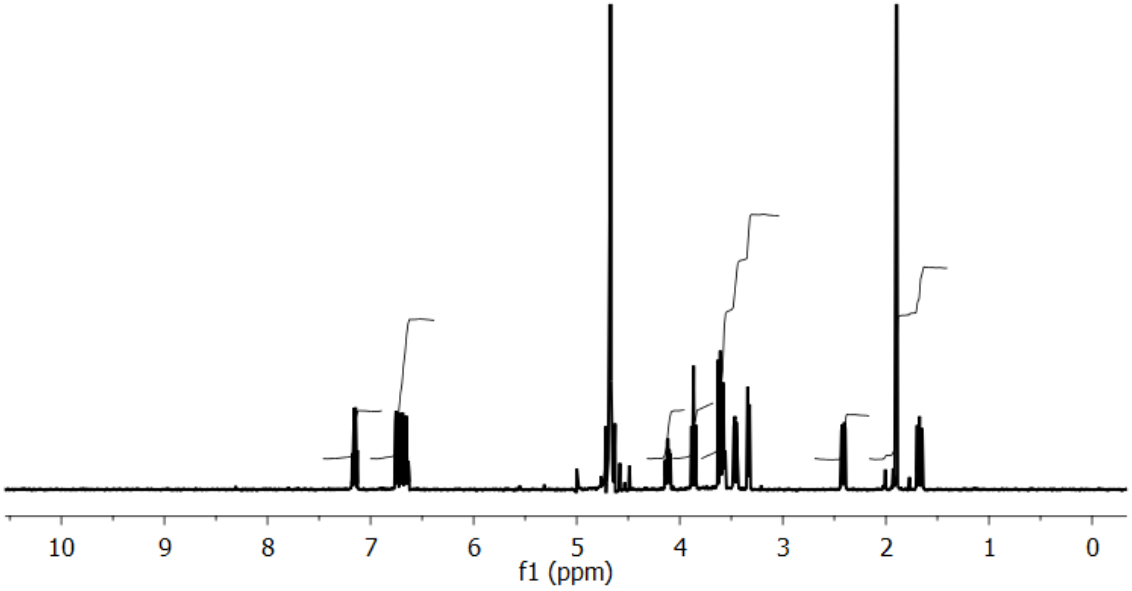

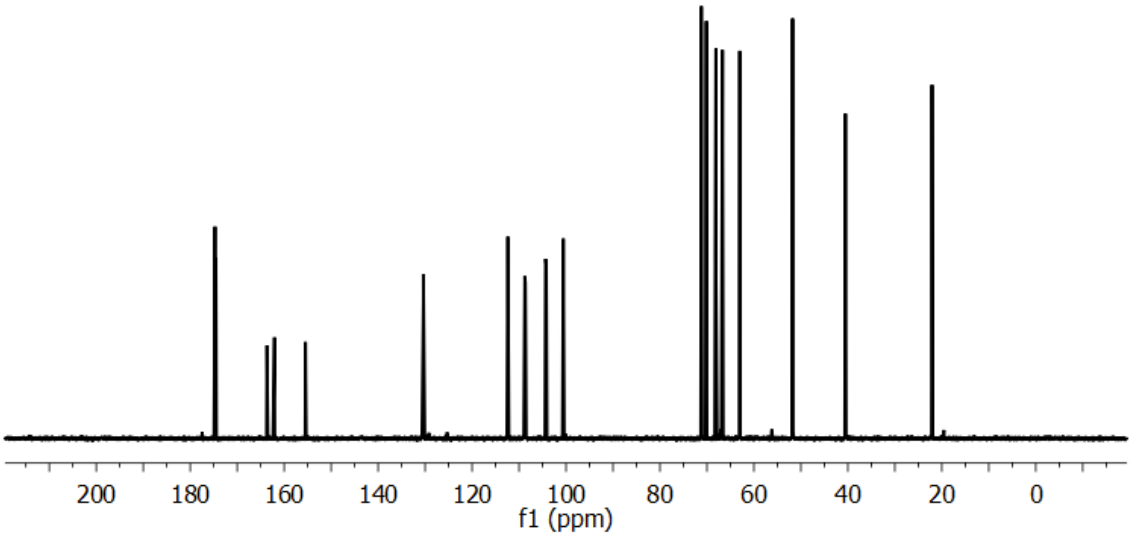

4-fluorophenyl β-D-*N*-acetylneuraminide (4FP-βNeuAc) (1d)

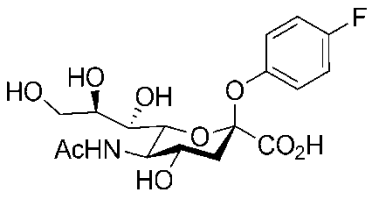

1d

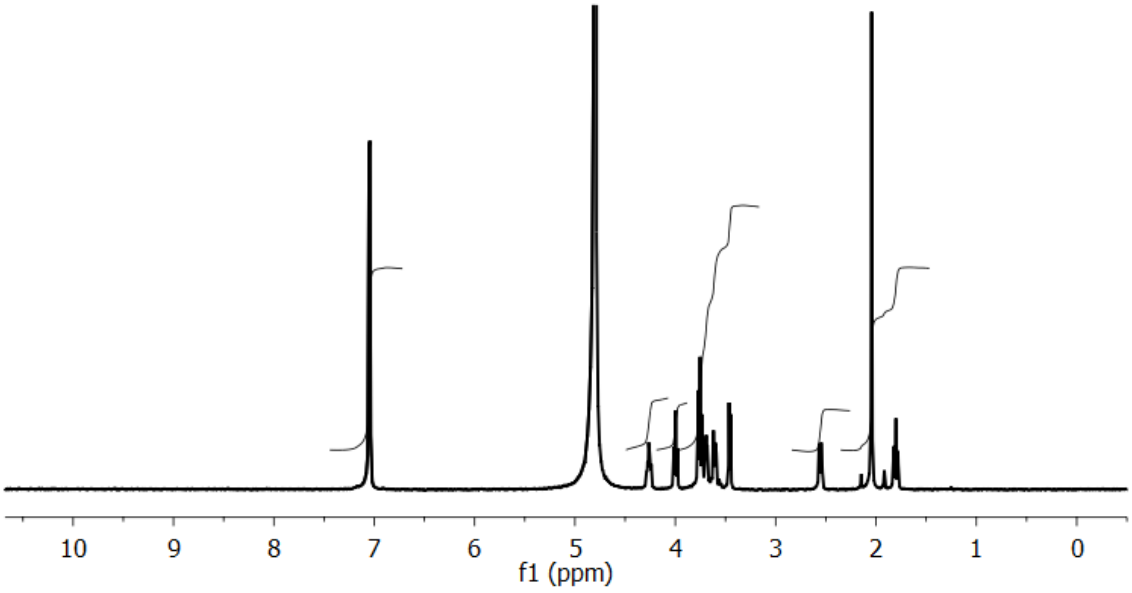

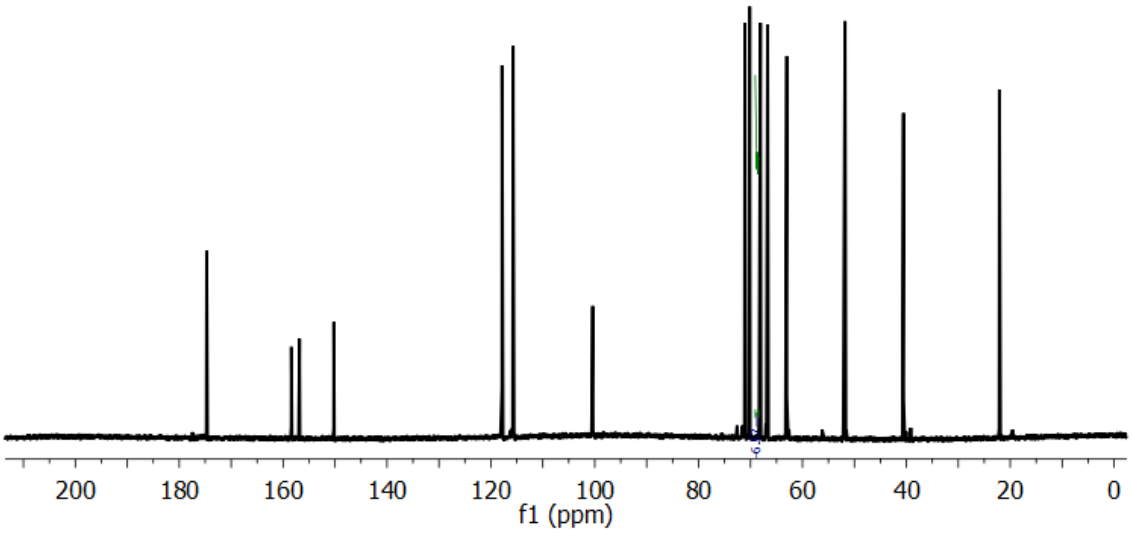

2,3-difluorophenyl β-D-*N*-acetylneuraminide (23DFP-βNeuAc) (1e)

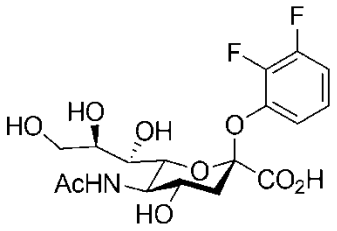

1e

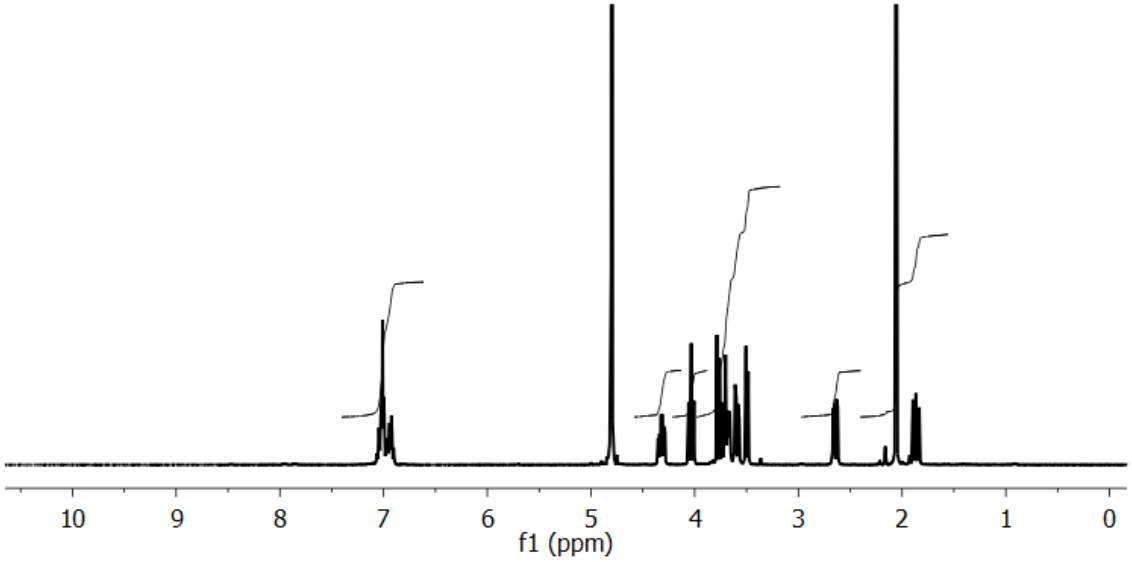

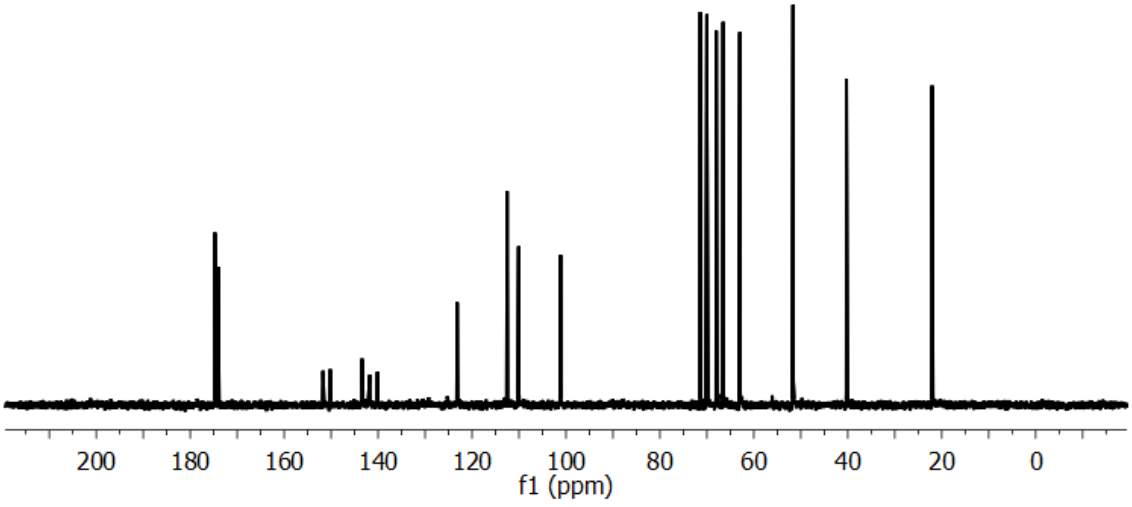

2,5-difluorophenyl β-D-*N*-acetylneuraminide (25DFP-βNeuAc) (1f)

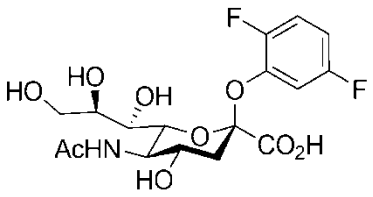

1f

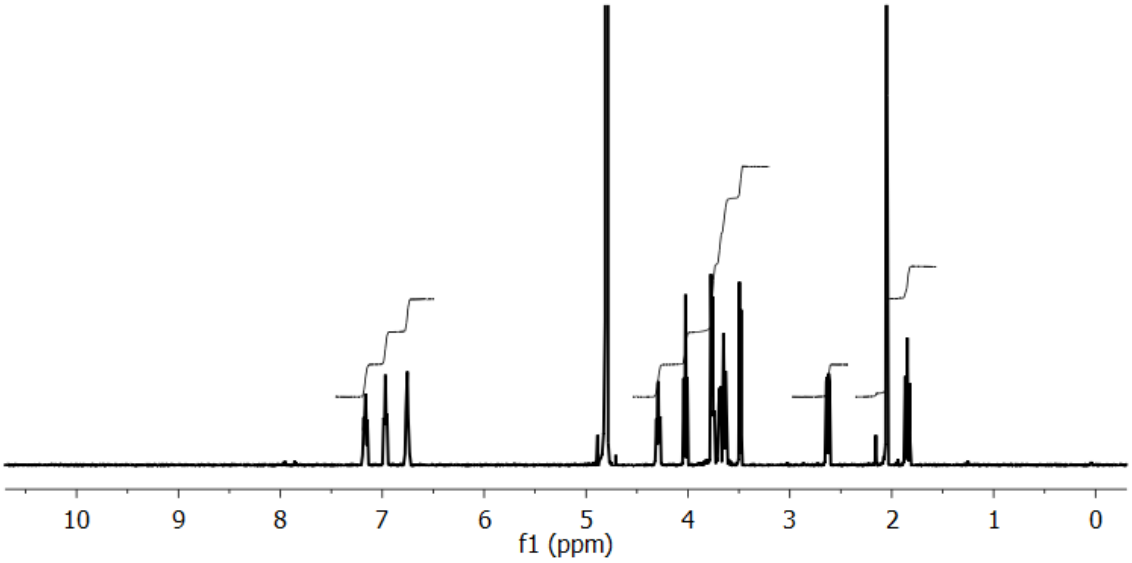

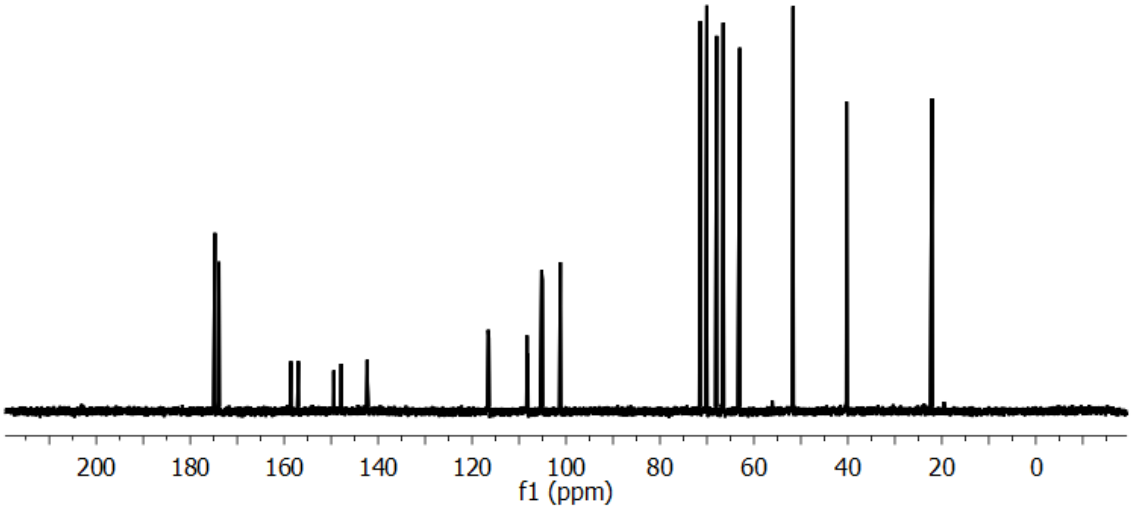

2,6-difluorophenyl β-D-*N*-acetylneuraminide (26DFP-βNeuAc) (1g)

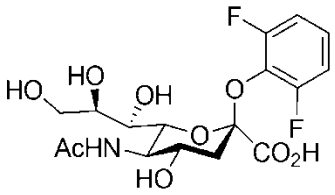

1g

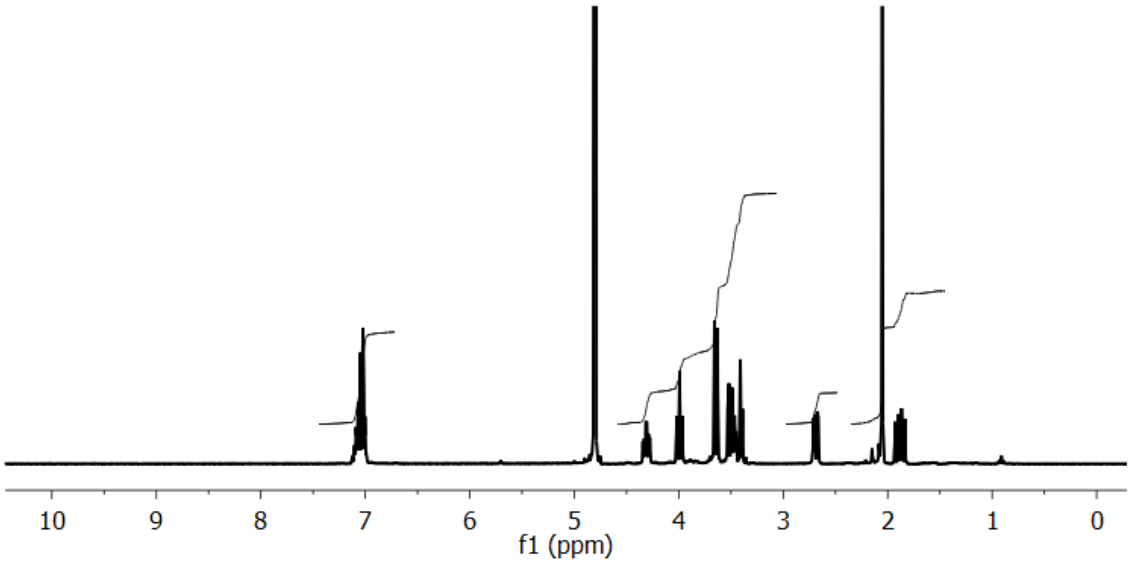

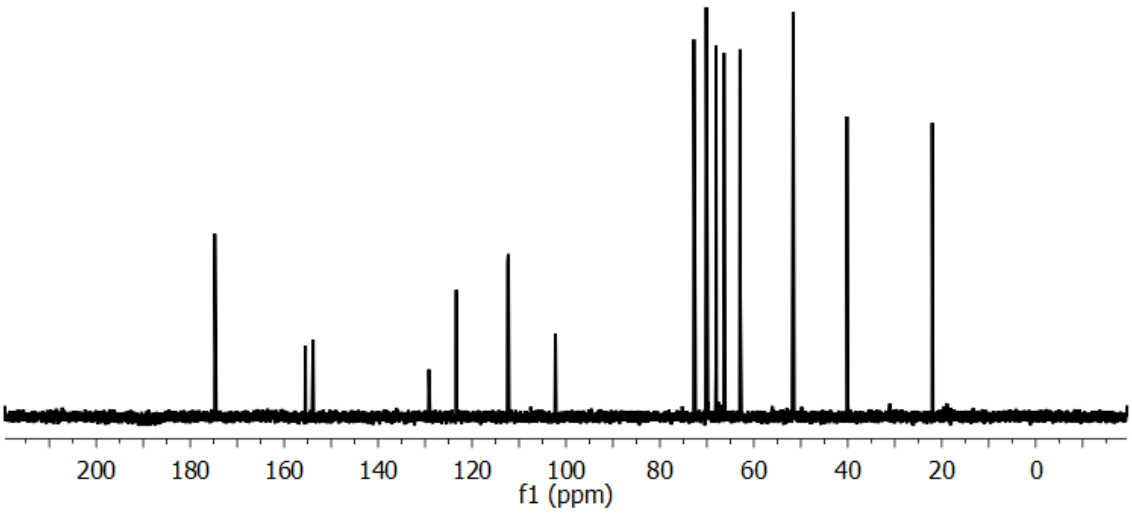

3,5-difluorophenyl β-D-*N*-acetylneuraminide (35DFP-βNeuAc) (1h)

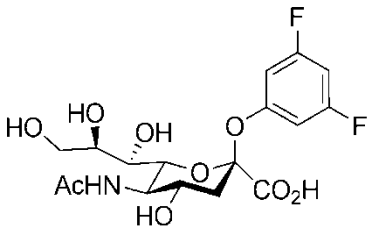

1h

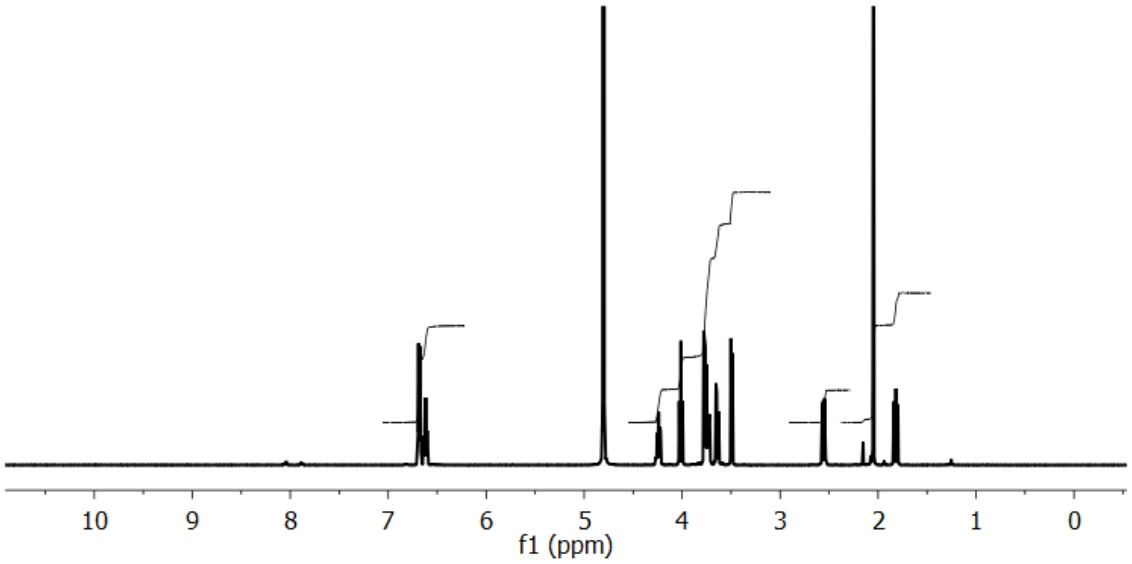

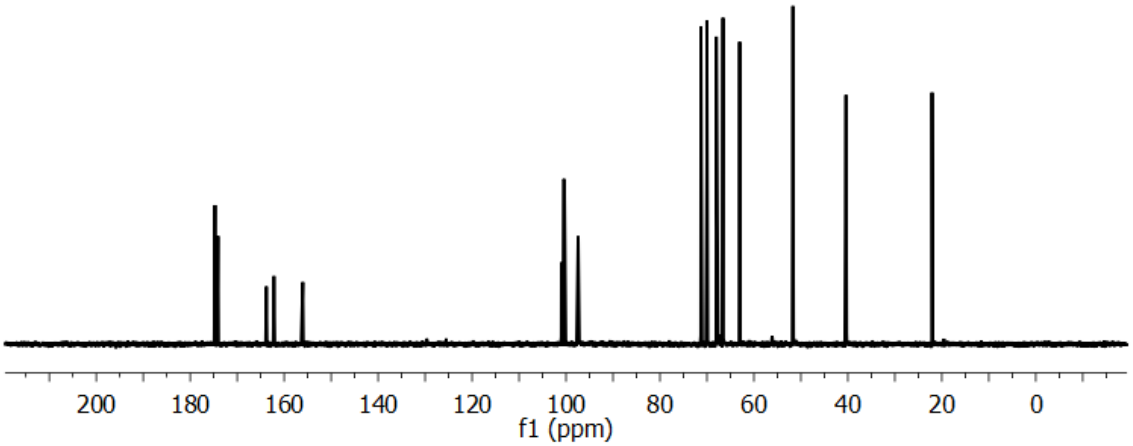

2.9 References

[1] Cantarel, B. L.; Coutinho, P. M.; Rancurel, C.; Bernard, T.; Lombard, V.; Henrissat, B. *Nucleic Acids Res* **2009**, *37*, D233.

[2] Davies, G., Sinnott, M. L., and Withers, S. G. In *Comprehensive Biological Catalysis.* ; Sinnott, M. L., Ed.; Academic Press: San Diego, 1998, p 119.

[3] Yip, V. L.; Withers, S. G. *Biochemistry* **2006**, *45*, 571.

[4] Tews, I., vanScheltinga, A. C. T., Perrakis, A., Wilson, K. S., and Dijkstra, B. W. *J Am Chem Soc* **1997**, *119*, 7954.

[5] Vocadlo, D. J., and Davies, G. J. *Curr Opin Chem Biol* **2008**, *12*, 539.

[6] Watson, J. N.; Dookhun, V.; Borgford, T. J.; Bennet, A. J. *Biochemistry* **2003**, *42*, 12682.

[7] Watts, A. G.; Oppezzo, P.; Withers, S. G.; Alzari, P. M.; Buschiazzo, A. *J Biol Chem* **2006**, *281*, 4149.

[8] Amaya, M. F., Watts, A. G., Damager, T., Wehenkel, A., Nguyen, T., Buschiazzo, A., Paris, G., Frasch, A. C., Withers, S. G., and Alzari, P. M. *Structure* **2004**, *12*, 775.

[9] Watts, A. G.; Damager, I.; Amaya, M. L.; Buschiazzo, A.; Alzari, P.; Frasch, A. C.; Withers, S. G. *J Am Chem Soc* **2003**, *125*, 7532.

[10] Watson, J. N.; Newstead, S.; Dookhun, V.; Taylor, G.; Bennet, A. J. *FEBS Lett* **2004**, *577*, 265.

[11] Lowry, T. H., and Richardson, K. S. *Mechanism and Theory in Organic Chemistry*; 3rd ed.; Harper & Row: New York, 1987.

[12] Fersht, A. R. *Enzyme Structure and Mechanism*; 2nd ed.; W.H. Freeman: New York, 1985.

[13] Banait, N. S., and Jencks, W. P. *J Am Chem Soc* **1995**, *113*, 7951.

[14] Huang, X., Surry, C., Hiebert, T., and Bennet, A. J *J Am Chem Soc* **1995**, *117*, 10614.

[15] Greig, I. R., Macauley, M. S., Williams, I. H., and Vocadlo, D. J *J Am Chem Soc* **2009**, *131*, 13415.

[16] Newstead, S.; Watson, J. N.; Knoll, T. L.; Bennet, A. J.; Taylor, G. *Biochemistry* **2005**, *44*, 9117.

[17] Watson, J. N.; Newstead, S.; Narine, A. A.; Taylor, G.; Bennet, A. J. *Chembiochem* **2005**, *6*, 1999.

[18] Watson, J. N.; Indurugalla, D.; Cheng, L. L.; Narine, A. A.; Bennet, A. J. *Biochemistry* **2006**, *45*, 13264.

[19] Dookhun, V.; Bennet, A. J. *J Am Chem Soc* **2005**, *127*, 7458.

[20] Sharma, M. N.; Eby, R. *Carbohydr Res* **1984**, *127*, 201.

[21] Gaskell, A.; Crennell, S.; Taylor, G. *Structure* **1995**, *3*, 1197.

[22] Segel, I. H. *Enzyme Kinetics: Behavior and Analysis of Rapid Equilibrium and Steady State Enzyme Systems*; Wiley: New York, 1975.

[23] Schowen, R. L. In *Isotope Effects on Enzyme-Catalyzed Reactions*; Cleland, W. W., O'Leary, M. H., Northrop, D. B., Eds.; University Park Press: Baltimore, 1977, p 64.

[24] Taylor, J. R. *An Introduction to Error Analysis: The Study of Uncertainties in Physical Measurements*; University Science Books: Mill Valley, Calif, 1982.

[25] Klepach, T.; Carmichael, I.; Serianni, A. S. *J Am Chem Soc* **2008**, *130*, 11892.

[26] Aisaka, K., Igarashi, A., and Uwajima, T. *Agric Biol Chem* **1991**, *55*, 997.

[27] Sakurada, K.; Ohta, T.; Hasegawa, M. *J Bacteriol* **1992**, *174*, 6896.

[28] Guo, X.; Sinnott, M. L. *Biochem J* **1993**, *294 (Pt 3)*, 653.

[29] Richard, J. P.; Westerfeld, J. G.; Lin, S. *Biochemistry* **1995**, *34*, 11703.

[30] Alvarez, F. J., and Schowen, R. L In *Secondary and Solvent Isotope Effects: Isotopes in Organic Chemistry*; Elsevier: Amsterdam , New York, 1987.

[31] Guo, X., Laver, W. G., Vimr, E., and Sinnott, M. L *J Am Chem Soc* **1994**, *116*, 5572.

[32] Chan, J.; Lewis, A. R.; Gilbert, M.; Karwaski, M. F.; Bennet, A. J. *Nat Chem Biol* **2010**, *6*, 405.

3 Chemical Insight into the Emergence of Influenza Virus Strains that are Resistant to Relenza

Fahimeh S. Shidmoossavee[a], *Jacqueline N. Watson*[b] *And Andrew J. Bennet*[a]

[a]Departments of Chemistry, Simon Fraser University, 8888 University Drive, Burnaby, British Columbia, V5A 1S6, Canada
[b]Departments of Molecular Biology and Biochemistry, Simon Fraser University, 8888 University Drive, Burnaby, British Columbia, V5A 1S6, Canada

This Chapter comprises the manuscript ″Chemical Insight into the Emergence of Influenza Virus Strains that are Resistant to Relenza″ written in the template for communications in Journal of American Chemical Society (JACS), and it has been submitted to JACS for publication.

Authors Contributions:

This project was designed by Prof. Andrew J. Bennet, and the author of this thesis performed all the experimental synthetic work of the compounds and the kinetic measurements. Dr. Jacqueline N. Watson cloned the genes and expressed the proteins.

3.1 Abstract

A reagent panel containing ten 4-substituted 4-nitrophenyl α-D-sialosides and a second panel of the corresponding sialic acid glycals were synthesized and used to probe the inhibition mechanism for two neuraminidases, the N2 enzyme from influenza type A virus and the enzyme from *Micromonospora viridifaciens*. For the viral enzyme the logarithm of the inhibition constant (K_i) correlated with neither the logarithm of the catalytic efficiency (k_{cat}/K_m) nor catalytic proficiency ($k_{cat}/K_m k_{un}$). This linear free energy relationship data supports the notion that these inhibitors, which include the therapeutic agent Relenza, are not transition state mimics for the enzyme-catalyzed hydrolysis reaction. Moreover, for the influenza enzyme a correlation (slope, 0.80 $\pm$ 0.08) is observed between the logarithms of the inhibition (K_i) and Michaelis (K_m) constants. We conclude that the free energy for Relenza binding to the influenza enzyme mimics the enzyme-substrate interactions at the Michaelis complex. Thus, an influenza mutational response to a 4-substituted sialic acid glycal inhibitor can weaken the interactions of the inhibitor to the viral neuraminidase without a concomitant decrease in free energy of binding for the substrate at the enzyme-catalyzed hydrolysis transition state. The current findings make it clear that new structural motifs and/or substitution patterns need to be developed in the search for a bona fide influenza viral neuraminidase transition state analog inhibitor.

3.2 Introduction

Recent reports highlight the threat of an avian influenza virus strain, such as H5N1, crossing the species barrier[1] and becoming transmissible in humans. Barring the development of new therapeutic strategies, a crossover virus such as this presents a

real threat of precipitating an influenza pandemic.[2] Current influenza therapeutics are designed to take advantage of the requirement of neuraminidase activity for viral pathogenicity.[3] Viral resistance to influenza therapeutics is an emerging medical problem, driven in part by the high mutational frequency of the virus.[2] Often, mutations that generate resistant strains[4-6] also attenuate viral infectivity.[7] However, continued selection pressure resulting from drug treatment results in permissive secondary mutations that allow the resistant virus to override the deleterious effects of the initial point mutation.[8]

An ongoing challenge to the development of therapeutic agents for treating influenza and controlling the spread of disease[3] is the design of selective inhibitors that engender a reduced risk of viral resistance. An ideal inhibitor would precisely mimic the neuraminidase-catalyzed glycosylation[9,10] or deglycosylation[11] transition state (TS). In such a case, a mutational response by the virus to a transition state analog (TSA) inhibitor that reduces binding avidity to the targeted viral neuraminidase must also, by virtue of the TS analogy, compromise the catalytic efficiency of this enzyme, resulting in reduced infectivity of the mutated strain of the influenza virus. If however, the inhibitor is not a transition state analog then a mutational response can lower the efficacy of the therapeutic without causing an obligatory decrease in the targeted enzymatic activity, a situation which permits the emergence of resistant strains and poses further risk to human health. Therefore, in order to design new influenza treatments with a reduced risk of provoking further viral resistance, it is imperative that we understand whether such inhibitors are true transition state analogs.

It is important to point out that, tight-binding inhibitors are not necessarily TSAs because binding interactions that occur in the enzyme:inhibitor complex may not replicate those at an enzymatic transition state. Once a tight-binding structural motif is

reported, its inhibitory potency is maximized by the synthesis of structures containing different functional groups, and the resultant best inhibitor is often presumed to be the best TSA. Thus, many tight-binding inhibitors are labeled as 'transition state analogues' based on chemical intuition rather than an in-depth scientific analysis. Indeed, the rapid emergence of influenza viral strains that are resistant to Relenza and possess catalytically competent mutant neuraminidases raises the question of whether this drug is a genuine transition state analogue as has often been presumed[12-14] or if its binding avidity to the viral enzyme is unrelated to the mechanism of catalysis. In order to test the presumed TS analogy for neuraminidase inhibitors like Neu2en5Ac (**2a,** Figure 3.1) and Relenza (**2h,** Figure 3.1) a detailed kinetic and theoretical analysis must be performed.

Scheme 3.1 shows the neuraminidase-catalyzed glycosylation mechanism in which the bound substrate in the accumulating Michaelis complex adopts a skew boat conformation,[11] while the pyranosyl ring conformation of the sialosyl-enzyme intermediate is a $^{2}C_{5}$ chair.[15] To understand the individual contributions to TS stabilization—knowledge that is critical for evaluating whether an inhibitor is a transition state analogue as well as for designing optimized TS mimics—a robust approach is to establish a linear free energy relationship (LFER) between catalysis and inhibitor binding.[16,17] Using this LFER method, inhibitors and corresponding substrates are systematically modified at a single position, and a comparison is made between the free energy for inhibitor binding to the enzyme (log K_i) and the free energy difference between the TSs for the first irreversible step and that for the uncatalyzed reaction (log $k_{cat}/K_m k_{un}$) for each substrate/inhibitor pair.[16,17] A correlation with a unit slope reveals that structural changes in the inhibitor parallel those at the TSs and that the core inhibitor structure is a genuine TSA.

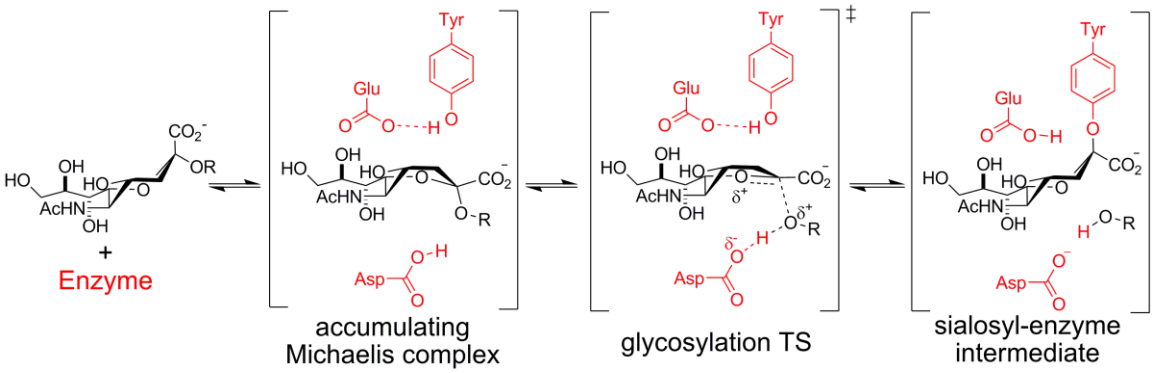

Scheme 3.1. Mechanism for the neuraminidase-catalyzed formation of the tyrosinyl bound intermediate: The key active site amino acid residues (Glu, Tyr, Asp) and the substrate are shown. The substrate is bound in a skew boat conformation and the sialosyl-enzyme intermediate is in a $^{2}C_{5}$ conformation[18]

With these factors in mind we aimed to test whether the ring geometry of these glycal inhibitors (including Neu2en5Ac **2a** and Relenza, **2h**), which are constrained by the ring double bond, orients the 4-substituent so that when bound the resultant interactions within the complex mimic those of the substrate at the glycosylation TS. We focused on these interactions because the 4-position is substituted with positively charged groups in two commercial influenza drugs Relenza (zanamivir) and Tamiflu (oseltamivir).

To perform these studies, we synthesized a panel of ten 4-nitrophenyl α-D-sialosides (**1a**: pNP-αNeu5Ac) as substrates, and the corresponding ten 4-substituted 5-acetamido-2,6-anhydro-3,5-dideoxy-D-*glycero*-D-*galacto*-non-2-enonic acids (**2a**: Neu2en5Ac) as inhibitors (Figure 3.1: **1a–j** and **2a–j**). We chose to make 4-nitrophenyl substrates because of: i) synthetic accessibility, ii) ease of monitoring kinetics, and iii) ability to measure uncatalyzed hydrolysis rate constants (k_{un}).

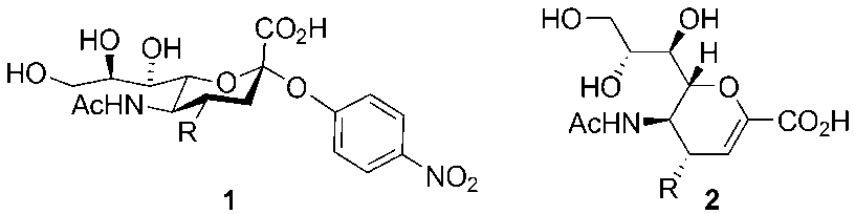

1

1a R = OH
1b R = N_3
1c R =1-triazolyl
1d R = NH_2
1e R = NHAc
1f R = NMe_2
1g R = NH^iPr
1h R = guanidino
1i R = H
1j R = OMe

2

2a R = OH
2b R = N_3
2c R =1-triazolyl
2d R = NH_2
2e R = NHAc
2f R = NMe_2
2g R = NH^iPr
2h R = guanidino
2i R = H
2j R = OMe

Figure 3.1. Synthesized substrates **1a-j** and inhibitors **2a-j**. Inhibitors Neu2en5Ac and Relenza are **2a** and **2h**, respectively.

3.3 Results and Discussion

3.3.1 Synthesis

Commercially available sialic acid (**3**) was transformed into **4**, and then converted into oxazoline (**5**) and azido (**6**) using known procedures (Scheme 3.2).[19] Reduction of glycal **6** gave **7**, which we used to make protected **2e–h** by: i) acetylation, **2e**, reductive amination, **2f** and **2g**, and iii) guanidylation, **2h**. Also, azide **6** underwent a [2,3]-cycloaddition with propynoic acid, which after decarboxylation gave protected **2c**. Selective hydrogenation of oxazoline **5** gave access to glycal **2i**, while selective methylation of **10** gave the 4-methoxy compounds. Reaction of **8**, formed by HCl addition to **6**,[19] with 4-nitrophenol gave glycoside **9**. Using identical reactions to those that converted **6** into protected **2b–h**; **9** was turned into protected *p*NP-*α*Neu5Ac analogs **1b–h**. Hydrogenation of oxazoline **5** gave access to 4-deoxy compound **1i**, while careful methylation of **10** (made in two steps from sialic acid), allowed synthesis of 4-methoxy

analog **1j**. Lastly, all protecting groups were removed using routine protocols to give substrates **1a–j** and inhibitors **2a–j**.

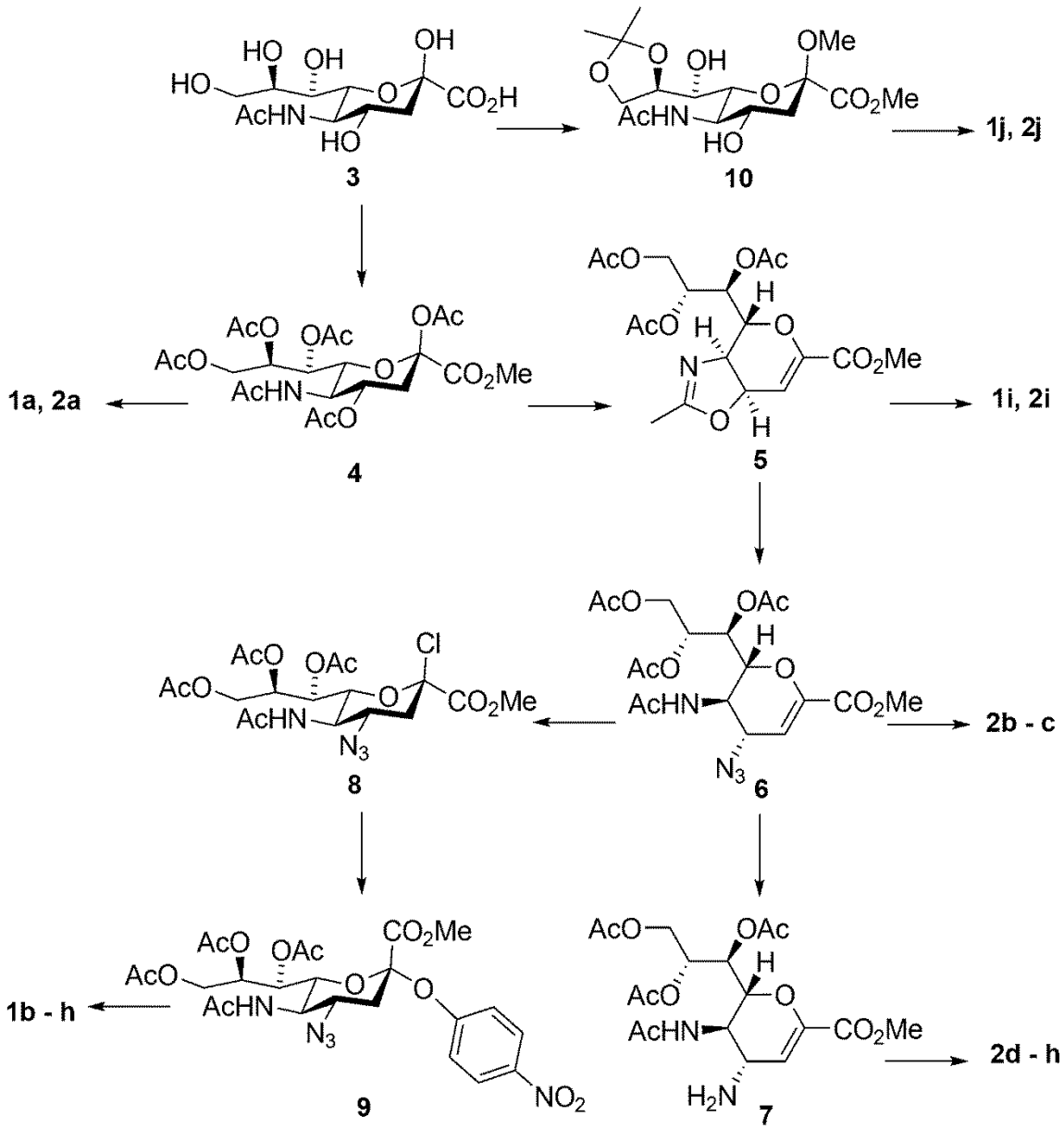

Scheme 3.2. Generalized synthetic routes to substrates **1a-j** and inhibitors **2a-j**. Reagents and yields for all steps are shown in Schemes 3.3-3.6 (Supporting Information).

3.3.2 Kinetics

In order to resolve whether good inhibitors are TSAs equivalent alterations are made to a panel of substrates and inhibitors. If these modifications have identical effects on enzymatic catalysis and inhibition, then a LFER with a slope of one will be measured (Eq 3.1)[17] and the inhibitor can be classified as a TSA.[17,20] In this equation, δ is the proportionality between K_i and ($K_m k_{un}/k_{cat}$) because any TSA is an imperfect mimic of the transition state.[17]

$$\log(K_i) = \log(K_m k_{un}/k_{cat}) + \delta \quad \text{(Eq 3.1)}$$

For a linear relationship to be valid between log K_i and log K_m/k_{cat} it is important that: (i) enzymatic kinetic parameters are measured under conditions in which glycosylation is kinetically significant, which in these cases occurs at non-optimal pH values,[21,22] thus, we monitored all kinetic parameters at a pH value of 8.03, (ii) the rate constants for the spontaneous, uncatalyzed, hydrolyses (k_{un}) are identical for all substrates, and (iii) the inhibitors are kinetically stable. Although glycals are known to undergo neuraminidase-catalyzed hydration these reactions are ~10^7–fold slower than hydrolysis.[23,24]

We conclude that our results, which are plotted in Figure 3.4 (Supporting Information), show that log(K_m/k_{cat}) correlates with log(K_i) for neither the influenza N2 (panel **a**) nor the *Mv*NA (panel **b**) enzymes. However, as noted above it is assumed that k_{un} is constant for all substrates. Consequently, we measured the rate constants for the uncatalyzed hydrolyses of **1a–j** (k_{un}) in order to determine whether the lack of correlation was caused by different intrinsic reactivities of the ten substrates. Notably, the spontaneous hydrolysis rate constants measured for the 4-deoxy (**1h**) through triazolyl

(**1c**) substrates span more than two orders of magnitude (Table 3.4, supporting information). The resultant plots of $\log(K_m \bullet k_{un}/k_{cat})$ versus $\log(K_i)$ are shown in Figure 3.2.

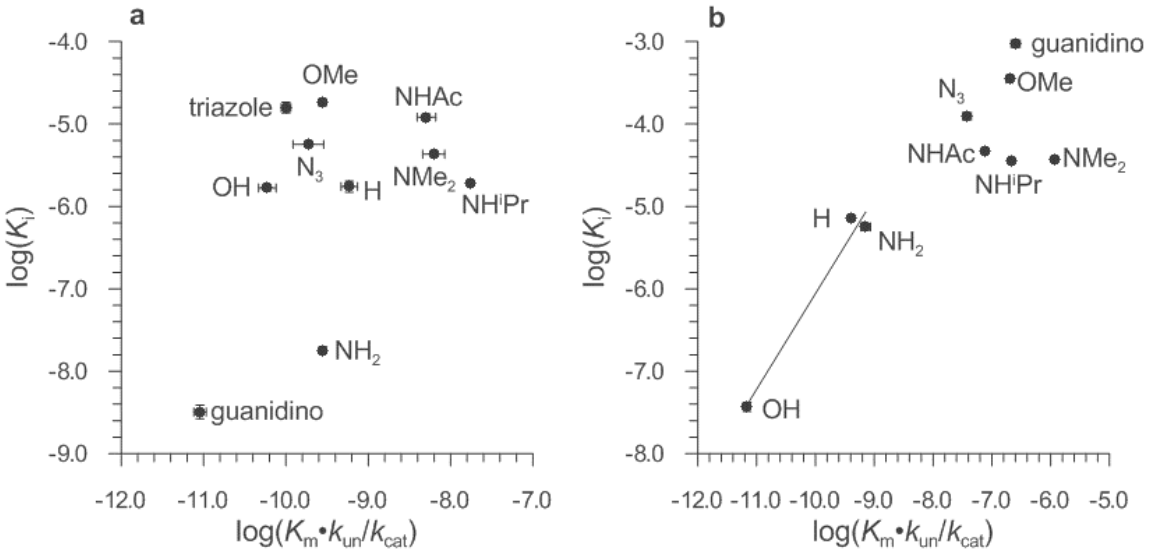

Figure 3.2. Neuraminidases: Linear free energy correlations. Plots of $\log(K_m \bullet k_{un}/k_{cat})$ for neuraminidase-catalyzed hydrolysis of pNP 4-substituted-sialosides (**1a–j**) versus $\log(K_i)$ for the corresponding glycal inhibitor (**2a–j**). Panel **a** displays data for the influenza N2 enzyme while panel **b** shows data for the *M. viridifaciens* neuraminidase. Error bars are shown or are encompassed within the symbol. The line shown in panel b is the best linear fit for the three smallest substituents (slope, 1.16 ± 0.18).

We are forced to conclude, contrary to the commonly held assumption, that sialic acid glycals, including Neu2en5Ac (**2a**) and Relenza (**2h**), are not TSA inhibitors for the influenza A N2 enzyme. That is, although the anomeric carbon of the substrate must be undergoing rehybridization towards an sp^2–like center at the glycosylation TS (Scheme 3.1) this does not necessarily enforce glycal inhibitors, which have sp^2 carbons at this position, to adopt a comparable ring conformation when bound to the enzyme (Figure 3.5, Supporting Information). Indeed, the characteristic increase in inhibition (lower K_i) with only a moderate increase in catalytic efficiency (k_{cat}/K_m) for the guanidino compounds (**1h** and **2h**) displays the hallmarks of nonproductive binding.[25] That is, during the catalytic cycle a component of free energy for **1h** binding to the enzyme is

expressed at the Michaelis complex but not at the hydrolytic TS. Such nonproductive binding in which the inhibitor binding mimics the enzyme-substrate interactions in the Michaelis complex, should give a correlation between log(K_i) and log(K_m).[17] A plot of log(K_m) versus log(K_i) for the influenza N2 data (Figure 3.2) gives a slope of 0.80 ± 0.08 (after omitting the point for the *N-iso*propyl substituent).

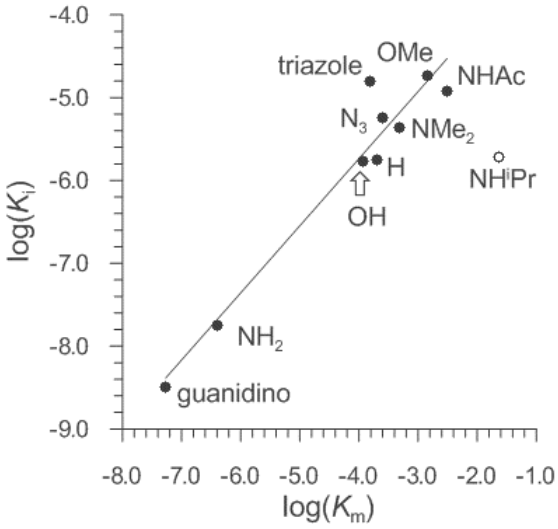

Figure 3.3. Plot of log(K_m) for the influenza catalyzed hydrolysis of pNP 4-substituted-sialosides versus log(K_i) of the correspond glycal inhibitor; the line represents the best linear fit (slope, 0.80 ± 0.08) to the data excluding that for 4-*N-iso*propyl compounds (hollow circle).

We conclude that Neu2en5Ac derivatives (**2a–j**), including Relenza **2h**, are potent ground state analog inhibitors of influenza N2 neuraminidase in which the constrained geometry of the glycal places the 4-substitutent so that its interactions with the enzyme mimic those in the Michaelis complex.

In contrast, the data for the *M. viridifaciens* neuraminidase (*Mv*NA) suggests that log(K_m•k_{un}/k_{cat}) and log(K_i) are correlated, albeit only for the three smallest substituents (Figure 3.2, panel **b**). Given that in the structure of this enzyme complexed with **2a**[26] the C4-OH group of Neu2en5Ac interacts strongly with an arginine residue (O–N distance is

~3Å) it is not surprising that interactions between substrates/inhibitors and *Mv*NA only exhibit TS analogy for small substituents. Of note, the influenza N2 and *Mv*NA enzymes are from different glycosyl hydrolase (GH) families,[27] (GH34 and GH33, respectively). It is therefore not too surprising that the glycosylation TSs for these two enzymes are different.

Importantly, it has been proposed, based on molecular modeling studies, that the Michaelis complex involving an influenza type A N1 enzyme and a 3- or 6-sialyllactoside substrate places the sugar ring into a $^{4}S_{2}$ or $B_{2,5}$ conformation, respectively.[28] Whereas, Chan et al used kinetic isotope effect (KIE) measurements to propose a $^{6}S_{2}$ skew-boat[11] distortion of the substrate in the accumulating Michaelis complex for the *Mv*NA-catalyzed reaction. Although deglycosylation is partly rate-limiting for influenza N2,[21,22] similar KIE experiments suggest that the Michaelis complex contains a distorted substrate.[21] The four low energy conformations for the glycal inhibitors (**2a**–**j**) are two half-chair ($^{6}H_{5}$ and $^{5}H_{6}$) and two boat ($^{4,O}B$ and $B_{4,O}$) conformations (Figure 3.5, Supporting Information). We suggest that for the influenza enzyme the glycal inhibitor binds in a $^{6}H_{5}$ half-chair conformation and that the interactions of the 4-substituent with the enzyme gives rise to no stabilization of the glycosylation TS as the Michaelis complex undergoes reaction to give the enzyme-bound intermediate in a $^{2}C_{5}$ chair conformation.[15]

The above analysis also explains reactivity differences for sialosyl-enzyme covalent intermediates formed between a series of influenza viral enzymes and 4-substituted 2,3-difluorosialic acids.[29] That is, the fluorinated sialosyl-enzyme intermediates (see Scheme 3.1 for the generic structure) containing either a guanidino or amino group at C-4 undergo deglycosylation at greatly reduced rates compared to the 4-OH derivative. This effect likely arises from nonproductive binding of the 4-substituent that is expressed at the enzyme-bound intermediate but not at the deglycosylation TS,

thus resulting in the sialosyl-enzyme intermediate being longer lived for the positively charged inhibitors.[29]

In conclusion, we show that, using rigorous LFER experiments, the hypothesis that Relenza and Neu2en5Ac are TSA inhibitors for influenza N2 neuraminidase, which is based on a presumed similarity between the glycal inhibitor and the oxacarbenium ion-like TS for enzymatic hydrolysis, is incorrect. Moreover, the influenza N2 enzyme and MvNA have different glycosylation TSs and we suggest an earlier TS for MvNA-catalyzed hydrolysis (less C–O bond cleavage), which is closer in structure to the Michaelis complex than is the influenza N2 TS. This difference in TS structure results in the 4-substituents of the glycal (Neu2en5Ac and Relenza) when bound to influenza N2 mimicking the interactions present in the Michaelis complex and not those at the glycosylation TS. That the addition of a guanidino group to the glycal results serendipitously in a dramatic increase in binding potency without a concomitant increase in stabilization of the glycosylation TS is ultimately the root cause for the ease with which the influenza virus generates resistant strains. Accordingly, resistant strains possess neuraminidases that have a reduced binding avidity to Relenza but are still active catalysts. Clearly, new structural motifs and/or substitution patterns need to be developed in the search for bona fide influenza neuraminidase TSAs. Such inhibitors should be less likely to provoke rapid emergence of resistant strains and their associated risk to human health.

3.4 Acknowledgement

This work was aided by a Natural Sciences and Engineering Re-search Council of Canada Discovery grant to AJB (121348-2007).

3.5 Supporting Information

Chemical Insight into the Emergence of Influenza Virus Strains that are Resistant to Relenza

Fahimah Shidmoossavee[a], *Jacqueline N. Watson*[b] *And Andrew J. Bennet*[a]

[a]Departments of Chemistry, Simon Fraser University, 8888 University Drive, Burnaby, British Columbia, V5A 1S6, Canada
[b]Departments of Molecular Biology and Biochemistry, Simon Fraser University, 8888 University Drive, Burnaby, British Columbia, V5A 1S6, Canada

3.5.1 Synthetic Experimental

3.5.1.1 General Information

All chemicals were of analytical grade or better and were purchased from Sigma-Aldrich unless noted otherwise. 4-Nitrophenyl 5-acetamido-2,6-anhydro-3,5-dideoxy-D-*glycero*-α-D-*galacto*-non-2-ulopyranosylonic acid, also known as *p*NP-α-Neu5Ac, and 5-acetamido-2,6-anhydro-3,5-dideoxy-D-*glycero*-D-*galacto*-non-2-enonic acid (Neu2en5Ac, which is also known as DANA) were made by following published procedures[30,31]. 4-Methylumbelliferyl 5-acetamido-2,6-anhydro-3,5-dideoxy-D-*glycero*-α-D-*galacto*-non-2-ulopyranosylonic acid was purchased from Sigma-Aldrich. ^{1}H- and ^{13}C-NMR spectra were acquired on a Bruker 600 MHz spectrometer, and chemical shifts are reported in parts per million and coupling constants (*J*) are given in hertz. Melting points were determined on a MPA100—automated melting point system. Optical rotations were measured on a Perkin-Elmer 341 polarimeter and are reported in units of deg cm^2g^{-1} (concentrations reported in units of g per 100 mL).

3.5.1.2 Synthesis and Characterization of Intermediates

2-Methyl-4,5-dihydro-(methyl (7,8,9-tri-*O*-acetyl-2,6-anhydro-3,4,5-trideoxy-D-*glycero*-D-*talo*-non-2-en)onate)[5,4-d]-1,3-oxazole (5)[32]

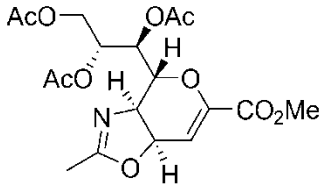

5

To a solution of fully protected sialic acid 4 (40 g, 75 mmol) in warm (40 °C) ethyl acetate (200 mL) trimethylsilyl trifluoromethanesulfonate (42 mL, 232 mmol) was added dropwise, over 10 min, under a nitrogen atmosphere as the solution was being cooled to 30 °C. After the addition was complete, the reaction mixture was warmed to

approximately 50 °C with stirring. After 3 h at this temperature the reaction mixture was poured into a vigorously stirred ice-cold mixture of saturated sodium bicarbonate (200 mL) and solid sodium bicarbonate (55 g). The resultant solution was filtered after 10 min, and the aqueous layer was separated and extracted with ethyl acetate (2 × 100 mL). The combined organic layers were then washed with brine (100 mL) and dried over sodium sulphate. The resulting solution was then concentrated under reduced pressure and the remaining residue was purified by column chromatography eluting with chloroform/acetone (3:1 v/v) to give a foamy solid (26 g, 83% yield); Mpt = 89–90 °C, $[\alpha]^{20}_{D}$ = –10.4 (c = 1.25, DMSO); ^{1}H NMR (600 MHz, $CDCl_3$): δ: 1.98, 2.03, 2.04, 2.13 (4 × s, 12 H, CH_3, 3 × OAc and oxazoline Me), 3.41 (dd, 1H, $J_{6,5}$= 10.1, $J_{6,7}$ = 2. 6, H-6), 3.79 (s, 3 H, OCH_3), 3.93 (m, 1 H, H-5), 4.20 (dd, 1 H, $J_{9',9}$ = 12.5, $J_{9',8}$ = 6.4, H-9´), 4.58 (dd, 1 H, $J_{9,9'}$ = 12.5, $J_{9,8}$ = 2.6, H-9), 4.80 (dd, 1 H, $J_{4,3}$ = 4.0, $J_{4,5}$ = 8.6, H-4), 5.42 (td, 1 H, $J_{8,9'}$ = 6.2, $J_{8,7}$ = 6.2, $J_{8,9}$ = 2.6, H-8), 5.61 (dd, 1 H, $J_{7,8}$ = 6.0, $J_{7,6}$ = 2.6, H-7), 6.36 (d, 1 H, $J_{3,4}$ = 4.0, H-3); ^{13}C NMR (150 MHz, $CDCl_3$) δ: 14.40, 20.86, 21.02, 21.09 (4 × CH_3), 52.79 (OCH_3), 62.22 (C-9), 62.27 (C-5), 69.06 (C-7), 79.51 (C-8), 72.48 (C-4), 76.97 (C-6), 107.80 (C-3), 147.38 (C-2- oxazole), 162.11 (C-2), 167.43 (C-1), 169.82, 170.04, 170.90 (3 × C=O). HRMS-FAB (*m*/*z*): [M + Na^+] calcd for $C_{18}H_{23}NO_{10}$, 436.1220; found, 436.1212

Methyl 5-acetamido-7,8,9-tri-*O*-acetyl-2,6-anhydro-4-azido-3,4,5-trideoxy-D-*glycero*-D-*galacto*-non-2-enonate (6)[32]

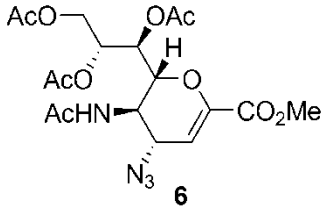

6

Trimethylsilyl azide (13 mL, 91 mmol) was added to a solution of oxazoline **5** (25 g, 60 mmol) in dry *tert*-butanol (200 mL) that was maintained under a nitrogen atmosphere. The reaction mixture was stirred at 80 °C for 12 h while a condenser circulating hot water (60 ºC) was used to prevent hydrazoic acid from condensing. After being cooled to room temperature, aqueous sodium nitrite (5.36 g in 26 mL) was added. Hydrochloric acid (6 M) was added dropwise to the mixture until effervescence has ceased. The reaction mixture was then extracted with ethyl acetate (130 mL) and water (130 mL). The organic layer was separated and washed with water (2 × 200 mL). The combined aqueous layers were extracted with ethyl acetate (2 × 60 mL) and the combined organic layers were then washed with aqueous $NaHCO_3$ (6%, 130 mL) and brine (130 mL) and dried over sodium sulphate. The resulting solution was concentrated to dryness under reduced pressure to give a foamy solid (20 g, 73% yield); Mpt = 91–92 °C, $[\alpha]^{20}_D$ = +81.6 (c = 0.54, CH_2Cl_2); ^{1}H NMR (600 MHz, $CDCl_3$) δ: 1.98, 2.03, 2.04, 2.11 (s, 12 H, CH_3), 3.78 (s, 3 H, $COOCH_3$), 3.82 (m, 1 H, H-5), 4.15 (dd, 1 H, $J_{9',9}$ = 12.4, $J_{9',8}$ = 6.6, H-9), 4.46 (dd, 1 H, $J_{4,5}$ = 8.7, $J_{4,3}$ = 2.8, H-4), 4.49 (dd, 1 H, $J_{6,5}$ = 9.9, $J_{6,7}$ = 2.5, H-6), 4.59 (dd, 1 H, $J_{9,9'}$ = 12.5, $J_{9,8}$ = 2.8, H-9), 5.31 (m, 1 H, H-8), 5.43 (dd, 1 H, $J_{7,8}$ = 5.5, $J_{7,6}$ = 2.5, H-7), 5.77 (d, 1 H, $J_{NH,5}$ = 8.7, NH), 5.95 (d, 1 H, $J_{3,4}$ = 2.8, H-3); ^{13}C NMR (150 MHz, $CDCl_3$) δ: 20.96, 21.00, 21.10, 23.59 (4 × CH_3), 48.99 (C-5), 52.83 (OCH_3), 57.65 (C-4), 62.15 (C-9), 67.91 (C-7), 70.80 (C-8), 75.81 (C-6), 107.68 (C-3), 145.34 (C-2), 161.70 (C-1), 170.27, 170.62, 170.80, 170.82 (4 × C=O). HRMS-FAB (*m*/*z*): [M +

Na^+] calcd for $C_{18}H_{24}N_4O_{10}$, 479.1390; found, 479.1376.

Methyl 5-acetamido-7,8,9-tri-*O*-acetyl-4-amino-2,6-anhydro-3,4,5-trideoxy-D-*glycero*-D-*galacto*-non-2-enonate (7)

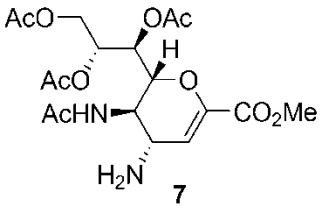

7

To a solution of azide **6** (3 g, 6.57 mmol) in THF (30 mL) triphenylphosphine (2 g, 7.62 mmol) was added and the resulting solution was stirred at rt for 12 h. Subsequently, water (6 mL) was added and the solution was stirred at rt for another 24 h. The reaction mixture was then concentrated and extracted with ethyl acetate (300 mL). The organic layer was dried over Na_2SO_4 and the solvent was removed under reduced pressure to obtain a yellow syrup. Purification involved column chromatography using ethyl acetate as the first eluent followed by ethyl acetate/methanol/water (10:2:1 v/v/v) to afford a yellow powder (2.26 g, 80% yield). Mpt = 130–131 °C; $[\alpha]^{20}_D$ = +62.1 (c = 0.46, CH_2Cl_2); ^{1}H NMR (600 MHz, $CDCl_3$) δ: 1.97, 2.03, 2.03, 2.09 (4 × s, 12 H, CH_3), 3.54 (m, 1 H, H-4), 3.76 (s, 3 H, OCH_3), 3.88 (q, 1 H, $J_{5,4}$ = $J_{5,NH}$ = 9.3, $J_{5,6}$ = 9.4, H-5), 4.16 (dd, 1 H, $J_{9',9}$ = 12.4, $J_{9',8}$ = 7.2, H-9′), 4.23 (dd, 1 H, $J_{6,5}$ = 9.7, $J_{6,7}$ = 2.7, H-6), 4.67 (dd, 1 H, $J_{9,9'}$ = 12.4, $J_{9,8}$ = 2.9, H-9), 5.30 (ddd, 1 H, $J_{8,9}$ = 2.8, $J_{8,9'}$ = 7.4, $J_{8,7}$ = 4.6, H-8), 5.48 (dd, 1 H, $J_{7,8}$ = 4.6, $J_{7,6}$ = 2.7, H-7), 5.62 (d, 1 H, $J_{NH,5}$ = 9.0, NH), 5.97 (d, 1 H, $J_{3,4}$ = 2.6, H-3). ^{13}C NMR (150 MHz, $CDCl_3$) δ: 21.19, 21.22, 21.35, 23.87 (4 × C, CH_3), 51.04 (C-4), 51.27 (C-5), 52.82 (OCH_3), 62.54 (C-9), 68.39 (C-7), 71.75 (C-8), 114.28 (C-3), 143.70 (C-2), 162.56 (C-1), 170.74, 171.06, 171.11 (4 × C=O). HRMS-FAB (*m*/*z*): [M + Na^+] calcd for $C_{18}H_{26}N_2O_{10}$, 453.1485; found, 453.1467.

Methyl 5-acetamido-7,8,9-tri-*O*-acetyl-2,6-anhydro-3,4,5-trideoxy-4-(1-triazolyl)-D-*glycero*-D-*galacto*-non-2-enonate (1S)

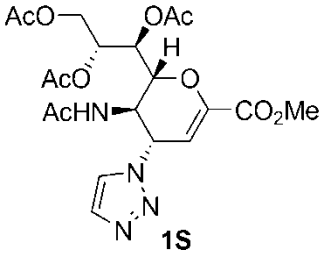

1S

Propynoic acid (0.35 mL, 5.66 mmol) was added to a solution of azide **6** (500 mg, 1.16 mmol) in toluene (3 mL) and the resulting solution was heated to reflux while being maintained under a nitrogen atmosphere for 2 h. The solvent was then evaporated under reduced pressure to give a yellow oil that was crystallized from ethyl acetate and diethyl ether to afford the triazole carboxylic acid as a white powder. This material was decarboxylated by heating, under vacuum, to its melting point in a 50 mL round bottomed flask for 1 h. The resultant brown residue was purified by column chromatography (ethyl acetate/methanol 15:1 v/v) to give a white powder (200 mg, 42% yield). Mpt = 110–111 °C; $[\alpha]^{20}_{D}$ = +276.6 (c = 0.047, CH_2Cl_2); ^{1}H NMR (600 MHz, $CDCl_3$) δ: 1.84, 2.04, 2.07, 2.07 (4 × s, 12 H, CH_3), 3.82 (s, 3 H, OCH_3), 4.17–4.24 (m, 2 H, H-5 and H-9´), 4.65 (dd, 1 H, $J_{9,9'}$ = 12.5, $J_{9,8}$ = 2.6, H-9), 4.77 (dd, 1 H, $J_{6,5}$ = 10.6, $J_{6,7}$ = 1.7, H-6), 5.38 (td, 1 H, $J_{8,9}$ = $J_{8,7}$ = 6.5, $J_{8,9'}$ = 2.6, H-8), 5.49 (dd, 1 H, $J_{7,8}$ = 5.7, $J_{7,6}$ = 1.8, H-7), 5.89 (dd, 1 H, $J_{4,5}$ = 10.0, $J_{4,3}$ = 2.4, H-4), 6.03 (d, 1 H, $J_{3,4}$ = 2.4, H-3), 6.12 (d, 1 H, $J_{NH,5}$ = 8.8, NH), 7.63 (d, 1 H, $J_{5',4'}$ = 0.9, H-4´-triazole), 7.68 (d, 1 H, $J_{4'5'}$ = 0.7, H-5´-triazole). ^{13}C NMR (150 MHz, $CDCl_3$) δ: 20.81, 20.83, 20.99, 23.11 (4 × C, CH_3), 49.15 (C-5), 52.81 (OCH_3), 57.56 (C-4), 62.06 (C-9), 67.76 (C-7), 70.65 (C-8), 76.27 (C-6), 107.02 (C-3), 122.60 (C-5´-triazole), 134.28 (C-4´-triazole), 145.97 (C-2), 161.31 (C-1), 170.16, 170.31, 170.73, 170.88 (4 × C=O). HRMS-FAB (*m*/*z*): [M + Na^+] calcd for $C_{20}H_{26}N_4O_{10}$, 505.1547; found, 505.1524.

Methyl 4,5-diacetamido-7,8,9-tri-*O*-acetyl-2,6-anhydro-3,4,5-trideoxy-D-*glycero*-D-*galacto*-non-2-enonate (2S)

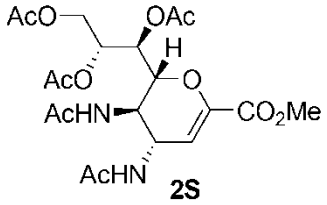

2S

To a solution of amine **7** (114 mg, 0.265 mmol) in CH_2Cl_2 (4 mL) were added acetic anhydride (0.5 mL, 5.30 mmol) and triethylamine (0.055 mL, 0.397 mmol), and the resulting solution was stirred at rt for 1 h. The resulting mixture was washed with saturated aqueous $NaHCO_3$ (4 × 4 mL), water (2 mL), brine (2 mL) and dried over Na_2SO_4. After evaporating the solvent under reduced pressure, a foamy solid was obtained (100 mg, 80% yield). Mpt 70–71 °C; $[\alpha]^{20}_D$ = +44.3 (c = 0.36, CH_2Cl_2); ^{1}H NMR (600 MHz, $CDCl_3$) δ: 1.88, 1.94, 2.04, 2.05, 2.07 (5 × s, 15 H, CH_3), 3.76 (s, 1 H, OCH_3), 4.15 (dd, 1 H, $J_{9',9}$ = 12.4, $J_{9',8}$ = 7.4, H-9´), 4.20 (q, 1 H, $J_{5,4}$ = $J_{5,NH}$ = 9.8, $J_{5,6}$ = 9.9, H-5), 4.26 (dd, 1 H, $J_{6,5}$ = 10.1, $J_{6,7}$ =2.3, H-6), 4.67 (dd, 1 H, $J_{9,9'}$ =12.4, $J_{9,8}$ = 2.7, H-9), 4.78 (td, 1 H, $J_{4,NH}$ = $J_{4,5}$ = 9.2, $J_{4,3}$ = 2.5, H-4), 5.28 (ddd, 1 H, $J_{8,9'}$ = 7.4, $J_{8,9}$ = 2.7, $J_{8,7}$ = 4.7, H-8), 5.48 (dd, 1 H, $J_{7,8}$ = 4.7, $J_{7,6}$ = 2.3, H-7), 5.88 (d, 1 H, $J_{3,4}$ = 2.5, H-3), 5.97 (d, 1 H, $J_{NH,4}$ = 8.8, NH), 6.13 (d, 1 H, $J_{NH,5}$ = 9.8, NH); ^{13}C NMR (150 MHz, $CDCl_3$) δ: 20.65, 20.80, 20.93, 23.12, 23.16 (5 × C, CH_3), 46.98 (C-5), 48.69 (C-4), 52.50 (OCH_3), 62.13 (C-9), 67.75 (C-7), 71.34 (C-8), 77.23 (C-6), 110.40 (C-3), 144.61 (C-2), 161.72 (C-1), 169.97, 170.39, 170.64, 171.03, 171.23 (5 × C=O). HRMS-FAB (*m*/*z*): [M + Na^+] calcd for $C_{20}H_{28}N_2O_{11}$, 495.1591; found, 495.1571.

Methyl 5-acetamido-7,8,9-tri-*O*-acetyl-2,6-anhydro-3,4,5-trideoxy-4-dimethylamino-D-*glycero*-D-galacto-non-2-enonate (3S)

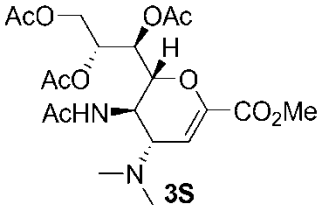

To a solution of amine **7** (100 mg, 0.232 mmol) in methanol (1 mL) was added formaldehyde solution (0.17 mL, 2.3 mmol), and the resulting solution was stirred at rt for 2 h. After adding $NaCNBH_3$ (22 mg, 0.35 mmol) to the solution, it was left at rt for 30 min. After the addition of glacial acetic acid (2 mL) the resultant solution was stirred for 10 min before being poured dropwise into a saturated $NaHCO_3$ solution (200 mL) over a period of 30 min. The product was then extracted with CH_2Cl_2 (3 × 200 mL), and the combined organic layers were washed with brine (200 mL) and dried over Na_2SO_4. After evaporating the solvent under reduced pressure, a white powder (66 mg, 62 %) was obtained. Mpt = 122–123 °C; $[\alpha]^{20}_D$ = +79.8 (c = 0.39, CH_2Cl_2); ^{1}H NMR (600 MHz, $CDCl_3$) δ: 1.93, 2.03, 2.04, 2.11, (4 × s, 12 H, CH_3), 2.29 (2 × s, 6 H, NCH_3), 3.34 (dd, $J_{4,5}$ = 8.6, $J_{4,3}$ = 2.7, H-4), 3.78 (s, 3 H, OCH_3), 4.15–4.21 (m, 2 H, H-5, H-9´), 4.26 (dd, 1 H, $J_{6,5}$ = 8.8, $J_{6,7}$ = 3.3, H-6), 4.63 (dd, 1 H, $J_{9,9'}$ = 12.3, $J_{9,8}$ = 3.0, H-9), 5.31–5.37 (m, 2 H, H-8, NH), 5.49 (m, 1 H, H-7), 6.08 (d, 1 H, $J_{3,4}$ = 3.0, H-3). ^{13}C NMR (150 MHz, $CDCl_3$) δ: 20.99, 21.08, 21.13, 23.75 (4 × C, CH_3), 41.33 (2 × C, NCH_3), 44.86 (C-5), 52.59 (OCH_3), 62.37, 62.46 (2 × C, C-4, C-9´), 68.52 (C-7), 71.29 (C-8), 109.39 (C-3), 145.22 (C-2), 162.16 (C-1), 170.36, 170.39, 170.59, 170.80 (4 × C=O). HRMS-FAB (*m*/*z*): [M + H^+] calcd for $C_{20}H_{30}N_2O_{10}$, 459.1979; found, 459.1961.

Methyl 5-acetamido-7,8,9-tri-*O*-acetyl-2,6-anhydro-4-isopropylamino-3,4,5-trideoxy-D-*glycero*-D-*galacto*-non-2-enonate (4S)

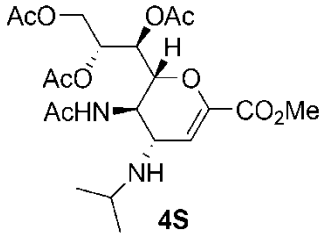

4S

To a solution of amine **7** (100 mg, 0.232 mmol) in methanol (1 mL) acetone (0.18 mL, 2.4 mmol) was added, and the resulting solution was stirred at rt for 2 h. $NaCNBH_3$ (20 mg, 0.32 mmol) was then added to the solution, which was stirred at rt overnight. After adding glacial acetic acid (2 mL), the resulting solution was stirred for 10 min and it was then added dropwise into sat. $NaHCO_3$ (200 mL) over a period of 30 min. The product was then extracted with CH_2Cl_2 (3 × 200 mL), and the combined organic layers were washed with brine (200 mL) and dried over Na_2SO_4. After evaporating the solvent under reduced pressure, a white powder (70 mg, 0.15 mmol) was obtained in a 64% yield. Mpt = 68–69 °C; $[\alpha]^{20}_D$ = +57.8 (c = 0.43, CH_2Cl_2); ^{1}H NMR (600 MHz, $CDCl_3$) δ: 1.01, 1.08, (2 × d, 6 H, J = 6.1, CH(CH_3)$_2$), 1.95, 2.02, 2.03, 2.09 (4 × s, 12 H, CH_3), 2.96 (m, 1 H, $(CH_3)_2$CH), 3.47 (dd, 1 H, $J_{4,5}$ = 7.1, $J_{4,3}$ = 3.2, H-4), 3.77 (s, 3 H, OCH_3), 3.86 (m, 1 H, H-5) 4.18 (dd, 1 H, $J_{9',9}$ = 12.2, $J_{9',8}$ = 6.8, H-9´), 4.39 (dd, 1 H, $J_{6,5}$ = 7.7, $J_{6,7}$ = 4.4, H-6), 4.55 (dd, 1 H, $J_{9,8}$ = 3.4, H-9), 5.41 (m, 1 H, H-8), 5.5–5.6 (m, 2 H, H-7, N-H), 6.06 (d, 1 H, $J_{3,4}$ = 3.2, H-3): ^{13}C NMR (150 MHz, $CDCl_3$) δ: 20.94, 20.99, 21.10, 22.88, 23.59, 23.98 (6 × C, CH_3), 46.98 ($(CH_3)_2$HC), 49.66 (C-5), 52.57 (2 × C, C-4, OCH_3), 62.17 (C-9), 68.40 (C-8), 76.50 (C-6), 112.25 (C-3), 142.90 (C-2), 162.60 (C-1), 170.16, 170.48, 170.51, 170.78 (4 × C=O). HRMS-FAB (m/z): [M + H$^+$] calcd for $C_{21}H_{32}N_2O_{10}$, 473.2135; found, 473.2126.

***N*,*N´*-Bis-*tert*-butoxycarbonylthiourea**[33]**:**

To a cold solution of thiourea (570 mg, 7.49 mmol) in dry THF (120 mL; 0 °C) was added NaH (1.35 g, 56.3 mmol). The resultant solution was stirred for 10 min under a N_2 atmosphere, when di-*tert*-butyl dicarbonate (3.8 mL, 16.5 mmol) was added. This mixture was stirred at rt for 2 h after which the reaction was quenched by adding aqueous $NaHCO_3$. (50 mL). Addition of water (70 mL) to the resulting mixture was followed by extraction using ethyl acetate (150 mL). The organic layer was then dried ($NaSO_4$) and the volatiles were removed under reduced pressure. The resultant crude product was purified by column chromatography (hexane/ethyl acetate 10:1 v/v/v) to give a white powder (1.5 g, 73 % yield). Mpt 124-125 °C; ^{13}C NMR (150 MHz, $CDCl_3$) δ: 28.03 (6 × C, C(CH_3)$_3$), 84.11 (2 × C, (CH_3)$_3C$)), 150.39 (C=S), 171.98 (C=O).

Methyl 5-acetamido-7,8,9-tri-*O*-acetyl-2,6-anhydro-4-[2,3-bis(tert-butoxycarbonyl)guanidino]-3,4,5-trideoxy-D-*glycero*-D-*galacto*-non-2-enonate (5S)[34]

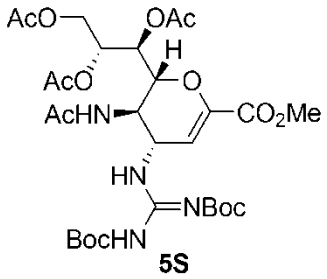

5S

To a solution of amine **7** (200 mg, 0.465 mmol) in anhydrous DMF (7 mL) were added *N*,*N´*-bis(*t*-butoxycarbonyl)thiourea (146 mg, 0.53 mmol) and triethylamine (19 mL, 136 mmol), and the solution was cooled to 0 °C. Subsequently, $HgCl_2$ (128 mg, 0.47 mmol) was added to the reaction which was stirred at 0 °C for 5 h. After concentrating under vacuum, the remaining residue was dissolved in ethyl acetate (20 mL) and it was filtered through celite and washed thoroughly with ethyl acetate. The filtrate was washed with water (40 mL) and brine (40 mL), and then dried over Na_2SO_4. The remaining

solution was concentrated to dryness under reduced pressure, and then it was purified by column chromatography (ethyl acetate/hexane 6:4 v/v) to afford white powder (160 mg, 51% yield). Mpt = 184–185 °C; $[\alpha]^{20}_{D}$ = +32.60 (0.28, CH_2Cl_2); ^{1}H NMR (600 MHz, $CDCl_3$) δ: 1.45, 1.46 (2 × s, 18 H, $C(CH_3)_3$), 1.85, 2.03, 2.05, 2.10 (4 × s, 12 H, CH_3), 3.78 (s, 3 H, OCH_3), 4.12 (dd, 1 H, $J_{9',9}$ = 12.5, $J_{9',8}$ = 7.1, H-9´), 4.19–4.27 (m, 2 H, H-5, H-6), 4.64 (dd, 1 H, $J_{9,9'}$ = 12.4, $J_{9,8}$ = 2.7, H-9), 5.12 (m, 1 H, H-4), 5.28 (ddd, 1 H, $J_{8,9'}$ = 7.5, $J_{8,7}$ = 5.0, $J_{8,9}$ = 2.7, H-8), 5.39 (dd, 1 H, $J_{7,8}$ = 5.0, $J_{7,6}$ = 1.5, H-7), 5.86 (d, 1 H, $J_{3,4}$ = 2.4, H-3), 6.00 (d, 1 H, $J_{NH,5}$ = 8.7, N-H), 8.46 (d, 1 H, $J_{NH,4}$ = 8.5, N-H), 11.33 (s, 1 H, ^{t}BocN-*H*); ^{13}C NMR (150 MHz, $CDCl_3$) δ: 21.03, 21.11, 21.16, 23.30 (4 × C, CH_3), 28.26, 28.47 (6 × C, 2 × $C(CH_3)_3$), 48.59 (C-5), 49.20 (C-4), 52.73 (OCH_3), 62.51 (C-9), 68.00 (C-7), 71.68 (C-8), 78.29 (C-6), 79.95, 84.17 (2 × C, 2 × $C(CH_3)_3$), 109.50 (C-3), 145.57 (C-2), 152.88 (N=$C(NH)_2$), 157.39 (*C*=O (Boc-NH)), 161.85, 163.08 (2 × C, *C*=O (Boc-N)), 170.44, 170.48, 170.81, 171.19 (4 × C=O). HRMS-FAB (*m*/*z*): [M + H^+] calcd for $C_{29}H_{44}N_4O_{14}$, 673.2932; found, 673.2937.

Methyl (5-acetamido-7,8,9-tri-*O*-acetyl-4-azido-3,4,5-trideoxy-D-*glycero*-β-D-*galacto*-non-2-ulopyranosyl)onate chloride (8)[35]

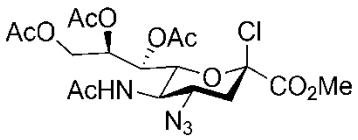

8

To a mixture of activated 4 Å molecular sieves (12 g) and dried LiCl (2.45 g, 57.8 mmol) compound **6** (5 g, 10.9 mmol) was added and the mixture of solids was stirred under vacuum (0.2 mm Hg) for 2 h. To this mixture, anhydrous degassed CH_3CN (125 mL) was added under a N_2 atmosphere and the resulting mixture was cooled to –30 °C. Subsequently, anhydrous HCl gas was bubbled through this mixture for 20 min while the

temperature was kept below –30 °C. After stirring the resultant mixture for 4 days at ambient temperature, volatiles were removed under reduced pressure, and CH_2Cl_2 (200 mL) was added to the residue. The solution was filtered through celite, which was washed thoroughly with CH_2Cl_2. Subsequently, the filtrate was washed with ice-cold water (100 mL), ice-cold saturated aqueous $NaHCO_3$ (2 × 100 mL), brine (100 mL) and the resultant solution was dried over Na_2SO_4. After evaporating the solvent under reduced pressure, a yellow foamy solid was obtained (4.3 g). Analysis of the crude product by ^{1}H NMR spectroscopy showed that it contained >85% of the desired product 8 and ~10% of starting material 6. This crude product was used for the next step without further purification. ^{1}H NMR (600 MHz, $CDCl_3$) δ: 2.00, 2.03, 2.05, 2.11 (s, 12 H, CH_3), 2.78 (dd, 1 H, $J_{3eq,4}$ = 14.2, $J_{3eq,4}$ = 4.6, H-3$_{eq}$), 3.73 (m, 1 H, H-5), 2.93 (s, 3 H, $COOCH_3$), 4.08 (dd, 1 H, $J_{9',9}$ = 12.6, $J_{9',8}$ = 5.6, H-9′), 4.23 (m, 1 H, H-4), 4.38 (dd, 1 H, $J_{9,9'}$ = 12.6, $J_{9,8}$ = 2.6, H-9), 4.50 (dd, 1 H, $J_{6,5}$ = 11.0, $J_{6,7}$ = 1.98, H-6), 5.16 (m, 1 H, H-8), 5.44 (dd, 1 H, $J_{7,6}$ = 2.2, $J_{7,8}$ = 7.2, H-7), 5.62 (d, 1 H, $J_{NH,5}$ = 9.2, NH); ^{13}C NMR (150 MHz, $CDCl_3$) δ: 20.97, 21.00, 21.12, 23.59 (4 × C, CH_3), 41.03 (C-3), 50.13 (C-5), 53.99 (OCH_3), 57.8 (C-4), 62.16 (C-9), 67.30 (C-7), 69.81 (C-8), 73.01 (C-6), 96.54 (C-2), 165.82 (C-1), 169.79, 170.50, 170.82, 170.84 (5 × C=O).

Methyl (4-nitrophenyl 5-acetamido-7,8,9-tri-*O*-acetyl-4-azido-3,4,5-trideoxy-D-*glycero*-α-D-*galacto*-non-2-ulopyranosid)onate (9)

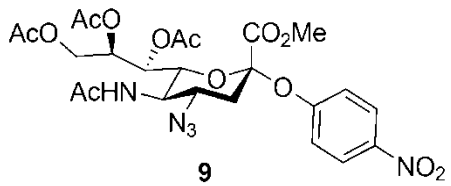

9

A solution of impure **8** (2 g) and 4-nitrophenol (5.70 g, 41 mmol) in dry CH_3CN (500 mL) was cooled in an ice-bath, following which *N*,*N*-diisopropylethylamine (10 mL,

59 mmol) was added and the resulting solution was stirred at 0 °C for 2 h. The reaction mixture was then allowed to warm to room temperature and stirring was continued for a further 18 h. Removal of the volatiles under reduced pressure afforded a yellow syrup which was dissolved in CH_2Cl_2 (600 mL) and washed with saturated $NaHCO_3$ (5 × 300 mL), H_2SO_4 (10%, 200 mL), brine (300 mL) and dried (Na_2SO_4). After filtration the volatiles were removed under reduced pressure and the crude product was purified by recrystallization from diethyl ether-dichloromethane to give a pale yellow powder (1.22 g, 50%). Mpt = 124–125 °C; $[\alpha]^{20}_D$ = +41.8 (c = 0.24, CH_2Cl_2); ^{1}H NMR (600 MHz, $CDCl_3$) δ: 2.02, 2.04, 2.11(4 × s, 12 H, CH_3), 2.75 (dd, 1 H, $J_{3e,3a}$ = 13.3, $J_{3e,4}$ = 4.5, H-3_{eq}), 3.30 (m, 1 H, OCH_3), 4.10-4.25 (m, 3 H, H-4, H-9, H-9´), 4.84 (dd, 1 H, $J_{6,5}$ = 10.77, $J_{6,7}$ = 1.4, H-6), 5.31 (dd, 1 H, $J_{7,8}$ = 9.4, $J_{7,6}$ = 1.6, H-7), 5.37 (ddd, 1 H, $J_{8,7}$ = 9.3, $J_{8,9´}$ = 4.4, $J_{8,9}$ = 2.6, H-8), 5.6 (d, 1 H, $J_{NH,5}$ = 8.31, NH), 7.13 (m, 2 H, Ar-H), 8.17 (m, 2 H, Ar-H); ^{13}C NMR (150 MHz, $CDCl_3$) δ: 20.73, 20.85, 21.01, 23.58, (4 × C, CH_3), 39.04 (C-3), 52.20 (C-5), 53.37 (OCH_3), 55.93 (C-4), 61.99 (C-9), 67.52 (C-7), 67.96 (C-8), 72.21 (C-6), 99.45 (C-2), 118.68 (2 × C, C-2´, C-6´), 125.66 (2 × C, C-3´, C-5´), 143.46 (C-4´), 158.95 (C-1´), 167.63 (C-1), 170.09, 170.54, 170.76, 170.81 (4 × C=O). HRMS-FAB (*m*/*z*): [M + Na^+] calcd for $C_{24}H_{29}N_5O_{13}$, 618.1660; found, 618.1648.

Methyl (4-nitrophenyl 5-acetamido-7,8,9-tri-*O*-acetyl-4-amino-3,4,5-trideoxy-D-*glycero*-α-D-*galacto*-non-2-ulopyranosid)onate (7S)

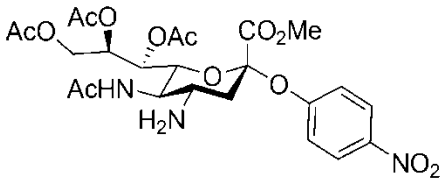

7S

Triphenylphosphine (0.65 g, 2.5 mmol) was added to a solution of azide **9** (1 g, 1.68 mmol) in THF (25 mL), and the resulting solution was stirred at rt for 12 h.

Subsequently, water (1.7 mL) was added to the solution and it was stirred at rt for another 24 h. The reaction mixture was then concentrated and extracted with ethyl acetate (150 mL). The organic layer was dried over Na_2SO_4 and the solvent was removed under reduced pressure to obtain a yellow syrup. The crude product was purified by column chromatography using ethyl acetate as the initial eluent followed by ethyl acetate/methanol/water 10:2:1 v/v/v) to afford a pale yellow powder (800 g, 83%). Mpt = 168–169 °C; $[\alpha]^{20}_D$ = +61.9 (c = 0.11, CH_2Cl_2); ^{1}H NMR (600 MHz, $CDCl_3$) δ: 1.96 (t, 1 H, $J_{3e,3a} = J_{3e,4}$ = 13.0, H-3_{ax}), 2.02, 2.03, 2.09, 2.18 (4 × s, 12 H, CH_3), 2.68 (dd, 1 H, $J_{3e,3a}$ = 13.3, $J_{3e,4}$ = 4.0, H-3_{eq}), 2.94 (m, 1 H, H-4), 3.54 (dd, 1 H, $J_{5,4} + J_{5,6}$ = 20.0, $J_{5,NH}$ = 10.3, H-5), 3.61 (s, 3 H, OCH_3), 4.13 (dd, 1 H, $J_{9',9}$ = 12.6, $J_{9',8}$ = 4.6, H-9´), 4.20 (dd, 1 H, $J_{9,9'}$ = 12.6, $J_{9,8}$ = 2.3, H-9), 4.61 (dd, 1 H, $J_{6,5}$ = 10.7, $J_{6,7}$ = 1.6, H-6), 5.31–5.42 (m, 3 H, H-7, H-8, N-H), 7.12 (m, 2 H, Ar-H), 8.16 (m, 2 H, Ar-H); ^{13}C NMR (150 MHz, $CDCl_3$) δ: 20.97, 20.98, 21.25, 23.82 (4 × C, CH_3), 42.34 (C-3), 49.38 (C-4), 53.30, 53.50 (2 × C, C-5, OCH_3), 62.30 (C-9), 67.64 (C-7), 68.69 (C-8), 74.02 (C-6), 100.18 (C-2), 118.65 (2 ×C, C-2´, C-6´), 125.87 (2 × C, C-3´, C-5´), 143.47 (C-4´), 159.48 (C-1´), 168.67 (C-1), 170.35, 170.49, 170.78, 171.12 (4 × C=O). HRMS-FAB (*m*/*z*): [M + Na^+] calcd for $C_{24}H_{31}N_3O_{13}$, 592.1755; found, 592.1744.

Methyl (4-nitrophenyl 5-acetamido-4-(1-triazolyl)-3,4,5-trideoxy-D-*glycero*-α-D-*galacto*-non-2-ulopyranosid)onate (6S)

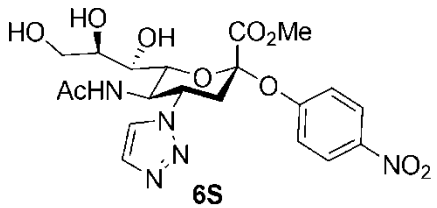

6S

To a solution of azide **9** (157 mg, 0.26 mmol) in toluene (2 mL) was added propynoic acid (0.1 mL, 1.62 mmol) and the reaction mixture was stirred at 65 °C for 3 h

under a N_2 atmosphere. After concentrating the solvent under reduced pressure, the oil residue was crystallized from ethyl acetate and ether to afford the triazole carboxylic acid as a white powder. Subsequently, this material was decarboxylated by heating it to its melting point under vacuum (0.2 mm Hg) while stirring for 30 min. The crude material was dissolved in dry methanol (6 mL), and subsequently a methanolic sodium methoxide solution (1.3 mL, 0.65 mmol) was added at 0 °C. After stirring the solution at 0 °C for 30 min, the solution was neutralized by the addition of Amberlite IR-120 resin ($NH4^+$ form). After filtering the mixture and washing the resin several times with methanol, the filtrate was concentrated under reduced pressure to give a brown syrup. The crude product was then purified by flash-column chromatography using ethyl acetate/methanol/water (10:2:1 v/v/v). The fractions containing 6S were combined and concentrated to give a solid residue (30 mg, 23% yield). Mpt = 141–142 °C; $[\alpha]^{20}_D$ = +16.18 (c = 0.068, MeOH); ^{1}H NMR (600 MHz, D2O) δ: 1.84 (s, 3 H, CH_3), 2.98 (t, 1 H, $J_{3a,3e} = J_{3e,4}$ = 13.2, H-3_{ax}), 3.17 (dd, 1 H, $J_{3e,3a}$ = 13.3, $J_{3e,4}$ = 3.3, H-3_{eq}), 3.65–3.74 (m, 2 H, H-7, H-9´), 3.82–3.90 (m, 5 H, $COOCH_3$, H-8, H-9), 4.54 (t, 1 H, $J_{5,4}$ = J5,6 = 9.8, H-5), 4.64 (d, 1 H, $J_{6,5}$ = 9.8, H-6), 5.02 (m, 1 H, H-4), 7.38 (m, 2 H, Ar-H), 7.84 (s, 1 H, H-4´-triazole), 8.11 (s, 1 H, H-5´-triazole), 8.29 (m, 2 H, Ar-H); ^{13}C NMR (150 MHz, D_2O) δ: 21.56 (CH_3), 37.20 (C-3), 49.75 (C-5), 53.77 (OCH_3), 57.93 (C-4), 63.16 (C-9), 67.93 (C-7), 70.38 (C-8), 74.56 (C-6), 100.20 (C-2), 119.98 (2 × C, C-2´-Ar, C-6´-Ar), 124.76 (C-5´-triazole), 125.80 (2 × C, C-3´-Ar, C-5´-Ar), 133.90 (C-4´-triazole), 143.60 (C-4´-Ar), 158.74 (C-1´), 168.96 (C-1), 174.00 (C=O). HRMS-FAB (m/z): [M + Na^+] calcd for $C_{20}H_{25}N_5O_{10}$, 518.1499; found, 518.1494.

Methyl (4-nitrophenyl 4,5-diacetamido-7,8,9-tri-*O*-acetyl-3,4,5-trideoxy-D-*glycero*-α-D-*galacto*-non-2-ulopyranosid)onate (8S)

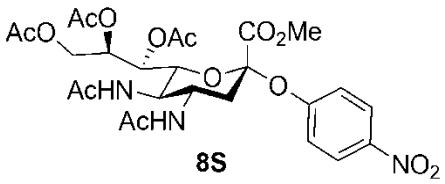

8S

To a solution of amine **7S** (102 mg, 0.18 mmol) in CH_2Cl_2 (5 mL) were added acetic anhydride (0.17 mL, 1.8 mmol) and triethylamine (0.036 mL, 0.26 mmol) at 0 ºC. After stirring for 1 h at 0 ºC the reaction mixture was washed with saturated aqueous $NaHCO_3$ (4 × 4 mL), water (2 mL), brine (2 mL) and dried (Na_2SO_4). After filtration the solvent was removed under reduced pressure to give a foamy solid (90 mg, 80%). Mpt = 154–155 °C; $[\alpha]^{20}_D$ = +36.9 (c = 0.27, CH_2Cl_2); ^{1}H NMR (600 MHz, $CDCl_3$) δ: 1.92, 1.94, 2.04, 2.07, 2.19 (5 × s, 15 H, CH_3), 2.75 (dd, 1 H, $J_{3e,3a}$ = 13.14, $J_{3e,4}$ = 3.8, H-3$_{eq}$), 3.63 (s, 3 H, OCH_3), 3.92–4.03 (m, 2 H, H-4, H-5), 4.09 (dd, 1 H, $J_{9',9}$ = 12.6, $J_{9',8}$ = 4.4, H-9′), 4.20 (dd, 1 H, $J_{9,9'}$ = 12.5, $J_{9,8}$ = 2.1, H-9), 4.60 (dd, 1 H, $J_{6,5}$ = 10.4, $J_{6,7}$ = 1.3, H-6), 5.34–5.40 (m, 2 H, H-7, H-8), 5.46 (d, 1 H, $J_{NH,5}$ = 9.4, NH), 5.91 (d, 1 H, J_{NH-4} = 7.9, NH); ^{13}C NMR (150 MHz, $CDCl_3$) δ: 20.83, 20.98, 21.23, 23.38, 23.39 (5 × C, CH_3), 39.72 (C-3), 48.29, 49.49 (2 × C, C-4, C-5), 53.56 (OCH_3), 62.25 (C-9), 67.27, 68.48 (2 × C, C-7, C-8), 74.56 (C-6), 99.81 (C-2), 118.65 (2 × C, C-2′, C-6′), 125.91 (2 × C, C-3′, C-5′), 143.61 (C-4′), 159.30 (C-1′), 168.32 (C-1), 169.85, 170.31, 170.82, 170.92, 171.98 (5 × C=O). HRMS-FAB (*m*/*z*): [M + Na^+] calcd for $C_{26}H_{33}N_3O_{14}$, 634.1860; found, 634.1854.

Methyl (4-nitrophenyl 5-acetamido-7,8,9-tri-*O*-acetyl-3,4,5-trideoxy-4-dimethylamino-D-*glycero*-α-D-*galacto*-non-2-ulopyranosid)onate (9S)

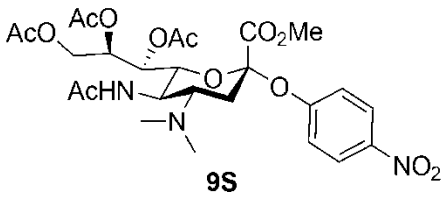

9S

To a solution of amine **7S** (100 mg, 0.17 mmol) in methanol (1 mL) was added an aqueous formaldehyde solution (0.13 mL, 1.76 mmol). The resulting solution was then stirred at rt for 2 h before $NaCNBH_3$ (16.64 mg, 0.26 mmol) was added to the mixture, which was then stirred for another 30 min. Following the dropwise addition of glacial acetic acid (1.5 mL) stirring was continued for 10 min. The solution was then transferred into ice-cold sat $NaHCO_3$ solution (150 mL) dropwise over a period of 30 min. The product was then extracted with CH_2Cl_2 (3 × 150 mL), and the combined organic layers were washed with brine (150 mL) and dried over Na_2SO_4. After evaporating the solvent under reduced pressure, the residue was crystallized from dichloromethane and diethyl ether to afford a yellow powder (70 mg, 68%). Mpt = 134−135 °C; $[\alpha]^{20}_D$ = +56.6 (c = 0.30, CH_2Cl_2); ^{1}H NMR (600 MHz, $CDCl_3$) δ: 1.95, 2.03, 2.10, 2.16 (4 × s, 12 H, CH_3), 2.24 (s, 6 H, NCH_3), 2.54 (dd, 1 H, $J_{3e,3a}$ = 13.1, $J_{3e,4}$ = 3.4, H-3_{eq}), 2.65 (td, 1 H, $J_{4,5}$ = $J_{4,3a}$ = 12.7, $J_{4,3e}$ = 3.3, H-4), 3.63 (s, 3 H, OCH_3), 4.01 (dd, 1 H, $J_{5,6}$ = 10.4, $J_{5,4}$ + $J_{5,NH}$ = 20.7, H-5), 4.08 (dd, 1 H, $J_{9',9}$ = 12.5, $J_{9',8}$ = 5.8, H-9´), 4.20 (dd, 1 H, $J_{9,9'}$ = 12.5, $J_{9,8}$ = 2.7, H-9), 4.47 (dd, 1 H, $J_{6,5}$ = 10.4, $J_{6,7}$ = 1.8, H-6), 5.11 (d, 1 H, $J_{NH,5}$ = 9.6, N-H), 5.31 (dd, 1 H, $J_{7,8}$ = 8.6, $J_{7,6}$ = 1.9, H-7), 5.36 (ddd, 1 H, $J_{8,7}$ = 8.58, $J_{8,9'}$ = 5.8, $J_{8,9}$ = 2.7, H-8), 7.13 (m, 2 H, Ar-H), 8.16 (m, 2 H, Ar-H); ^{13}C NMR (150 MHz, $CDCl_3$) δ: 20.98, 21.12, 21.26, 23.82 (4 × C, CH_3), 31.73 (C-3), 40.35 (2 × C, NCH_3), 47.25 (C-5), 53.29 (OCH_3), 60.91 (C-4), 62.59 (C-9), 68.03 (C-7), 68.93 (C-8), 75.67 (C-6), 101.12 (C-2), 118.64 (2 × C, C-2´, C-6´), 125.88 (2 × C, C-3´, C-5´), 143.43 (C-4´), 159.54 (C-1´), 168.71 (C-1),

170.39, 170.55, 170.61, 170.82 (4 × C=O). HRMS-FAB (*m*/*z*): [M + H^+] calcd for $C_{26}H_{35}N_3O_{13}$, 598.2248; found, 598.2243.

Methyl (4-nitrophenyl 5-acetamido-7,8,9-tri-*O*-acetyl-3,4,5-trideoxy-4-isopropylamino-D-*glycero*-α-D-*galacto*-non-2-ulopyranosid)onate (10S)

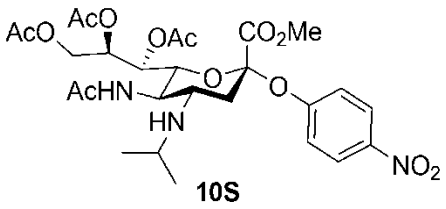

10S

To a solution of amine **7S** (102 mg, 0.18 mmol) in methanol (1 mL) was added acetone (0.14 µL, 1.86 mmol), and the resulting solution was stirred at rt for 2 h. Subsequently, $NaCNBH_3$ (18 mg, 0.286 mmol) was added to the solution, which was stirred at rt overnight. After adding glacial acetic acid (1.5 mL) to the solution and stirring for 10 min, the solution was transferred into ice-cold sat $NaHCO_3$ solution (150 mL) dropwise over a period of 30 min. The product was then extracted with CH_2Cl_2 (3 × 150 mL), and the combined organic layers were washed with brine (150 mL) and dried over Na_2SO_4. After evaporating the solvent under reduced pressure, a white powder (90 mg, 82%) was obtained. Mpt = 176–177 °C; $[\alpha]^{20}_D$ = +42.2 (c = 0.38, CH_2Cl_2); ^{1}H NMR (600 MHz, $CDCl_3$) δ: 0.94, 1.01 (2 × d, 6 H, *J* = 6.2, $CH(CH_3)_2$), 1.85 (t, 1 H, $J_{3a,3e} = J_{3a,4}$ = 12.7, H-3_{ax}), 1.99, 2.03, 2.07, 2.17 (4 × s, 12 H, CH_3), 2.73 (dd, 1 H, $J_{3e,3a}$ = 13.5, $J_{3e,4}$ = 3.9, H-3_{eq}), 2.85 (sept, 1 H, $(CH_3)_2C$-H), 2.94 (td, 1 H, $J_{4,5} + J_{4,3a}$ = 22.7, $J_{4,3e}$ = 3.4, H-4), 3.44 (m, 1 H, H-5), 3.65 (s, 3 H, OCH_3), 4.14 (dd, 1 H, $J_{9',9}$ = 12.5, $J_{9',8}$ = 5.1, H-9′), 4.21 (dd, 1 H, $J_{9,9'}$ = 12.5, $J_{9,8}$ = 2.4, H-9), 4.65 (m, 1 H, H-6), 5.27–5.34 (m, 2 H, N-H, H-7), 5.37 (ddd, 1 H, $J_{8,7}$ = 8.9, $J_{8,9'}$ = 5.11, $J_{8,9}$ = 2.5, H-8), 7.14 (m, 2 H, Ar-H), 8.15 (m, 2 H, Ar-H). ^{13}C NMR (150 MHz, $CDCl_3$) δ: 20.96, 21.00, 21.25, 22.83, 23.79, 24.40 (6 ×C, CH_3), 40.76 (C-3), 46.40 ($CH(CH_3)_2$), 51.74, 52.14 (2 × C, C-4, C-5), 53.25 (OCH_3),

62.39 (C-9), 67.97 (C-7), 68.73 (C-8), 73.74 (C-6), 100.59 (C-2), 118.97 (2 × C, C-2´, C-6´), 125.81 (2 × C, C-3´, C-5´), 143.50 (C-4´), 159.51 (C-1´), 168.48 (C-1), 170.33, 170.62, 170.77, 171.07 (4 × C=O). HRMS-FAB (*m*/*z*): [M + Na^+] calcd for $C_{27}H_{37}N_3O_{13}$, 634.2224; found, 634.2211.

Methyl (4-nitrophenyl 5-acetamido-7,8,9-tri-*O*-acetyl-4-[2,3-bis(tert-butoxycarbonyl)guanidino]-3,4,5-trideoxy-D-*glycero*-α-D-*galacto*-non-2-ulopyranosid)onate (11S)

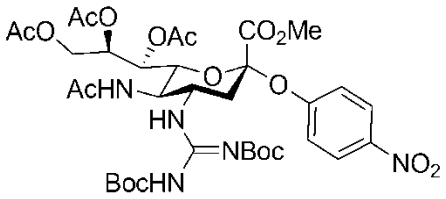

11S

N,*N*´-bis(*tert*-butoxycarbonyl)thiourea (52.8 mg, 0.19 mmol) and triethylamine (7 mL, 50 mmol) were added to a solution of amine **7S** (90 mg, 0.16 mmol) in anhydrous DMF (3 mL). The reaction mixture was cooled to 0 °C when $HgCl_2$ (46 mg, 0.17 mmol) was added and the resulting solution was stirred at 0 °C for 5 h under a N_2 atmosphere. The reaction mixture was concentrated under vacuum and the remaining residue was dissolved in ethyl acetate (10 mL), which was then filtered through celite, and the celite was thoroughly washed with ethyl acetate. The resultant filtrate was washed with water (10 ml) and brine (10 ml), and dried over sodium Na_2SO_4. The solution was concentrated under reduced pressure to give a residue that was purified by column chromatography (ethyl acetate/hexane: 6/4 v/v) to afford a white powder (80 mg, 61%). Mpt = 117-118 °C; $[\alpha]^{20}_D$ = +17.5 (c = 0.11, CH_2Cl_2); ^{1}H NMR (600 MHz, $CDCl_3$) δ: 1.47, 1.48 (2 × s, 18 H, $C(CH_3)_3$), 1.86, 2.04, 2.07, 2.18 (4 × s, 12 H, CH_3), 2.80 (dd, 1 H, $J_{3e,3a}$ = 13.1, $J_{3e,4}$ = 4.3, H-3_{eq}), 3.66 (s, 3 H, OCH_3), 4.00–4.10 (m, 2 H, H-5, H-9´), 4.18–4.26 (m, 2 H, H-4, H-9), 4.51 (dd, 1 H, $J_{6,5}$ = 10.5, $J_{6,7}$ = 1.8, H-6), 5.29 (dd, 1 H, $J_{7,8}$ = 8.7, $J_{7,6}$ = 1.8, H-7),

5.37 (ddd, 1 H, $J_{8,7}$ = 8.7, $J_{8,9}$ = 5.8, $J_{8,9'}$ = 2.78, H-8), 6.07 (d, 1 H, $J_{NH,5}$ = 9.3, N-H), 7.15 (m, 2 H, Ar-H), 8.17 (m, 2 H, Ar-H), 8.52 (d, 1 H, $J_{NH,4}$ = 7.5, N-H), 11.30 (s, 1 H, BocN-H); ^{13}C NMR (150 MHz, $CDCl_3$) δ: 21.01, 21.08, 21.31, 23.31 (4 × C, CH_3), 28.25, 28.47, (6 × C, 2 × C(CH_3)$_3$), 39.30 (C-3), 48.32 (C-4), 51.01 (C-5), 53.58 (OCH_3), 62.58 (C-9), 67.70 (C-7), 68.89 (C-8), 75.20 (C-6), 790.96, 84.25, (2 × C, 2 × C(CH_3)$_3$), 99.73 (C-2), 118.68 (2 × C, C-2′, C-6′), 125.88 (2 × C, C-3′, C-5′), 143.52 (C-4′), 152.99 (N=C(NH)$_2$), 157.02 (C=O (Boc-NH)), 159.31 (C-1′), 163.12 (C=O (Boc-N)), 168.23 (C-1), 170.27, 170.40, 170.84, 171.16 (4 × C=O). HRMS-FAB (*m*/*z*): [M + Na^+] calcd for $C_{35}H_{49}N_5O_{17}$, 834.3021; found, 834.3011.

Methyl (5-acetamido-7,8,9-tri-*O*-acetyl-2,6-anhydro-2,3,4,5-tetradeoxy-D-*glycero*-D-*galacto*-non-2-enpyranosyl)onate (12S)[36]

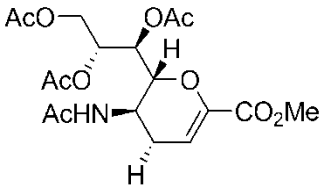

12S

To a solution of oxazoline **5** (554 mg, 1.34 mmol) in dry dioxane (40 mL) was added Pd/C (10% Pd, 100 mg, 0.094 mmol) and the resulting mixture was hydrogenated for 10 h under an atmospheric pressure at room temperature. After filtration over celite, the catalyst was removed and the filtrate was concentrated under reduced pressure. The remaining residue was purified by column chromatography with ethyl acetate/methanol (18:1) to afford the product as a yellowish white solid (380 mg, 68%). Mpt 46–47 °C; $[\alpha]^{20}_D$ = +17.27 (c = 0.11, MeOH); ^{1}H NMR (600 MHz, $CDCl_3$) δ: 1.97, 2.05, 2.06, 2.11 (4 × s, 12 H, CH_3), 2.20 (m, 1H, H-4$_{eq}$), 2.61 (ddd, 1 H, $J_{4a,4e}$ = 19.20, $J_{4a,5}$ = 5.9, $J_{4a,3}$ = 4.0, H-4$_{ax}$), 3.78 (s, 3H, OCH_3), 4.17 (t, 1 H, $J_{6,5}$ = $J_{6,7}$ = 5.84, H-6), 4.23 (dd, 1 H, $J_{9',9}$= 12.26, $J_{9',8}$ = 7.26, H-9′), 4.35 (m, 1 H, H-5), 4.57 (dd, 1 H, $J_{9,9'}$ = 12.26, $J_{9,8}$ = 3.40, H-9),

5.22 (dt, 1 H, $J_{8,7}$ = 7.30, $J_{8,9}$ = $J_{8,9'}$ = 3.62, H-8), 5.43 (m, 1 H, H-7), 5.85 (d, 1 H, $J_{NH,5}$ = 8.9, NH), 6.10 (t, 1 H, $J_{3,4a}$ = $J_{3,4e}$ = 4.1, H-3); ^{13}C NMR (150 MHz, $CDCl_3$) δ: 20.64, 20.73, 20.86, 23.10 (4 × CH_3), 26.32 (C-4), 42.01 (C-5), 52.26 (OCH_3), 61.70 (C-9), 68.29 (C-7), 70.49 (C-8), 76.17 (C-6), 109.37 (C-3), 142.54 (C-2), 162.23 (C-1), 170.13, 170.36, 170.70 (4 × C=O). HRMS-FAB (*m*/*z*): [M + H^+] calcd for $C_{18}H_{25}NO_{10}$, 416.1557; found, 416.1561.

Methyl [methyl (5-acetamido-7,8,9-tri-*O*-acetyl-3,4,5-trideoxy-α and *β*-D-manno-non-3-en-2-ulopyranosid)onate (13S)[37]

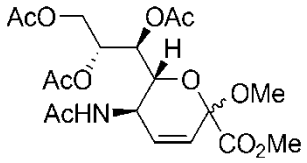

13S

β/α (≈ 8/2)

To a solution of compound **5** (1g, 2.42 mmol) in dry dichloromethane (20 mL) was added methanol (2 mL, 50 mmol) and followed by addition of a solution of $BF_3.OEt_2$ (0.3 mL, 2.5 mmol) in dichloromethane (4 mL). The resultant mixture was then stirred for 3 h under a N_2 atmosphere at room temperature. The solution was then washed with saturated $NaHCO_3$ (20 mL) water (20 mL) and brine (20 mL), and the resulting solution was dried over anhydrous Na_2SO_4. After evaporating the solvent under reduced pressure, the remaining residue was purified by flash column chromatography using dichromethane:methanol (15:1 v/v) to afford yellowish white powder 13S as a mixture of β-anomer/α-anomer (8:2) (870 mg, 80%). β-anomer: ^{1}H NMR (500 MHz, $CDCl_3$) δ: 1.97, 2.03, 2.08, 2.14 (4× s, 12 H, CH_3), 3.28 (s, 3 H, OCH_3), 3.80 (s, 3 H, $COOCH_3$), 4.04 (dd, 1 H, $J_{6,5}$ = 10.3, $J_{6,7}$ = 2.3, H-6), 4.23 (dd, 1 H, $J_{9',9}$ = 12.1, $J_{9',8}$ = 6.1, H-9), 4.65−4.59 (m, 2 H, H-9, H-5), 5.31 (td, 1 H, $J_{8,9'}$ = $J_{8,7}$ = 6.3, $J_{8,9}$ = 2.4, H-8), 5.38 (dd, 1 H, $J_{7,8}$ = 5.6, $J_{7,6}$ = 2.3, H-7), 5.50 (d, 1 H, $J_{NH,5}$ = 9.6, NH), 5.90 (s, 2 H, H-3, H-4); ^{13}C NMR (150 MHz,

$CDCl_3$) δ: 20.87, 20.90, 21.15, 23.43 (4 × CH_3), 43.29 (C-5), 52.18 (O CH_3), 52.99 ($COOCH_3$), 62.35 (C-9), 68.27 (C-7), 70.58 (C-6), 71.11 (C-8), 96.64 (C-2), 125.93 (C-3), 133.90 (C-4), 167.63 (C-1), 170.0, 170.28, 170.58, 170.74 (4 × C=O). HRMS-FAB (*m*/*z*): [M + Na^+] calcd for $C_{19}H_{27}NO_{11}$, 468.1482; found, 468.1508.

Methyl [methyl (5-acetamido-7,8,9-tri-*O*-acetyl-3,4,5-trideoxy-*α* and *β*-D-manno-non-2-ulopyranosid)onate (14S)

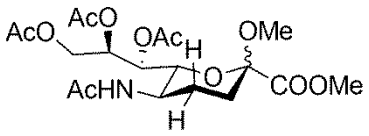

14S

β/α (≈ 8/2)

To a solution of α and β anomers **13S** (500 mg, 1.12 mmol) in dry dioxane (30 mL) was added Pd/C (10% Pd, 80 mg, 0.075 mmol,) and the resulting mixture was then hydrogenated for 10 h under atmospheric pressure at room temperature. The catalyst was then removed by filtration over celite, and the filtrate was concentrated under reduced pressure to afford the product as a mixture of α and β anomers 14S (480 mg, 95%) as a yellowish white solid. The crude was used for the next step without further purification. β-anomer: ^{1}H NMR (500 MHz, $CDCl_3$) δ: 1.85, 1.97, 2.01, 2.08 (4× s, 12 H, CH_3), 1,75−1.85 (m, 4 H, H-3_{eq}, H-3_{ax}, H-4_{eq}, H-4_{ax}), 3.21 (s, 3 H, OCH_3), 3.74 (s, 3 H, $COOCH_3$), 3.80 (dd, 1 H, $J_{6,5}$ = 10.35, $J_{6,7}$ = 2.48, H-6), 3.95 (m, 1 H, H-5), 4.08 (dd, 1 H, $J_{9,9'}$ = 11.7, $J_{9',8}$ = 7.94, 1 H, H-9′), 4.80 (dd, 1 H, $J_{9,9'}$ = 12.4, $J_{9,8}$ = 2.4, H-9), 5.17 (m, 1 H, H-8), 5.36 (dd, 1 H, $J_{7,8}$ = 3.5, $J_{7,6}$ = 2.5, H-7), 5.73 (d, 1 H, $J_{NH,5}$ = 9.8, NH); ^{13}C NMR (150 MHz, $CDCl_3$) δ: 20.80, 20.82, 21.06, 23.31 (4 × CH_3), 25.70, 31.68 (C-3, C-4), 43.69 (C-5), 51.15 (OCH_3), 52.56 ($COOCH_3$), 62.64 (C-9), 68.93 (C-7), 72.35 (C-8), 72.78 (C-6), 98.03 (C-2), 168.70 (C-1), 169.73, 170.26, 170.65, 170.83 (4 × C=O). HRMS-FAB (*m*/*z*): [M + H^+] calcd for $C_{19}H_{29}NO_{11}$, 448.1819; found, 448.1823.

5-Acetamido-3,4,5-trideoxy-D-*manno*-non-2-ulosonic acid (α and β) (15S)

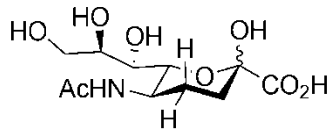

15S

β/α (≈ 8/2)

To a solution of α and β anomers **14S** (450 mg, 1.01 mmol) in dry methanol (20 mL) a methanolic sodium methoxide solution (5 mL, 2.54 mmol) was added at 0 °C. After the resulting solution was stirred at 0 °C for 30 min, it was neutralized by addition of Amberlite IR-120 resin (H^+ form). After filtering the mixture, the resin was washed thoroughly with methanol, and filtrate was concentrated under reduced pressure to give a solid residue which was dissolved in a 3:1 v/v THF/H_2O solution (10 mL) at 0 °C. Subsequently, to the resulting solution was added LiOH.H_2O (84 mg, 2 mmol), and the reaction mixture was stirred at 0°C for 30 min. After neutralizing the mixture using Amberlite IR-120 resin (H^+ form), it was filtered and the resin was washed thoroughly with water. The filtrate was then concentrated under reduced pressure to give a solid residue which was dissolved in HCl (10 mL, 0.025 M). Subsequently, Amberlite IR-120 resin (H^+ form) (650 mg) was added to the solution and the resulting mixture was heated at 70 °C for 16 h. The resin was removed by filtration and it was washed with water (10 mL). The solvent was evaporated and the residue was dried under high vacuum for 15 h to give the compound 15S as a mixture of α and β anomers (200 mg, 67% overall yield) which was used for the next step without further purification. β-anomer: ^{1}H NMR (500 MHz, D_2O) δ: 1.75 (m, 1 H, H-4_{eq}), 1.87–2.04 (m, 2 H, H-3_{ax}, H-3_{eq}), 2.04 (s, 3 H, CH_3), 2.17 (m, 1 H, H-4_{ax}), 3.54–3.65 (m, 2 H, H-8, H-9´), 3.75 (dd, 1 H, $J_{9,9'}$ = 12.36, $J_{9,8}$ = 2.56, H-9), 3.90 (m, 1 H, H-5), 4.22 (d, 1 H, $J_{7,8}$ = 7.4, H-7), 4.64 (s, 1 H, H-6); ^{13}C NMR (150 MHz, D_2O) δ: 21.06 (C-4), 21.81 (CH_3), 27.74 (C-3), 45.72 (C-5), 61.99 (C-9), 71.40

(C-8), 78.39 (C-7), 78.73 (C-6), 105.52 (C-2), 170.71 (C-1), 173.65 (C=O). HRMS-FAB (*m*/*z*): [M + Na^+] calcd for $C_{11}H_{19}NO_8$, 316.1008; found, 316.1007.

Methyl (4-nitrophenyl 5-acetamido-3,4,5-trideoxy-*β*-D-manno-non-2-ulopyranosyl)onate (18S)

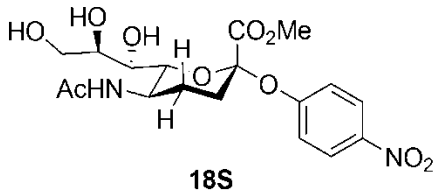

18S

To a solution of compound **15S** (150 mg, 0.51 mmol) in dry methanol (20 mL) was added Amberlite IR-120 resin (H^+ form, 800 mg) and the reaction mixture was stirred under N_2 atmosphere at room temperature for 3 h. The resin was filtered and it was washed thoroughly with methanol. After evaporating methanol under reduced pressure, the remaining residue (crude 16S) was dissolved in acetyl chloride (10 mL, 140 mmol) at 0 °C. A mixture of MeOH (2 mL, 50 mmol) and glacial acetic acid (4 mL, 70 mmol) was then added dropwise to the resulting solution. The flask was sealed and the reaction mixture was stirred for 48 h at room temperature. The solution was evaporated to dryness to afford the crude chloride **17S**, which was added to a solution of 4-nitrophenol (570 mg, 4.09 mmol) in dry acetonitrile (40 mL) at 0 °C. To this mixture diisopropylethyl amine (1 mL, 5.7 mmol) was added and the resulting solution was stirred for 48 h while the temperature was gradually changed from 0 °C to room temperature. The volatiles were then removed and the resulting residue was dissolved in dichloromethane (60 mL). The organic phase was then washed with saturated solution of $NaHCO_3$ (5 × 30 mL), 10% H_2SO_4 (20 mL) brine (30 mL), and dried (Na_2SO_4). After evaporating the solvent under reduced pressure, the remaining residue was dissolved in dry methanol (10 mL) and a methanolic sodium methoxide solution (2.6 mL, 1.3 mmol)

was then added at 0 °C. The resulting solution was stirred at 0 °C for 30 min, and then it was neutralized by addition of Amberlite IR-120 resin (H^+ form). The resin was removed by filtration and it was washed thoroughly with methanol. The filtrate was concentrated under reduced pressure to give a solid residue which was purified by flash column chromatography using dichromethane:methanol (15:1 v/v) to afford the product 18S, (45 mg, 20%) as a yellow solid. Mpt 108–109 °C; $[\alpha]^{20}_D$ = + 23.93 (0.04, MeOH); 1H NMR (600 MHz, D2O) δ: 1.56 (tdd, 1 H, $J_{4a,4e}$ = 16.9 $J_{4a,3a}$ = $J_{4a,5}$ = 12.4, $J_{4a,3e}$ = 4.2, H-4_{ax}), 1.90 (s, 3 H, CH_3), 1.98-2.12 (m, 2 H, H-3_{ax}, H-4_{eq}), 2.44 (dt, 1 H, $J_{3e,3a}$ = $J_{3e,4e}$ = 14.6, $J_{3e,4a}$ = 4.1, H-3_{eq}), 3.46 (dd, 1 H, $J_{7,8}$ = 9.2, $J_{7,6}$ = 1.4, H-7), 3.55 (dd, 1 H, $J_{9',9}$ = 11.0, $J_{9',8}$ = 5.3, H-9´), 3.69–3.77 (m, 2 H, H-8, H-9), 4.01 (td, 1 H, $J_{5,4}$ = $J_{5,6}$ = 11.3, $J_{5,4e}$ = 4.2, H-5), 4.19 (dd, 1 H, $J_{6,5}$ = 10.6, $J_{6,7}$ = 1.5, H-6), 7.25 (m, 2 H, Ar-H), 8.12 (m, 2 H, Ar-H); ^{13}C NMR (150 MHz, D_2O) δ: 21.88 (CH_3), 25.16 (C-4), 31.83 (C-3), 43.89 (C-5), 53.39 (COO*C*H_3), 63.12 (C-9), 68.06 (C-7), 70.22 (C-8), 76.14 (C-6), 101.00 (C-2), 119.47 (C-2´, C-6´), 125.68 (C-3´, C-5´), 143.19 (C-4´), 159.06 (C-1´), 170.21 (C-1), 174.23 (C=O). HRMS-FAB (m/z): [M + Na^+] calcd for $C_{18}H_{24}N_2O_{10}$, 451.1329; found, 451.1332.

Methyl (methyl 5-acetamido-3,5-dideoxy-D-*glycero*-β-D-*galacto*-non-2-ulopyranosid)onate (19S)[38]

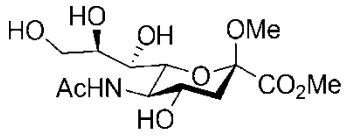

19S

Sialic acid (5 g, 13.7 mmol) was dissolved in dry methanol (300 mL) and Amberlite IR-120 resin (H^+ form, 3 g) was added and the mixture was refluxed for 48 h. The resin was removed by filtration and it was thoroughly washed with methanol. The filtrate was concentrated to dryness and then the residue was dissolved in methanol (60 mL) with heating at 45 °C. After reducing the volume of methanol to its half amount, the

solution was left in freezer (–20 °C) overnight. The resultant crystals were collected by filtration and the filtrate was again left at –20 °C overnight to afford a second crop of crystals. The combined solids were dried and the overall yield of Neu5Ac methyl ester methyl ketoside **19S** was 4.3 g (93%). Mpt 119−120 °C; $[\alpha]^{20}_{D}$ = –35.59 (c = 0.54, MeOH); ^{1}H NMR (500 MHz, D_2O) δ: 1.78 (t, 1 H, $J_{3a,3e} = J_{3a,4}$ = 12.3, H-3_{ax}), 2.04 (s, 3 H, CH_3), 2.39 (dd, 1 H, $J_{3e,3a}$ = 13.3, $J_{3e,4}$ = 4.9, H-3_{eq}), 3.27 (s, 3 H, OCH_3), 3.58 (d, 1 H, $J_{6,5}$ = 9.7, H-6), 3.66 (dd, 1 H, $J_{9',9}$ = 12.1, $J_{9',8}$ = 5.8, H-9´), 3.79–3.95 (m, 7 H, $COOCH_3$, H-5, H-7, H-8, H-9), 4.04 (dt, 1 H, $J_{4,3a} = J_{4,5}$ = 12.5, $J_{4,3e}$ = 4.6, H-4); ^{13}C NMR (150 MHz, D_2O) δ: 22.06 (CH_3), 39.18 (C-3), 50.99 (OCH_3), 51. 68, 69.82, 70.52 (3 × s, C-5, C-7, C-8), 53.53 ($COOCH_3$), 63.35 (C-9), 66.40 (C-4), 68.0 (C-6), 99.18 (C-2), 170.38 (C-1), 174.79 (C=O). HRMS-FAB (*m*/*z*): [M + Na^+] calcd for $C_{13}H_{23}NO_9$, 360.1271; found, 360.1280.

Methyl (methyl 5-acetamido-3,5-dideoxy-8,9-*O*-isopropylidene-D-*glycero*-β-D-*galacto*-non-2-ulopyranosid)onate (10)[38]

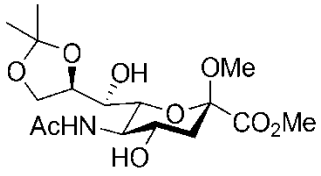

10

To a solution of methyl ketoside **19S** (4 g, 11.85 mmol) in anhydrous acetone (100 mL, dried over 4Å molecular sieves) was added *p*-toluenesulfonic acid (110 mg, 0.64 mmol). After stirring the reaction mixture at room temperature for 4 h, triethylamine (1 mL) was added to neutralize the acid. After the volatiles were evaporated the resulting thick syrup was crystallized from diethyl ether to afford **10** as white crystals (3.8 g, 10.07 mmol, 85%). Mpt 176−177 °C; $[\alpha]^{20}_{D}$ = –26.09 (c = 0.46, MeOH); ^{1}H NMR (500 MHz, D_2O) δ: 1.29, 1.37 (2 × s, 6 H, $C(CH_3)_2$), 1.76 (dd, 1 H, $J_{3a,3e}$ = 12.8, $J_{3a,4}$ = 11.3, H-3_{ax}),

2.07 (s, 3 H, CH_3), 2.43 (dd, $J_{3e,3a}$ = 13.0, $J_{3a,4}$ = 4.9, H-3_{eq}), 3.25 (s, 3 H, OCH_3), 3.47 (m, 1 H, H-7), 3.57 (m, 1 H, H-6), 3.81–3.91 (m, 6 H, $COOCH_3$, H-5, 4-OH, 7-OH), 3.97–4.07 (m, 2 H, H-4, H-9´), 4.13 (dd, 1 H, $J_{9,9'}$ = 8.9, $J_{9,8}$ = 6.2, H-9), 4.28 (dt, 1 H, $J_{8,9'}$ = $J_{8,9'}$ = 8.3, $J_{8,7}$ = $J_{8,9}$ = 5.9, H-8), 6.26 (d, 1 H, $J_{NH,5}$ = 7.9, NH); ^{13}C NMR (150 MHz, D_2O) δ: 23.34 (CH_3), 25.49, 27.16 (2 × C, C(*C*H_3)$_2$), 40.67 (C-3), 51.16 (OCH_3), 52.88 (COO*C*H_3), 53.23 (C-5), 67.03 (C-4), 67.92 (C-9), 70.48 (C-7), 71.90 (C-6), 74.45 (C-8), 99.21 (C-2), 109.07 (*C*(CH$_3$)$_2$), 168.90 (C-1), 173.40 (C=O). HRMS-FAB (*m*/*z*): [M + Na^+] calcd for $C_{16}H_{27}NO_9$, 400.1584; found, 400.1599.

Methyl (methyl 5-acetamido-3,4,5-trideoxy-4-methoxy-8,9-*O*-isopropylidene-D-*glycero*-β-D-*galacto*-2-nonulopyranosid)onate (20S)

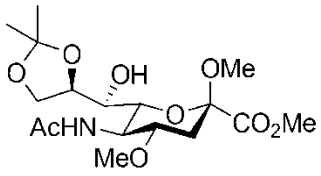

20S

Sodium hydride (177 mg, 7.40 mmol) was added to a solution of compound **1**0 (2 g, 5.29 mmol) in dry acetonitrile (20 mL) at 0 °C under a nitrogen atmosphere. After stirring for 15 min at 0 °C under nitrogen atmosphere, dimethyl sulfate (0.7 mL, 7.50 mmol) was added to the solution, and stirring was continued for an additional 20 min. After filtering the reaction mixture through celite, the filtrate was concentrated to dryness under reduced pressure, and the resultant residue was purified by flash column chromatography (dichloromethane:methanol 20:1 v/v) to give 20S (1.7 g, 82%). Mpt 182−183 °C; $[\alpha]^{20}_D$ = –20.21 (c = 0.46, MeOH); ^{1}H NMR (500 MHz, $CDCl_3$) δ: 1.31, 1.38 (2 × s, 6 H, C(CH_3)$_2$), 1.66 (dd, $J_{3a,3e}$ = 12.8, $J_{3a,4}$ = 11.0, H-3_{ax}), 2.08 (s, 3 H, CH_3), 2.59 (dd, 1 H, $J_{3e,3a}$ = 12.9, $J_{3e,4}$ = 4.7, H-3_{eq}), 3.29 (s, 3 H, 4-OCH_3), 3.33 (s, 3 H, 2-OCH_3), 3.47 (d, 1 H, $J_{7,8}$ = 8.4, H-7), 3.58 (d, 1 H, $J_{6,5}$ = 10.5, H-6), 3.73 (td, 1 H, $J_{4,3a}$ = $J_{4,5}$ =

10.6, $J_{4,3e}$ = 4.7, H-4), 3.80 (s, 3 H, $COOCH_3$), 3.91 (m, 1 H, H-5), 4.02 (dd, 1 H, $J_{9,9'}$ = 8.6, $J_{9',8}$ = 5.5, H-9´), 4.15 (dd, 1 H, $J_{9,9'}$ = 8.6, $J_{9,8}$ = 6.3, H-9), 4.33 (dt, 1 H, $J_{8,7}$ = $J_{8,9}$ = 8.3, $J_{8,9'}$ = 5.9, H-8), 5.46 (d, 1 H, $J_{NH,5}$ = 7.6, NH); ^{13}C NMR (150 MHz, $CDCl_3$) δ: 23.30 (CH_3), 25.37, 27.04 (2 × C, C(CH_3)$_2$), 36.61 (C-3), 51.01 (C-5), 51.17 (4-OCH_3), 52.66 ($COOCH_3$), 55.57 (2-OCH_3), 67.95 (C-9), 70.28 (C-7), 72.07 (C-6), 74.13 (C-8), 75.03 (C-4), 99.07 (C-2), 108.83 (C(CH_3)$_2$), 168.48 (C-1), 172.73 (C=O). HRMS-FAB (*m*/*z*): [M + Na^+] calcd for $C_{17}H_{29}NO_9$, 414.1740; found, 414.1757.

Methyl (5-acetamido-3,4,5-trideoxy-4-methoxy-D-*glycero*-β-D-*galacto*-non-2-ulopyranosid)onate (23S)[38]

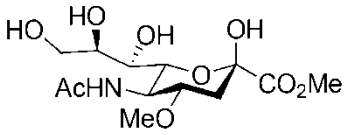

23S

To a solution of compound **20S** (1.5 g, 3.83 mmol) in a mixture of methanol and water (15 mL, 1:1 v/v) was added NaOH (8 mL, 1 N), and the resulting mixture was stirred at room temperature for 1h. After neutralizing the reaction mixture with Amberlite IR-120 resin (H^+ form), it was filtered and the resin was washed with water. The filtrate was then concentrated to dryness under reduced pressure to leave a solid residue (crude 21S) which was subsequently dissolved in HCl (25 mL, 0.025 M). To the resultant solution was then added Amberlite IR-120 resin (H^+ form, 1.5 g) and it was stirred over night at 70 °C. The resin was then removed by filtration and washed with water. The solvent was fully evaporated under reduced pressure and the remaining residue was dried under high vacuum to afford 4-methoxy substituted Neu5Ac 22S. This material was dissolved in methanol (120 mL) to which Amberlite IR-120 resin (H^+ form, 3.5g) was added. After stirring the reaction for 3 h at rt under a nitrogen atmosphere, the resin was removed by filtration and it was washed thoroughly with methanol. The filtrate was

concentrated to dryness under reduced pressure to afford **23S** as a pinkish white solid (1.1 g, 85% overall yield). Mpt 190−191°C (dec); $[\alpha]^{20}_{D}$ = –19.05 (c = 0.42, MeOH); ^{1}H NMR (500 MHz, D_2O) δ: 1.81 (dd, 1 H, $J_{3a,3e}$ = 13.0, $J_{3a,4}$ = 11.4, H-3_{ax}), ¸2.05 (s, 3 H, CH_3), 2.50 (dd, 1 H, $J_{3e,3a}$ = 13.1, $J_{3e,4}$ = 4.7, H-3_{eq})¸, 3.39 (s, 3 H, OCH_3), 3.55 (dd, 1 H, $J_{7,8}$ = 9.3, $J_{7,6}$ = 1.0, H-7), 3.62 (dd, 1 H, $J_{9',9}$ = 11.9, $J_{9',8}$ = 6.2, H-9´), 3.73 (ddd, 1 H, $J_{8,7}$ = 9.1, $J_{8,9'}$ = 6.3, $J_{8,9}$ = 2.6, H-8), 3.77−3.88 (m, 5 H, $COOCH_3$, H-4, H-9), 3.98 (t, 1 H, $J_{5,4}$ = $J_{5,6}$ = 10.3, H-5), 4.08 (dd, 1 H, $J_{6,5}$ = 10.6, $J_{6,7}$ = 1.0, H-6). ^{13}C NMR (150 MHz, D_2O) δ: 22.19 (CH_3), 35.74 (C-3), 50.25 (C-5), 53.74 ($COOCH_3$), 56.24 (OCH_3), 63.19 (C-9), 67.88 (C-7), 69.78 (C-8), 70.46 (C-6), 75.75 (C-4), 95.04 (C-2), 174.78 (C-1), 181.36 (C=O). HRMS-FAB (*m*/*z*): [M + Na^+] calcd for $C_{13}H_{23}NO_9$, 360.1271; found, 360.1265.

Methyl (5-acetamido-3,4,5-trideoxy-7,8,9-tri-*O*-acetyl-4-methoxy-D-*glycero*-β-D-*galacto*-non-2-ulopyranosyl)onate chloride (24S)

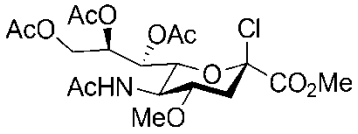

24S

To a solution of compound **23S** (500 mg, 1.5 mmol) in acetyl chloride (30 mL, 420 mmol) at 0 °C a mixture of MeOH (6 mL, 150 mmol) and glacial acetic acid (12 mL, 210 mmol) was added. The reaction vessel was then sealed and the mixture was stirred for 48 h at rt. The resultant solution was then concentrated to dryness and the residue was recrystallized from diethyl ether-dichloromethane to afford 24S (530 mg, 73%) as a white solid. This material was used directly without further purification.

Methyl (4-nitrophenyl 5-acetamido-3,4,5-trideoxy-4-methoxy-α-D-*glycero*-D-*galacto*-non-2-ulpyranosid)onate (25S) and methyl (5-acetamido-2,6-anhydro-3,4,5-trideoxy-4-methoxy-D-*glycero*-D-*galacto*-non-2-en)onate (26S)

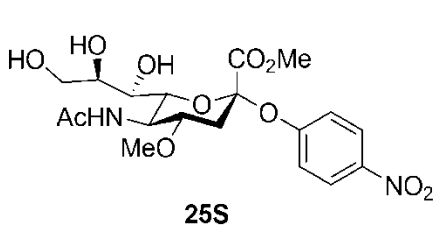

25S

&

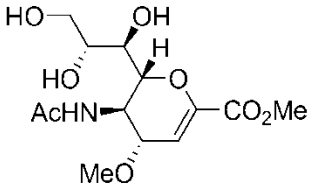

26S

Compound **24S** (500 mg, 1.04 mmol) and 4-nitrophenol (1.4 g, 10.07 mmol) were dissolved in cooled (0 °C) dry acetonitrile (100 mL) to which Hunig's base (1.5 mL, 15.7 mmol) was added. The resulting solution was stirred for 48 h while the temperature was gradually changed from 0 °C to room temperature. After the volatiles had been removed under reduced pressure the residue was dissolved in dichloromethane (150 mL). This organic phase was washed with saturated solution of $NaHCO_3$ (5 × 80 mL), 10% H_2SO_4 (50 mL) brine (80 mL), and dried over Na_2SO_4. After evaporating the solvent under reduced pressure, the remaining residue was dissolved in dry methanol (20 mL) and a methanolic sodium methoxide solution (5.2 mL, 2.6 mmol) was then added at 0 °C. The resulting solution was stirred at 0 °C for 30 min, and then it was neutralized by addition of Amberlite IR-120 resin (H^+ form). The resin was removed by filtration and washed thoroughly with methanol. The combined filtrates were concentrated under reduced pressure to give a solid residue which was purified by flash column chromatography using dichloromethane:methanol (10:1 v/v) to afford **25S** (150 mg, 32%) as a yellow powder and **26**S (30 mg, mol, 9.6%) as a pale yellow powder.

Compound 25S: Mpt 84−85°C; $[\alpha]^{20}_D$ = +48.02 (c = 0.23, MeOH); ^{1}H NMR (500 MHz, D_2O) δ: 2.04–2.15 (m, 4 H, CH_3, H-3_{ax}), 3.03 (dd, 1 H, $J_{3e,3a}$ = 13.2, $J_{3e,4}$ = 4.4, H-3_{eq}), 3.45 (s, 3 H, OCH_3), 3.62 (d, 1 H, $J_{7,8}$ = 9.3, H-7), 3.63–3.70 (m, 2 H, H-4, H-9´), 3.81 (s, 3 H, $COOCH_3$), 3.82–3.93 (m, 2 H, H-8, H-9), 4.10 (t, 1 H, $J_{5,6}$ = $J_{5,4}$ = 10.3, H-5),

4.27 (d, 1 H, $J_{6,5}$ = 10.7, H-6), 7.32 (m, 2 H, Ar-H), 8.27 (m, 2 H, Ar-H). ^{13}C NMR (150 MHz, D_2O) δ: 22.05 (CH_3), 36.66 (C-3), 49.85 (C-5), 53.64 (COO*C*H_3), 56.62 (OCH_3), 63.14 (C-9), 67.99 (C-7), 70.38 (C-8), 74.10 (C-6), 75.86 (C-4), 100.68 (C-2), 119.85 (C-2´, C-6´), 125.75 (C-3´, C-5´), 143.47 (C-4´), 158.89 (C-1´), 169.52 (C-1), 174.87 (C=O). HRMS-FAB (*m*/*z*): [M + Na^+] calcd for $C_{19}H_{26}N_2O_{11}$, 481.1434; found, 481.1429.

Compound 26S: Mpt 153−154°C; $[\alpha]^{20}_D$ = + 23.96 (c = 0.096, MeOH); ^{1}H NMR (500 MHz, D_2O) δ: 2.09 (s, 3 H, CH_3), 3.46 (s, 3 H, OCH_3), 3.66–3.72 (m, 2 H, H-7, H-9´), 3.86 (s, 3 H, $COOCH_3$), 3.91 (d, 1 H, $J_{9,9'}$ = 12.0, H-9), 3.95 (dd, 1 H, $J_{8,7}$ = 9.1, $J_{8,9'}$ = 6.7, H-8), 4.26 (t, 3 H, $J_{5,4}$ = $J_{5,6}$ = 9.4, H-5), 4.33–4.37 (m, 2 H, H-4, H-6), 6.23 (d, 1 H, $J_{3,4}$ = 2.4, H-3). ^{13}C NMR (150 MHz, D_2O) δ: 22.03 (CH_3), 46.72 (C-5), 52.93 (COO*C*H_3), 55.46 (OCH_3), 62.96 (C-9), 67.86 (C-8), 75.67 (C-4), 76.16 (C-6). HRMS-FAB (*m*/*z*): [M + Na^+] calcd for $C_{13}H_{21}NO_8$, 342.1165; found, 342.1185.

3.5.1.3 Synthesis and Characterization of Substrates and Inhibitors

General procedure for the deprotection to obtain glycals (**2b–2g**) and (**2i**) and sialosides (**1b**) and (**1d–1g**)

The related protected 4-substituted Neu5Ac2en derivative (**6**, **7**, **1S–4S** or **12S**) or the related 4-substituted *p*NP-αNeu5Ac (**9** or **7S–10S**) was dissolved in dry methanol (600 equiv), to which a methanolic sodium methoxide solution (2.5 equiv) was added at 0 °C. After stirring at 0 °C for 30 min, the solution was neutralized by the addition of Amberlite IR-120 resin (NH_4^+ form) and the resin, which was removed by filtration, was then washed several times with methanol. The combined filtrate was concentrated under reduced pressure, and the resulting residue was dissolved in a 3:1 v/v THF/H_2O solution (H_2O, 150 equiv). After adding LiOH.H_2O (2 equiv), the mixture was stirred at 0 °C for 30 min. Subsequently, the solution was neutralized using Amberlite IR-120 resin (NH_4^+

form) and filtered. The resin was then washed thoroughly with methanol, and filtrate was concentrated under reduced pressure to give a solid residue which was recrystallized from methanol and diethyl ether. The so-obtained solid material was then dissolved in H_2O and lyophilized to give the final product as a fluffy powder.

General Procedure for Deprotection to Obtain Compounds (2h) and (1h)

To a solution of the protected *p*NP-4-guanidino-αNeu5Ac **11S** or 4-guanidino-Neu5Ac2en **5S** in dry methanol (600 equiv) was added a methanolic sodium methoxide solution (2.5 equiv) at 0 °C. The resulting solution was stirred at 0 °C for 30 min, and then it was neutralized by Amberlite IR-120 resin (NH_4^+ form). After filtering the mixture, the resin was washed several times with methanol, and combined filtrate was concentrated under reduced pressure. The remaining residue was dissolved in a 3:1 v/v THF/H_2O solution (H_2O, 150 equiv) and treated with $LiOH.H_2O$ (2 equiv) at 0 °C. After stirring the mixture at 0 °C for 30 min, the solution was neutralized using Amberlite IR-120 resin (NH_4^+ form) and filtered. The resin was then washed thoroughly with methanol, and filtrate was concentrated under reduced pressure to give a solid residue. This solid was subsequently dissolved in dichloromethane 50 equiv to which trifluoroacetic acid (40 equiv) was added dropwise at 0 °C. The reaction mixture was warmed to rt and stirring was continued for a further 5 h. After which, the solution was concentrated under reduced pressure to afford a solid residue that was crystallized from methanol and diethyl ether to give the desired final compounds.

General Procedure for the Deprotection to Obtain Glycal (2j) and Sialosides (1c), (1i) and (1j)

Deacetylated 4-OMe-Neu5Ac2en **26S**, *p*NP-4-triazolyl-αNeu5Ac **6S**, *p*NP-4-H-αNeu5Ac **18S**, or *p*NP-4-OMe-αNeu5Ac **25S** was dissolved in a 3:1 v/v THF/H_2O solution (H_2O, 150 equiv) to which LiOH.H_2O (2 equiv) had been added and, the mixture was stirred at 0 °C for 30 min. Then, the solution was neutralized using Amberlite IR-120 resin (NH_4^+ form) and filtered. The resin was then washed thoroughly with methanol, and the filtrate was concentrated under reduced pressure to give a solid residue that was recrystallized from methanol/diethyl ether to give colorless crystals, which were then dissolved in water and lyophilized to give final product as fluffy solid.

5-Acetamido-2,6-anhydro-4-azido-3,4,5-trideoxy-D-*glycero*-D-*galacto*-non-2-enonic acid (2b)

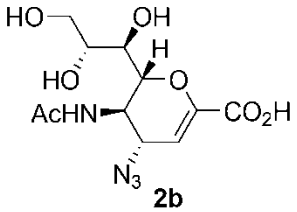

2b

(35 mg, 61%). Mpt = 140 °C (dec); $[\alpha]^{20}_D$ = 57.8 (*c* = 0.22, MeOH). ^{1}H NMR (600 MHz, D_2O) δ: 2.10 (s, 1 H, CH_3), 3.66–3.69 (m, 2 H, H-7, H-9´), 3.92 (dd, 1 H, $J_{9,9'}$ = 11.9, $J_{9,8}$ = 2.1, H-9), 3.97 (ddd, 1 H, $J_{8,9'}$ =9.8, $J_{8,7}$ = 6.3, $J_{8,9}$ = 2.51, H-8), 4.23 (t, 1 H, $J_{5,4}$ = $J_{5,6}$ = 10.0, H-5), 4.31–4.36 (m, 2 H, H-4, H-6), 5.73 (d, 1 H, $J_{3,4}$ = 2.0, H-3); ^{13}C NMR (150 MHz, D_2O) δ: 21.62 (CH_3), 47.26 (C-5), 58.80 (C-4), 62.62 (C-9), 67.59 (C-7), 69.27 (C-8), 74.76 (C-6), 102.88 (C-3), 148.93 (C-2), 168.63 (C-1), 174.07 (C=O). HRMS-FAB (*m*/*z*): [M + H^+] calcd for $C_{11}H_{16}N_4O_7$, 317.1097; found, 317.1090.

5-Acetamido-2,6-anhydro-3,4,5-trideoxy-4-(1-triazolyl)-D-*glycero*-D-*galacto*-non-2-enonic acid (2c)

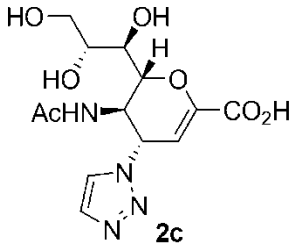

2c

(20 mg, 0.06 mmol, 60%). Mpt 145 °C (dec); $[\alpha]^{20}_{D}$ = +45.00 (*c* 0.05, MeOH). ^{1}H NMR (600 MHz, D_2O) δ: 1.93 (s, 3 H, CH_3), 3.69 (dd, 1 H, $J_{9',9}$ = 11.9, $J_{9',8}$ = 6.2, H-9´), 3.74 (m, 1 H, H-7), 3.93 (dd, 1 H, $J_{9,9'}$ = 11.9, $J_{9,8}$ = 2.5, H-9), 4.02 (m, 1 H, H-8), 4.44 (t, 1 H, $J_{5,4}$ = $J_{5,6}$ = 10.3, H-5), 4.63 (m, 1 H, H-6), 5.63 (dd, 1 H, $J_{4,5}$ = 9.7, $J_{4,3}$ = 2.0, H-4), 6.05 (d, 1 H, $J_{3,4}$ = 2.2, H-3), 7.86 (s, 1 H, H-4´), 8.11 (s, 1 H, H-5´). ^{13}C NMR (150 MHz, D_2O) δ: 20.97 (CH_3), 47.91 (C-5), 58.83 (C-4), 62.34 (C-9), 67.25 (C-7), 69.08 (C-8), 74.97 (C-6), 103.43 (C-3), 123.66 (C-5´), 133.63 (C-4´), 147.72 (C-2), 166.30 (C-1), 173.00 (C=O). HRMS-FAB (*m*/*z*): [M − H^+] calcd for $C_{13}H_{18}N_4O_7$, 341.1097; found, 341.1097.

5-Acetamido-4-amino-2,6-anhydro-3,4,5-trideoxy-D-*glycero*-D-*galacto*-non-2-enonic acid (2d)

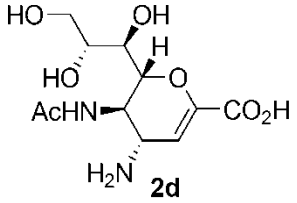

2d

(45 mg, 65%). Mpt = 102 °C (dec); $[\alpha]^{20}_{D}$ = +23.0 (*c* = 0.30, MeOH). ^{1}H NMR (600 MHz, D_2O) δ: 2.09 (s, 3 H, CH_3), 3.62–3.67 (m, 2 H, H-7, H-9´), 3.72 (dd, 1 H, $J_{4,5}$ = 9.4, $J_{4,3}$ = 2.1, H-4), 3.90 (dd, 1 H, $J_{9,9'}$ = 11.9, $J_{9,8}$ = 2.6, H-9), 3.95 (m, 1 H, H-8), 3.99 (t, 1 H, $J_{5,4}$ = $J_{5,6}$ = 10.0, H-5), 4.19 (appd, 1 H $J_{6,5}$ = 10.5, H-6), 5.67 (d, 1 H, $J_{3,4}$ = 2.17, H-3); ^{13}C NMR (150 MHz, D_2O) δ: 21.64 (CH_3), 48.99, 49.13 (2 × C, C-4, C-5), 62.67 (C-9),

67.77 (C-7), 69.32 (C-8), 74.86 (C-6), 106.73 (C-3), 147.35 (C-2), 169.22 (C-1), 174.37 (C=O). HRMS-FAB (*m*/*z*): [M + H^+] calcd for $C_{11}H_{18}N_2O_7$, 291.1192; found, 219.1189.

4,5-Diacetamido-2,6-anhydro-3,4,5-trideoxy-D-*glycero*-D-*galacto*-non-2-enonic acid (2e)

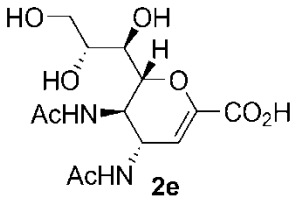

2e

(28 mg, 56%). Mpt = 236 °C (dec); $[\alpha]^{20}_D$ = +7.70 (*c* 0.26, MeOH). ^{1}H NMR (600 MHz, D_2O) δ: 2.00, 2.02 (2 × s, 6 H, CH_3), 3.65–3.68 (m, 2 H, H-7, H-9´), 3.91 (dd, 1 H, $J_{9,9'}$ = 11.76, $J_{9,8}$ = 1.8, H-9), 3.97 (m, 1 H, H-8), 4.13 (t, 1 H, $J_{5,4}$ = $J_{5,6}$ = 10.1, H-5), 4.35 (appd, 1 H, $J_{6,5}$ = 10.7, H-6), 4.78 (m, 1 H, H-4), 5.57 (d, 1 H, $J_{3,4}$ = 1.7, H-3); ^{13}C NMR (150 MHz, D_2O) δ: 21.48, 21.51 (2 × C, CH_3), 47.44, 47.73 (2 × C, C-4, C-5), 62.66 (C-9), 67.69 (C-7), 69.31 (C-8), 74.95 (C-6), 105.08 (C-3), 148.24 (C-2), 168.98 (C-1), 173.91, 173.98 (2 × C=O). HRMS-FAB (*m*/*z*): [M + Na^+] calcd for $C_{13}H_{20}N_2O_8$, 355.1117 found, 355.1118.

5-Acetamido-2,6-anhydro-3,4,5-trideoxy-4-dimethylamino-D-*glycero*-D-*galacto*-non-2-enonic (2f)

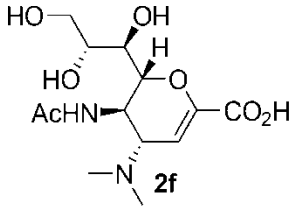

2f

(18 mg, 40%). Mpt = 208 °C (dec); $[\alpha]^{20}_D$ = +58.93 (*c* 0.18, MeOH). ^{1}H NMR (600 MHz, D_2O) δ: 2.06 (s, 3 H, CH_3), 2.29 (2 × s, 6 H, NCH_3), 3.59–3.68 (m, 3 H, H-7, H-4, H-9´), 3.91 (dd, 1 H, $J_{9,9'}$ = 11.5, $J_{9,8}$ = 1.9, H-9), 3.96 (m, 1 H, H-8), 4.14 (appd, 1 H, $J_{6,5}$ = 10.1, H-6), 4.26 (t, 1 H, $J_{5,6}$ = $J_{5,4}$ = 9.8, H-5), 5.82 (d, 1 H, $J_{3,4}$ = 1.9, H-3); ^{13}C NMR

(150 MHz, D_2O) δ: 21.73 (CH_3), 39.03 (2 × C, NCH_3), 43.33 (C-5), 60.89 (C-7), 62.69 (C-4), 68.00 (C-9´), 69.32 (C-8), 75.43 (C-6), 103.13 (C-3), 149.21 (C-2), 169.07 (C-1), 173.86 (C=O). HRMS-FAB (*m*/*z*): [M + H^+] calcd for $C_{13}H_{22}N_2O_7$, 319.1505; found, 319.1513.

5-Acetamido-2,6-anhydro-4-isopropylamino-3,4,5-trideoxy-D-*glycero*-D-*galacto*-non-2-enonic (2g)

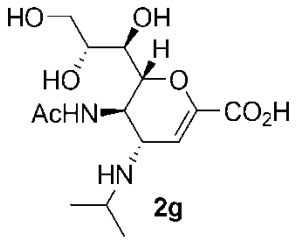

2g

(22 mg, 50%). Mpt 190 °C (dec); $[\alpha]^{20}_D$ = +25.3 (*c* = 0.12, MeOH). ^{1}H NMR (600 MHz, D_2O) δ: 1.09 (2 × d, 6 H, *J* = 6.3, $CH(CH_3)_2$), 2.08 (s, 3 H, CH_3), 3.06 (septet, 1 H, *J* = 6.6, $(CH_3)_2C$-*H*), 3.61–3.68 (m, 3 H, -H-7, H-4, H-9´), 3.91 (dd, 1 H, $J_{9,9'}$ = 11.99, $J_{9,8}$ = 1.8, H-9), 3.96 (m, 1 H, H-8), 4.01 (t, 1 H, $J_{5,4}$ = $J_{5,6}$ = 9.2, H-5), 4.19 (appd,, 1 H, *J* = 9.5, H-6), 5.82 (d, 1 H, $J_{3,4}$ = 1.7, H-3); ^{13}C NMR (150 MHz, D_2O) δ: 20.73, 21.57, 21.60 (3 × C, CH_3), 44.79 ($C(CH_3)_2$), 47.84 (C-5), 51.60 (C-4), 62.69 (C-9´), 68.36 (C-8), 75.09 (C-6), 106.11 (C-3), 146.98 (C-2), 169.51 (C-1), 174.15 (C=O). HRMS-FAB (*m*/*z*): [M + H^+] calcd for $C_{14}H_{24}N_2O_7$, 333.1662; found, 333.1671.

5-Acetamido-2,6-anhydro-4-guanidino-3,4,5-trideoxy-D-*glycero*-D-*galacto*-non-2-enonic acid (2h)

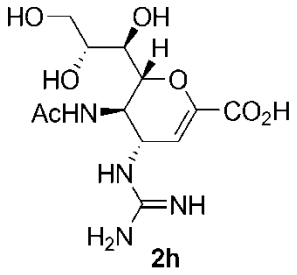

2h

(31 mg, 63%). Mpt 268 °C (dec); $[\alpha]^{20}_{D}$ = +9.1 (*c* = 0.11, MeOH). ^{1}H NMR (600 MHz, D_2O) δ: 2.06 (s, 3 H, CH_3), 3.66–3.71 (m, 2 H, H-7, H-9´), 3.92 (dd, 1 H, $J_{9,9'}$ = 11.9, $J_{9,8}$ = 2.63, H-9), 3.98 (ddd, 1 H, $J_{8,9'}$ = 9.7, $J_{8,7}$ = 5.9, $J_{8,9}$ = 2.33, H-8), 4.25 (t, 1 H, $J_{5,4}$ = $J_{5,6}$ = 9.9, H-5), 4.41 (m, 1 H, H-6), 4.48 (dd, 1 H, $J_{4,5}$ = 9.3, $J_{4,3}$ = 2.31, H-4), 5.67 (d, 1 H, $J_{3,4}$ = 2.4, H-3); ^{13}C NMR (150 MHz, D_2O) δ: 21.47 (CH_3), 47.24 (C-5), 50.65 (C-4), 62.56 (C-9), 67.65 (C-7), 69.28 (C-8), 74.91 (C-6), 103.53 (C-3), 148.57 (C=N), 156.53 (C-2), 168.49 (C-1), 173.93 (C=O). HRMS-FAB (*m*/*z*): [M + H^+] calcd for $C_{12}H_{20}N_4O_7$, 333.1410; found, 333.1409.

5-Acetamido-2,6-anhydro-2,3,4,5-tetradeoxy-D-*glycero*-D-*galacto*-non-2-enonic acid (2i)

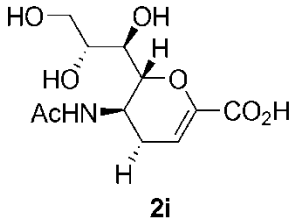

2i

(60 mg, 86%). Mpt > 200°C (dec); $[\alpha]^{20}_{D}$ = –3.70 (*c* = 0.40, MeOH). ^{1}H NMR (600 MHz, D_2O) δ: 2.04 (s, 3 H, CH_3), 2.26 (ddd, 1 H, $J_{4e,4a}$ = 18.3, $J_{4e,5}$ = 9.8, $J_{4e,3}$ = 2.9, H-4_{ax}), 2.53 (dt, 1 H, $J_{4a,4e}$ = 18.4, $J_{4a,3}$ = $J_{4a,5}$ = 5.7, H-4_{ax}), 3.65−3.69 (m, 2 H, H-7, H-9´), 3.90 (dd, 1 H, $J_{9,9'}$ = 11.9, $J_{9,8}$ = 2.7, H-9), 3.96 (ddd, 1 H, $J_{8,9'}$ = 9.2, $J_{8,7}$ = 6.3, $J_{8,9}$ = 2.8, H-8), 4.03 (dd, 1 H, $J_{6,5}$ = 9.5, $J_{6,7}$ = 1.4, H-6), 4.18 (td, 1 H, $J_{5,6}$ = $J_{5,4e}$ = 9.7, $J_{5,4e}$ = 6.1,

H-5), 5.92 (dd, 1 H, $J_{3,4a}$ = 5.4, $J_{5,4e}$ = 2.9, H-3); ^{13}C NMR (150 MHz, D_2O) δ: 21.98 (CH_3), 26.90 (C-4), 42.66 (C-5), 63.13 (C-9), 68.47 (C-7), 70.0 (C-8), 75.53 (C-6), 105.62 (C-3), 146.88 (C-2), 170.36 (C-1), 174.08 (C=O). HRMS-FAB (*m*/*z*): [M + Na^+] calcd for $C_{11}H_{17}NO_7$, 298.0902; found, 298.0912.

5-acetamido-2,6-anhydro-3,4,5-trideoxy-4-methoxy-D-*glycero*-D-*galacto*-non-2-enonic acid (2j)

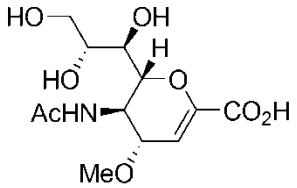

2j

(15 mg, 0.05 mmol, 83%) as a pale yellow powder. Mpt >200 °C (dec); $[\alpha]^{20}_D$ = +25.55 (c = 0.09, MeOH);); ^{1}H NMR (600 MHz, D_2O) δ: 2.07 (s, 3 H, CH_3), 3.43 (s, 3 H, OCH_3), 3.64 (d, 1 H, $J_{7,8}$ = 9.4, H-7), 3.67 (dd, 1 H, $J_{9',9}$ = 11.9, $J_{9',8}$ = 6.3, H-9´), 3.89 (dd, 1 H, $J_{9,9'}$ = 12.0, $J_{9,8}$ = 2.6, H-9), 3.94 (ddd, 1 H, $J_{8,7}$ = 9.1, $J_{8,9'}$ = 6.3, $J_{8,9}$ = 2.6, H-8), 4.22–4.29 (m, 2 H, H-5, H-6), 4.34 (m, 1 H, H-4), 6.00 (d, $J_{3,4}$ = 2.2, H-3); ^{13}C NMR (150 MHz, D_2O) δ: 21.77 (CH_3), 46.49 (C-5), 54.92 (OCH_3), 62.76 (C-9), 67.79 (C-7), 69.49 (C-8), 75.42 (C-6), 75.67 (C-4), 106.32 (C-3), 146.81 (C-2), 167.34 (C-1), 174.25 (C=O). HRMS-FAB (*m*/*z*): [M + Na^+] calcd for $C_{12}H_{19}NO_8$, 328.1008; found, 328.0992.

4-Nitrophenyl 5-acetamido-4-azido-3,4,5-trideoxy-α-D-*glycero*-D-*galacto*-non-2-ulpyranosylonic acid (1b)

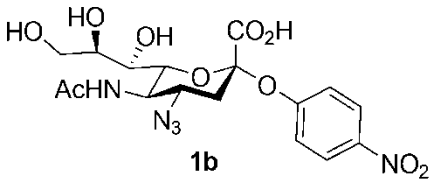

1b

60% yield (25 mg); Mpt = 232 °C (dec); $[\alpha]^{20}_D$ = +15.9 (*c* = 0.31, MeOH). ^{1}H NMR (600 MHz, D_2O) δ: 2.04–2.11 (m, 4 H, CH_3, H-3_{ax}), 2.88 (dd, 1 H, $J_{3e,3a}$ = 12.5, $J_{3e,4}$ = 4.5,

H-3_{eq}), 3.64–3.67 (m, 2 H, H-7, H-9´), 3.77 (m, 1 H, H-4), 3.86–3.88 (m, 2 H, H-8, H-9), 4.13 (t, 1 H, $J_{5,4}$ = $J_{5,6}$ = 10.4, H-5), 4.31 (dd, 1 H, $J_{6,5}$ = 10.5, $J_{6,7}$ = 1.4, H-6), 7.31 (m, 2 H, Ar-H), 8.35 (m, 2 H, Ar-H); ^{13}C NMR (150 MHz, D_2O) δ: 21.57 (CH_3), 37.17 (C-3), 49.27 (C-5), 58.25 (C-4), 62.36(C-9), 67.61 (C-7), 70.67 (C-8), 73.47 (C-6), 101, 16 (C-2), 119.40 (2 × C, C-2´, C-4´), 125.12 (2 × C, C-3´, C-5´), 142.66 (C-4´), 159.21 (C-1´), 172.63 (C-1), 174.42 (C=O). HRMS-FAB (*m*/*z*): [M + Na^+] calcd for $C_{17}H_{21}N_5O_{10}$, 478.1186; found, 478.1183.

4-Nitrophenyl 5-acetamido-3,4,5-trideoxy-4-(1-triazolyl)-α-*D*-*glycero*-D-*galacto*-non-2-ulpyranosylonic acid (1c)

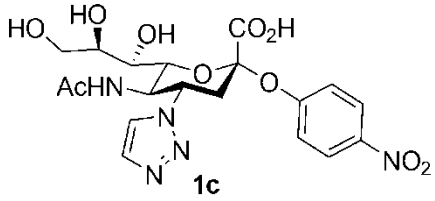

1c

(15 mg, 43%). Mpt = 168 °C (dec); $[\alpha]^{20}_D$ = +16.3 (*c* = 0.06, MeOH). ^{1}H NMR (600 MHz, D_2O) δ: 1.84 (s, 3 H, CH_3), 2.83 (t, 1 H, $J_{3a,3e}$ = $J_{3e,4}$ = 12.8, H-3_{ax}), 3.09 (dd, 1 H, $J_{3e,3a}$ = 12.9, $J_{3e,4}$ = 4.4, H-3_{eq}), 3.65–3.70 (m, 2 H, H-7, H-9´), 3.87–3.94 (m, 2 H, H-8, H-9), 4.50–4.56 (m, 2 H, H-5, H-6), 4.90 (m, 1 H, H-4), 7.36 (m, 2 H, Ar-H), 7.83 (d, 1 H, $J_{4´,5´}$ = 0.9, H-4´-triazole), 8.15 (d, 1 H, $J_{5´,4´}$ = 0.9, H-5´-triazole), 8.27 (m, 2 H, Ar-H); ^{13}C NMR (150 MHz, D_2O) δ: 21.05 (CH_3), 37.52 (C-3), 49.47 (C-5), 58.72 (C-4), 62.31 (C-9), 67.71 (C-7), 70.80 (C-8), 73.69 (C-6), 101.66 (C-2), 119.56 (2 × C, C-2´-Ar, C-6´-Ar), 124.38 (C-5´-triazole), 125.12 (2 × C, C-3´-Ar, C-5´-Ar), 133.35 (C-4´-triazole), 142.69 (C-4´-Ar), 159.32 (C-1´), 171.73 (C-1), 173.45 (C=O). HRMS-FAB (*m*/*z*): [M + Na^+] calcd for $C_{19}H_{23}N_5O_{10}$, 504.1343; found, 504.1335.

4-Nitrophenyl 5-acetamido-4-amino-3,4,5-trideoxy-α-D-*glycero*-D-*galacto*-non-2-ulpyranosylonic acid (1d)

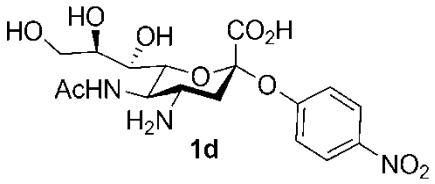

1d

(22 mg, 47%). Mpt = 144 °C (dec); $[\alpha]^{20}_{D}$ = +38.4 (*c* = 0.21, MeOH). ^{1}H NMR (600 MHz, D_2O) δ: 2.06 (s, 3 H, CH_3), 2.20 (t, 1 H, $J_{3a,3e}$ = $J_{3a,4}$ = 12.5, H-3_{ax}), 2.90 (dd, 1 H, $J_{3e,4}$ = 12.9, $J_{3e,4}$ = 4.0, H-3_{eq}), 3.48 (m, 1 H, H-4), 3.62–3.65 (m, 2 H, H-7, H-9´), 3.83–3.88 (m, 2 H, H-8, H-9), 4.24 (t, $J_{5,4}$ = $J_{5,6}$ = 10.1, H-5), 4.36 (m, 1 H, H-6), 7.28 (m, 2 H, Ar-H), 8.21 (m, 2 H, Ar-H). ^{13}C NMR (150 MHz, D_2O) δ: 21.60 (CH_3), 36.20 (C-3´), 47.52 (C-5), 49.38 (C-4), 62.23 (C-9), 67.48 (C-7), 70.69 (C-8), 73.26 (C-6), 101.17 (C-2), 119.26 (2 × C, C-2´-Ar, C-6´-Ar), 125.09 (2 × C, C-3´-Ar, C-5´-Ar), 142.59 (C-4´), 159.23 (C-1´), 171.63 (C-1), 174.59 (C=O). HRMS-FAB (*m*/*z*): [M + H^+] calcd for $C_{17}H_{23}N_3O_{10}$, 430.1462; found, 430.1464.

4-Nitrophenyl 4,5-diacetamido-3,4,5-trideoxy-α-D-*glycero*-D-*galacto*-non-2-ulpyranosylonic acid (1e)

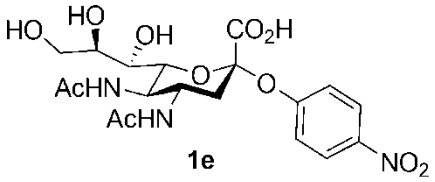

1e

(20 mg, 60%). Mpt = 146 °C (dec); $[\alpha]^{20}_{D}$ = +28.10 (*c* = 0.32, MeOH). ^{1}H NMR (600 MHz, D_2O) δ: 2.01 (s, 6 H, CH_3), 2.08 (t, 1 H, $J_{3a,3e}$ = $J_{3a,3e}$ = 12.2, H-3a), 2.74 (m, 1 H, H-3_{eq}), 3.62–3.66 (m, 2 H, H-7, H-9´), 3.85–3.87 (m, 2 H, H-8, H-9), 4.05–4.14 (m, 2 H, H-4, H-5), 4.34 (m, 1 H, H-6), 7.32 (m, 2 H, Ar-H), 8.25 (m, 2 H, Ar-H); ^{13}C NMR (150 MHz, D_2O) δ: 21.44 (CH_3), 37.61 (C-3), 47.34 (C-4), 49.12 (C-5), 62.36 (C-9), 67.78 (C-7), 70.81 (C-8), 73.81 (C-6), 101.53 (C-2), 119.44 (2 × C, C-2´, C-4´), 125.12 (2 × C, C-

3´, C-5´), 142.63 (C-4´), 159.36 (C-1´), 171.91 (C-1), 173.30, 174.21 (2 × C=O). HRMS-FAB (*m*/*z*): [M + Na^+] calcd for $C_{19}H_{25}N_3O_{11}$, 494.1387; found, 494.1384.

4-Nitrophenyl 5-acetamido-3,4,5-trideoxy-4-dimethylamino-α-D-glycero-D-galacto-non-2-ulpyranosylonic acid (1f)

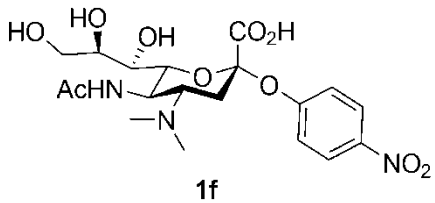

1f

(15 mg, 45%). Mpt = 130–131 °C (dec); $[\alpha]^{20}_D$ = + 30.21 (*c* = 0.15, MeOH). ^{1}H NMR (600 MHz, D_2O) δ: 2.00 (t, 1 H, $J_{3a,3e}$ = $J_{3a,4}$ = 12.6, H-3_{ex}), 2.05 (s, 3 H, CH_3), 2.31 (s, 6 H, $N(CH_3)_2$), 2.71 (dd, 1 H, $J_{3e,3a}$ = 12.7, $J_{3e,4}$ = 3.8, H-3_{eq}), 2.95 (td, 1 H, $J_{4,3a}$ = $J_{4,5}$ = 12.1, $J_{4,3e}$ = 3.4, H-4), 3.58 (d, 1 H, $J_{7,8}$ = 8.8, H-7), 3.63 (dd, 1 H, $J_{9,9'}$ = 12.5, $J_{9',8}$ = 6.7, H-9´), 3.84–3.86 (m, 2 H, H-8, H-9), 4.14–4.21 (m, 2 H, H-5, H-6), 7.29 (m, 2 H, Ar-H), 8.23 (m, 2 H, Ar-H). ^{13}C NMR (150 MHz, D_2O) δ: 22.25 (CH_3), 30.69 (C-3), 39.17 ($N(CH_3)_2$), 46.50 (C-5), 60.52 (C-4), 62.79 (C-9), 68.48 (C-7), 71.41 (C-8), 75.09 (C-6), 103.33 (C-2), 119.99 (C-2´, C-6´), 125.56 (C-3´,C-5´), 143.02 (C-4´), 160.07 (C-1´), 172.85 (C-1), 174.52 (C=O). HRMS-FAB (*m*/*z*): [M + H^+] calcd for $C_{19}H_{27}N_3O_{10}$, 458.1775; found, 458.1777.

4-Nitrophenyl 5-acetamido-3,4,5-trideoxy-4-isopropylamino-α-D-*glycero*-D-*galacto*-non-2-ulopyranosylonic acid (1g)

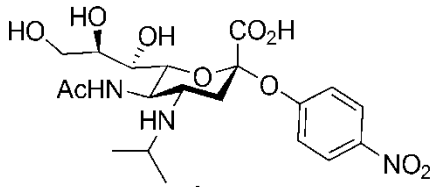

1g

(23 mg, 52%). Mpt = 140 °C (dec); $[\alpha]^{20}_D$ = +37.5 (*c* = 0.21, MeOH). ^{1}H NMR (600 MHz, D_2O) δ: 1.31, 1.35 (2 × D, 6 H, *J* = 6.36, $CH(CH_3)_2$), 2.08 (s, 3 H, OCH_3), 2.25 (t, 1

H, $J_{3a,3}$e = $J_{3a,4}$ = 11.7, H-3$_{ax}$), 2.93 (dd, 1 H, $J_{3e,3a}$ = 13.4, $J_{3e,4}$ = 4.2, H-3$_{eq}$), 3.54–3.69 (m, 4 H, H-4, H-7, H-9′, $(CH_3)_2$C-H), 3.87–3.93 (m, 2 H, H-8, H-9), 4.29–4.32 (m, 2 H, H-5, H-6), 7.30 (m, 2 H, Ar-H), 8.25 (m, 2 H, Ar-H); ^{13}C NMR (150 MHz, D_2O) δ: 17.34, 18.82 (2 × C, C(CH_3)$_2$), 21.66 (OCH_3), 33.78 (C-3), 47.09, 47.60 (2 × C, C-5, $C(CH_3)_2$), 52.90 (C-4), 62.20 (C-9), 67.49 (C-7), 70.78 (C-8), 73.11 (C-6), 101.37 (C-2), 119.09 (2 × C, C-2′-Ar, C-4′-Ar), 125.16 (2 × C, C-3′-Ar, C-5′-Ar), 142.61 (C-4′), 159.21 (C-1′), 171.72 (C-1), 174.59 (C=O). HRMS-FAB (*m*/*z*): [M + Na^+] calcd for $C_{20}H_{29}N_3O_{10}$, 494.1751; found, 494.1743.

4-Nitrophenyl 5-acetamido-3,4,5-trideoxy-4-guanidino-α-D-*glycero*-D-*galacto*-non-2-ulpyranosylonic acid (1h)

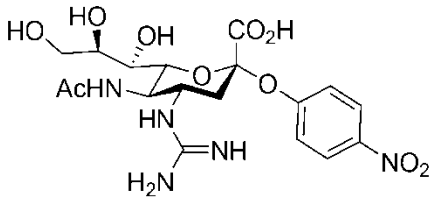

1h

(20 mg, 55%). Mpt = 124 °C (dec); $[\alpha]^{20}_D$ = +16.8 (*c* = 0.18, MeOH). ^{1}H NMR (600 MHz, D_2O) δ: 2.04 (s, 3 H, CH_3), 2.18 (t, 1 H, $J_{3a,3e}$ = $J_{3a,4}$ = 12.4, H-3$_{ax}$), 2.85 (dd, 1 H, $J_{3e,3a}$ = 13.5, $J_{3e,4}$ = 4.3, H-3$_{eq}$), 3.65–3.68 (m, 2 H, H-7, H-9′), 3.80 (m, 1 H, H-4), 3.86–3.90 (m, 2 H, H-8, H-9), 4.16 (t, 1 H, $J_{5,4}$ = $J_{5,6}$ = 10.0, H-5), 4.38 (m, 1 H, H-6), 7.32 (m, 2 H, Ar-H), 8.25 (m, 2 H, Ar-H). ^{13}C NMR (150 MHz, D_2O) δ:21.40 (CH_3), 37.50 (C-3), 49.44 (C-5), 50.69 (C-4), 62.26 (C-9), 67.65 (C-7), 70.80 (C-8), 73.23 (C-6), 101.47 (C-2), 119.44 (2 × C, C-2′, C-6′), 125.10 (2 × C, C-3′, C-5′), 142.65 (C-4′), 156.16 (C=N), 159.30 (C-1′), 172.05 (C-1), 174.21 (C=O). HRMS-FAB (*m*/*z*): [M + H^+] calcd for $C_{18}H_{25}N_5O_{10}$, 472.1680; found, 472.1679

4-Nitrophenyl (5-acetamido-3,4,5-trideoxy-α-D-*manno*-non-2-nonulopyranosylonic acid) (1i)

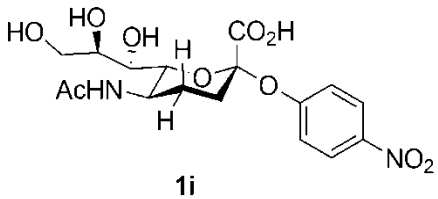

1i

(30 mg, ,75%) as yellowish white powder. Mpt 130−131 °C; $[\alpha]^{20}_{D}$ = + 10.27 (c = 0.15, MeOH); ^{1}H NMR (600 MHz, D_2O) δ: 1.63 (qd, 1 H, $J_{4a,4e} = J_{4a,3e} = J_{4a,5}$ = 13.6, $J_{4a,3e}$ = 4.0, H-4_{ax}), 2.01 (s, 3 H, CH_3), 2.05 (td, 1 H, $J_{3a,3e} = J_{3a,4a}$ = 13.6, $J_{3a,4e}$ = 4.54, H-3_{ax}), 2.16 (m, 1 H, H-4_{eq}), 2.50 (dt, 1 H, $J_{3e,3a} = J_{3e,4e}$ = 13.7, $J_{3e,4a}$ = 4.3, H-3_{eq}), 3.61–3.66 (m, 2 H, H-9´, H-7), 3.84–3.88 (m, 2 H, H-9, H-8), 4.07 (td, 1 H, $J_{5,6} = J_{5,4a}$ = 10.3, $J_{5,4e}$ = 4.5, H-5), 4.15 (dd, 1 H, $J_{6,5}$ = 10.3, $J_{6,7}$ = 1.03, H-6), 7.28 (m, 2 H, Ar-H), 8.22 (m, 2 H, Ar-H); ^{13}C NMR (150 MHz, D_2O) δ: 21.96 (CH_3), 25.95 (C-4), 32.05 (C-3), 44.26 (C-5), 62.80 (C-9), 68.44 (C-7), 71.49 (C-8), 76.09 (C-6), 103.25 (C-2), 119.73 (C-2´, C-6´), 125.61 (C-3´, C-5´), 142.88 (C-4´), 160.35 (C-1´), 173.75 (C-1), 174.33 (C=O). HRMS-FAB (m/z): [M – H^+] calcd for $C_{17}H_{21}N_2O_{10}$, 413.1196; found, 413.1194.

4-Nitrophenyl 5-acetamido-3,4,5-trideoxy-4-methoxy-D-*glycero*-α-D-*galacto*-non-2-ulopyranosylonic acid (1j)

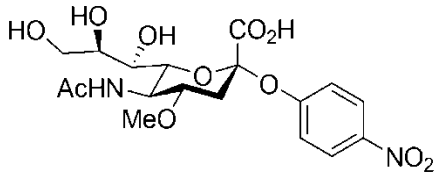

1j

(100 mg, 72%) as yellow powder. Mpt 172−173°C (dec); $[\alpha]^{20}_{D}$ = +61.79 (c = 0.18, MeOH); ^{1}H NMR (600 MHz, D_2O) δ: 1.97 (dd, 1 H, $J_{3a,3e}$ = 12.8, $J_{3a,4}$ = 10.8, H-3_{ax}), 2.04 (s, 3 H, CH_3), 2.96 (dd, 1 H, $J_{3e,3a}$ = 12.9, $J_{3e,4}$ = 4.6, H-3_{eq}), 3.43 (s, 3 H, OCH_3), 3.55–3.59 (m, 2 H, H-4, H-7), 3.64 (dd, 1H, $J_{9,9'}$ = 11.8, $J_{9',8}$ = 6.2, H-9´), 3.84–3.88 (m, 2

H, H-8, H-9), 4.04 (t, 1 H, $J_{5,6}$ = $J_{5,4}$ = 10.0, H-5), 4.14 (d, 1 H, $J_{6,5}$ = 10.6, H-6), 7.27 (m, 2 H, Ar-H), 8.21 (m, 2 H, Ar-H); ^{13}C NMR (150 MHz, D_2O) δ: 21.79 (CH_3), 37.13 (C-3), 49.81 (C-5), 56.29 (OCH_3), 62.55 (C-9), 67.95 (C-7), 71.08 (C-8), 73.56 (C-6), 76.90 (C-4), 102.22 (C-2), 119.47 (C-2´, C-6´), 125.43 (C-3´, C-5´), 142.76 (C-4´), 159.84 (C-1´), 172.96 (C-1), 174.73 (C=O). HRMS-FAB (*m*/*z*): [M + Na^+] calcd for $C_{18}H_{24}N_2O_{11}$, 467.1278; found, 467.1257.

3.5.2 Supporting Schemes

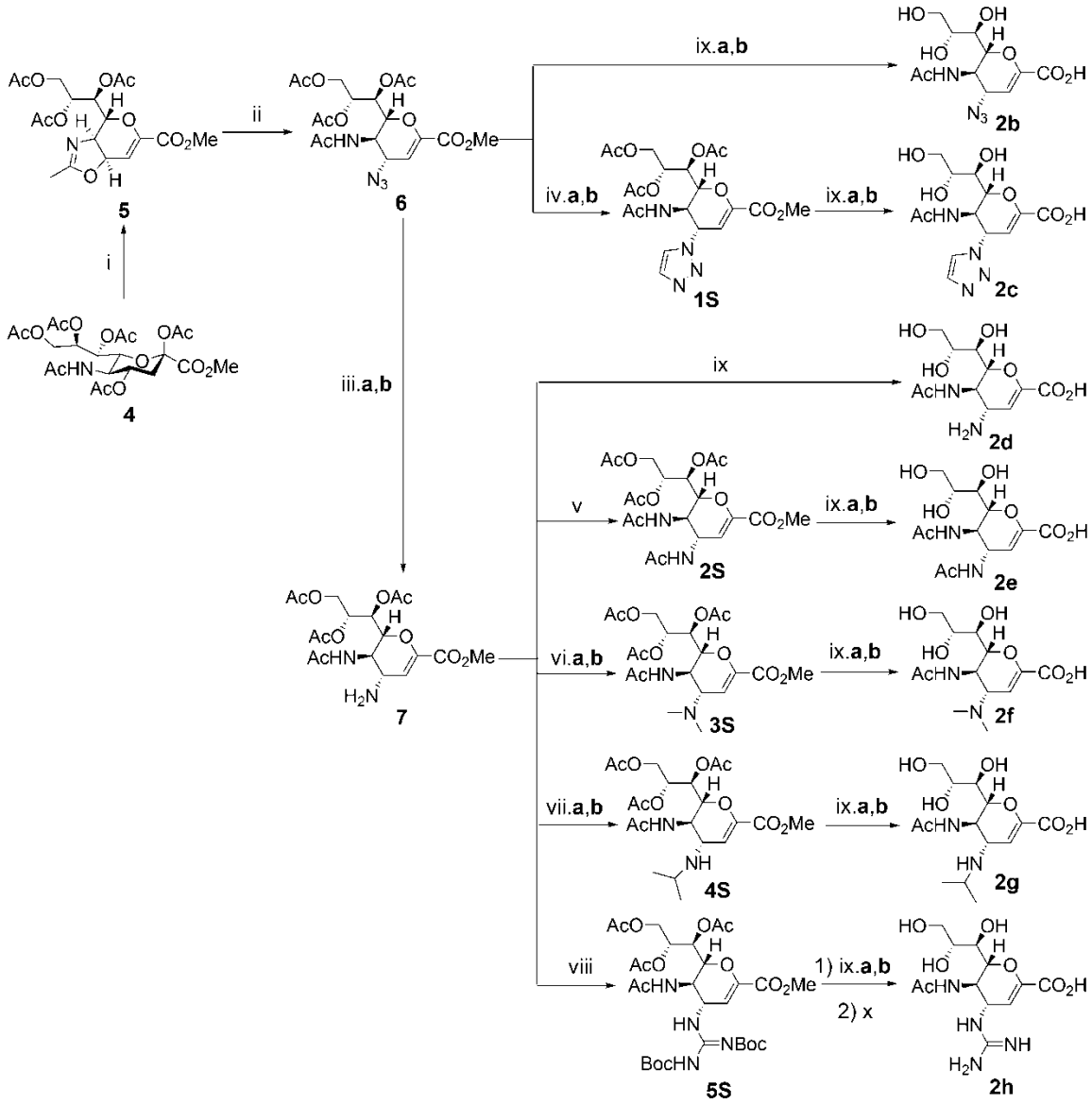

Scheme 3.3. Reagents and conditions: (i) TMSOTf (3 equiv), EtOAc, 50°C, 3 h, 83%; (ii) $TMSN_3$ (1.5 equiv), tert-BuOH, 80 °C, 2 h, 73% ; (iii) a. PPh_3 (1.15 equiv), THF, 2 h, rt; b. H_2O, (50 equiv), rt, 24 h, 80 %; (iv) a. CHCCOOH (5 equiv), Toluene, 2 h, reflux; b. Heat to melt point under vacuum, 42%; (v) Ac_2O (20 equiv), Et_3N (1.5 equiv), CH_2Cl_2, rt, 1 h, 80 %; (vi) a. HCOH (10 equiv), MeOH, rt, 2 h; b. $NaCNBH_3$ (1.5 equiv), rt, 30 min, 62%; (vii) a. H_3CCOCH_3 (10 equiv), MeOH, rt, 2 h; b. $NaCNBH_3$ (1.5 equiv), rt, overnight, 64 %; (viii) N,N´-di-Boc-thiourea (1.14 equiv), Et_3N (300 equiv), $HgCl_2$ (1 equiv), DMF, 5 h, 0°, 51%; (ix) a. NaOMe (2.5 equiv), MeOH (dry), 0 °C, 30 min; b. LiOH (2 equiv), THF/H_2O (3:1), 0 °C, 30 min 40–65%; (x) TFA (40 equiv), CH_2Cl_2, 5 h, 0°C to rt, 63%.

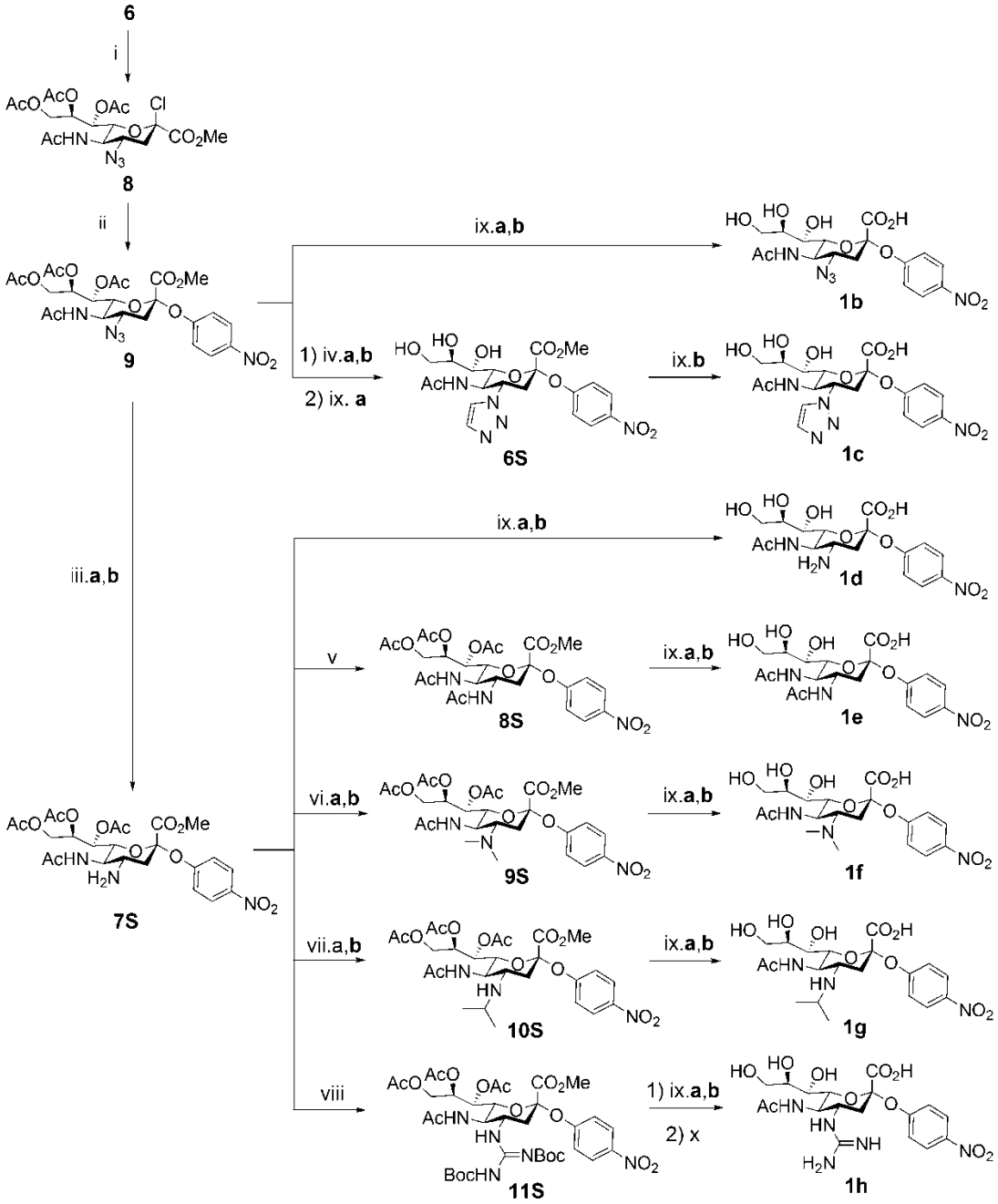

Scheme 3.4. Reagents and conditions: (i) HCl (gas), CH_3CN, Molecular sieves (4Å), LiCl (5.3 equiv), rt, 4 days, 85%; (ii) 4-Nitrophenol (10 equiv), Hunig's base (15 equiv), CH_3CN, rt, 18 h, 50 %; (iii) a. PPh_3 (1.5 equiv), THF, 12 h, rt; b. H_2O, (50 equiv), rt, 24 h, 83 %; (iv) a. CHCCOOH (6 equiv), Toluene, 3 h, reflux; b. Heat to melt point under vacuum, 23% for 6S (overall iv and ix.a); (v) Ac_2O (10 equiv), Et_3N (1.4 equiv), CH_2Cl_2, rt, 1 h, 80 %; (vi) a. HCOH (10 equiv), MeOH, rt, 12 h; b. $NaCNBH_3$ (1.5 equiv), rt, 30 min, 68%; (vii) a. H_3CCOCH_3 (10 equiv), MeOH, rt, 12 h; b. $NaCNBH_3$ (1.5 equiv), rt, 10 min, 82 %; (viii) *N*,*N*´-di-^{t}Boc-thiourea (1.2 equiv), Et_3N (300 equiv), $HgCl_2$ (1 equiv), DMF, 5 h, 0°C, 61%; (ix) a. NaOMe (2.5 equiv), MeOH (dry), 0 °C; b. LiOH (2 equiv), THF/H_2O (3:1), 0 °C, 43–60%; (x) TFA (40 equiv), CH_2Cl_2, 5 h, 0°C to rt, 55%.

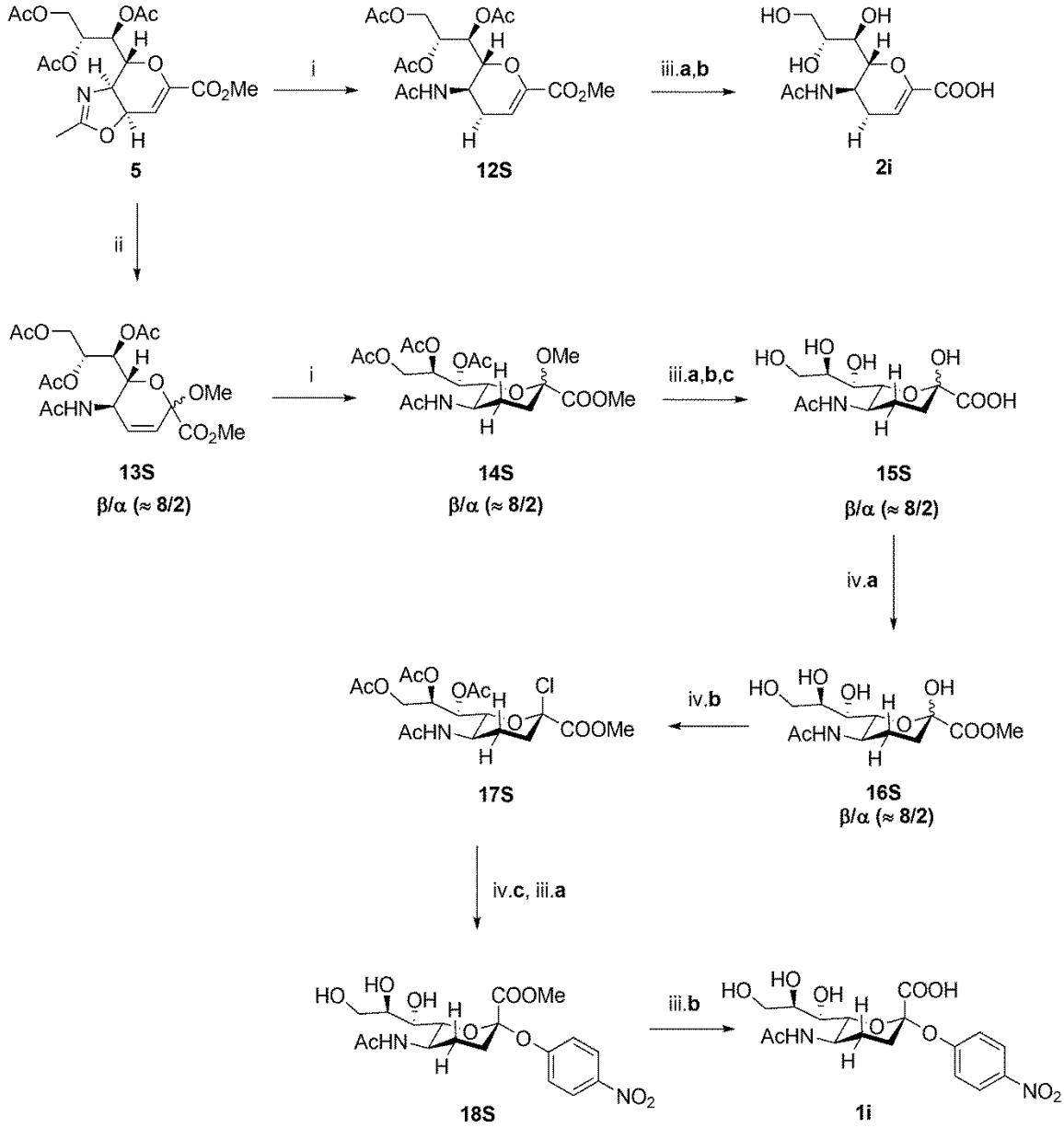

Scheme 3.5. Reagents and conditions: (i) H_2 (gas), Pd/C (10% Pd, 0.07 equiv), Dioxane, rt, 10 h, 68% for 12S and 95% for 14S; (ii) Methanol (20 equiv), BF_3-OEt_2 (1 equiv), CH_2Cl_2, rt, 3 h, N_2 atmosphere, 80 %; (iii) a. NaOMe (2.5 equiv), MeOH (dry), 0 °C; b. LiOH (2 equiv), THF/H_2O (3:1), 0 °C, 30 min; c. HCl (0.025 M), Amberlite IR-120 (H+), 70°C, 16 h, 67% for 15S (overall iii.a,b,c), 86% for 2i (iii.a,b) and 75% for 1i (only iii.b); (iv) a. MeOH, Amberlite IR-120 (H^+), N_2 atmosphere, rt, 3 h; b. MeOH (100 equiv), AcCl (275 equiv), AcOH (137 equiv), rt, 48 h; c. 4-Nitrophenol (8 equiv), Hunig's base (11 equiv), CH_3CN, rt, 48 h, 20 % for 18S (overall iv.a,b,c and iii. a).

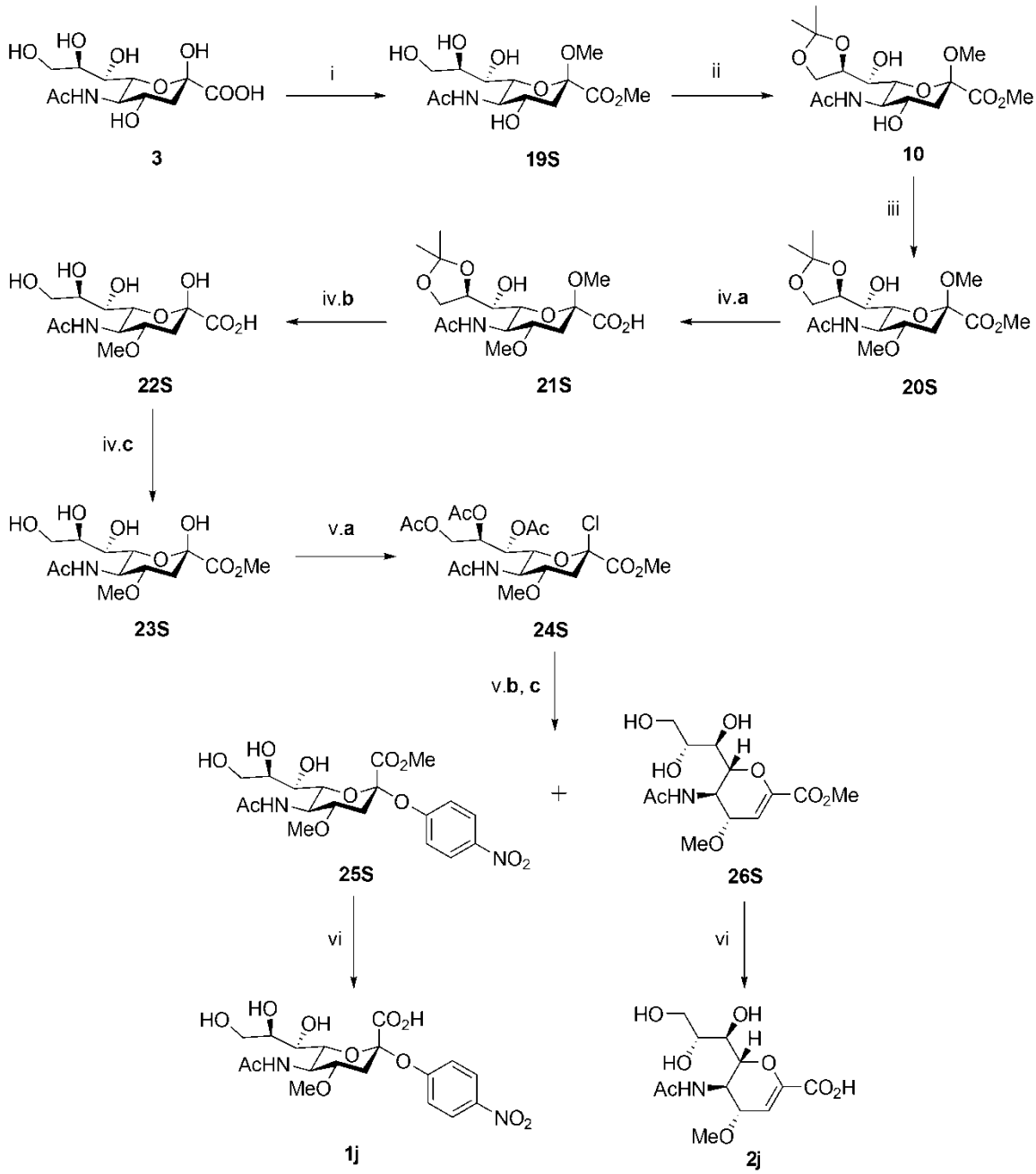

Scheme 3.6. Reagents and conditions: (i) Amberlite IR-12 (H^+), MeOH, reflux, 48 h, 93%; (ii) Acetone, PTSA (0.05 equiv), rt, 4 h, 85%; (iii) NaH (1.4 equiv), Me_2SO_4 (1.4 equiv), 0°C, 20 min, 82%; (iv) a. MeOH/H_2O (1:1), NaOH (2 equiv), rt, 1 h; b. HCl (0.025 M), Amberlite IR-120 (H+), 70°C, 16 h; c. MeOH, Amberlite IR-120 (H^+), N_2 atmosphere, rt, 3 h, 85% for 23S (overall iv.a,b,c); (v) a. MeOH (100 equiv), AcCl (280 equiv), AcOH (140 equiv), rt, 48 h; b. 4-Nitrophenol (10 equiv), Hunig's base (15 equiv), CH_3CN, rt, 48 h; c. NaOMe (2.5 equiv), MeOH (dry), 0 °C, 42% for the mixture of 25S/26S (7.7:2.3) (overall v.a,b,c). (vi) LiOH (2 equiv), THF/H_2O (3:1), 0 °C, 30 min, 72% for 1j and 83% for 2j.

3.5.3 Supporting Figures

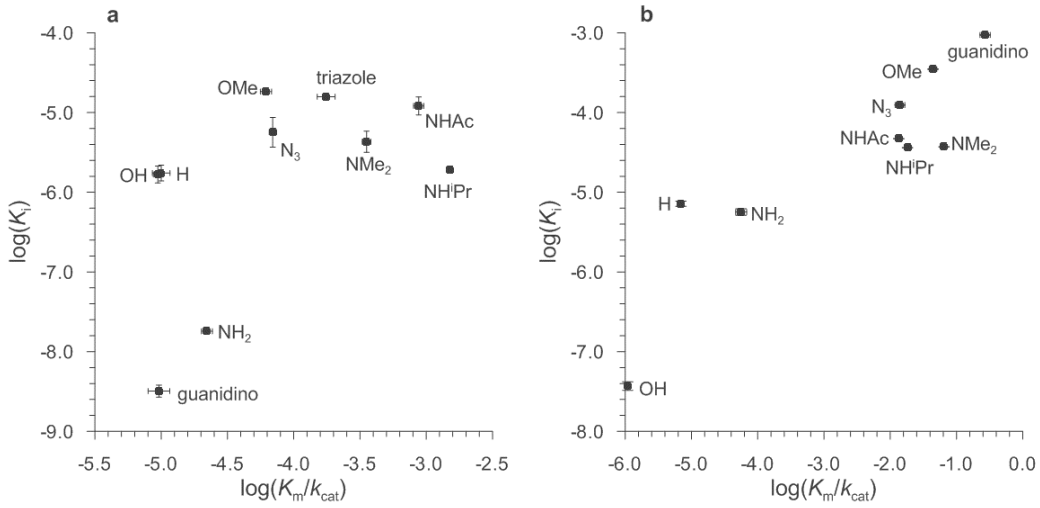

Figure 3.4. Neuraminidases: Linear free energy correlations. Plots of log(K_m/k_{cat}) for a neuraminidase-catalyzed hydrolysis of pNP 4-substituted-sialosides (**1a–j**) versus log(K_i) for the corresponding glycal inhibitor (**2a–j**). Panel **a** displays the data for the influenza N2 enzyme while panel **b** shows the results for the *Micromonospora viridifaciens* neuraminidase. Error bars are shown or are encompassed within the symbol diameter.

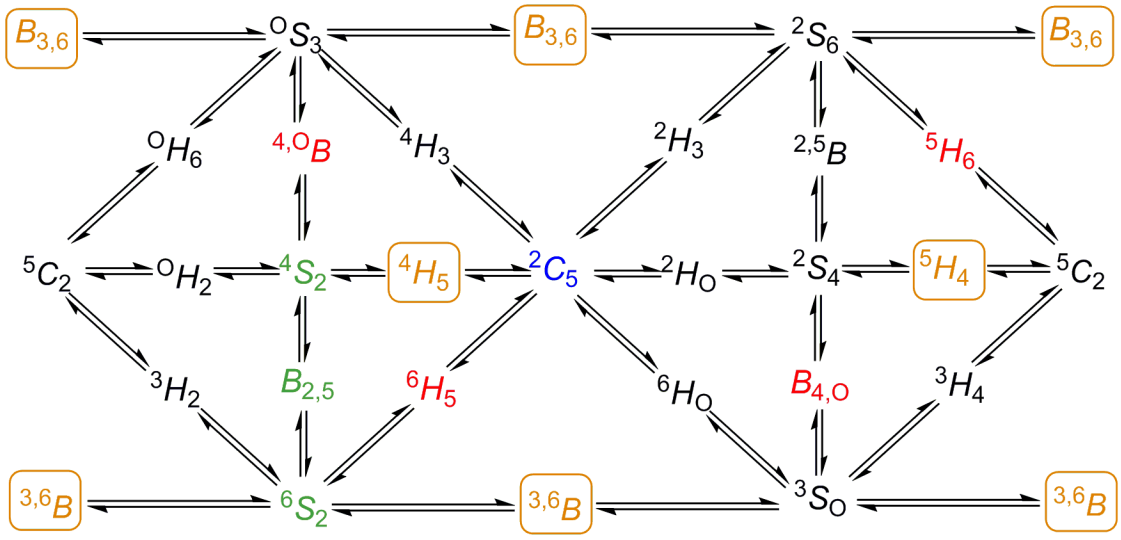

Figure 3.5. A transverse Mercator projection of the conformational itinerary for sialosyl units. The four low-energy conformations of DANA (Neu2en5Ac) are shown in red, the three proposed conformations for the Michaelis complex between a neuraminidase and substrate are highlighted in green[14,23], the conformation of the natural galactoside substrate and sialosyl-intermediate is shown in blue lettering and the four lowest energy conformations of a sialyl oxacarbenium ion are boxed in orange.

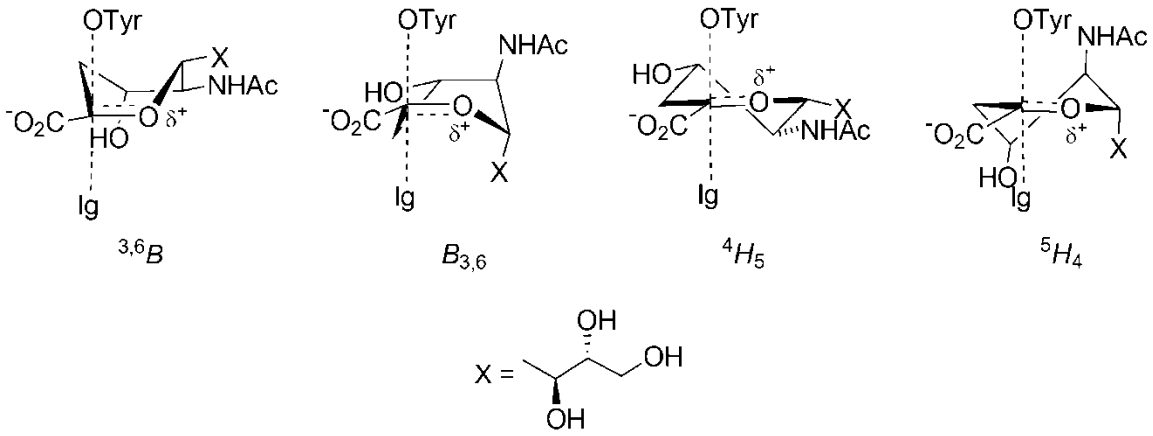

Figure 3.6. Structural representations of the four possible low energy conformations of a sialyl oxacarbenium ion

3.5.4 Kinetics Experimental

3.5.4.1 General Information

Enzymatic catalytic efficiencies (k_{cat}/K_m) and inhibitory potencies (K_i) were measured under conditions in which the glycosylation step is kinetically significant, which, in these cases, occurs at a non-optimal pH (8.05).[21,22,39] The catalytic efficiencies (k_{cat}/K_m) of the influenza N2 and *Mv*NA were generally calculated by fitting the kinetic data to the Michaelis-Menten equation. All inhibitor binding constants were calculated by measuring an IC_{50} value, at a single substrate (**1a**: *p*NP-*α*Neu5Ac) concentration and correcting this value to zero substrate as detailed by Segel.[40] However, as several substrates exhibited either large or small K_m values we used other kinetic protocols to calculate their k_{cat}/K_m values. The rate constants for the spontaneous hydrolyses of **1a**–**j** were measured at various temperatures and extrapolated to give k_{uncat} at 37 °C (Table 3.4).

3.5.4.2 Enzyme kinetic Measurements (Influenza N2 and *Micromonospora Viridifaciens* Neuraminidases)

The enzyme-catalyzed hydrolysis of compounds **1a–j** was monitored at 400 nm and at 37 °C using a Cary 3E spectrophotometer equipped with a Peltier temperature controller. All hydrolysis reactions were performed at a pH value of 8.03 using an identical buffering system to that reported by Chong *et al*[41]. Specifically, the buffer contained 50 mM 2-(*N*-morpholino)ethanesulfonic acid (MES), 50 mM N-[tris(hydroxymethyl)methyl]-3-aminopropanesulfonic acid (TAPS), 0.1 M ethanolamine and 20 mM $CaCl_2$.

Kinetic parameters for substrates in which K_m was in the range 5–5000 μM were measured from a minimum of seven initial rate measurements within a substrate concentration of at least $K_m/4$ to $4K_m$. Each 0.4 mL reaction mixture containing substrate and buffer was incubated at 37 °C for 1min before addition of an enzyme stock solution that contained bovine serum albumin (BSA: concentration in the reaction mixture was 0.01%). The rate versus substrate concentration data were fitted to a standard Michaelis–Menten equation using a nonlinear least-squares program (Prism).

For substrates that possessed high K_m values (> 5 mM) the parameter V_{max}/K_m was calculated using initial rate measurements at five different substrate concentrations. The slope of the resultant straight line (V_{max}/K_m) when corrected for the enzyme concentration gives k_{cat}/K_m.

For tight binding substrates (K_m < 5 μM) were estimated by either monitoring the pseudo first-order rate constant for the enzyme-catalyzed hydrolysis of a very low concentration of substrate (2 μM) or by measuring k_{cat} values under saturating conditions and estimating K_m by monitoring the decrease in the rate of hydrolysis of *p*NP-*α*Neu5Ac in the presence of varying concentrations of the tight-binding substrate (competitive

inhibition assay) to give an apparent K_m value, which was used to calculate K_m values by correcting for the concentration of *p*NP-*α*Neu5Ac in the assay.

3.5.4.3 Measurement of Inhibitor Affinities (Influenza and *Micromonospora Viridifaciens* Neuraminidases)

The estimation of K_i values involved measurement of IC_{50} values at a single concentration of substrate (20 μM of *p*NP-*α*Neu5Ac for influenza N2 and 0.5 μM of 4-MU-αNeu5Ac for *M. viridifaciens* neuraminidase). Specifically, the rate of hydrolysis of *p*NP-αNeu5Ac (influenza N2) or 4-MU-αNeu5Ac (MvNA) was monitored in the presence of at least eight different concentrations of inhibitor **2a–j** at a pH of 8.03 (buffered as above) and 37 °C. The measured initial rate versus inhibitor concentration data were fit to a standard inhibition model using a nonlinear least squares program (Prism). These calculated IC_{50} values were corrected for the concentration of substrate to give K_i values using a standard equation.[40]

3.5.4.4 Spontaneous Hydrolyses of *p*NP-Sialosides

The hydrolyses of 4-substituted *p*NP-αNeu5Acs were performed in triplicate at three or four temperatures and the resulting k_{obs} versus 1/T data was fit to the Eyring equation and the value for k_{uncat} at 37 °C was calculated. All spontaneous hydrolysis reactions were conducted in 1 mL cuvettes using a refurbished Cary-14 UV-Vis spectrophotometer (OLIS). The change in absorbance at 400 nM was monitored during the hydrolysis of each substrate (20 μM) at a pH of 8.03 (50 mM MES, I = 0.3, $NaClO_4$). The absorbance data versus time were fit to a standard first-order rate equation using a computer program (Prism) to give the rate constant and standard deviation for the three runs.

3.5.4.5 Kinetic Data

Table 3.1. Kinetic Parameters of Influenza Sialidase Catalyzed Hydrolysis of pNP-αNeu5Ac and 4-Substituted Derivatives of pNP-αNeu5Ac at 37 °C and pH 8.03.

Substrates	Compound	K_m(μM)	k_{cat} (s^{-1})	$10^{-3} \times k_{cat}/K_m$ (M^{-1} s^{-1})
pNP-αNeu5Ac	1a	120 ± 27	12.6 ± 1.1	106 ± 26
4-N_3-pNP-αNeu5Ac	1b	250 ± 100	3.66 ± 0.64	14.4 ± 6.2
4-(1-Triazolyl)-pNP-αNeu5Ac	1c	151 ± 12	0.859 ± 0.023	5.69 ± 0.47
4-NH_2-pNP-αNeu5Ac	1d	–	–	45.2 ± 0.7
4-NHAc-pNP-αNeu5Ac	1e	3100 ± 700	3.53 ± 0.45	1.14 ± 0.30
4-NMe_2-pNP-αNeu5Ac	1f	490 ± 130	1.39 ± 0.21	2.82 ± 0.86
4-NHiPr-pNP-αNeu5Ac[a]	1g	~ 23000	~ 4.6	0.664 ± 0.045
4-Guanidino-pNP-αNeu5Ac	1h	0.054 ± 0.006	0.00560 ± 0.00095	104 ± 18
4-H-pNP-αNeu5Ac	1i	200 ± 40	19.9 ± 1.7	100 ± 23
4-OMe-pNP-αNeu5Ac	1j	1450 ± 60	23.6 ± 0.4	16.2 ± 0.7

Table 3.2. Kinetic Parameters for the *M. viridifaciens* Sialidase-Catalyzed Hydrolysis of pNP-αNeu5Ac and 4-Substituted Derivatives of pNP-αNeu5Ac at 37 °C and pH 8.03.

Substrates	Compound	K_m(μM)	k_{cat} (s^{-1})	$10^{-3} \times k_{cat}/K_m$ (M^{-1} s^{-1})
pNP-αNeu5Ac	1a	6.33 ± 0.75	5.80 ± 0.21	916 ± 114
4-N_3-pNP-αNeu5Ac	1b	–	–	0.0713 ± 0.0001
4-(1-Triazolyl)-pNP-αNeu5Ac	1c	N.D.[a]	N.D.[a]	N.D.[a]
4-NH_2-pNP-αNeu5Ac	1d	263 ± 23	4.68 ± 0.17	17.8 ± 1.7
4-NHAc-pNP-αNeu5Ac	1e	–	–	0.0744 ± 0.0003
4-NMe_2-pNP-αNeu5Ac	1f	–	–	0.0154 ± 0.0001
4-NHiPr-pNP-αNeu5Ac	1g	–	–	0.0550 ± 0.0002
4-Guanidino-pNP-αNeu5Ac	1h	–	–	0.00370 ± 0.00001
4-H-pNP-αNeu5Ac	1i	260 ± 17.5	37.6 ± 1.3	144 ± 11
4-OMe-pNP-αNeu5Ac	1j	~ 14000	~ 0.27	0.0226 ± 0.0002

[a] N.D. = not determined.

Table 3.3. Calculated K_i Values for Neu2en5Ac and 4-Substituted Derivatives of Neu2en5Ac with the Sialidases from Influenza Type A N2 and *M. Viridifaciens* at 37 °C and pH 8.03.

K_i (μM)			
Inhibitor	**Compound #**	**Influenza N2**	***Micromonospora viridifaciens***
Neu2en5Ac	**2a**	1.67 ± 0.13	0.037 ± 0.003
4-N_3-Neu2en5Ac	**2b**	5.66 ± 0.34	124 ± 21
4-(1-Triazolyl)-Neu2en5Ac	**2c**	15.8 ± 2.5	N.D.[a]
4-NH_2-Neu2en5Ac	**2d**	0.018 ± 0.002	5.64 ± 1.08
4-NHAc-Neu2en5Ac	**2e**	12.1 ± 1.1	47.0 ± 3.9
4-NMe_2-Neu2en5Ac	**2f**	4.30 ± 0.32	37.2 ± 2.0
4-NHiPr-Neu2en5Ac	**2g**	1.91 ± 0.09	36.2 ± 2.9
4-Guanidino-Neu2en5Ac	**2h**	0.0032 ± 0.0006	940 ± 170
4-H-Neu2en5Ac	**2i**	1.74 ± 0.26	7.18 ± 0.56
4-OMe-Neu2en5Ac	**2j**	18.3 ± 1.8	350 ± 45

[a] N.D. = not determined.

Table 3.4. Calculated Rate Constants for the Spontaneous Hydrolyses of pNP-αNeu5Ac and 4-Substituted Derivatives of pNP-αNeu5Ac at 37 °C and pH 8.03 (μ = 0.3, NaClO4).

Substrate	**Compound #**	$10^5 \times k_{uncat}$ (s^{-1})
pNP-αNeu5Ac	**1a**	0.63 ± 0.01
4-N_3-pNP-αNeu5Ac	**1b**	0.270 ± 0.003
4-(1-Triazolyl)-pNP-αNeu5Ac	**1c**	0.057 ± 0.006
4-NH_2-pNP-αNeu5Ac	**1d**	1.27 ± 0.01
4-NHAc-pNP-αNeu5Ac	**1e**	0.580 ± 0.004
4-NMe_2-pNP-αNeu5Ac	**1f**	1.76 ± 0.04
4-NHiPr-pNP-αNeu5Ac	**1g**	1.16 ± 0.02
4-Guanidino-pNP-αNeu5Ac	**1h**	0.094 ± 0.007
4-H-pNP-αNeu5Ac	**1i**	5.89 ± 0.01
4-OMe-pNP-αNeu5Ac	**1j**	0.450 ± 0.002

3.5.5 NMR Spectra

5-Acetamido-2,6-anhydro-4-azido-3,4,5-trideoxy-D-*glycero*-D-*galacto*-non-2-enonic acid (2b)

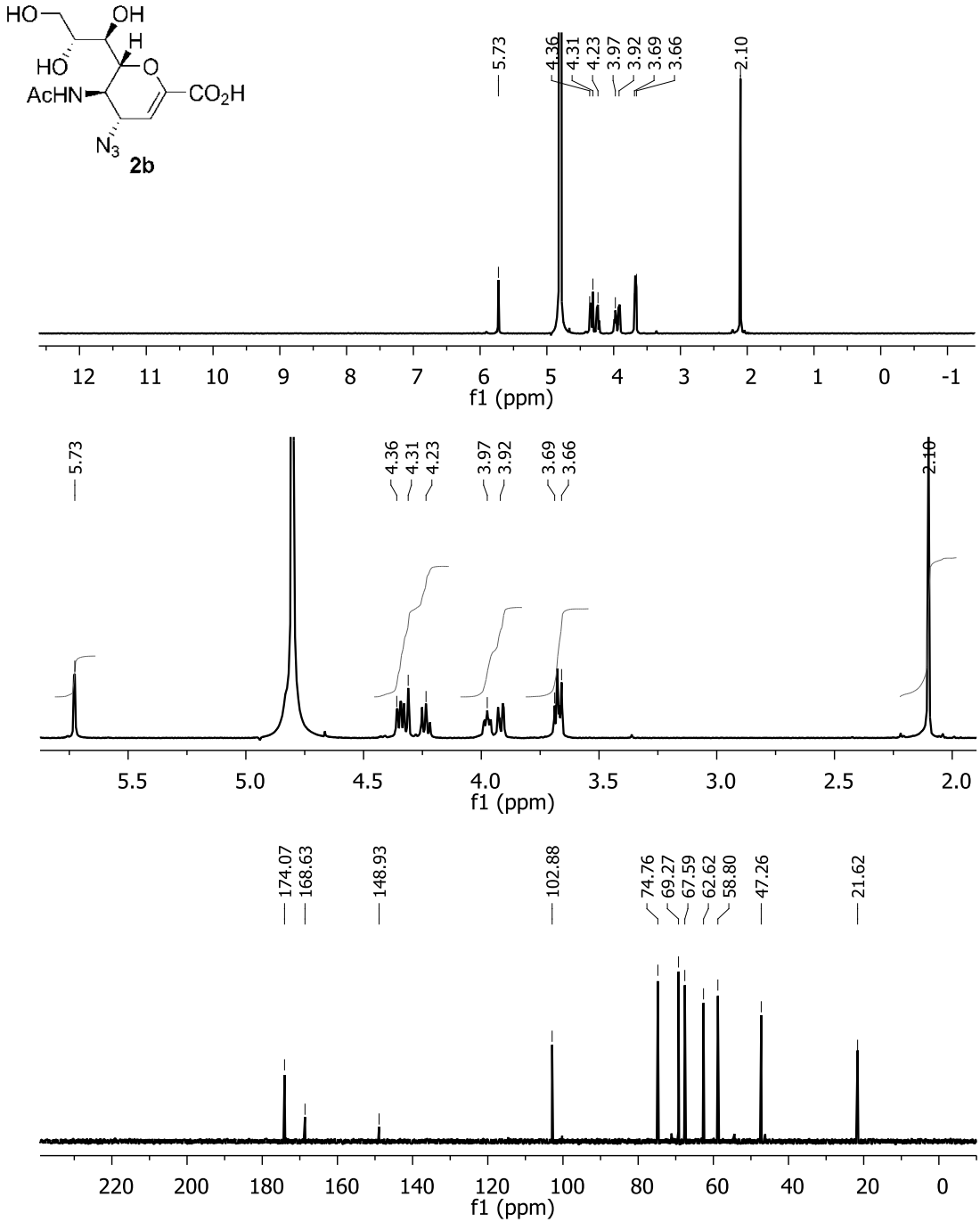

5-Acetamido-2,6-anhydro-3,4,5-trideoxy-4-(1-triazolyl)-D-*glycero*-D-*galacto*-non-2-enonic acid (2c)

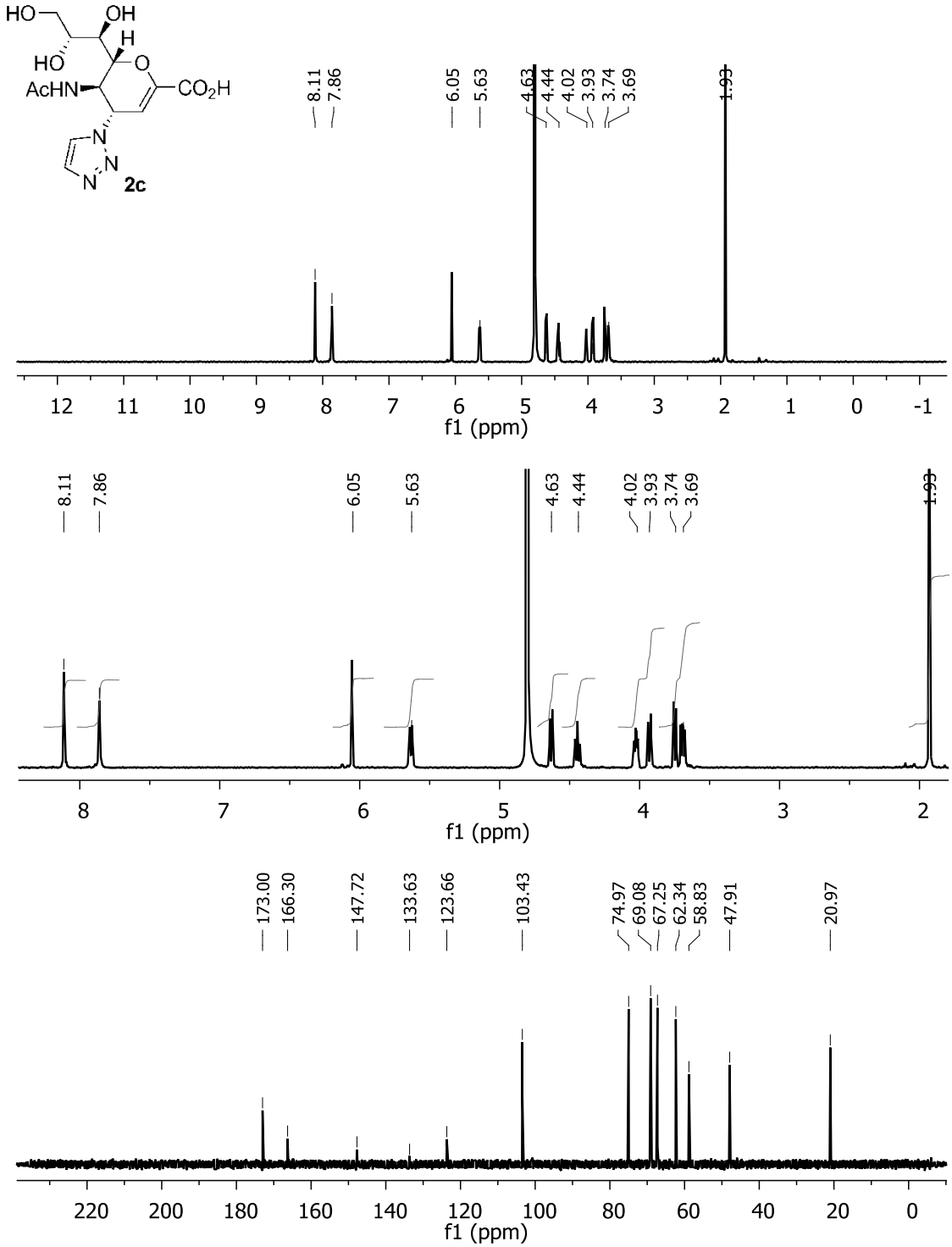

5-Acetamido-4-amino-2,6-anhydro-3,4,5-trideoxy-D-*glycero*-D-*galacto*-non-2-enonic acid (2d)

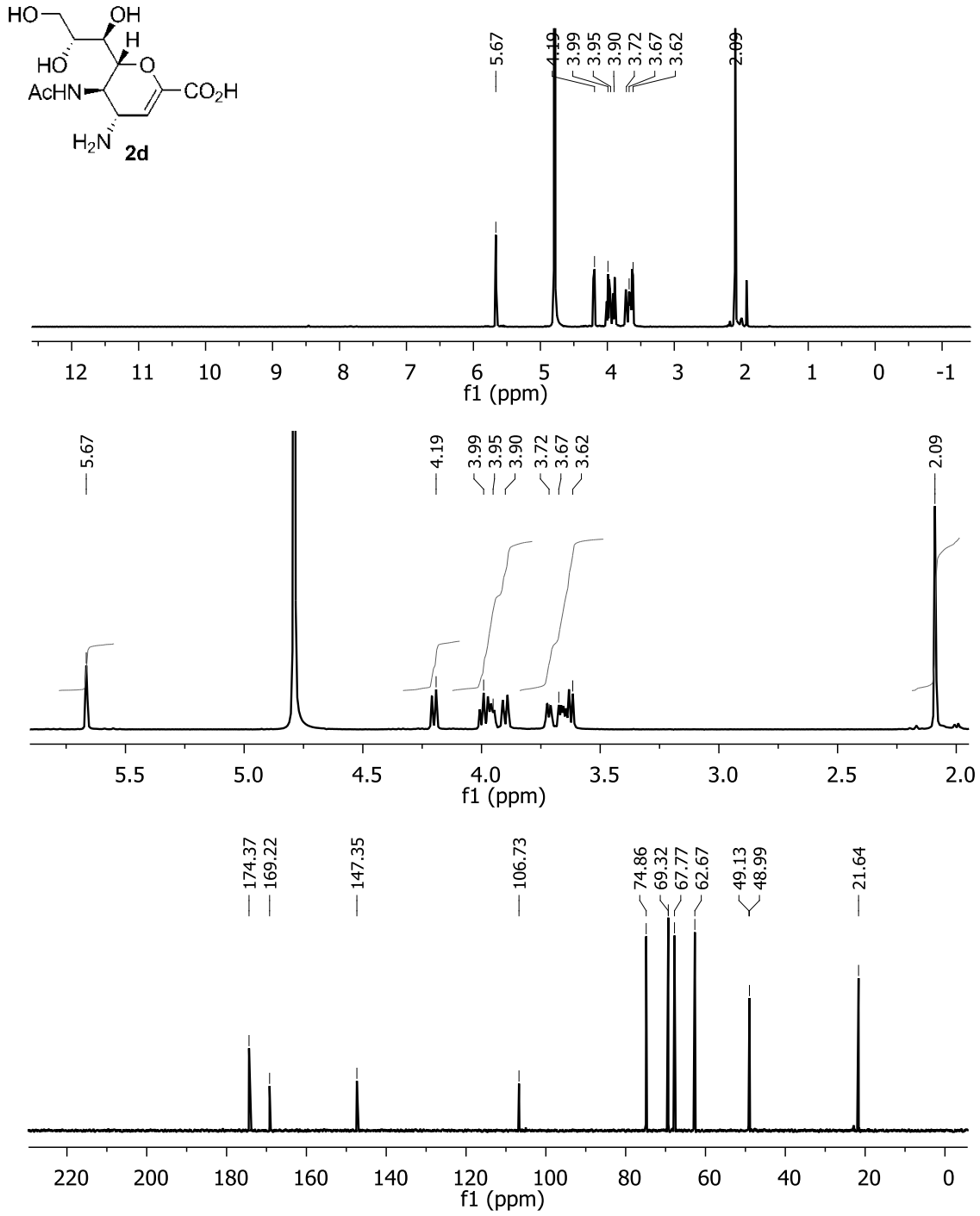

4,5-Diacetamido-2,6-anhydro-3,4,5-trideoxy-D-*glycero*-D-*galacto*-non-2-enonic acid (2e)

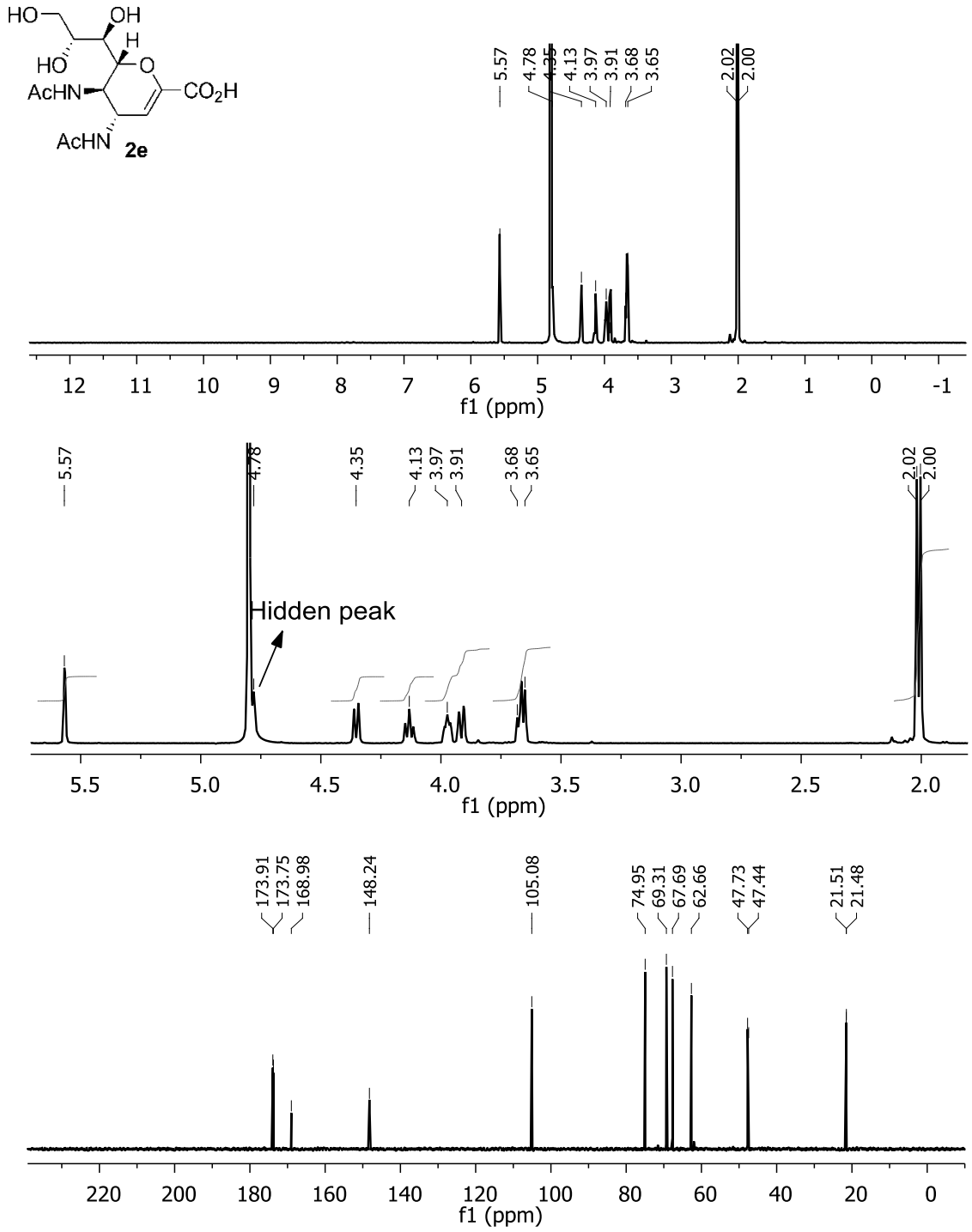

5-Acetamido-2,6-anhydro-3,4,5-trideoxy-4-dimethylamino-D-*glycero*-D-*galacto*-non-2-enonic (2f)

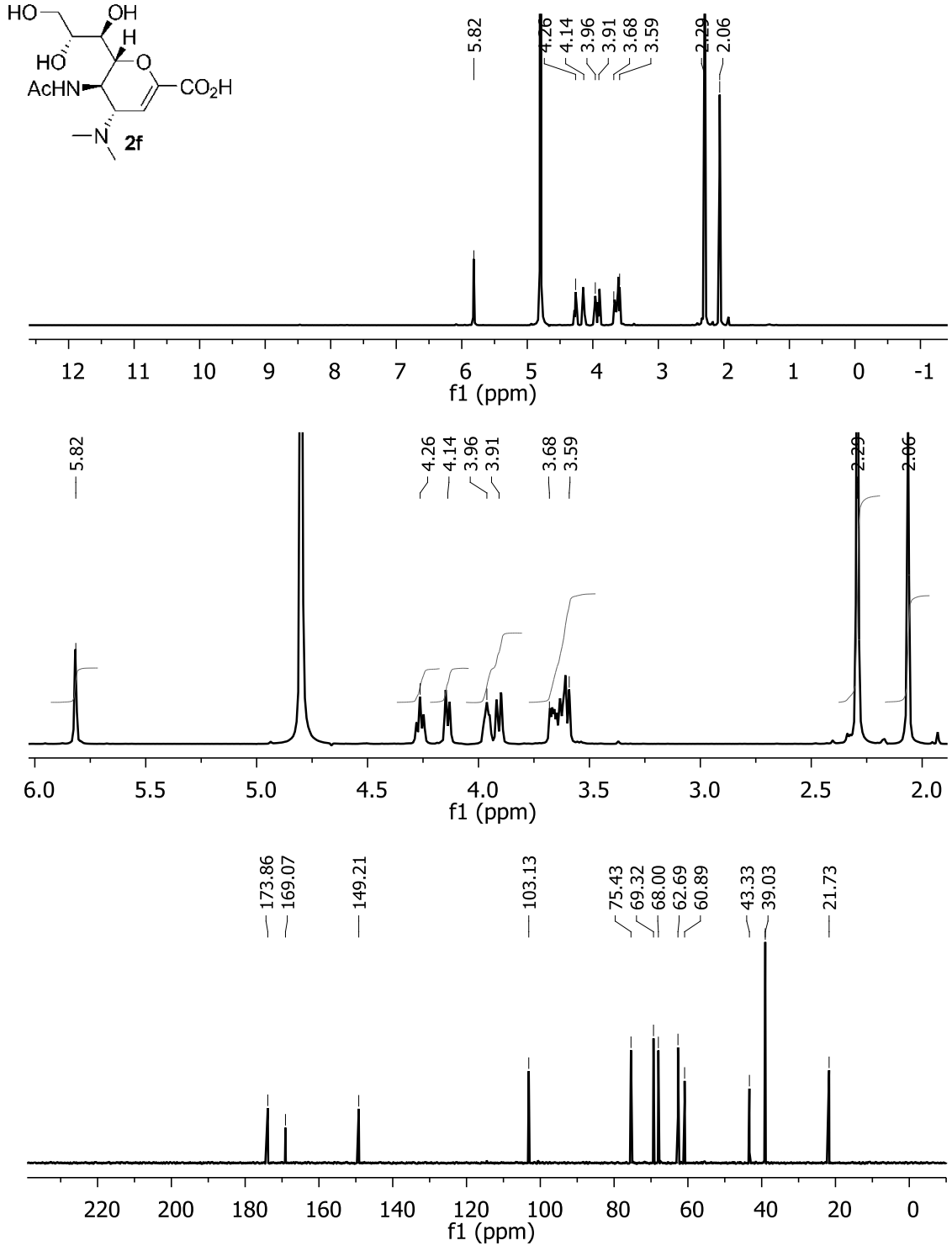

5-Acetamido-2,6-anhydro-4-isopropylamino-3,4,5-trideoxy-D-*glycero*-D-*galacto*-non-2-enonic (2g)

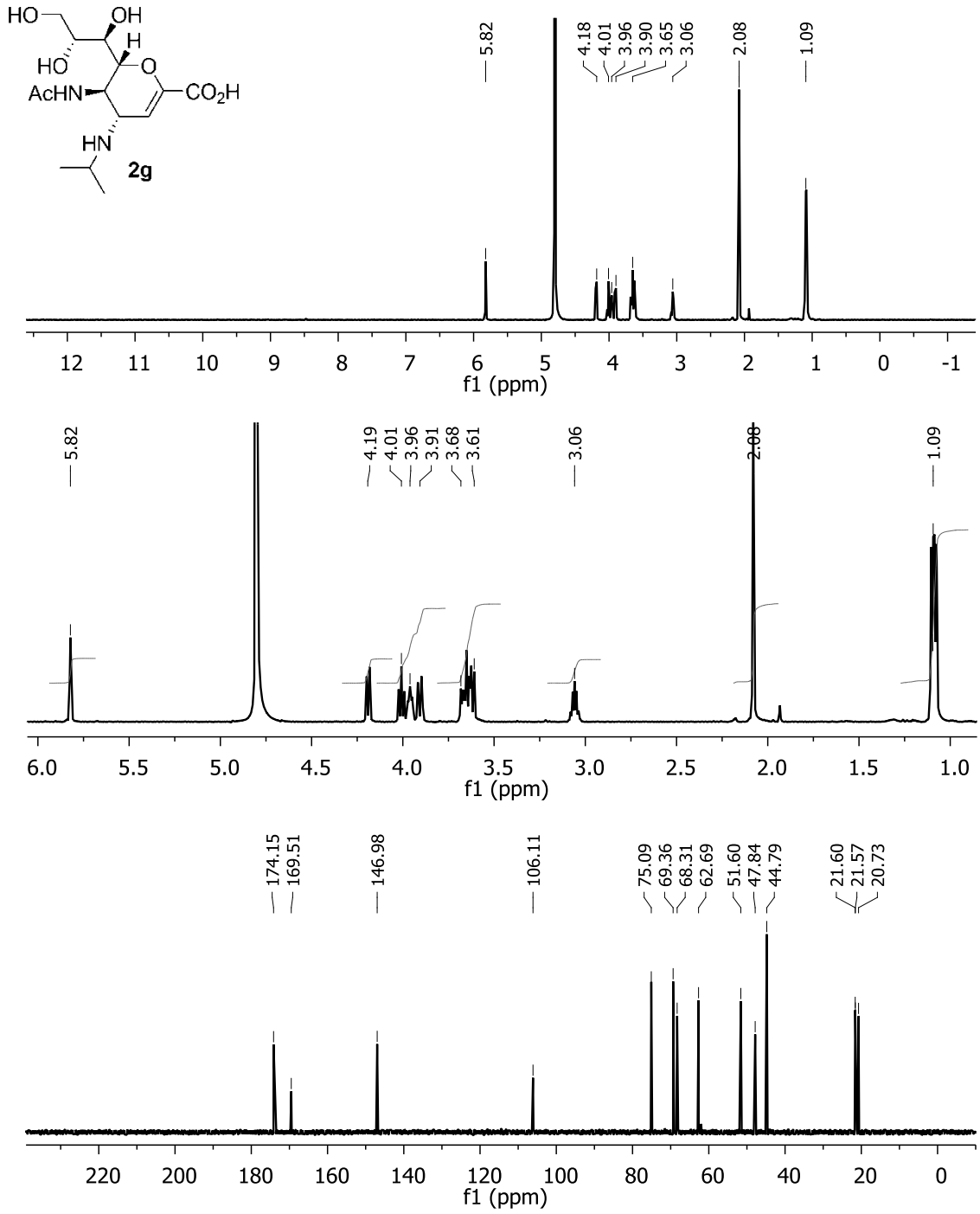

5-Acetamido-2,6-anhydro-4-guanidino-3,4,5-trideoxy-D-*glycero*-D-*galacto*-non-2-enonic acid (2h)

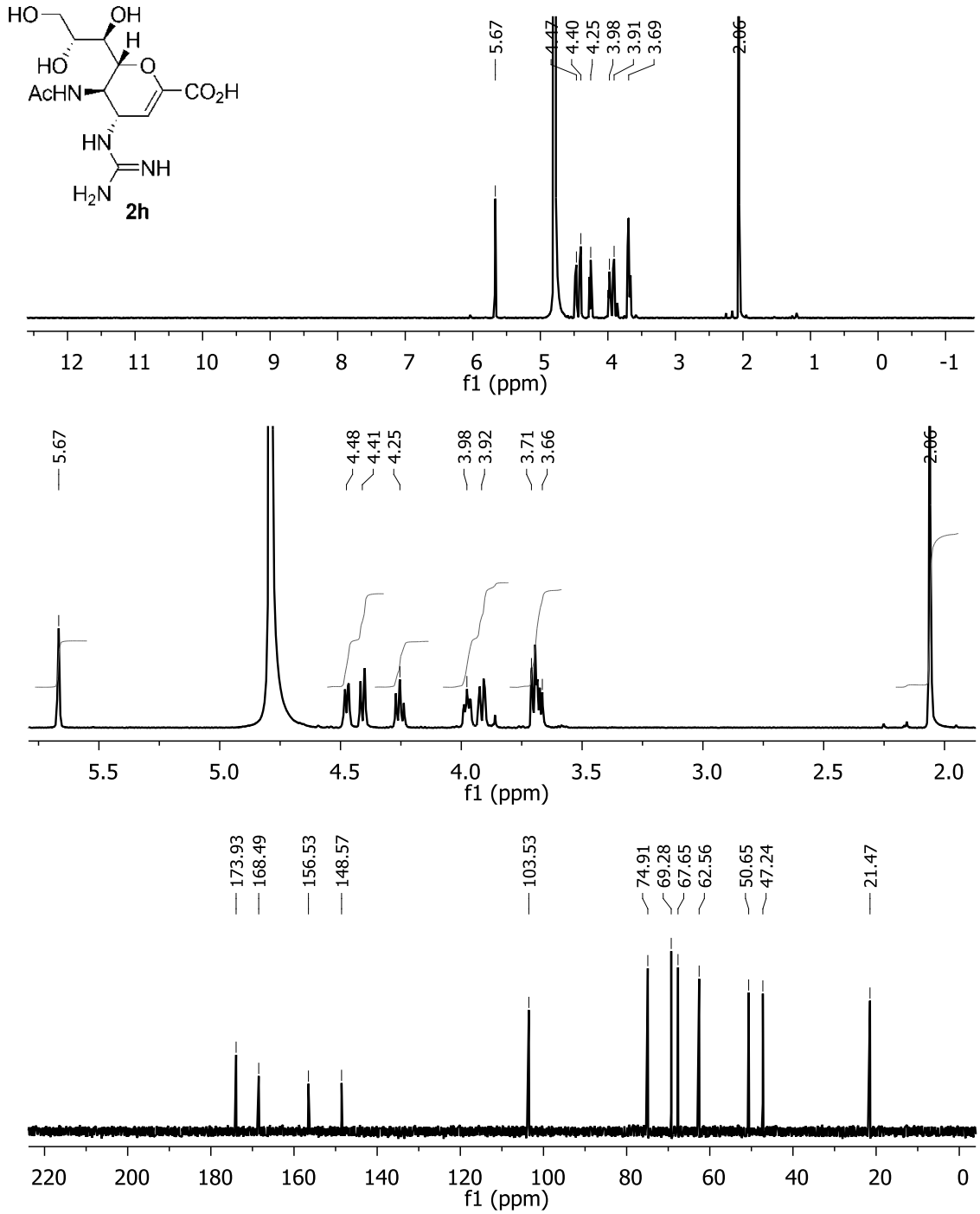

5-Acetamido-2,6-anhydro-2,3,4,5-tetradeoxy-D-*glycero*-D-*galacto*-non-2-enonic acid (2i)

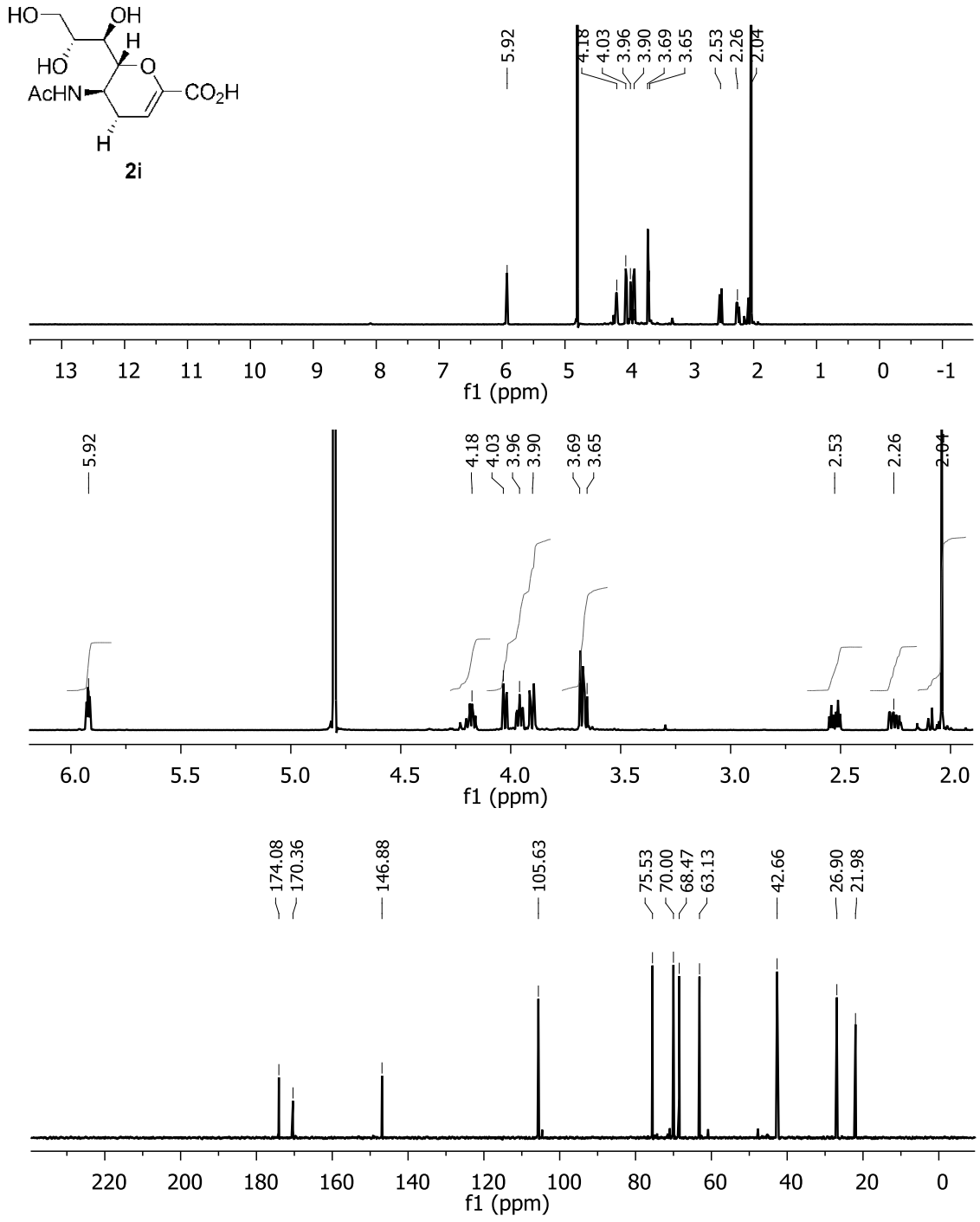

5-acetamido-2,6-anhydro-3,4,5-trideoxy-4-methoxy-D-*glycero*-D-*galacto*-non-2-enonic acid (2j)

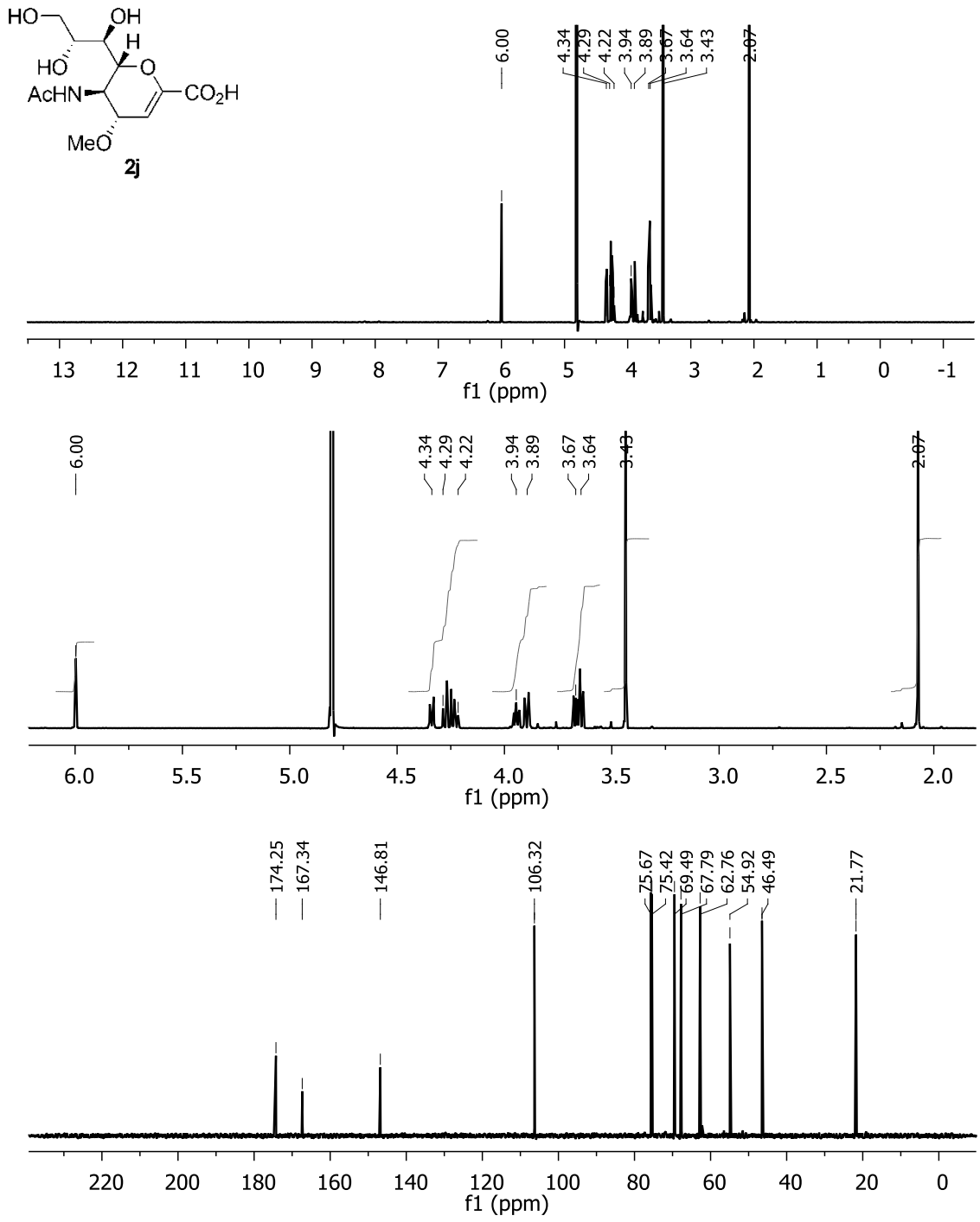

4-Nitrophenyl 5-acetamido-4-azido-3,4,5-trideoxy-α-D-*glycero*-D-*galacto*-non-2-ulpyranosylonic acid (1b)

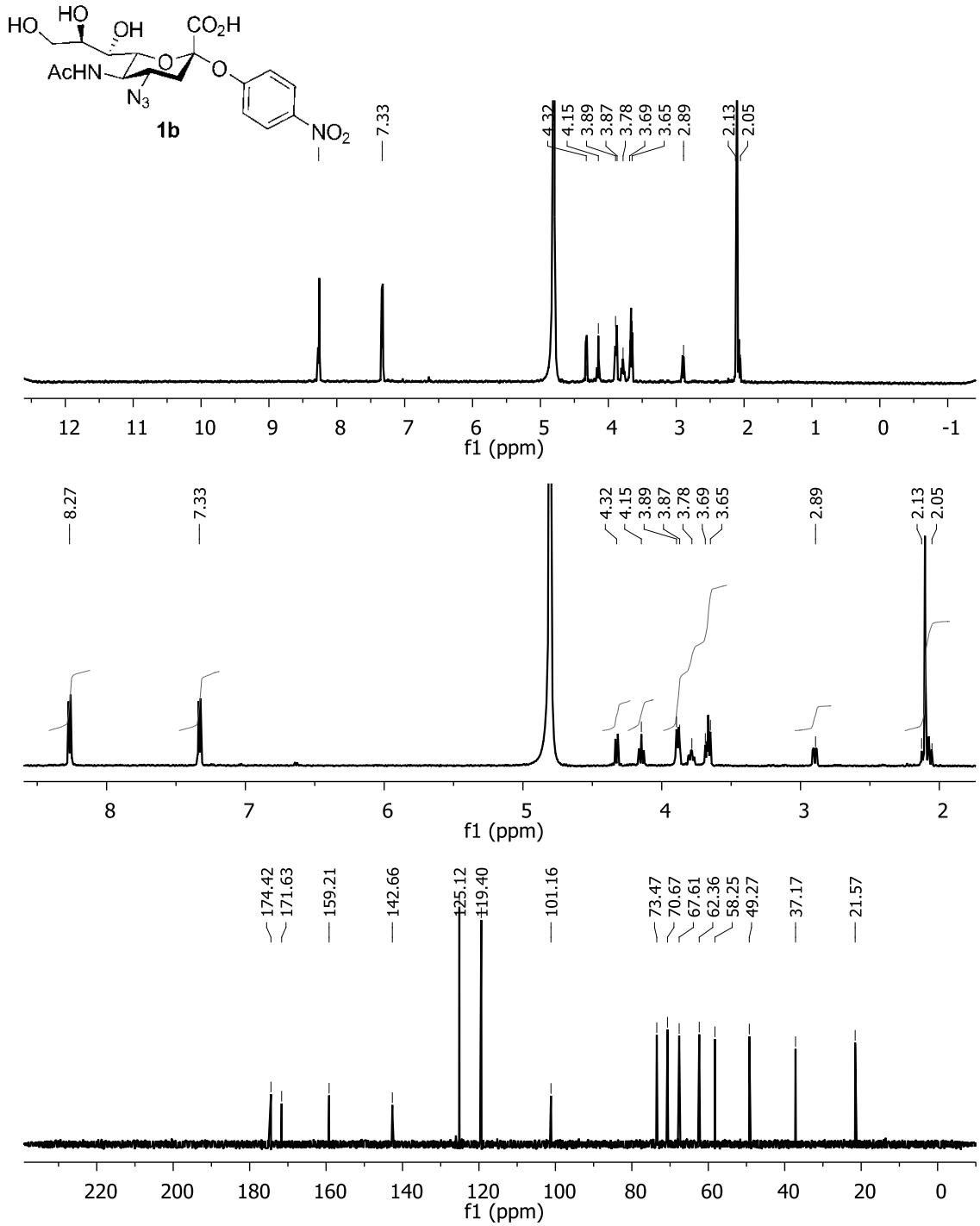

4-Nitrophenyl 5-acetamido-3,4,5-trideoxy-4-(1-triazolyl)-α-*D*-*glycero*-D-*galacto*-non-2-ulpyranosylonic acid (1c)

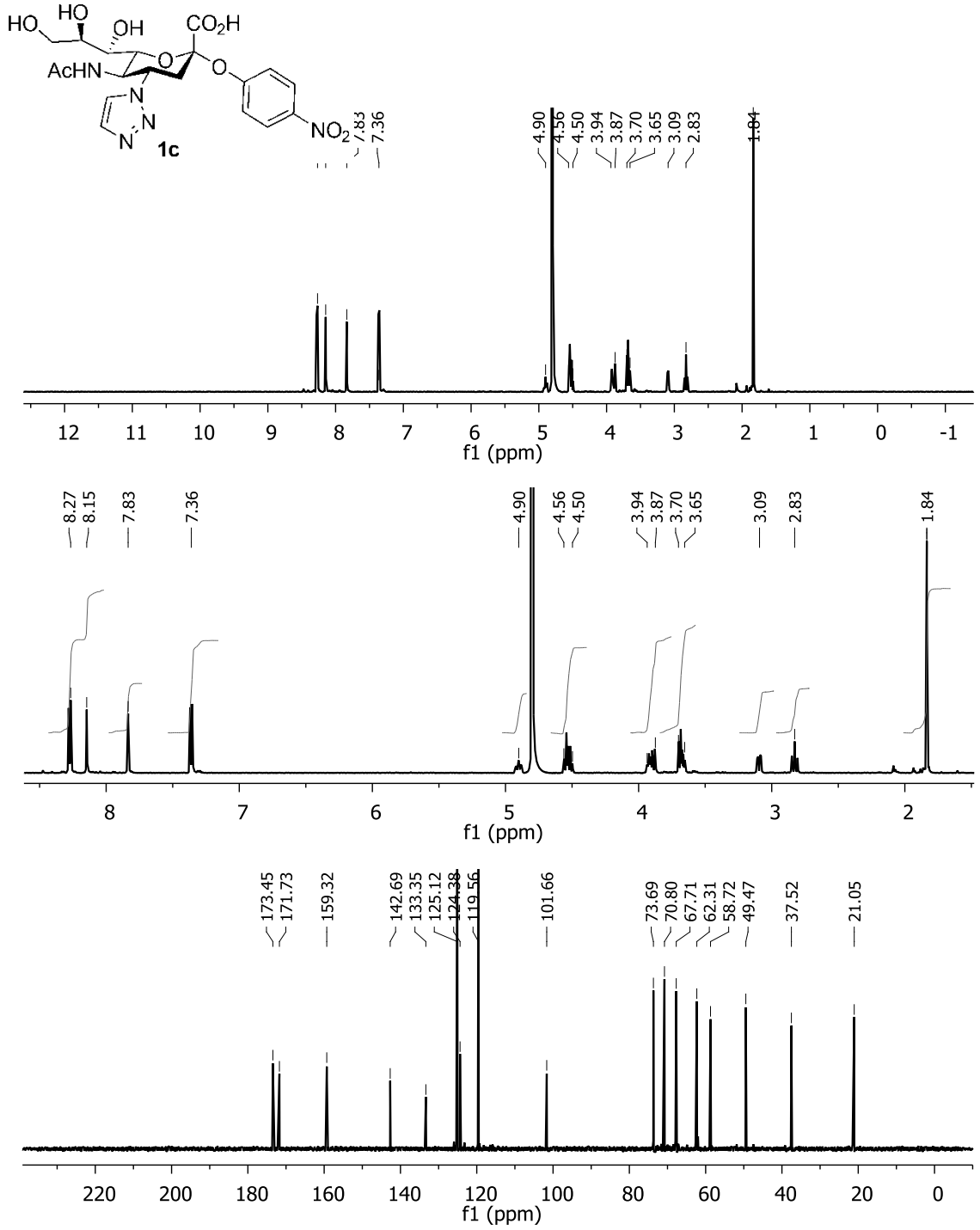

4-Nitrophenyl 5-acetamido-4-amino-3,4,5-trideoxy-α-D-*glycero*-D-*galacto*-non-2-ulpyranosylonic acid (1d)

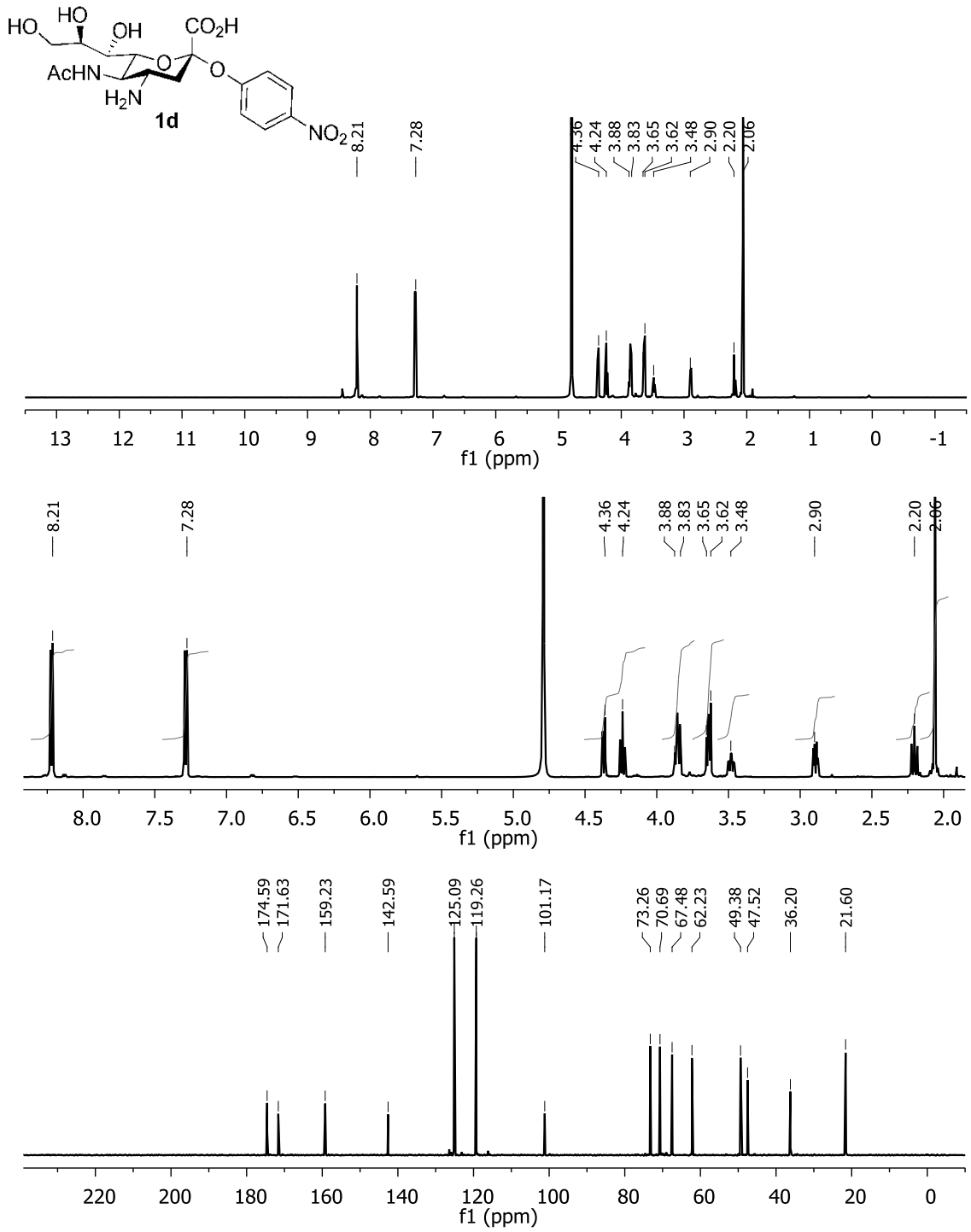

4-Nitrophenyl 4,5-diacetamido-3,4,5-trideoxy-α-D-*glycero*-D-*galacto*-non-2-ulpyranosylonic acid (1e)

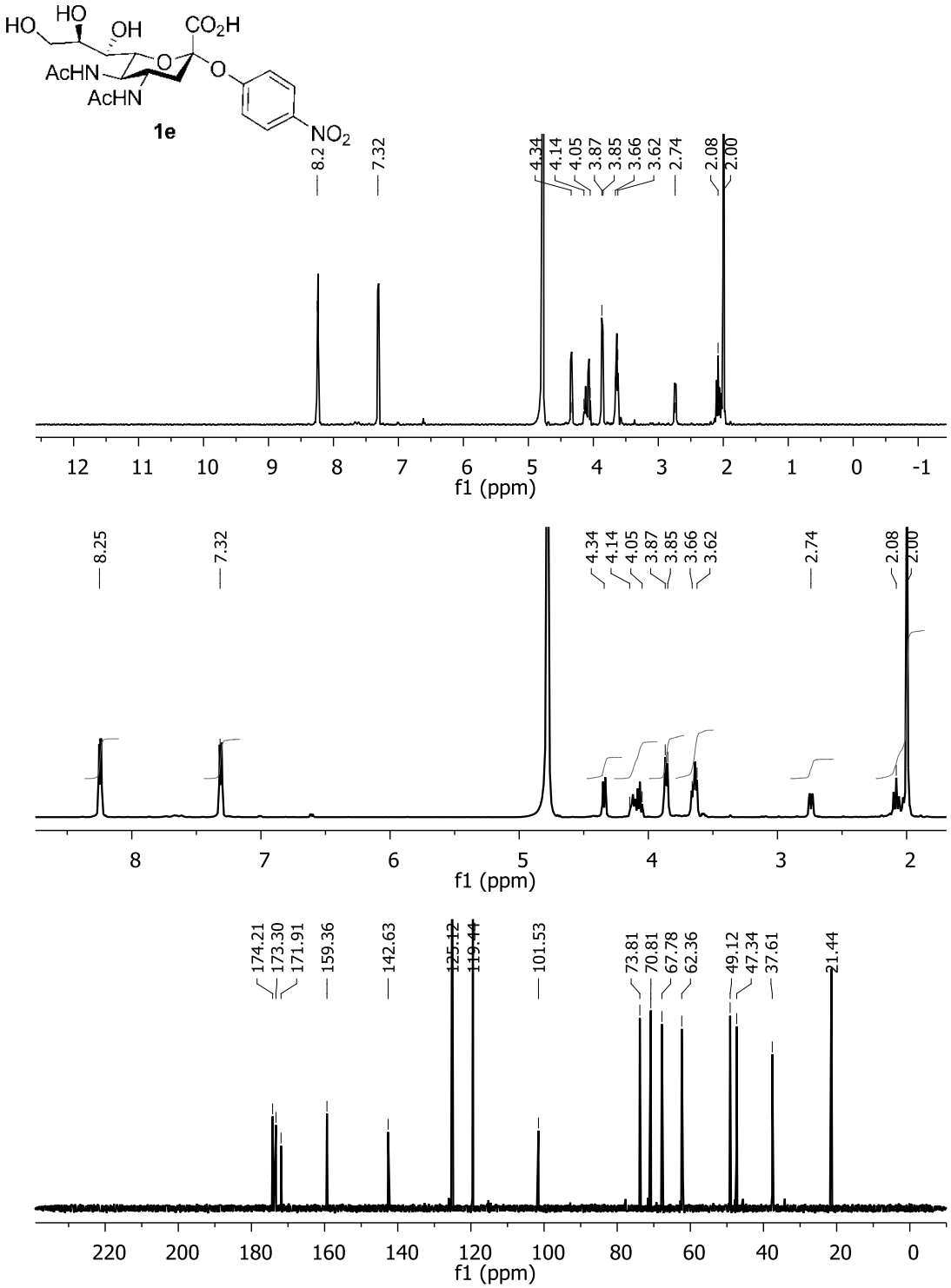

4-Nitrophenyl 5-acetamido-3,4,5-trideoxy-4-dimethylamino-α-D-glycero-D-galacto-non-2-ulpyranosylonic acid (1f)

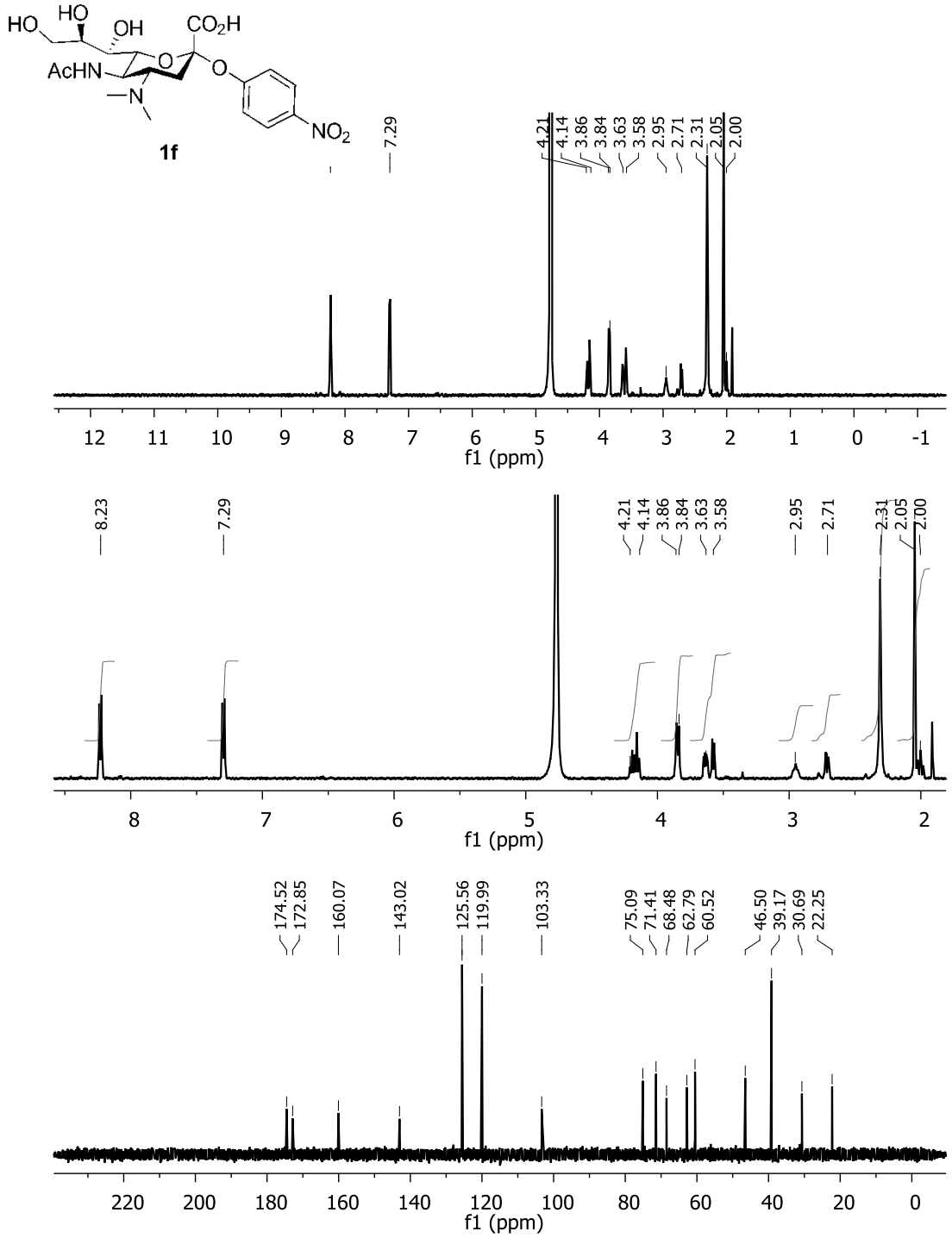

4-Nitrophenyl 5-acetamido-3,4,5-trideoxy-4-isopropylamino-α-D-*glycero*-D-*galacto*-non-2-ulopyranosylonic acid (1g)

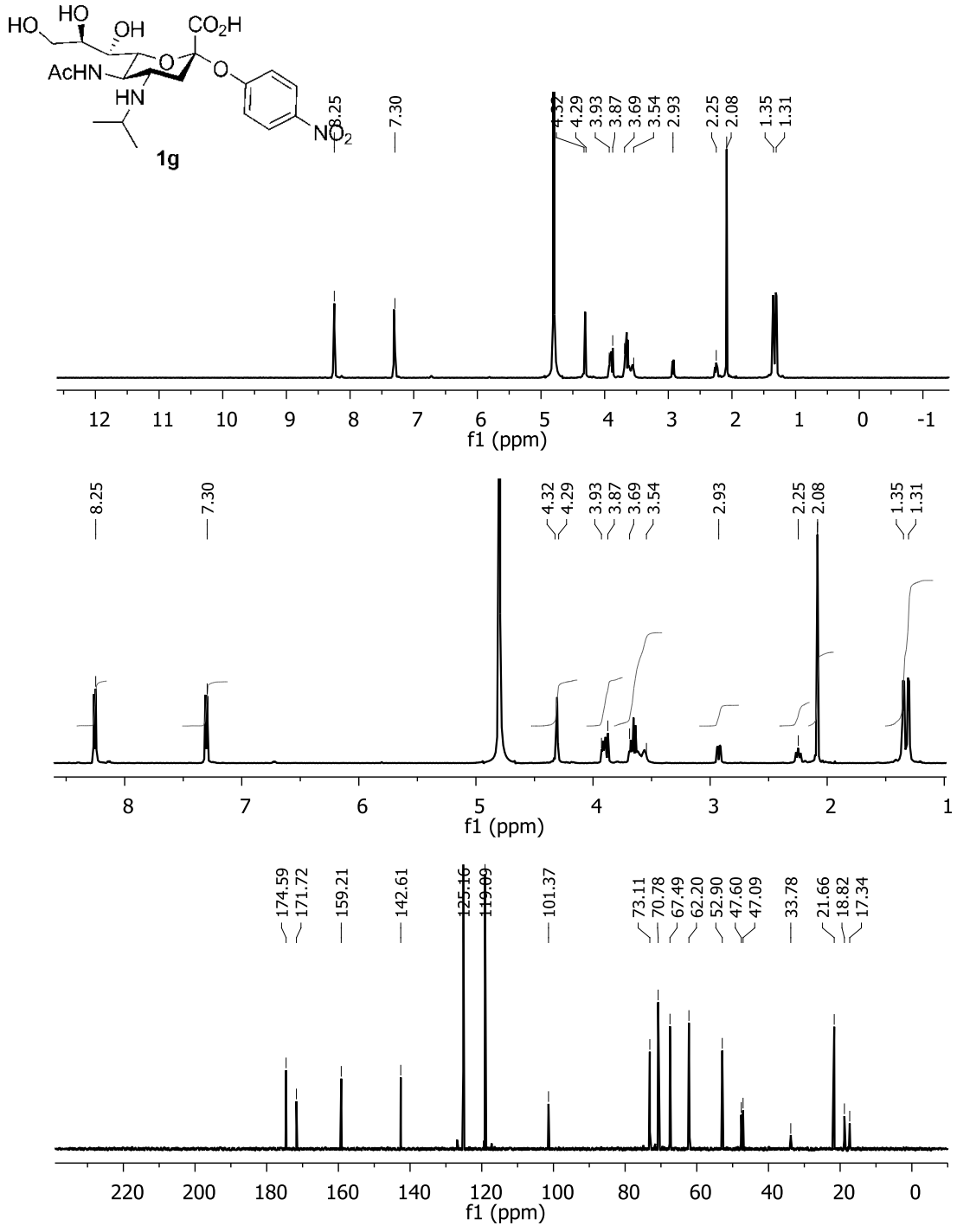

4-Nitrophenyl 5-acetamido-3,4,5-trideoxy-4-guanidino-α-D-*glycero*-D-*galacto*-non-2-ulpyranosylonic acid (1h)

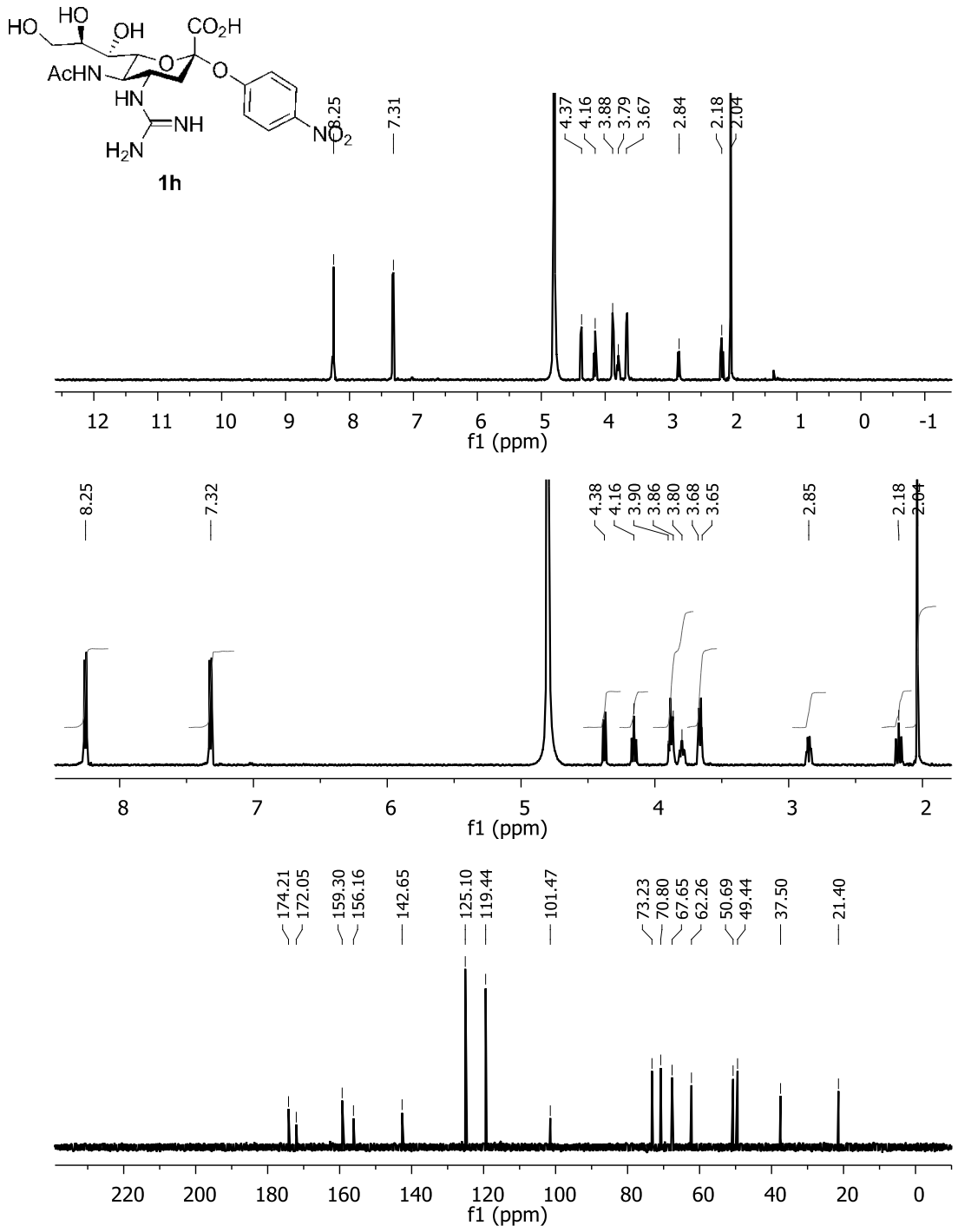

4-Nitrophenyl (5-acetamido-3,4,5-trideoxy-α-D-*manno*-non-2-nonulopyranosylonic acid) (1i)

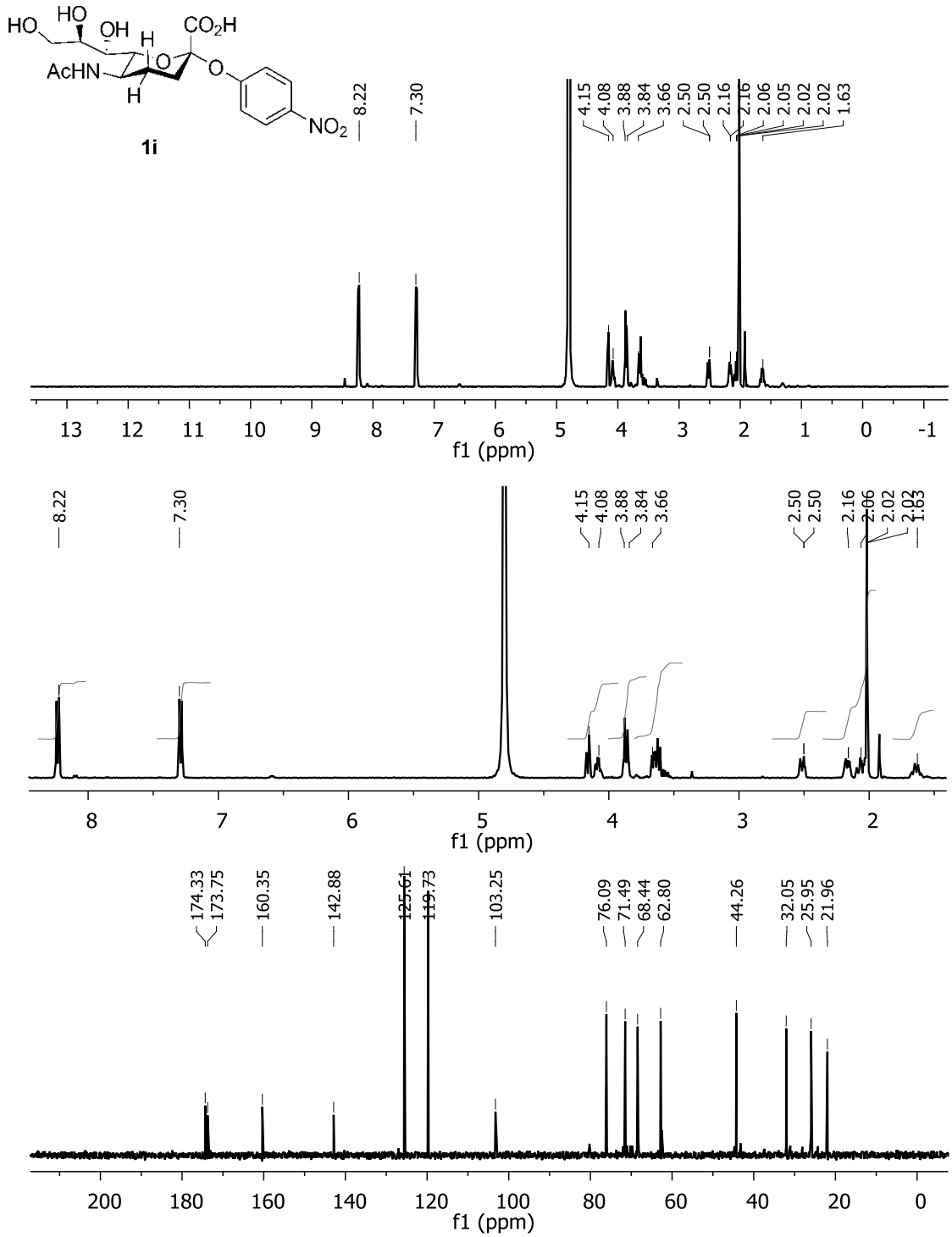

4-Nitrophenyl 5-acetamido-3,4,5-trideoxy-4-methoxy-D-*glycero*-α-D-*galacto*-non-2-ulopyranosylonic acid (1j)

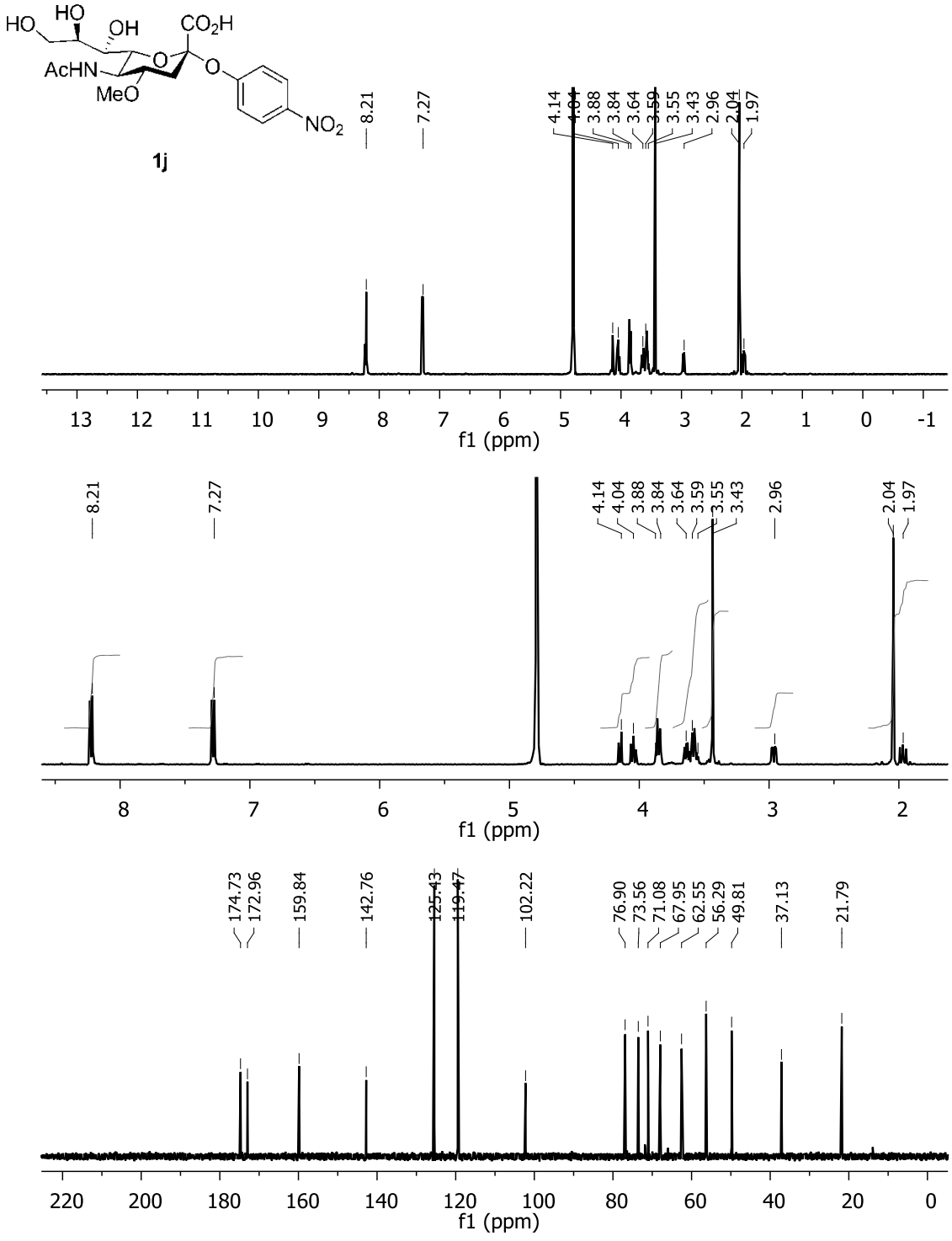

3.6 References

[1] Kuiken, T.; Holmes, E. C.; McCauley, J.; Rimmelzwaan, G. F.; Williams, C. S.; Grenfell, B. T. *Science* **2006**, *312*, 394.

[2] Ghedin, E.; Sengamalay, N. A.; Shumway, M.; Zaborsky, J.; Feldblyum, T.; Subbu, V.; Spiro, D. J.; Sitz, J.; Koo, H.; Bolotov, P.; Dernovoy, D.; Tatusova, T.; Bao, Y. M.; St George, K.; Taylor, J.; Lipman, D. J.; Fraser, C. M.; Taubenberger, J. K.; Salzberg, S. L. *Nature* **2005**, *437*, 1162.

[3] von Itzstein, M. *Influenza Virus Sialidase - A Drug Discovery Target*; Springer: Basel, 2012.

[4] Molla, A.; Kati, W.; Carrick, R.; Steffy, K.; Shi, Y.; Montgomery, D.; Gusick, N.; Stoll, V. S.; Stewart, K. D.; Ng, T. I.; Maring, C.; Kempf, D. J.; Kohlbrenner, W. *J Virol* **2002**, *76*, 5380.

[5] McKimm-Breschkin, J. L. *Antiviral Res* **2000**, *47*, 1.

[6] Gubareva, L. V.; Robinson, M. J.; Bethell, R. C.; Webster, R. G. *J Virol* **1997**, *71*, 3385.

[7] Ives, J. A.; Carr, J. A.; Mendel, D. B.; Tai, C. Y.; Lambkin, R.; Kelly, L.; Oxford, J. S.; Hayden, F. G.; Roberts, N. A. *Antiviral Res* **2002**, *55*, 307.

[8] Bloom, J. D.; Gong, L. I.; Baltimore, D. *Science* **2010**, *328*, 1272.

[9] Chan, J.; Lewis, A. R.; Gilbert, M.; Karwaski, M. F.; Bennet, A. J. *Nat Chem Biol* **2010**, *6*, 405.

[10] Chan, J.; Lewis, A. R.; Indurugalla, D.; Schur, M.; Wakarchuk, W.; Bennet, A. J. *J Am Chem Soc* **2012**, *134*, 3748.

[11] Chan, J.; Lu, A.; Bennet, A. J. *J Am Chem Soc* **2011**, *133*, 1877.

[12] Murrell, M.; Porotto, M.; Weber, T.; Greengard, O.; Moscona, A. *J Virol* **2003**, *77*, 309.

[13] Vavricka, C. J.; Liu, Y.; Kiyota, H.; Sriwilaijaroen, N.; Qi, J.; Tanaka, K.; Wu, Y.; Li, Q.; Li, Y.; Yan, J.; Suzuki, Y.; Gao, G. F. *Nat Commun* **2013**, on line.

[14] Amaya, M. F.; Buschiazzo, A.; Nguyen, T.; Alzari, P. M. *J Mol Biol* **2003**, *325*, 773.

[15] Newstead, S. L.; Potter, J. A.; Wilson, J. C.; Xu, G. G.; Chien, C. H.; Watts, A. G.; Withers, S. G.; Taylor, G. L. *J Biol Chem* **2008**, *283*, 9080.

[16] Bartlett, P. A.; Marlowe, C. K. *Biochemistry* **1983**, *22*, 4618.

[17] Mader, M. M.; Bartlett, P. A. *Chem Rev* **1997**, *97*, 1281.

[18] Watts, A. G.; Oppezzo, P.; Withers, S. G.; Alzari, P. M.; Buschiazzo, A. *J Biol Chem* **2006**, *281*, 4149.

[19] Chandler, M.; Bamford, M. J.; Conroy, R.; Lamont, B.; Patel, B.; Patel, V. K.; Steeples, I. P.; Storer, R.; Weir, N. G.; Wright, M.; Williamson, C. *J Chem Soc Perk T 1* **1995**, 1173.

[20] Wolfenden, R. *Biophys Chem* **2003**, *105*, 559.

[21] Chong, A. K. J.; Pegg, M. S.; Taylor, N. R.; von Itzstein, M. *Eur J Biochem* **1992**, *207*, 335.

[22] Guo, X.; Laver, W. G.; Vimr, E.; Sinnott, M. L. *J Am Chem Soc* **1994**, *116*, 5572.

[23] Flashner, M.; Kessler, K.; Tanenbaum, S. W. *Arch Biochem Biophys* **1983**, *221*, 188.

[24] Xu, G. G.; Kiefel, M. J.; Wilson, J. C.; Andrew, P. W.; Oggioni, M. R.; Taylor, G. L. *J Am Chem Soc* **2011**, *133*, 1718.

[25] Richard, J. P.; Westerfeld, J. G.; Lin, S. *Biochemistry* **1995**, *34*, 11703.

[26] Gaskell, A.; Crennell, S.; Taylor, G. *Structure* **1995**, *3*, 1197.

[27] Henrissat, B.; Bairoch, A. *Biochem J* **1996**, *316*, 695.

[28] Raab, M.; Tvaroška, I. *J Mol Biol* **2011**, *17*, 1445.

[29] Kim, J. H.; Resende, R.; Wennekes, T.; Chen, H. M.; Bance, N.; Buchini, S.; Watts, A. G.; Pilling, P.; Streltsov, V. A.; Petric, M.; Liggins, R.; Barrett, S.; McKimm-Breschkin, J. L.; Niikura, M.; Withers, S. G. *Science* **2013**, *340*, 71.

[30] Eschenfelder, V.; Brossmer, R. *Carbohydr Res* **1987**, *162*, 294.

[31] Rothermel, J.; Faillard, H. *Carbohydr Res* **1990**, *196*, 29.

[32] Chandler, M. e. a. *J Chem Soc, Perkin Trans* **1995**, *1*.

[33] Iwanowicz, E. J.; Poss, M. A.; Lin, J. *Synth Commun* **1993**, *23*.

[34] Wen, W. H.; Wang, S. Y.; Tsai, K. C.; Cheng, Y. S.; Yang, A. S.; Fang, J. M.; Wong, C. H. *Bioorg Med Chem* **2010**, *18*, 4074.

[35] Sabesan, S.; Neira, S.; Wasserman, Z. *Carbohydr Res* **1995**, *267*, 239.

[36] Schreiner, E. Z., Erich; Kleineidam, Reinhard G.; Schauer, Roland *Liebigs Ann Chem* **1991**, *2*, 129

[37] Ikeda, K., Ueno, Y., Kitani, S., Nishino, R. & Sato, M. *Synlett* **2008**, 1027.

[38] Srivastava, O. S., Geeta; Du, Minghui; Hingsgaul, Ole; Bundle, David R. *US 6420552 B1 20020716* **2002**.

[39] Narine, A. A.; Watson, J. N.; Bennet, A. J. *Biochemistry* **2006**, *45*, 9319.

[40] Segel, I. H. *Enzyme Kinetics: Behavior and Analysis of Rapid Equilibrium and Steady State Enzyme Systems*; Wiley: New York, 1975.

[41] Chong, A. K.; Pegg, M. S.; Taylor, N. R.; von Itzstein, M. *Eur J Biochem* **1992**, *207*, 335.

4 Simultaneous Measurements of Multiple Kinetic Isotope Effects by NMR Spectroscopy

Fahimeh S. Shidmoossavee, Andrew R. Lewis, Matthew J. Courtemanche & Andrew J. Bennet

Department of Chemistry, Simon Fraser University, 8888 University Drive, Burnaby, British Columbia, V5A 1S6, Canada

This Chapter describes a project which is still in progress. This work is focused on developing a NMR-based technique to precisely measure KIE (kinetic isotope effect) values in sialidase-catalyzed hydrolysis of a series of synthesized natural analogue substrates. These techniques are: i) one dimensional NMR spectroscopy (^{13}CNMR), and ii) two dimensional NMR spectroscopies (HETCOR and HSQC).

Authors Contributions:

This project was designed by Prof. Andrew J. Bennet, and the author of this thesis performed the experimental synthetic work to make all isotopologues, the kinetic measurements using ^{13}C-NMR, HETCOR and HSQC spectroscopies, deconvoluted all spectra and analyzed all data. Dr. Andrew Lewis wrote the pulse sequences used for the quantitative ^{13}C-NMR, HETCOR, and HSQC experiments, ran trial experiments, trained the author of this thesis how to operate the NMR spectrometer, run the actual experiments, and how to use the *Mathematica* program scripts. Mr. Matthew Courtemanche helped with the experimental syntheses.

4.1 Abstract

The present work involves developing one dimensional (1D) and two dimensional (2D) nuclear magnetic resonance (NMR) spectroscopic methods for the simultaneous measurement of several kinetic isotope effects (KIEs) on sialidase-catalyzed reactions. The main purpose of this work is to develop a novel method that precisely measures multiple KIE values in a single solution. Technique development proceeds by performing the experiments on a panel of six singly- and doubly- labelled phenyl α-sialyl-(2$\rightarrow$6)-β-D-1-thiolactosides as natural substrate analogues for *Micromonospora viridifaciens* sialidase-catalyzed hydrolysis, with the goal of modeling the TS and comparing it to the already solved TS structure for *Vibrio cholerae* sialidase[1]. Continuous, quantitative 1D- and 2D-NMR spectra acquired during the course of the enzymatic reactions are deconvoluted using a combination of computer programs in order to calculate multiple KIE values simultaneously. The results obtained using 1D-NMR (^{13}C-NMR) spectroscopy are presented in full detail in this chapter; however, the measurement of KIEs using 2D-NMR (HETCOR[1] and HSQC[2]) spectroscopy is still under progress, and the preliminarily results of the 2D experiments are also presented in this chapter.

4.2 Introduction

The measurement of kinetic isotope effects is a powerful tool that is used to investigate enzyme mechanisms as the magnitude of these effects provides useful information about the chemical and physical changes that are occurring during a catalytic cycle. Importantly, kinetics isotope effects (KIEs) provide information about the

[1] Heteronuclear Correlation
[2] Heteronuclear Single Quantum Coherence

structure of transition states along the reaction coordinate. However, there is one severe limitation associated with this technique which arises from the often small rate differences (a few percent) that result from isotopic substitution. Standard techniques that are ordinarily used to measure primary hydrogen KIEs are not often sensitive enough to measure the small changes associated with heavy atom substitution. Therefore, an ongoing challenge exists to develop new approaches to improve this situation. The most accurate methods to measure isotope effects on an enzymatic reaction are competitive methods, which require the reaction of unlabelled and labelled reactants to be carried out in the same vessel. Such experiments eliminate systematic errors arising from differences in temperature, pH, concentration and other variables that can occur in separate rate constant measurements.

The theory behind all competitive KIE measurements is that, as any reaction proceeds, the remaining starting material becomes fractionally enriched in the slower-reacting isotopologue while simultaneously the product is enriched in the faster reacting isotopologue. The KIE can be calculated by measuring isotopologue ratios in the remaining starting material and by use of the following equation (Eq 4.1) [2,3] where R_0 is the ratio of heavy isotopologue to light isotopologue at time = 0 (before adding enzyme) and R is this ratio (after adding enzyme) at a specific fraction of reaction (F_L) for the light isotopologue.

$$R/R_0 = (1-F_L)^{(1/KIE)-1} \quad \text{(Eq 4.1)}$$

In case of normal KIE (KIE $>$ 1), when the enzymatic reaction is near to completion, the ratio R/R_0 tends to ∞ as F_L asymptotically approaches 1 (Figure 4.1).

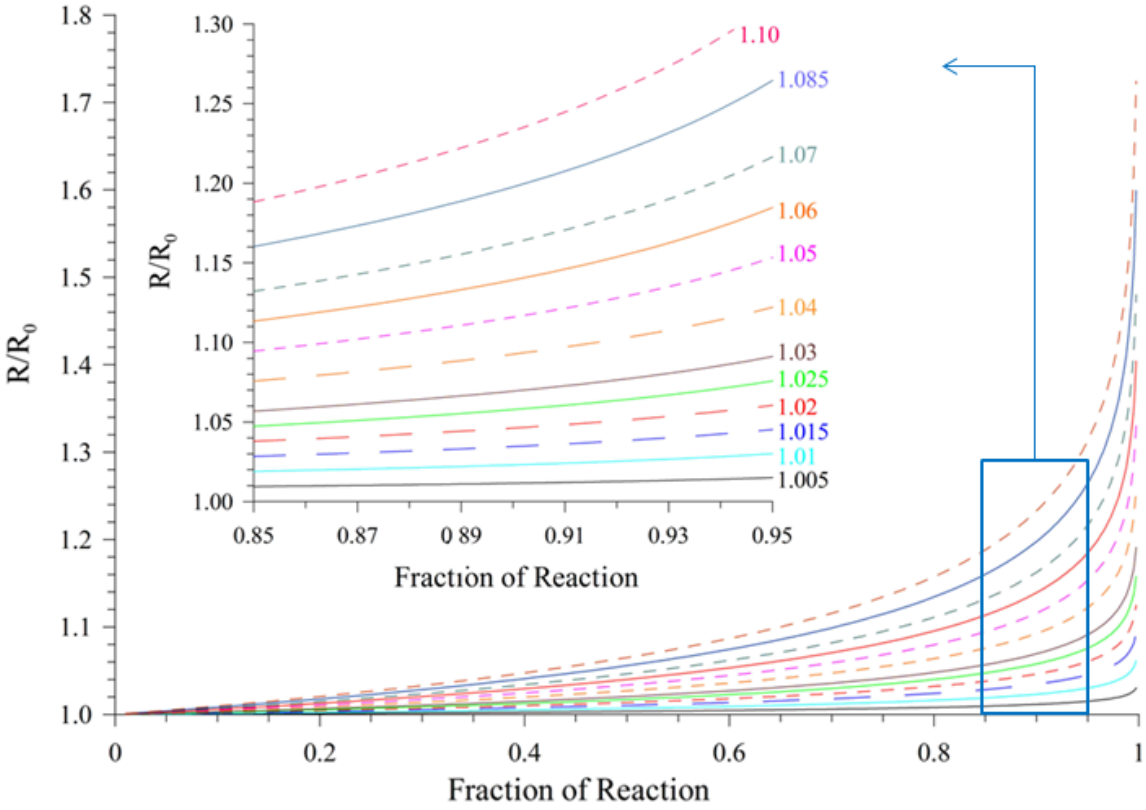

Figure 4.1. Plots of R/R_0 vs. F_L for various KIE Values (calculated using Eq 4.1). The corresponding KIE values are indicated (zoomed area).

Note. (Graph credit: Andrew. J. Bennet)

Therefore, in a competitive measurement of a KIE, it is crucial to obtain precise measurements of the ratios of the isotopologues during the reaction course. Isotope-ratio mass spectrometry (IRMS), nuclear magnetic resonance (NMR) spectroscopy and radiochemical methods are the most commonly used techniques for competitive measurements of isotope effects. Each of these methods has its own limitations such as the need for selective degradations (without isotopic fractionation) of materials into small molecules suitable for isotope ratio MS analysis. Singleton et al used a ^{13}C-NMR spectrometer to measure KIEs using natural abundance of ^{13}C and in order to overcome the low sensitivity of ^{13}C-NMR spectroscopy, this method required the use of large quantities of materials.[2] Recently, Chan et al reported an improved and sensitive ^{13}C-

NMR-based approach for KIE measurements that allows continuous data collection throughout the reaction time course[4]. This innovative method permits straightforward and precise determination of KIEs and is based on differences in the isotopic composition of atoms adjacent to a probe nucleus (^{13}C). Utilizing synthetically enriched ^{13}C materials means that only small quantities (a few milligrams) of reactants are needed for each KIE measurement. The various isotopologues involved in the reaction are distinguishable either by the isotopic chemical shift perturbations (**a**, Figure 4.2), or by differences in their one-bond coupling constants (**b**, Figure 4.2).

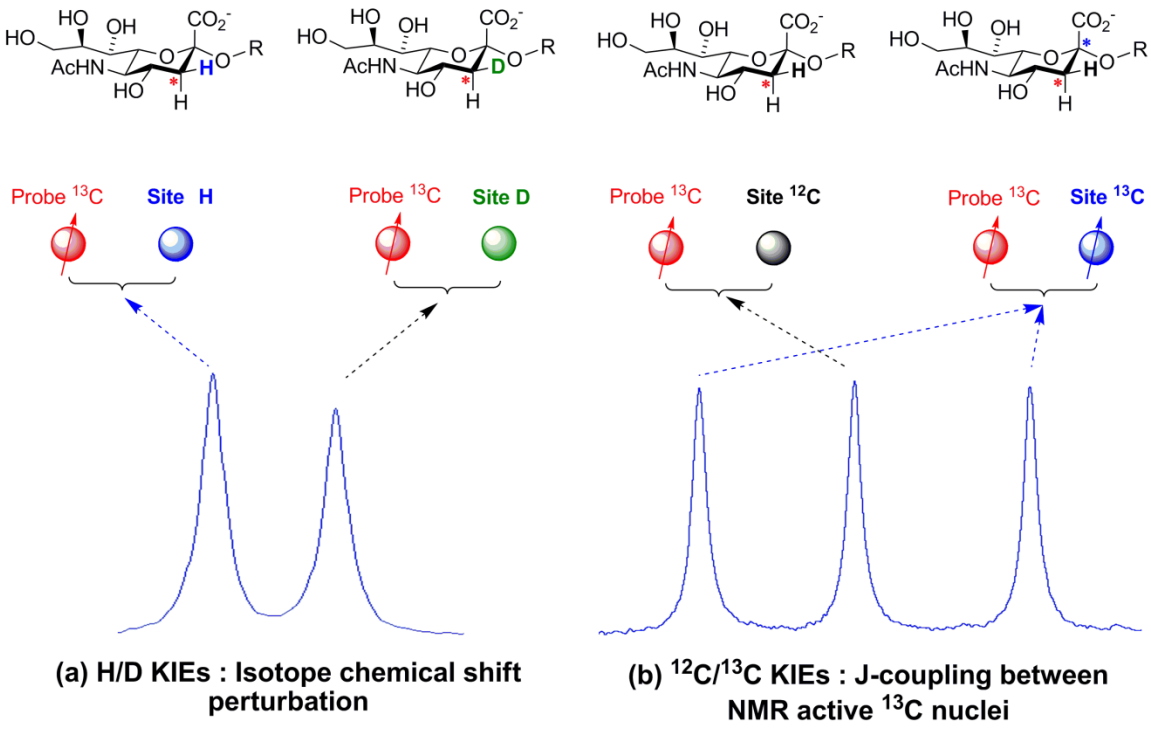

Figure 4.2. Use of ^{13}C nucleus to probe an adjacent isotopic composition

Note. Modified picture from *Nat. Chem. Biol.* 2010, page 405.[4]

In the current project we describe the development of one-dimensional (^{13}C) and two-dimensional (HETCOR and HSQC) NMR spectroscopic techniques for measuring multiple kinetic isotope effects simultaneously. These techniques are demonstrated

using the *Micromonospora viridifaciens* sialidase-catalyzed hydrolysis of a series of synthesized ^{13}C- and ^{2}H-labelled substrates (**1a-f**, Figure 4.3). This work substantially extends the NMR-based technique developed by Chan et al[4] which utilizes substrates site-specifically enriched in ^{13}C to probe adjacent isotopic composition.

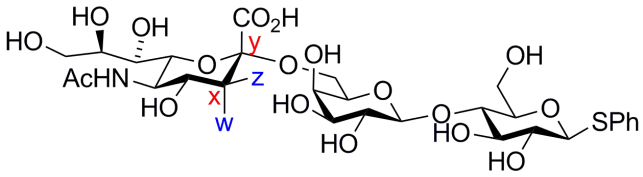

Neu5Acα2,6LacβSPh (1a-f)

KIE	Substrate	Positions Labelled			
		x	y	z	w
Anomeric Carbon	**1a**	^{13}C	^{12}C	^{1}H	^{1}H
	1b	^{13}C	^{13}C	^{1}H	^{1}H
Equatorial Proton at C-3	**1a**	^{13}C	^{12}C	^{1}H	^{1}H
	1e	^{13}C	^{12}C	^{2}H	^{1}H
Axial Proton at C-3	**1a**	^{13}C	^{12}C	^{1}H	^{1}H
	1c	^{13}C	^{12}C	^{1}H	^{2}H
Anomeric Carbon on Deuterated C-3 (eq)	**1e**	^{13}C	^{12}C	^{2}H	^{1}H
	1f	^{13}C	^{13}C	^{2}H	^{1}H
Anomeric Carbon on Deuterated C-3 (ax)	**1c**	^{13}C	^{12}C	^{1}H	^{2}H
	1d	^{13}C	^{13}C	^{1}H	^{2}H

Figure 4.3. Synthesized labelled derivatives of Neu5Acα2,6LacβSPh[3] (**1a-f**) and multiple kinetic isotope effects measured when a mixture of the natural analogue substrates (**1a-f**) are hydrolyzed simultaneously with *M. viridifaciens* sialidase.

Simultaneous KIE measurements of all six labelled substrates (**1a-f)** in the same NMR tube minimize systematic errors, to allow for precise detection of the small differences (often only a few percent) in reaction rate constants that arise from isotopic substitution. Specifically, KIEs will be determined using both one dimensional ^{13}C and two dimensional (HSQC and HETCOR) NMR spectroscopic methods. Of note, in

[3] Neu5Acα2,6LacβSPh is the abbreviation used for phenyl α-sialyl-(2$\rightarrow$6)-β-1-thiolactoside

comparison to one dimensional ^{13}C-NMR spectroscopy, two dimensional NMR spectra should provide faster access to isotopologue-specific integral data because the problem of peak overlap is considerably decreased by the additional dimension. This reduced overlap should make quantitation of the various compounds in the reaction easier and therefore result in more precise and accurate KIE measurements. KIEs measured using a proton detected 2D–NMR spectroscopic method should also be more accurate than 1-D ^{13}C methods because of the intrinsically better signal to noise ratios. Eventually, the development of improved techniques for KIEs measurement (e.g. by two dimensional NMR spectroscopy) will facilitate efforts to model sialidase transition state structures. Better knowledge of TS structural differences in sialidases (such as those found in drug-resistant influenza type A strains), may lead to new strategies for drug development.

4.3 Substrate Synthesis

4.3.1 Materials

All chemicals and biochemicals were of analytical grade or better and were purchased from Sigma-Aldrich unless noted otherwise. Sodium (3-^{13}C)- and (2,3 $^{13}C_2$) pyruvates were purchased from Cambridge Isotope Laboratories. *N*-acetyl-D-mannosamine (**ManAc**) and *E.Coli* Neu5Ac Aldolase were purchased from Codexis. Cytidine 5'-triphosphate disodium salt was purchased from 3B scientific Corp. CMP-Neu5Ac synthase from *Neisseria meningitides*[5] and α-2,6-sialyltransferase from *Vibrionaceae photobacterium* sp. JT-ISH-224[6] were expressed according to the reported procedures. ^{1}H- and ^{13}C-NMR spectra were acquired on a Bruker 600 MHz spectrometer equipped with a QNP cryoprobe, chemical shifts are listed in parts per million, and coupling constants (*J*) are given in hertz. Melting points were determined on

a MPA100—automated melting point system. Optical rotations were measured on a Perkin-Elmer 341 polarimeter and concentrations are reported in units of g per 100 mL.

4.3.2 Phenyl 4-*O*-(*β*-D-galactopyranosyl)-1-thio-β-D-glucopyranoside (4)

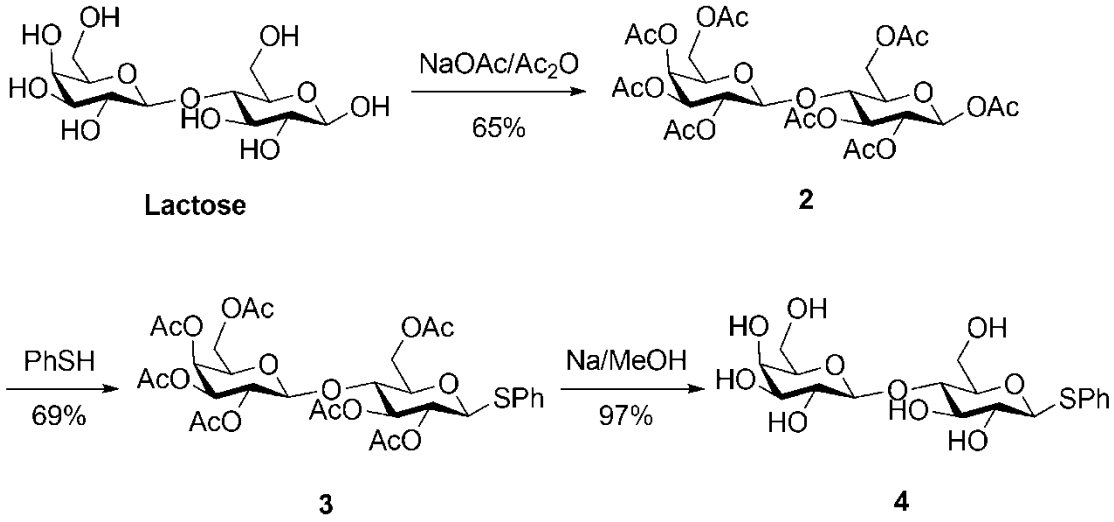

Scheme 4.1. Synthetic route used for the production of phenyl 4-*O*-(*β*-**D**-galactopyranosyl)-1-thio-β-D-glucopyranoside (**4**)

To a hot (~100 °C) suspension of sodium acetate (25 g, 0.30 mol) in acetic anhydride (350 mL), lactose was gradually added (62.5 g, 0.17 mol) over 1 h. After each addition of lactose, the reaction was initiated by directly heating the flask using a gas torch until the mixture started to boil. After all the lactose was added, the reaction mixture was cooled to rt and left at this temperature for 30 min, and it was then poured onto crushed ice (1 L) and stirred overnight. The precipitated product was filtered off, washed with water and recrystallized from ethanol to yield the *β*-anomer of peracetylated lactose (**2**, 71 g, 65% yield). Subsequently, a mixture of this peracetylated lactose (**2**, 20 g, 0.03 mol) and activated 3 Å molecular sieves (80 g) was dried under vacuum for 1 h. To the resulting solid, thiophenol (10 mL, 0.10 mol) and dry CH_2Cl_2 (1200 mL) were

added under a N_2 atmosphere, and the mixture was then stirred for 1 h. Then, BF_3-diethyl ether (25.4 mL, 0.21 mol) in CH_2Cl_2 (100 mL) was added and the mixture was stirred overnight under a N_2 atmosphere at room temperature. The resultant mixture was filtered through celite, and washed thoroughly with CH_2Cl_2. The combined filtrates were washed with saturated $NaHCO_3$ (3 $\times$ 1 L), water (1 L) and brine (1 L), and the resulting solution was dried over anhydrous Na_2SO_4. After evaporating the solvent under reduced pressure, a solid residue was obtained, which was recrystallized from ethanol to yield **3** as white crystals (15 g, 69% yield). Subsequently, lactoside **3** (10 g, 13.7 mmol) was dissolved in dry methanol (400 mL), and a 2 M methanolic sodium methoxide solution (10 mL) was added at 0 °C. The resulting solution was stirred at 0 °C for 2.5 h and was then neutralized by adding Amberlite IR-120 resin (H^+ form). The mixture was filtered and the resin was thoroughly washed with methanol. Subsequently, the filtrate was concentrated under reduced pressure to give thiophenyl lactoside **4** as a white solid (5.8 g, 97%). Mpt 216–217 °C; $[\alpha]^{20}_D$ = -33.18 (c = 1.1, MeOH); ^{1}H NMR (600 MHz, D_2O) δ: 3.44 (t, 1 H, $J_{2,1} = J_{2,3}$ = 8.7, H-2^{II}), 3.57 (t, 1 H, $J_{2,1} = J_{2,3}$ = 8.7, H-2^{I}), 3.62–3.87 (m, 8 H, H-3^{I}, H-3^{II}, H-4^{II}, H-5^{I}, H-5^{II}, H-$6_b{}^{I}$, H-$6_a{}^{III}$, H-$6_b{}^{II}$), 3.92–4.01 (m, 2 H, H-$6_a{}^{I}$, H-4^{I}), 4.47 (d, 1 H, $J_{1,2}$ = 7.8, H-1^{I}), 4.85 (d, 1 H, $J_{1,2}$ = 9.9, H-1^{II}), 7.39–7.48(m, 3 H, Ar-H), 7.58–7.64(m, 2 H, Ar-H); ^{13}C NMR (150 MHz, D_2O) δ: 59.65 (C-6^{I}), 60.55 (C-6^{II}), 68.08 (C-4^{I}), 70.47 (C-2^{I}), 70.98 (C-2^{II}), 72.04 (C-3^{I}), 77.47, 75.31, 74.87 (C-5^{I}, C-5^{II}, C-3^{II}), 78.23 (C-4^{II}), 86.65 (C-1^{II}), 102.38 (C-1^{I}), 131.39, 131.20, 128.86, 127.67 (Ar). HRMS-FAB (*m*/*z*): [M+Na^+] calcd for $C_{18}H_{26}O_{10}S$, 457.113889; found, 457.113719.

4.3.3 Synthesis of Labelled Sialic Acids (6a-f)[7,8]

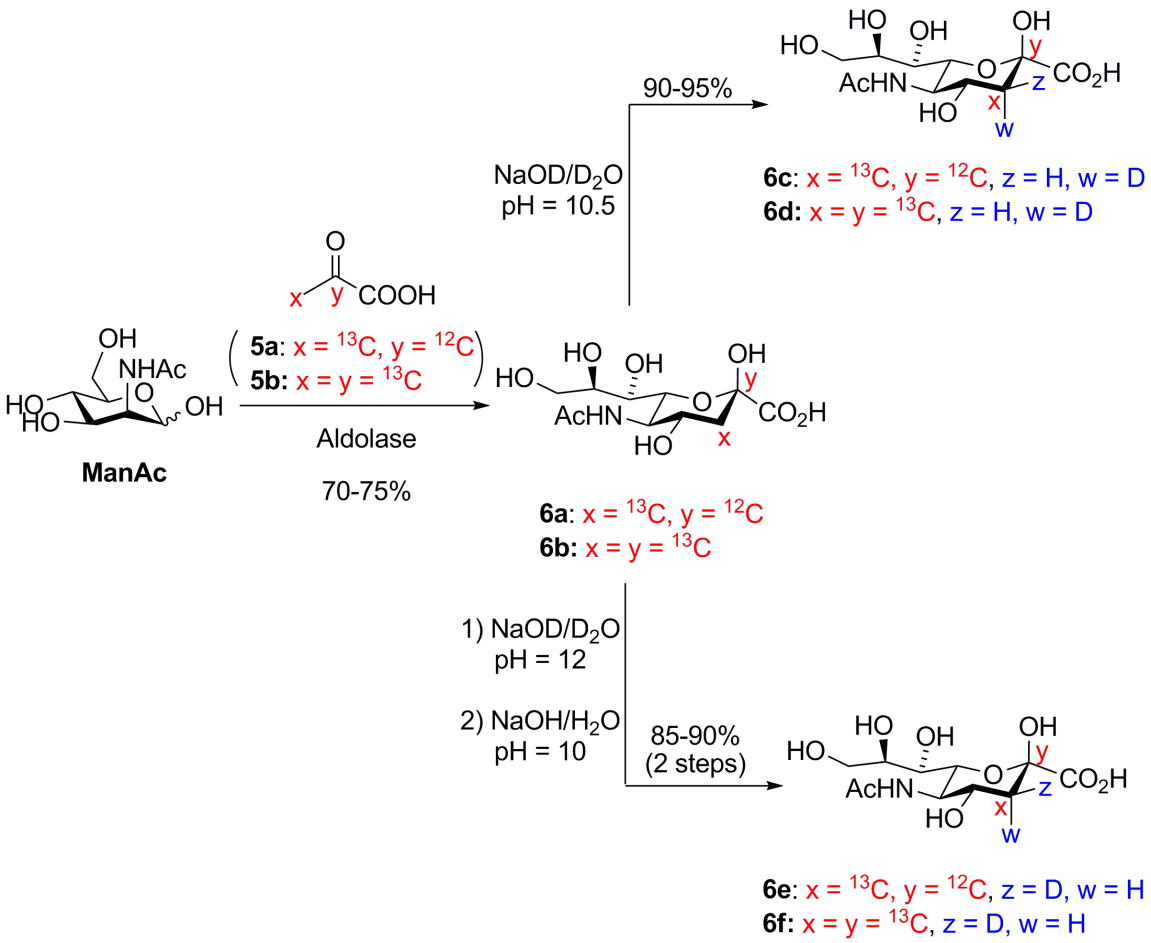

Scheme 4.2. Chemo-enzymatic synthesis of labelled sialic acids (**6a-f**)

To a solution of *N*-acetyl-D-mannosamine (**ManAc**, 10 g, 45 mmol), and the appropriate ^{13}C-labelled sodium pyruvate (**5a** or **5b,** ~1 g**,** ~9 mmol) in deionized water (12 mL) were added aldolase (20 mg, 0.2 μm) and BSA (1 mg) dissolved in water (1 mL) at pH = 7.5. After incubating for 2 days at 37 °C, the mixture was heated to 70 °C for 15 min. The resultant mixture was then cooled to rt and centrifuged (3500 RPM) for 30 min. The supernatant was subsequently concentrated and purified by anion exchange column (formate form) chromatography eluting initially with water to remove excess ManAc and then with 2 M formic acid. Fractions containing the ^{13}C labelled sialic acid were

combined and freeze dried to give the corresponding ^{13}C labelled sialic acids (**6a** or **6b**, ~ 2 g, 70-75% yield) as white solids.

Incorporation of deuterium at the axial position of C–3 in ^{13}C labelled sialic acids (**6a** and **6b**) was achieved by dissolving **6a** or **6b** in D_2O and adjusting the pD to 10.5. The exchange reaction (via the acyclic keto form) was monitored by ^1H-NMR spectroscopy, and when the integration of the peak at δ1.70 ppm (H-ax) decreased by about 70%, the reaction was stopped by the addition of Amberlite IR-120 resin (H^+ form), filtered and then lyophilized to give either a mixture of **6c**/**6a** (~7:3) or **6d**/**6b** (~7:3). Incorporation of deuterium at the equatorial position of C–3 in ^{13}C labelled sialic acids (**6a** and **6b**) was accomplished in two steps. First, **6a** or **6b** were dideuterated by performing the exchange reaction at a pD of 12 for 24 h, by which time both ^1H-signals at C-3 had disappeared and the dideuterio compounds were isolated as described above. The specifically *pro-S* deuterated compounds were made by back-exchanging the dideuterated compounds in water at a pH of 10 for 5 h when the integration for the peak at δ 1.70 ppm (H-ax) was 70% more than the integration of peak at δ 2.70 ppm (H-eq). Upon workup as above, a mixture of **6e**/**6a** (~7:3) or **6f**/**6b** (~7:3) was obtained as white solids (85-95% yield). All of the labelled sialic acids (**6a-f**) showed the predicted ^1H-NMR and ^{13}C-NMR spectra, consistent with incorporation of the appropriate isotopes (^2H and ^{13}C). As all deuterium incorporation experiments gave isotopically labelled (^2H < 100 atom%) as opposed to substituted (~100 atom%) sialic acids, no further characterization was done, and only (2-^{13}C) labelled sialic acid (**6a**) was characterized as follows:

3-^{13}C β-Neu5Ac (6a) (containing 5% of α-anomer): Mpt 170 °C (dec); $[\alpha]^{20}_D$ = –0.4 (c = 0.7, H_2O); ^1H NMR (600 MHz, D_2O) δ: 1.90 (dt, 1 H, $J_{3a,^{13}C}$ = 129.7, $J_{3a,3e}$ = $J_{3a,4}$ = 12.2, H-3_{ax}), 2.06 (s, 3 H, CH_3), 2.33 (ddd, 2 H, $J_{3e,^{13}C}$ = 133.5, $J_{3e,3a}$ = 13.1, $J_{3e,4}$ = 4.6),

3.58 (d, 1 H, $J_{7,8}$ = 9.2, H-7), 3.64 (dd, 1 H, $J_{9b,9a}$ = 11.8, $J_{9b,8}$ = 6.3, H-9_b), 3.77 (ddd, 1 H, $J_{8,7}$ = 8.9, $J_{8,9b}$ = 6.2, $J_{8,9a}$ = 2.4, H-8), 3.86 (dd, 1 H, $J_{9a,9b}$ = 11.9, $J_{9a,8}$ = 2.4, H-9_a), 3.95 (t, 1 H, $J_{5,6}$ = $J_{5,4}$ = 10.3, H-5), 4.03–4.13(m, 2 H, H-4 and H-6); ^{13}C NMR (150 MHz, D_2O) δ: 21.59 (CH_3), 38.37 (C-3), 51.59 (C-5), 62.69 (C-9), 66.26 (d, $J_{C\text{-}4,C\text{-}3}$ = 35.8, C-4), 67.77 (C-7), 69.67 (C-8), 69.93 (C-6), 94.82 (d, $J_{C\text{-}2,C\text{-}3}$ = 41.0, C-2), 174.37, 172.98 (C=O and C-1). HRMS-FAB (*m/z*): [M + Na^+] calcd for $C_{10}{}^{13}CH_{19}NO_9$, 333.098557; found, 333.098282.

4.3.4 Synthesis of ^{13}C- and ^{2}H-Labelled Derivatives of Neu5Acα2,6LacβSPhs (1a-f)[7]

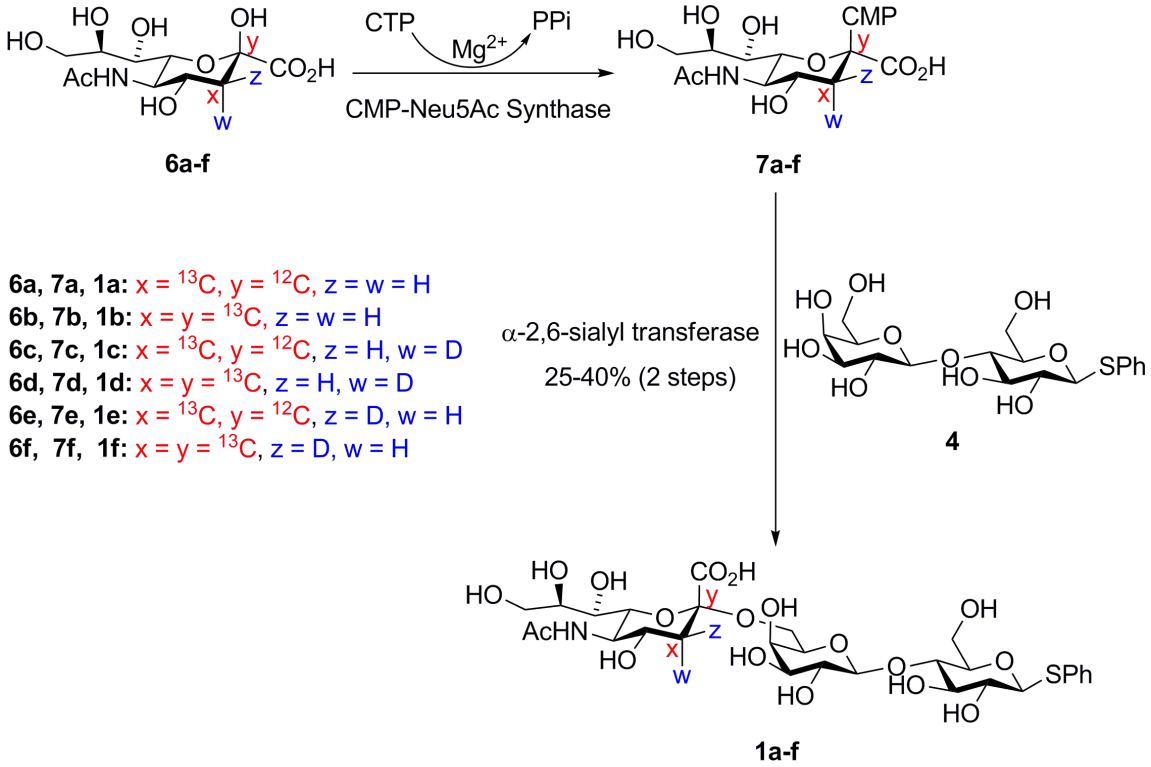

Scheme 4.3. Chemo-enzymatic synthesis of ^{13}C- and ^{2}H-labelled derivatives of Neu5Acα2,6LacβSPh (**1a-f**)

Labelled sialic acids (**6a–f**, ~100 mg, ~0.32 mmol) were converted into the corresponding CMP-sialic acids **7a–f** by incubation with CMP-Neu5Ac synthase (1 mL of

expression supernatant) in the presence of cytidine 5'-triphosphate disodium salt (212 mg, 0.59 mmol) in a solution containing Tris buffer (1 M; 3.6 mL), $MgCl_2$ (1 M; 1.4 mL), and pyrophosphatase (100 μL, 0.1 U/mL) at 37 ºC and pH = 8 (the pH was adjusted by adding NaOH prior to addition of CMP-Neu5Ac synthase) for 3 h. After centrifuging the reaction mixture (15 min, 3500 rpm), the supernatant was directly reacted with thiophenyl β-lactoside **4** in the presence of α2,6–sialyltransferase (500 μL of expression supernatant) and this mixture was incubated at 37 ºC overnight. After the reaction was complete, the mixture was purified by loading into a reversed-phase C18 sep-pack cartridge and eluting successively with water and 1:20 v/v MeCN/H_2O. Fractions containing the product were lyophilized to give the corresponding labelled ^{13}C- and ^{2}H-labelled derivatives of Neu5Acα2,6LacβSPh (**1a-f**, 60-90 mg, 25-40% yield). All the labelled Neu5Acα2,6LacβSPhs (**1a-f**) showed the predicted ^{1}H NMR and^{13}C NMR spectra consistent with incorporation of the appropriate isotopes (^{2}H and ^{13}C) in the sialic acid moiety. Labelled Neu5Acα2,6LacβSPhs (**1a**) was characterized: Mpt 230 °C (dec); $[\alpha]^{20}_{D}$ = -38.69 (c = 0.2, H_2O); ^{1}H NMR (600 MHz, D_2O) δ: 1.72 (dt, 1 H, $^{2}J_{3a,C\text{-}13}$ = 129.9, $J_{3a,3e}$ = $J_{3a,4}$ = 12.1, H-3_{ax}), 2.03 (s, 3H, CH_3), 2.70 (ddd, 1 H, $^{2}J_{3e,C\text{-}13}$ = 134.4, $J_{3e,3a}$ = 12.4, $J_{3e,4}$ = 4.6, C-3_{eq}), 3.42 (dd, 1 H, $J_{2,1}$ + $J_{2,3}$ = 18.7, H-2^{II}), 3.50–3.57 (m, 2 H, H-2^{I} and H-7^{III}), 3.59 (dd, $J_{9b,9a}$ = 10.4, $J_{9b,8}$ = 3.7, H-$9_a{}^{III}$), 3.61– 3.74 (m, 7 H, H-3^{I}, H-3^{II}, H-4^{II}, H-4^{III}, H-5^{I}, H-5^{II}, H-$6_b{}^{II}$), 3.77–3.82 (m, 2 H, H-$6_b{}^{I}$, H-8^{III}), 3.82–3.91 (m, 3 H, H-5^{III}, H-6^{III}, H-$6_a{}^{II}$), 3.91–3.99 (m, 3 H, H-4^{I}, H-$6_a{}^{I}$, H-$9_a{}^{III}$), 4.42 (d, 1H, $J_{1,2}$ = 7.9, H-1^{I}), 4.83 (d, 1 H, $J_{1,2}$ = 10.0, H-2^{II}), 7.37–7.45 (m, 3 H, Ar-H), 7.57–7.61 (m, 2 H, Ar-H); ^{13}C NMR (150 MHz, D_2O) δ: 22.09 (CH_3), 40.13 (C-3), 51.80 (C-5), 60.32 C-6^{I}), 62.66 (C-6^{II}), 63.63 (C-9^{III}), 68.49 (d, $^{1}J_{4,3}$ = 19.6, C-4^{III}), 68.55 68.30 (C-4^{I} and C-7^{III}) 70.79 (C-2^{I}) 71.32 (C-2^{II}) 71.85 (C-6^{III}) 79.32, 78.56, 76.01, 73.74, 72.54, 72.38 (C-3^{I}, C3^{II}, C-4^{II}, C-5^{I}, C-5^{II}, C-8^{III}) 86.92 (C-1^{I}) 100.29 (d, $^{1}J_{2,3}$ = 43.0, C-2^{III}) 103.20 (C-1^{I}) 131.79, 129.34, 128.18 (Ar)

174.91, 173.49 (C-1^{III} and C=O). HRMS-FAB (*m*/*z*): [M - Na^+] calcd for $C_{28}{}^{13}C\ H_{43}NO_{18}S$, 749.212660; found, 749.212799.

4.4 Kinetics Spectroscopy

4.4.1 Acquisition of ^{13}C-NMR Spectra

NMR spectra were acquired on a Bruker AVANCE II spectrometer equipped with a QNP cryoprobe operating at 600 MHz for ^{1}H, 150 MHz for ^{13}C, and 92 MHz for ^{2}H. The reaction solvent was H_2O containing 3% D_2O for spectral locking. Manual shimming was performed by adjusting the various parameters in order to obtain an optimal ^{1}H NMR spectrum with peaks exhibiting close to Lorentzian shape and showing excellent signal to noise. Proton T_1 values of labelled Neu5Acα2,6LacβSPhs (**1a-f**) were measured using a standard inversion recovery pulse sequence and the values ranged from 300–400 ms for the axial and equatorial protons at position 3 of sialosides (**1a-f**). Carbon-13 T_1 values were also obtained in a similar way and the values for C3 and C2 of labelled Neu5Acα2,6LacβSPhs (**1a-f**) were determined to be in a range of 200–400 ms and 4–5 s, respectively.

In a typical experiment, the six synthesized labelled Neu5Acα2,6LacβSPhs (**1a-f**) (~0.5 mg of each) were dissolved in H_2O (~500 µL) containing 3% D_2O. 2–^{13}C Labelled glycine (~ 0.05 mg) was added as an internal standard. The pH of the mixture was then adjusted to 5.2 with NaOAc buffer (final concentration of 100 mM) and the resulting solution was transferred into a standard NMR tube. Prior to adding the *Micromonospora viridifaciens* sialidase (10-20 µl, 0.05-0.10 µg/mL), the magnetic field was manually shimmed to obtain symmetrical (ideally close to Lorentzian) peak shapes having good signal to noise. One ^{1}H NMR and one ^{13}C NMR spectrum were then acquired. The

sample was removed from the magnet, the enzyme added and the sample re-inserted into the NMR probe. The magnetic field was then re-shimmed and the probe re-tuned before sequentially acquiring more than fifty quantitative proton- and deuterium-decoupled ^{13}C (^{13}C {^{1}H,^{2}H}) NMR spectra.

4.4.2 Deconvolution of ^{13}C-NMR Spectra

During sialidase-catalyzed reactions, the first formed isotopologue products of hydrolysis are labelled α-sialic acids that mutarotate to afford an equilibrium mixture enriched in the more thermodynamically stable labelled β-sialic acids (Figure 4.4). In a typical ^{13}C {^{1}H,^{2}H} spectrum acquired during the sialidase-catalyzed reaction, the enriched 3-^{13}C in labelled α-sialosides, labelled α-sialic acids, labelled β-sialic acids, and [2-^{13}C]-glycine appear as shown in Figure 4.5.

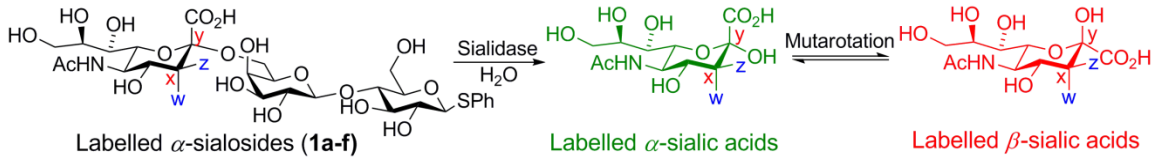

Figure 4.4. Sialidase-catalyzed hydrolysis of labelled Neu5Acα2,6LacβSPhs (**1a-f**). The asterisk (*) stands for ^{13}C

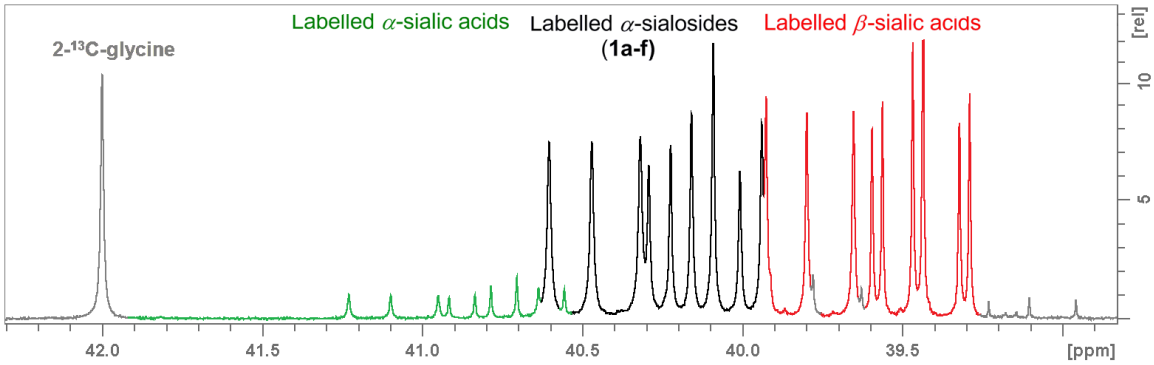

Figure 4.5. A typical ^{13}C\{1H, 2H\} spectrum acquired in the middle of sialidase-catalyzed hydrolysis of labelled Neu5Acα2,6LacβSPhs (**1a-f**).

Focusing on the six isotopologues (**1a-f**) in the acquired ^{13}C {^{1}H,^{2}H} spectrum during sialidase-catalyzed reaction, the enriched 3-^{13}C in each isotopologue appears as shown in Figure 4.6.

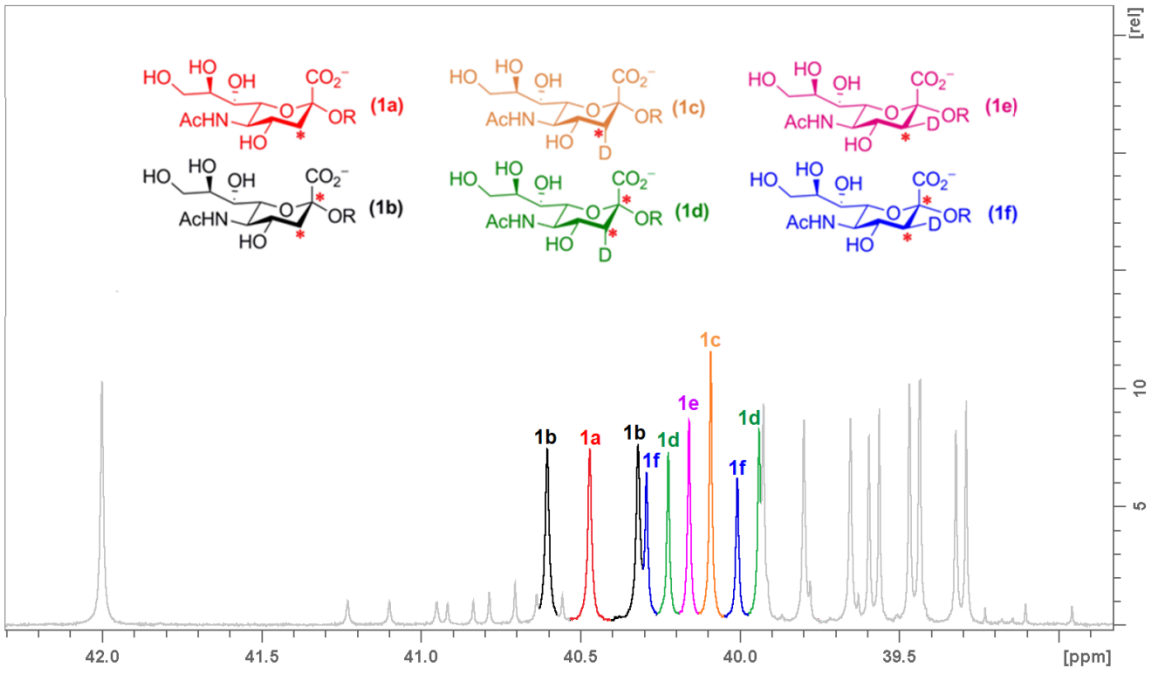

Figure 4.6. Marked signals related to the enriched 3-^{13}C of labelled Neu5Acα2,6LacβSPhs (**1a-f**). The asterisk (*) stands for ^{13}C and R = Phenyl 4-O-(β-d-galactopyranosyl)-1-thio-β-D-glucopyranoside

The resulting series of quantitative ^{13}C {^{1}H,^{2}H} spectra were deconvoluted by performing the following operations:

i) all spectra were carefully phased and baseline corrected manually using Bruker's *Topspin* software.

ii) each spectrum's chemical shift scale was calibrated by setting the chemical shift of the C2 signal of the internal standard (2-^{13}C)-glycine to be 42 ppm.

iii) three (of the more than fifty acquired) ^{13}C {^{1}H,^{2}H} spectra were selected from the beginning, the middle, and the end of the reaction (**a**, **b**, and **c**; Figure 4.7). Using

Bruker's *Topspin* software, these three spectra were co-added to create a single sum spectrum (**d**, Figure 4.7).

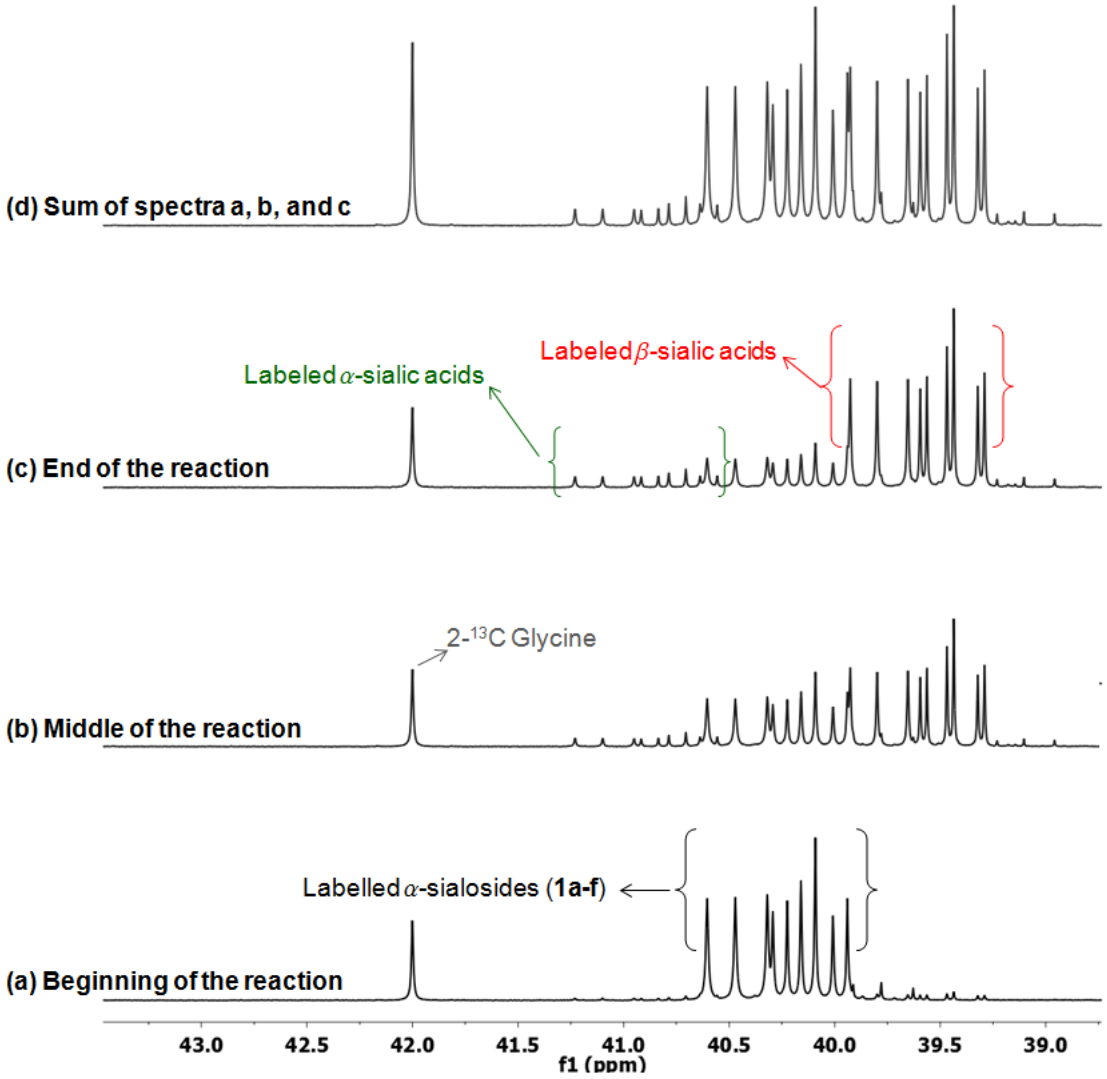

Figure 4.7. Three stacked ^{13}C {^{1}H,^{2}H} spectra (**a**, **b**, **c**) are selected from the beginning, the middle and the end of the *Micromonospora Viridifaciens*-sialidase catalyzed hydrolysis of natural substrate analogues (**1a-f**). Spectrum **d** is the sum of **a**, **b** and **c** created by using Bruker *topspin* software.

iv) This sum spectrum (**d**) was then fit to a series of mixed Gaussian-Lorentzian peaks using a special script written by Dr. D. Brouwer[9]. This fitting utilized the least-square "NonlinearRegress" function in a *Mathematica* notebook[10]. The chemical

shift range deconvoluted (38.6–42.8 ppm) covers all of the relevant peaks from the 2-^{13}C-glycine, substrates **1a-f,** and the products of hydrolysis (α- and β-sialic acids). From this analysis, the peak positions, peak widths at half-height, and optimal combination of Lorentzian and Gaussian (L/G) shapes of the individual peaks that best matched the sum spectrum (**d**) were determined. The calculated Mathematica fit for the sum spectrum (**d**) is shown in red color in Figure 4.8, while the sum spectrum (**d**) is in black (covered by the red spectrum). The goodness of fit is shown by the blue line (residual), which is the difference between the sum spectrum and the calculated fit. The two green lines indicate the standard deviation of the noise level in the original spectrum (determined from a region without any peaks).

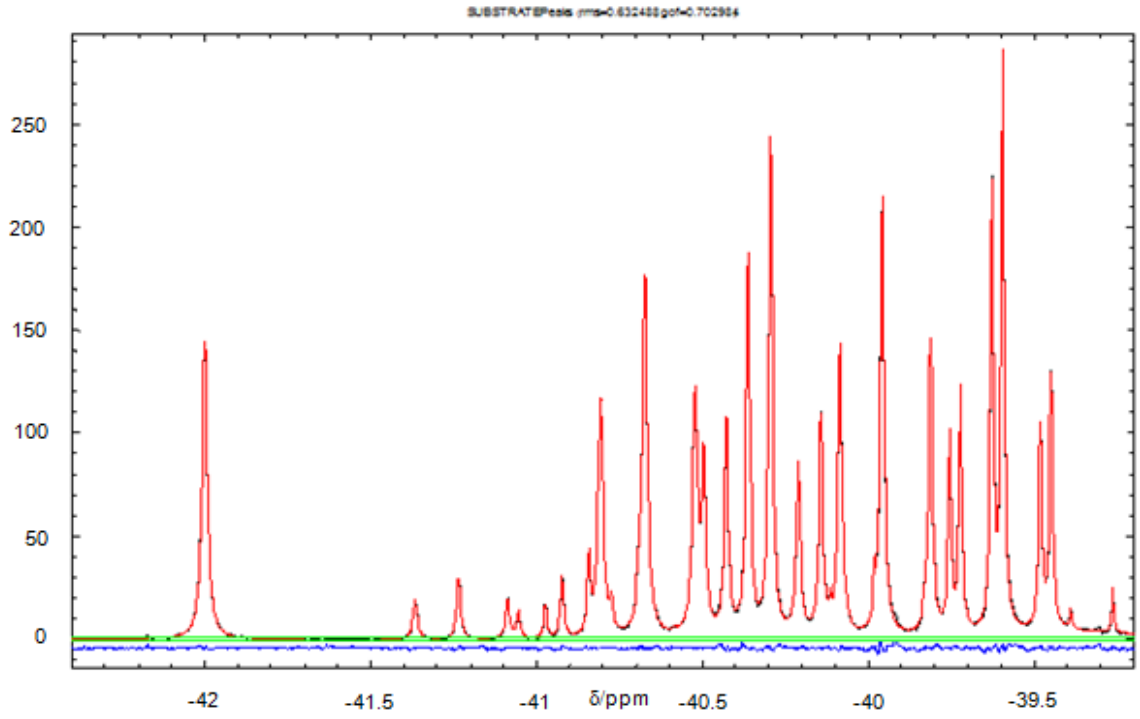

Figure 4.8. Fit for the sum spectrum (**d**, Figure 4.7) using least-squares ″nonlinear Regression″ function in *Mathematica*. The original sum spectrum (**d**) is in black which is covered under the calculated fit spectrum (red). The difference between spectrum **d** and the fit is shown in blue (residual).

v) The custom *Mathematica* non-linear regression script was then used to fit all other individual quantitative ^{13}C {^{1}H,^{2}H} spectra. In each case, the fitting parameters obtained from the optimal *Mathematica* fit of the sum spectrum (**d**) were used as initial parameters, keeping the peak positions, peak widths at half-height, and the G/L mix of each peak fixed while allowing only the peak heights to be varied during the fitting procedure. In each ^{13}C {^{1}H,^{2}H} spectrum, there are thirty peaks to be fit by the *Mathematica* algorithm: nine peaks from labelled substrates (**a**, Figure 4.7), nine peaks from labelled α–sialic acids which are the first products of hydrolysis (**c**, Figure 4.7), nine peaks from labelled β–sialic acids (which are formed by mutarotation of α-sialic acids, **c**, Figure 4.7), one peak from 2-^{13}C glycine (**b**, Figure 4.7), and eight small peaks associated with dideuterated materials.

vi) Finally, the peak areas are normalized by dividing peak areas for reactants (labelled substrates) by the area of the 2-^{13}C glycine peak in the same spectrum. In each spectrum, the fraction of reaction (F_L) was obtained for the lighter isotopomer, and R/R_0 for the corresponding fraction of reaction was calculated. These data were then analyzed using a non-linear least squares fit to Eq 4.1 in the ″Prism-4″ software.

4.4.3 Acquisition of 2D-NMR (HETCOR and HSQC) Spectra

HETCOR:

2-Dimensional ^{13}C-^{1}H HETCOR spectra were acquired on a Bruker AVANCE II spectrometer equipped with a 5 mm QNP cryoprobe and operating at 600 MHz for ^{1}H, 150 MHz for ^{13}C, and 92 MHz for ^{2}H. The reactions were carried out in 600 MHz-grade NMR tubes (5 mm diameter) with the sample maintained at 298 K. H_2O containing 3%

D_2O (for spectral field locking) was used as the solvent. The HETCOR pulse sequence used in this experiment (written by Dr. Andrew Lewis, see Appendix, page 240) was modified to balance the last echo, to apply simultaneous (and inverse gated) ^1H and ^2H decoupling during FID acquisition, and to permit ^2H field-locking to remain active during the recycle delay only. 90-Degree (hard) pulse lengths were determined on the actual samples and found to be 9.38 µs (26.65 kHz r.f. field) and 11.25 µs (22.22 kHz r.f. field) for ^{13}C and ^1H, respectively. 180-Degree (hard) pulse lengths were set to twice these durations. These r.f field strengths were more than adequate to excite the spectral regions of interest. Decoupling was achieved using a GARP4 composite pulse decoupling with an 80 µs pulse length on the ^1H channel and 300 µs on the ^2H channel. Transmitter offsets were set to 2.2 ppm for the ^1H and ^2H channels, and 40 ppm for ^{13}C. The 1/4*J* delay was set assuming a 1-bond ^1H-^{13}C J coupling of 132 Hz (closely matching the values measured for the actual compounds used, which ranged from 130-134 Hz), and the dead time (DE) was set to 4.5 µs.

Based upon longitudinal (T_1) spin relaxation arguments, the intrinsic sensitivity of an NMR experiment (i.e., the S/N divided by the square root of the time required to detect one FID) is maximized when using a recycle delay of 1.27 x T_1 of the initially excited nucleus (^1H for the HETCOR experiment used here). However, because a relatively long FID acquisition time (3.39 s) was used (and the simultaneous GARP4 ^1H and ^2H decoupling applied therein could produce unacceptably high r.f. duty cycles), a recycle delay (D1) of 1.5 s was used. After 16 dummy scans, 4 co-added transients (scans) per t1 increment were acquired using a spectral width (SW) of 4 ppm in both the ^{13}C (F2) and ^1H (F1) dimensions. The number of complex points along the indirect (^1H) dimension was set to optimize the experimental time while providing acceptable resolution (basically 4 well-separated peaks in this dimension in the region acquired).

The high ^{13}C sensitivity of the QNP cryoprobe produced relatively long-lasting FIDs. Therefore in order to acquire data with acceptable peak shapes and spectral resolution in the direct (^{13}C) dimension, the FID acquisition time was set to 3390 ms. This permitted application of an exponential decay window function to the ^{13}C time domain data which had several benefits including: i) efficiently suppressing any residual truncation artifacts, ii) ensuring better peak shapes, and iii) producing minimal baseline distortions. Thus 400 (complex) t1 increments, each containing 4096 complex points per FID, were acquired for a total acquisition time of 2.25 h per spectrum.

Data processing used double Fourier transformation using 4-fold and 5-fold zero filling in the ^{13}C and ^{1}H dimensions respectively, QSINE (shifted) window function was applied to the ^{1}H dimension, 4 Hz exponential line broadening in the ^{13}C dimension, and careful manual phase correction followed by automatic spline baseline correction in both dimensions. Chemical shift referencing was achieved by setting the glycine peak to 3.53 ppm and 42 ppm in the ^{13}C and ^{1}H dimensions, respectively. This produced data with resolutions of 0.15 and 1.17 Hz per point in the ^{13}C and ^{1}H dimensions respectively (peaks had at least 10 points above half-height). Note that because the HETCOR experiment is ^{13}C-detected, there is (virtually) no signal from the solvent (water), which permitted use of the highest possible receiver gains, and thus provided data with the maximum dynamic range attainable on the spectrometer used.

In a typical experiment, a 500 μL solution containing the six synthesized substrates **1a-f** (~0.5 mg of each), 2–^{13}C labelled glycine (~0.05 mg) as the internal standard and sodium acetate buffer (final concentration of 100 mM, pH = 5.2), all dissolved in H_2O containing 3% D_2O, is transferred into a 5 mm diameter NMR tube. Prior to adding the *M. viridifaciens* sialidase (10-20 μL, 0.05-0.10 μg/mL), the magnetic field is manually shimmed to obtain optimal Lorentzian peak shapes and increased

signal to noise, and then ^{1}H-NMR (one), ^{13}C-NMR (one), and HETCOR (one) spectra are acquired. After addition of the enzyme, re-shimming the magnetic field, and re-tuning the probe, more than thirty consecutive HETCOR spectra (135 min per spectrum) are acquired as the enzymatic reaction progresses for a period of 3-4 days.

HSQC:

2-Dimensional ^{1}H-^{13}C HSQC spectra were acquired on a Bruker AVANCE II spectrometer equipped with a 5 mm TCI cryoprobe and operating at 600 MHz for ^{1}H, 150 MHz for ^{13}C, and 92 MHz for ^{2}H. The reactions were carried out in H_2O as solvent (containing 3% D_2O for spectral field locking) with the sample maintained at 298 K. Because the HSQC experiment is ^{1}H detected, there is a very strong signal arising from the solvent used (97% H_2O). Various water suppression techniques were tried, however all methods gave baseline or other peak shape distortions that made the 2-D spectra unsuitable for reliable and accurate peak volume determination. Therefore the reactions were carried out in 5 mm Shigemi NMR tubes (Figure 4.9), which were susceptibility-matched to D_2O. The Shigemi tubes contained approx. 250 µL of solution (20 mm depth of filling in the tube, i.e. matching the r.f. coil length), and therefore reduced the total volume of H_2O present by a factor of 2. The use of Shigemi tubes had several advantages including: i) reducing (by ca. 1/2) the amount of isotopically-labelled substrates required per experiment, ii) permitting data with a far higher dynamic range to be acquired vs. a regular 5 mm tube (due to lower intensity water signal), iii) maintaining the highest possible r.f. field (pulse) homogeneity, and iv) not adversely impacting peak shapes (shimming) nor compromising the signal-to-noise dramatically.

Figure 4.9. Shigemi NMR tube

The HSQC pulse sequence used in this experiment (written by Dr. Andrew Lewis, see Appendix, page 242) was modified to apply ^{13}C decoupling during FID acquisition and ^{2}H decoupling throughout the pulse sequence (including FID acquisition), except during the recycle delay (where ^{2}H field-locking was activated). 90-Degree (hard) pulse lengths were determined on the actual samples and found to be 11.1 µs (22.52 kHz r.f. field) and 9.63 µs (26.65 kHz r.f. field) for ^{13}C and ^{1}H respectively. 180-Degree (hard) pulse lengths were set to twice these durations. Decoupling was achieved using a GARP4 composite pulse decoupling with a 55 µs pulse length on the ^{13}C channel and 175.5 µs on the ^{2}H channel. Transmitter offsets were set to 2.2 ppm for the ^{1}H and ^{2}H channels, and 40 ppm for ^{13}C. The 1/4*J* and 1/8*J* delays were set based on a 1-bond ^{1}H-^{13}C *J* coupling of 132 Hz, the dead time (DE) was set to 10 µs. With ^{1}H T_1 relaxation times between 0.46 and 1.3 s, and with $t2_{max}(^{1}H)$ = 568 ms, the inter-scan delay should be between 0.10 s and 1.15 s (i.e. 1.27 x T1 – AQ) based on T_1-optimized arguments (i.e. 1.27 x T_1). However, simultaneous GARP4 ^{2}H and ^{13}C decoupling during signal detection would have yielded an unacceptably high r.f. duty cycle (and also increased sample heating) using such short delays between FID acquisition. Hence, the 2D spectra were acquired with a recycle delay of 1.5 s. SINE-shaped gradient pulses were 500 µs in duration, and a 1 ms trim pulse was applied on the ^{1}H channel. After a 16 dummy scans, 4 co-added scans per t1 increment were acquired using a spectral width (SW) of 12 ppm in ^{1}H (F2) dimension, and 4 ppm in the ^{13}C (F1) dimension. Based on similar arguments outlined for HETCOR experiment above, the number of complex

points along the ^{13}C dimension was set so that $t1_{max}(^{13}C)$ (set to 993 ms) was greater than 5 × $T_2(^{13}C)$ (~ 600 ms). Similarly, $t2_{max}(^{1}H)$ was set to 568 ms (> 5 x $T_2(^{1}H)$ = 180 ms). Hence 1200 complex t1 increments, each containing 8192 complex points per FID, were acquired for a total acquisition time of 3.5 h per spectrum. Data processing used double Fourier transformation using 2-fold zero filling in both the ^{13}C and ^{1}H dimensions, 7 Hz and 1 Hz exponential line broadening were used for the ^{13}C and ^{1}H dimensions respectively, followed by careful manual phase correction and automatic spline baseline correction in both dimensions. This produced data with resolutions of 0.30 and 0.88 Hz per point in the ^{1}H and ^{13}C dimensions respectively. Chemical shift referencing was achieved by setting the glycine reference peak to 3.53 ppm and 42 ppm in the ^{13}C and ^{1}H dimensions, respectively.

In a typical experiment, the six synthesized substrates **1a-f** (~0.25-0.3 mg of each) and 2–^{13}C labelled glycine (~0.03 mg) as internal standard were dissolved in H_2O (~250 μL) containing 3% D_2O. The pH of the solution was adjusted to 5.2 using sodium acetate buffer (final concentration of 100 mM). The resulting solution was transferred into the Shigemi tube (outer tube), and the insert tube was then applied cautiously in order to prevent any bubbles being formed in the solution. If bubbles were present in the solution, the insert was pushed up and down slowly for couple of times to get rid of the bubbles. The probe was tuned and the magnetic field was manually shimmed, and one ^{1}H-NMR, one ^{13}C-NMR, and one HSQC spectra were acquired prior to adding the *M. viridifaciens* sialidase (~6-10 μL, 0.02-0.05 μg/mL). After addition of the enzyme, the magnetic field was re-shimmed and probe was re-tuned, and more than thirty consecutive HETCOR spectra (135 min per spectrum) are acquired as the enzymatic reaction progresses for a period of 3-4 days.

4.4.4 Deconvolution of 2D-NMR (HETCOR and HSQC) Spectra

Initial HETCOR and HSQC experiments have been very promising because the degree of peak overlap is considerably decreased compared to standard 1D (^{13}C-NMR) spectra; however, peak fitting is more challenging for 2D-NMR spectra and optimization of a reliable deconvolution method is still in progress.

Spectra (**a**) and (**b**) in Figure 4.10 represent decoupled ^{13}C-^{1}H HETCOR and ^{1}H-^{13}C HSQC spectra; respectively, which were acquired in the middle of sialidase-catalyzed hydrolysis of labelled Neu5Acα2,6LacβSPhs (**1a-f**). As was mentioned earlier, the first products of hydrolysis are labelled α-sialic acids which then mutarotate to an equilibrium mixture that favours the β-sialic acids. It is obvious from the spectra that all peaks are well separated and resonances for the labelled $\alpha-$ and $\beta-$sialic acids (reaction products) appear in two different rows because the protons of sialic acids at C-3 are more shielded relative to those of the labelled sialosides. Moreover, interfering peaks from residual dideuterated substrates are absent (there is no attached proton that can be detected). Therefore, peak overlapping from the resonances of sialic acid and sialoside isotopologues has been minimized.

In both spectra (HETCOR and HSQC), the peaks related to labelled α-sialosides appear in the region between 39.7 to 40.6 ppm along the F2 dimension and 1.6-2.8 ppm along the F1 dimension. The peaks related to the enriched 3-^{13}C in the six isotopologues (**1a-f**) in HETCOR and HSQC spectra are shown as (**a**, Figure 4.11) and (**b**, Figure 4.11), respectively.

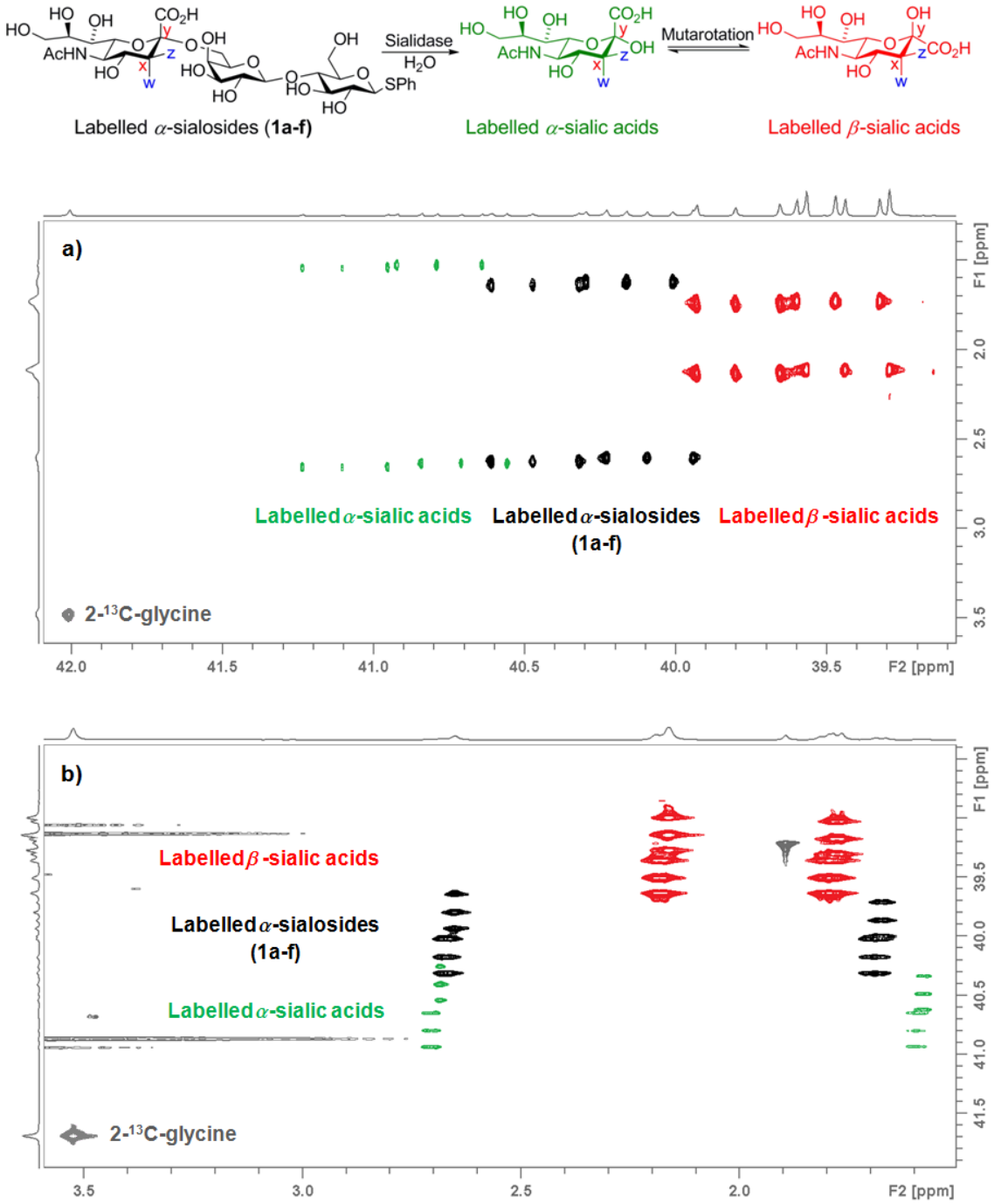

Figure 4.10. ^{1}H HETCOR (**a**) and ^{1}H-^{13}C HSQC (**b**) spectra acquired in the middle of sialidase-catalyzed hydrolysis of labelled Neu5Acα2,6LacβSPhs (**1a-f**)

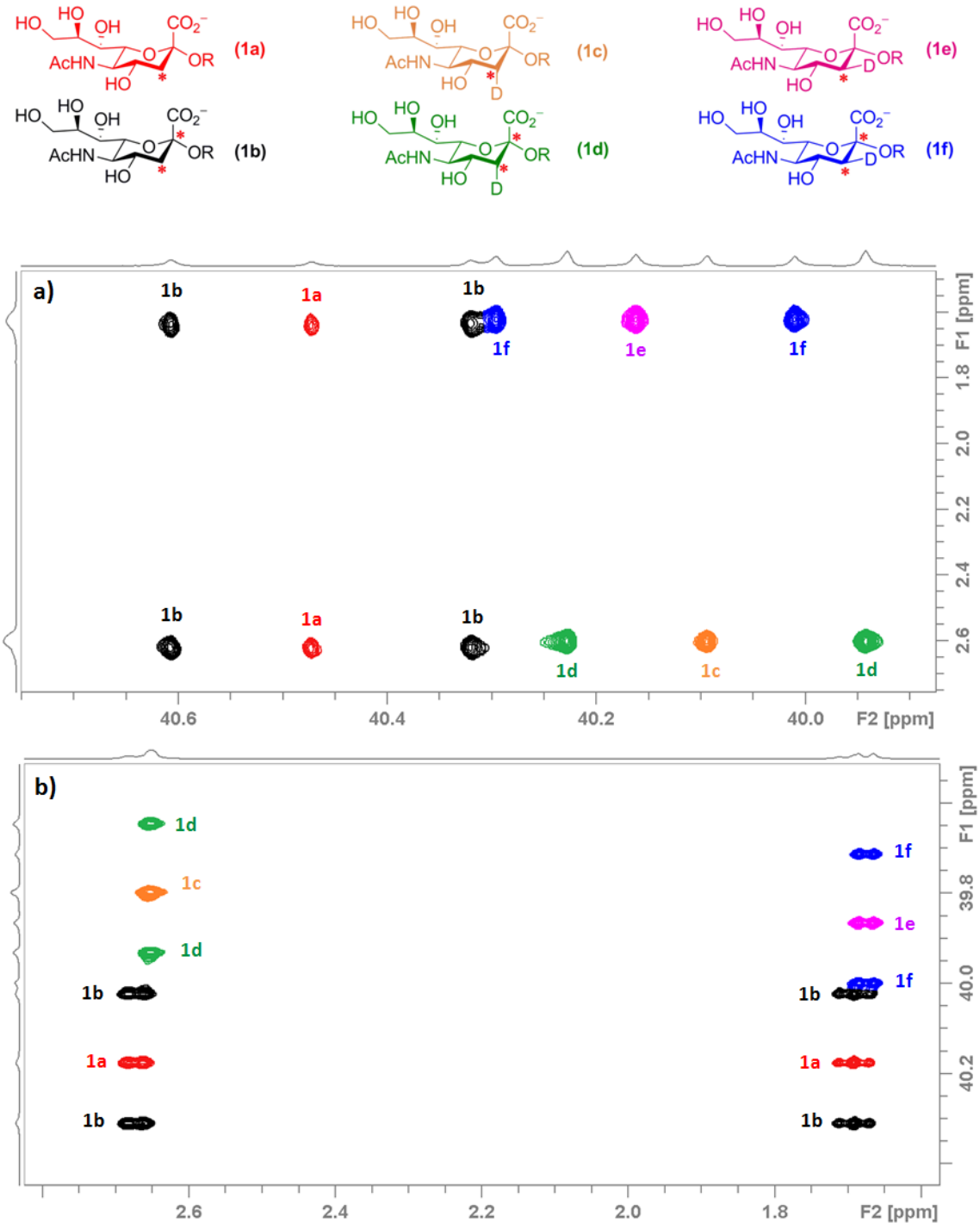

Figure 4.11. The labelled peaks corresponding to the enriched 3-^{13}C of labelled Neu5Acα2,6LacβSPhs (**1a-f**) in (**a**) ^{13}C-^{1}H HETCOR and (**b**) ^{1}H-^{13}C HSQC. The asterisk (*) stands for ^{13}C and R = Phenyl 4-O-(β-d-galactopyranosyl)-1-thio-β-D-glucopyranoside

Despite the inherent advantages mentioned above that should make measuring multiple KIE values more precise when using a mixture of isotopologues, integration of peak in the 2D NMR spectra is a challenging proposition because there are a limited number of programs that fit two dimensional peaks. Bruker's *Topspin* 3 program has a 2D-deconvolution routine; however, after numerous attempts, this option was considered to be not very useful for quantitative measurements of KIEs. An example of using 2D-deconvolution option in Bruker's *Topspin* 3 program is shown in Figure 4.12 which represents the deconvolution of one of the four peaks from isotopologue **1b** in the HETCOR spectrum (**a**, Figure 4.11). Spectrum **a** (Figure 4.12) represents the actual experimental peak, spectrum **b** is the calculated fit created by Bruker's *Topspin* 3 program for the peak in spectrum **a** and spectrum **c** is a representation of the peaks in **a** and **b** overlayed on each other.

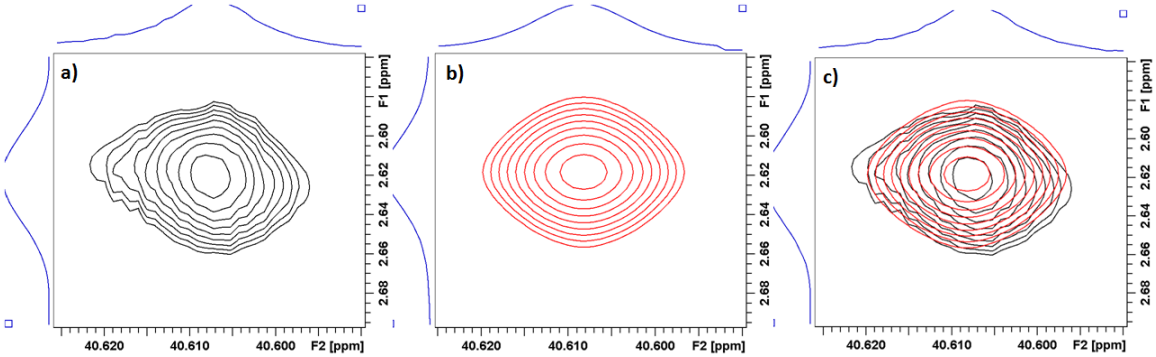

Figure 4.12. (**a**) One of the four experimental peaks related to the isotopologue **1b** (spectrum **a**, Figure 4.11); (**b**) the fit calculated for 2D-peak in spectrum **a** by 2D-deconvolution routine in Bruker's *Topspin* 3 program, (**c**) overlay of **a** and **b**

There is an obvious problem associated with this technique as the overlaid peaks (**c**, Figure 4.12) fit imperfectly. In order to use the 2D-deconvolution routine in Bruker's *Topspin* 3 program, the two dimensional peaks have to be highly symmetric, and to improve this situation, the appropriate pulse parameters are being modified for the acquisition of 2D-NMR spectra.

2D-deconvolution option in *Topspin* is problematic for the peaks in the HSQC spectra because most of the individual peaks in HSQC are split due to ^{1}H-^{1}H couplings ($J_{3eq,3ax}$ and $J_{3ax,4}$) which are not decoupled during the HSQC pulse sequence.

Another technique which is showing great promise for determining the volume of peaks in two dimensional spectra (related to a method described by Murkin et al.[11]) is outlined here. Note however that this technique needs to be improved and has not yet allowed us to measure KIE values. In this process, the spectra are first calibrated by adjusting the C2 signal of the internal standard (2-^{13}C)-glycine to be at chemical shifts of 42 ppm along the ^{13}C axis and 3.53 along the ^{1}H axis. Then, one individual set of peaks (singlet in case of HETCOR and singlet, doublet or triplet in case of HSQC) is manually picked. For example one of the peaks from α-sialoside **1b** (spectrum **b**, Figure 4.11) is selected, phased and the baseline is corrected along both F1 and F2 dimensions using Bruker's *Topspin* software to produce the symmetric peak as shown in spectrum **a** (Figure 4.13). More than twenty rows are then extracted from the selected peak along the ^{1}H-axis. This extraction can be applied to both axes (F1 or F2); however, in the HSQC spectra, the peaks are more easily phased along the ^{1}H axis, a situation which makes deconvolution easier. After extracting more than twenty 1D extracts from the 2D peak, they are summed using Bruker's *Topspin* 3 program (**b**, Figure 4.13). The summed 1D extract is then fitted using the least-square fitting script in a *Mathematica* notebook within a selected chemical shift range (1.25–2.35 ppm in this example) as shown in diagram **c** (Figure 4.13). In this diagram, an excellent fit is produced by the *Mathematica* program (red line) that is overlaid on the experimental summed 1D extract (black line), to give a smooth residual (blue line), showing the very minimal differences between the fit and the experimental summed 1D extract.

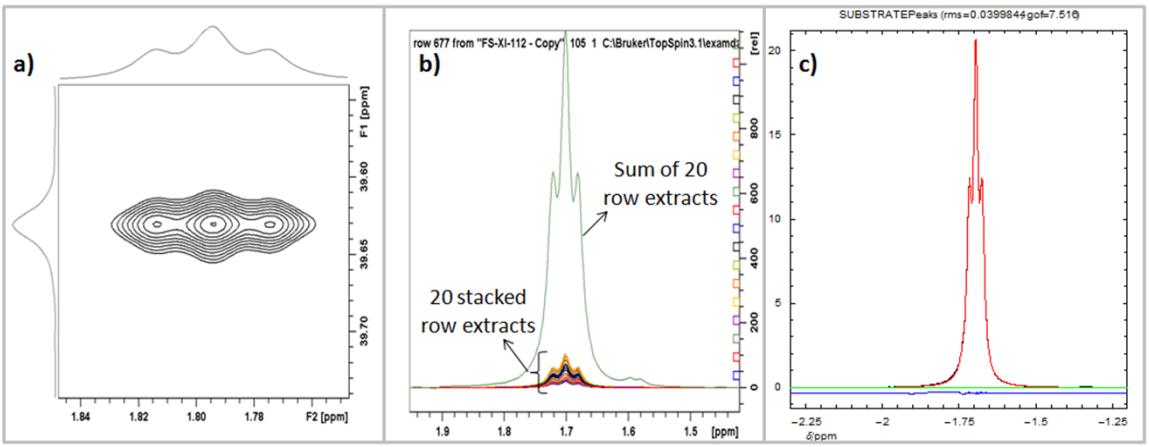

Figure 4.13. (**a**) One of the 2D peaks related to isotopologue **1b** which is picked up from the spectrum **b** (Figure 4.11); (**b**) representation of stacked rows extracted from 2D peak shown in **a** and the sum of these extracts created by Bruker's *Topspin* 3 program; (**c**) the fit for the summed 1D extract in **b** calculated by *Mathematica* program

The selected peak is similarly processed in all other spectra that were acquired at different fractions of reaction, and in each case the summed 1D extract is fit using the *Mathematica* notebook, the peak positions, peak widths at half-height and G/L mix of the peaks is fixed while leaving the heights of the peaks as the only variable. Finally, the summed 1D extract peaks in each spectrum is normalized by dividing the peak area (produced by *Mathematica*) by that obtained for the 2-^{13}C glycine peak in the same spectrum, which was obtained using the same process.

All other peaks related to the isotopologues (**1a-f**) are phased and processed separately in the similar way. In each spectrum, the fraction of reaction (F_L) is obtained for the lighter isotopomer, and R/R_0 for the corresponding fraction of reaction is calculated. This data is then analyzed using a non-linear least squares fit to Eq 4.1 in the ″Prism-4″ software.

Even though this technique is very promising, not all of the peaks could be successfully fit in *Mathematica* notebook because of aberrant phasing. This phasing

issue needs to be resolved when acquiring the 2D-NMR spectra and is currently under investigation.

4.4.5 Results

Even though, measuring KIE for all six labelled substrates simultaneously in the same NMR tube minimizes systematic errors tremendously, the large number of peaks in the spectra makes the fitting process challenging with regard to 1D-NMR (^{13}C-NMR) spectroscopy. The main problem arises from peak overlaps of starting materials. This problem is mitigated by using 2D-NMR (HETCOR and HSQC) spectroscopy as discussed earlier; however, deconvolution of the 2D-NMR spectra is still ongoing. Therefore, only the results obtained using 1D-NMR (^{13}C-NMR) spectroscopy are presented in this thesis. The conditions for acquiring quantitative ^{13}C {^{1}H,^{2}H} spectra, were optimized by running many enzymatic experiments and non enzymatic runs.

4.4.5.1 Anomeric ^{13}C KIE (^{13}(*V*/*K*))

To measure a ^{13}C-KIE on k_{cat}/K_m (^{13}(*V*/*K*)) for the anomeric carbon (C-2), the pair of substrate isotopologues needed is the singly and doubly ^{13}C-labelled Neu5Acα2,6LacβSPhs (**1a** and **1b**). The corresponding peaks related to these compounds are shown in Figure 4.14, which presents a typical ^{13}C {^{1}H,^{2}H} spectrum acquired at the beginning of *M. viridifaciens* sialidase-catalyzed hydrolysis of a mixture of **1a-f**. After running an experiment, the integrations for these peaks (as explained in section 4.4.2) were used to calculate the ratios of R/R_0 for successive spectra acquired during an experiment. The fraction of reaction for the lighter isotopologue (F_L) was also calculated for each spectrum (as explained in section 4.4.2). The data from three separate runs of the same experiment (*M. viridifaciens* sialidase-catalyzed hydrolysis of

1a-f) were analyzed by non-linear least squares fitting using a Prism-4 program. This produced the best fit lines to Eq 4.1 resulting in three plots (Figure 4.15) and three calculated ^{13}C-KIE values. The KIE on k_{cat}/K_m ($^{13}(V/K)$) for the three separate runs are 1.030 ± 0.001 (**run 1**), 1.027 ± 0.001 (**run 2**), and 1.029 ± 0.002 (**run 3**).

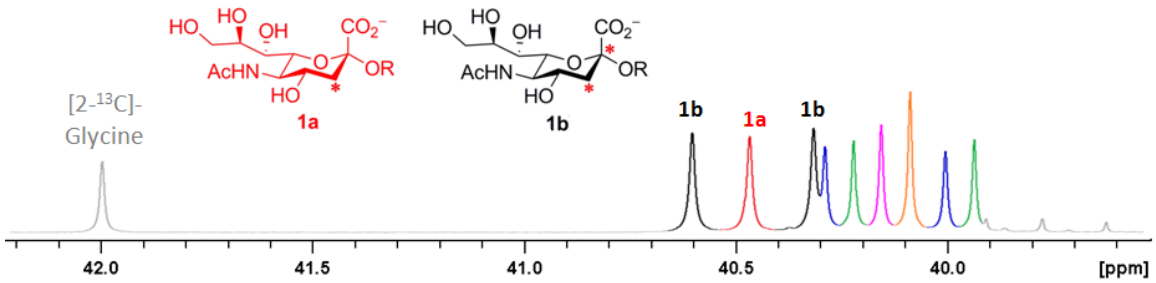

Figure 4.14. The labeled peaks corresponding to singly- (**1a**) and doubly-labelled (**1b**) Neu5Acα2,6LacβSPhs in a typical ^{13}C {^{1}H,^{2}H} spectrum acquired in the beginning of *M. viridifaciens* sialidase-catalyzed hydrolysis of **1a-f**. The asterisk (*) stands for ^{13}C and R = Phenyl 4-O-(β-D-galactopyranosyl)-1-thio-β-D-glucopyranoside.

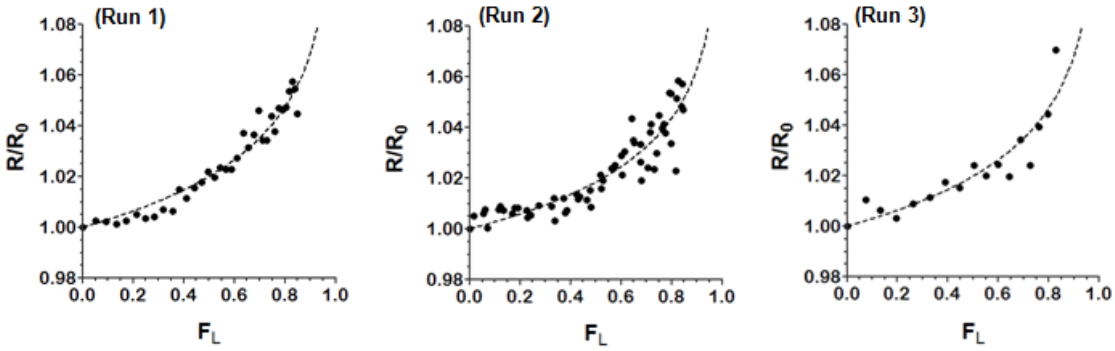

Figure 4.15. Plots obtained (using Eq 4.1 and *Prism* program) by fitting the experimental data corresponding to singly- (**1a**) and doubly-labelled (**1b**) Neu5Acα2,6LacβSPhs during *M.viridifaciens* sialidase catalyzed hydrolysis of **1a-f**. The obtained KIE values for $^{13}(V/K)$ are 1.030 ± 0.001 (**run 1**), 1.027 ± 0.001 (**run 2**), and 1.029 ± 0.002 (**run 3**).

4.4.5.2 Deuterium Effect on C-3 ($^{D}(V/K)$)

Secondary deuterium kinetic isotope effects on k_{cat}/K_m ($^{D}(V/K)$) at C-3 were also determined by analyzing the data related to the peaks corresponding to the isotopologue pairs of (**1a** and **1e**, Figure 4.16) and (**1a** and **1c**, Figure 4.18). The Prism plots of the resulting fits of the kinetic data for three separate runs for each effect ($^{3S\text{-}D}(V/K)$ and

$^{3R\text{-}D}(V/K)$) are displayed in Figure 4.17 and Figure 4.19, respectively. The deuterium KIE values for $^{3S\text{-}D}(V/K)$, are 0.987 ± 0.001 (**run 1**), 0.985 ± 0.001 (**run 2**), and 0.986 ± 0.001 (**run 3**). The deuterium KIE values for $^{3R\text{-}D}(V/K)$, are 0.988 ± 0.001 (**run 1**), 0.975 ± 0.001 (**run 2**), and 0.989 ± 0.001 (**run 3**).

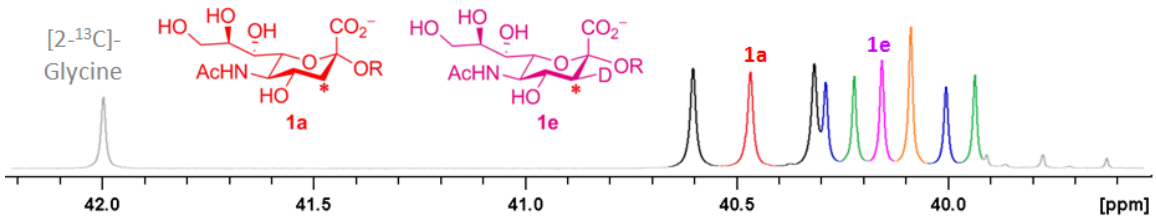

Figure 4.16. The labelled peaks corresponding to not deuterated (**1a**) and deuterated (**1e**) ^{13}C-labelled Neu5Acα2,6LacβSPhs in a typical ^{13}C {^{1}H,^{2}H} spectrum acquired in the beginning of *M. viridifaciens* sialidase-catalyzed hydrolysis of **1a-f**. The asterisk (*) stands for ^{13}C and R = Phenyl 4-O-(β-D-galactopyranosyl)-1-thio-β-D-glucopyranoside.

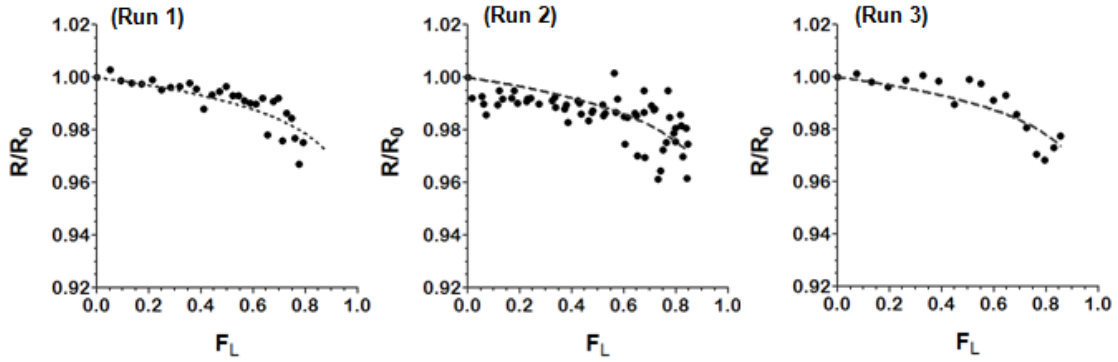

Figure 4.17. Plots obtained (using Eq 4.1 and *Prism* program) by fitting the experimental data corresponding to non-deuterated (**1a**) and deuterated (**1e**) ^{13}C-labelled Neu5Acα2,6LacβSPhs during *M. viridifaciens* sialidase catalyzed hydrolysis of **1a-f**. The obtained KIE values for $^{3S\text{-}D}(V/K)$ are 0.987 ± 0.001 (**run 1**), 0.985 ± 0.001 (**run 2**), and 0.986 ± 0.001 (**run 3**).

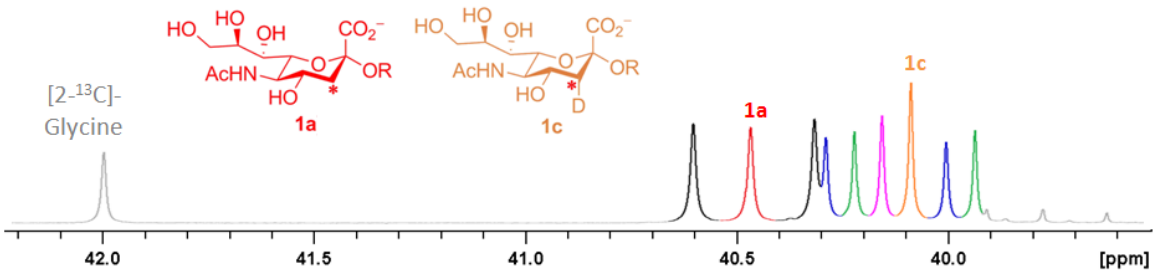

Figure 4.18. The labelled peaks corresponding to not deuterated (**1a**) and deuterated (**1c**) ^{13}C-labelled Neu5Acα2,6LacβSPhs in a typical ^{13}C {^{1}H,^{2}H} spectrum acquired in the beginning of *M. viridifaciens* sialidase-catalyzed hydrolysis of **1a-f**. The asterisk (*) stands for ^{13}C and R = Phenyl 4-O-(β-D-galactopyranosyl)-1-thio-β-D-glucopyranoside.

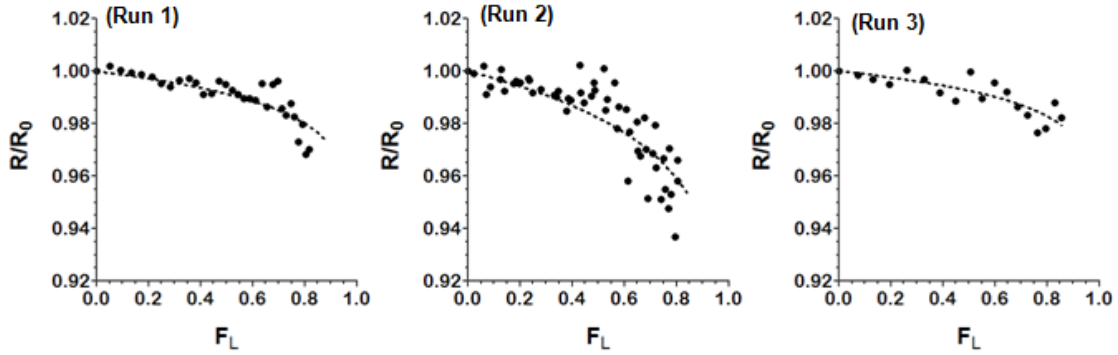

Figure 4.19. Plots obtained (using Eq 4.1 and *Prism* program) by fitting the experimental data corresponding to non-deuterated (**1a**) and deuterated (**1c**) ^{13}C-labelled Neu5Acα2,6LacβSPhs during *M. viridifaciens* sialidase catalyzed hydrolysis of **1a-f**. The obtained KIE values for $^{3R\text{-}D}$(V/*K*) are 0.988 ± 0.001 (**run 1**), 0.975 ± 0.001 (**run 2**), and 0.989 ± 0.001 (**run 3**).

4.4.5.3 Anomeric ^{13}C KIE on Deuterated Materials (^{13}(*V*/K)$_{3S\text{-}D}$ & ^{13}(*V*/K)$_{3R\text{-}D}$)

To determine if the ^{13}C isotope effect (2-^{13}C) is sensitive to deuterium substitution (3-D), the substrate pairs (**1e** and **1f**) and (**1c** and **1d**) (the corresponding peaks for these compounds in the ^{13}C-NMR spectra are shown in Figure 4.20 and Figure 4.22) were analyzed in the same manner (section 4.4.2), and the best fit lines to Eq 4.1 were produced for each pair as shown in Figures 4.21 and 4.23. The measured ^{13}C-KIE values on k_{cat}/K_m when a deuterium is incorporated in the equatorial position of C-3 (^{13}(*V*/*K*)$_{3S\text{-}D}$) for three separate runs are 1.003 ± 0.001 (**run 1**), 1.000 ± 0.001 (**run 2**), and 0.997 ± 0.002 (**run 3**). The ^{13}C-KIE values on k_{cat}/K_m for an axially deuterated

substrate ($^{13}(V/K)_{3R\text{-}D}$) are 1.028 ± 0.001 (**run 1**), 1.033 ± 0.001 (**run 2**), and 1.025 ± 0.002 (**run 3**).

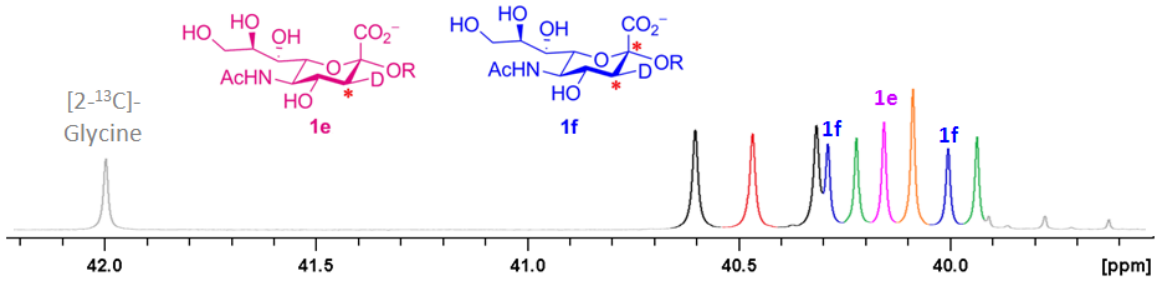

Figure 4.20. The arrows show the peaks corresponding to deuterated, singly ^{13}C-labelled (**1e**) and deuterated doubly ^{13}C-labelled (**1f**) Neu5Acα2,6LacβSPhs in a typical ^{13}C {^{1}H,^{2}H} spectrum acquired in the beginning of *M. viridifaciens* sialidase-catalyzed hydrolysis of **1a-f**. The asterisk (*) stands for ^{13}C and R = Phenyl 4-O-(β-D-galactopyranosyl)-1-thio-β-D-glucopyranoside

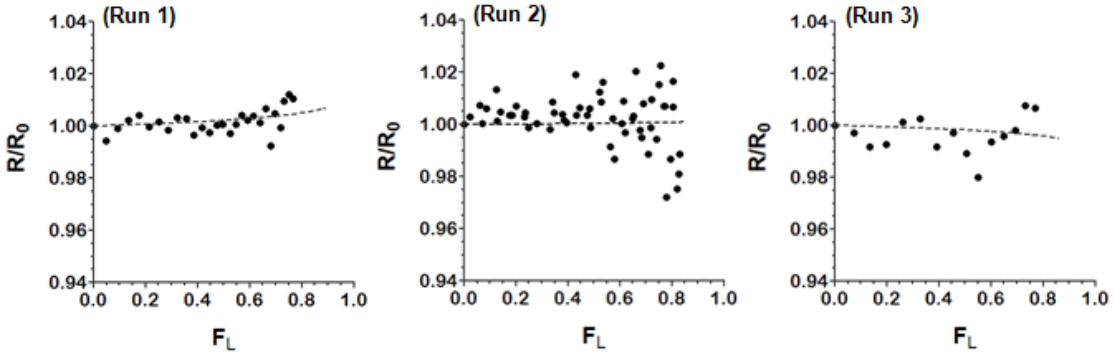

Figure 4.21. Plots obtained (using Eq 4.1 and *Prism* program) by fitting the experimental data corresponding to deuterated, singly ^{13}C-labelled (**1e**) and deuterated doubly ^{13}C-labelled (**1f**) Neu5Acα2,6LacβSPhs during *M. viridifaciens* sialidase catalyzed hydrolysis of **1a-f**. The obtained KIE values on $^{13}(V/K)_{3S\text{-}D}$ are 1.003 ± 0.001 (**run 1**), 1.000 ± 0.001 (**run 2**), and 0.997 ± 0.002 (**run 3**).

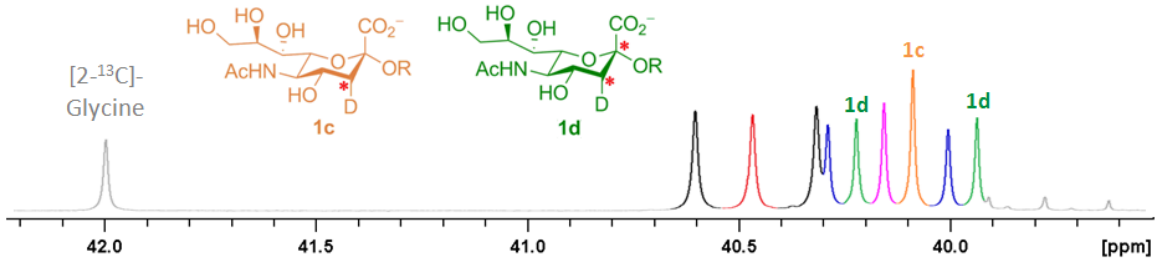

Figure 4.22. The labelled peaks corresponding to deuterated, singly ^{13}C-labelled (**1c**) and deuterated doubly ^{13}C-labelled (**1d**) Neu5Acα2,6LacβSPhs in a typical ^{13}C {^{1}H,^{2}H}. The prior spectrum acquired in the beginning of *M. viridifaciens* sialidase-catalyzed hydrolysis of **1a-f**. The asterisk (*) stands for ^{13}C and R = Phenyl 4-O-(β-D-galactopyranosyl)-1-thio-β-D-glucopyranoside.

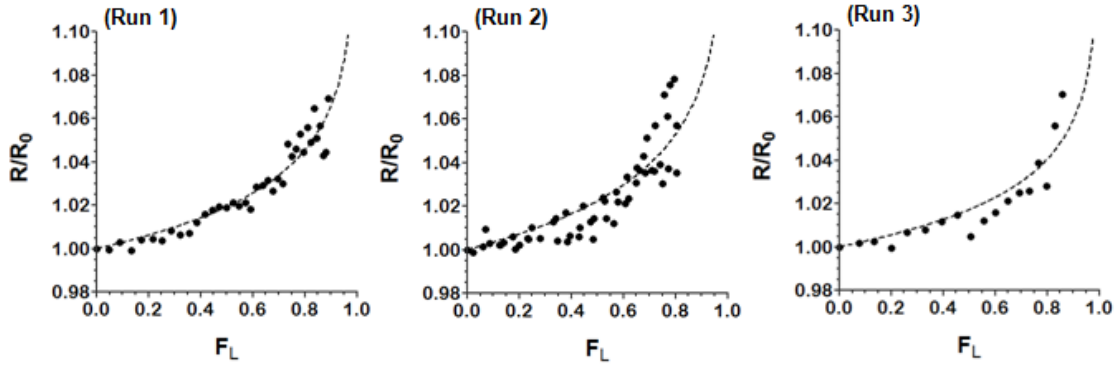

Figure 4.23. Plots obtained (using Eq 4.1 and *Prism* program) by fitting the experimental data corresponding to deuterated, singly ^{13}C-labelled (**1c**) and deuterated doubly ^{13}C-labelled (**1d**) Neu5Acα2,6LacβSPhs during *M. viridifaciens* sialidase catalyzed hydrolysis of **1a-f**. The obtained KIE values on $^{13}(V/K)_{3R\text{-}D}$ are 1.028 ± 0.001 (**run 1**), 1.033 ± 0.001 (**run 2**), and 1.025 ± 0.002 (**run 3**).

4.5 Discussion

Recently Murkin et al.[11] reported the measurement of KIEs using 2D-NMR spectroscopy. They utilized a series of ^{1}H-^{13}C HSQC spectra to measure a single KIE value. The goal of this research is to use 2D-NMR spectroscopy to measure multiple KIEs simultaneously. Measured KIE values for the *M. viridifaciens* sialidase-catalyzed hydrolysis will eventually help us to characterize the transition state structure(s). However, before discussing this issue, an understanding of competitive KIE measurements and the relationship between intrinsic and apparent KIEs in enzyme-

catalyzed reactions is necessary.

4.5.1 Kinetics of Competitive Measurement of Isotope Effects on Enzyme-Catalyzed Reactions

In enzyme-catalyzed reactions, any KIE values that is determined by using a competitive method (both isotopologues are present in the same solution) only reports on *V*/*K* (k_{cat}/K_m) irrespective of the isotopologue concentrations. In contrast, non-competitive measurements can provide KIE values for *V* (k_{cat}), K_m and *V*/*K* (k_{cat}/K_m). To illustrate this point, the simplest enzyme mechanism suitable for one isotopologue is shown in Scheme 4.4:

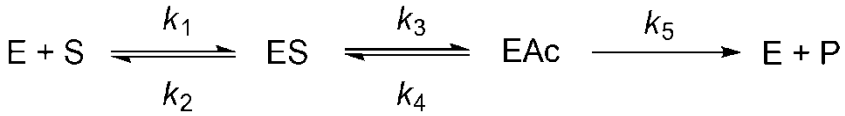

Scheme 4.4. Simplified kinetic scheme for one isotopologue (S) involved in a competitive reaction.

In this scheme, ES is the Michaelis-Menten complex, and EAc represents either a second Michaelis-Menten complex or a reaction intermediate, and k_5 represents the step in which the isotope sensitive chemical reaction of S occurs; therefore, the rate of the reaction can be shown as Eq 4.2:

$$\nu = k_5[\mathrm{EAc}] \quad \text{(Eq 4.2)}$$

By applying the steady-state condition to [EAc], it can be shown that:

$$\frac{d[\mathrm{EAc}]}{dt} = 0 = k_3[\mathrm{ES}] - k_4[\mathrm{EAc}] - k_5[\mathrm{EAc}]$$

$$[\mathrm{EAc}] = \frac{k_3[\mathrm{ES}]}{(k_4 + k_5)} \quad \text{(Eq 4.3)}$$

Since the concentration of each enzyme species can be expressed in terms of free enzyme $([E]_T = [E] + [ES] + [EAc])$, Eq 4.2 can be rewritten as Eq 4.4:

$$\frac{\nu}{[E]_T} = \frac{\frac{k_3 k_5}{(k_4 + k_5)}[ES]}{[E] + [ES]\left(\frac{k_3 + k_4 + k_5}{(k_4 + k_5)}\right)} \quad \text{(Eq 4.4)}$$

Similarly, the steady-state condition is applied to ES to afford the expression shown in Eq 4.5:

$$\frac{d[ES]}{dt} = 0 = k_4[EAc] + k_1[E][S] - k_3[ES] - k_2[ES]$$

$$\text{therefore,} \quad [ES] = \frac{k_1(k_4 + k_5)[E][S]}{(k_2 k_5 + k_3 k_5 + k_2 k_4)} \quad \text{(Eq 4.5)}$$

Now, combining equations 4.4 and 4.5 results in Eq 4.6 (**a**):

$$\text{a)}\ \frac{\nu}{[E]_T} = \frac{\frac{k_3 k_5}{(k_3 + k_4 + k_5)}[S]}{\frac{k_2 k_5 + k_3 k_5 + k_2 k_4}{k_1 k_4 + k_1 k_3 + k_1 k_5} + [S]} \quad \text{(Eq 4.6)}$$

where,

$$\text{b)}\ k_{cat} = \frac{k_3 k_5}{(k_3 + k_4 + k_5)}, \quad \text{c)}\ K_m = \frac{k_2 k_5 + k_3 k_5 + k_2 k_4}{k_1 k_4 + k_1 k_3 + k_1 k_5},$$

$$\text{d)}\ \frac{k_{cat}}{K_m} = \frac{k_1 k_3 k_5}{k_2 k_5 + k_3 k_5 + k_2 k_4}$$

Identical equations can be derived for the other isotopologue (S') whose kinetic scheme is shown as below:

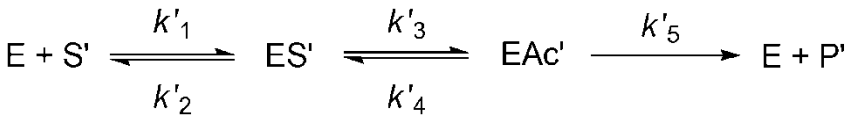

Scheme 4.5. Simplified kinetic scheme for the second isotopologue (S') in the same solution as the first isotopologue (S, Scheme 4.4)

In a competitive method, the light and heavy isotopologues (S'and S) are present in the same mixture; therefore, when S occupies the active site of enzyme, it becomes unavailable to S', and vice-versa. Hence, S and S' behave such that they are competitive inhibitors toward each other. Therefore, the total enzyme concentration is expressed as Eq 4.7:

$$[E]_T = [E] + [ES] + [EAc] + [ES'] + [EAc'] \quad \text{(Eq 4.7)}$$

Since we are interested in ratio of reaction rates ($\nu_S/\nu_{S'}$), and considering Eqs 4.3, 4.5, and 4.7, it can be shown that:

$$\frac{\nu_S}{\nu_{S'}} = \frac{k_5[EAc]}{k_5'[EAc']} = \frac{\frac{k_3 k_5[ES]}{(k_4 + k_5)}}{\frac{k_3' k_5'[ES']}{(k_4' + k_5')}} = \frac{\frac{k_1 k_3 k_5}{(k_2 k_5 + k_3 k_5 + k_2 k_4)}[S]}{\frac{k_1' k_3' k_5'}{k_2' k_5' + k_3' k_5' + k_2' k_4'}[S']} \quad \text{(Eq 4.8)}$$

Based on the expression for k_{cat}/K_m that is shown in Eq 4.6, the equation 4.8 can be simplified to give Eq 4.9:

$$\frac{\nu_S}{\nu_S'} = \frac{\frac{k_{cat}}{K_m}[S]}{\frac{k_{cat}'}{K_m'}[S']} \quad \text{(Eq 4.9)}$$

Thus when competitive intermolecular methods are used to determine kinetic isotope effect, the result is a ratio of second-order rate constants. Therefore, if $k = \nu_S / [S]$ and $k' = \nu_S' / [S']$, then

$$\frac{k}{k'} = \frac{\frac{k_{cat}}{K_m}}{\frac{k_{cat}'}{K_m'}} = \frac{\frac{V}{K}}{\frac{V'}{K'}} \quad \text{(Eq 4.10)}$$

In conclusion, the KIE (i.e. *k/k'*) in an enzyme-catalyzed reaction containing two isotopologues is determined by *V*/*K* (k_{cat}/K_m), regardless of the starting substrate concentrations.

4.5.2 The Apparent and Intrinsic Isotope Effects in Enzyme-Catalyzed Reactions

When measuring kinetic isotope effects, there is a profound distinction between non-enzymatic and enzymatic reactions. That is, in most non-enzymatic reactions, a chemical (isotope sensitive) step is usually rate-limiting, and the KIE is directly interpreted in terms of the bonds being made and broken at the transition state. However, in an enzyme-catalyzed reaction, the observed KIE is often not solely associated with the chemical step in which isotopic substitutions participate. In fact, the magnitude of an observed kinetic isotope effect is often lower than the intrinsic isotope effect (isotope effect on the bond-breaking/making step) as an enzymatic reaction involves multistep processes. These steps usually are physical steps, substrate binding and product release, which can have transition state free energies that are similar to those for the isotope-sensitive step. Even though correlating KIEs to transition state structure is more difficult (sometimes it is even precluded) with a less than full

expression of an intrinsic KIE; it can provide useful information about the relative rates and sequences of different steps in the mechanism.[12]

The degree of attenuation in the observed KIE can be quantified by commitment factors, which were first introduced by Northrop.[13] The concept of commitment to catalysis as well as the relationship between intrinsic isotope effect and apparent isotope effect in their simplest form, can be understood by considering a minimal enzymatic mechanism illustrated in Scheme 4.6.

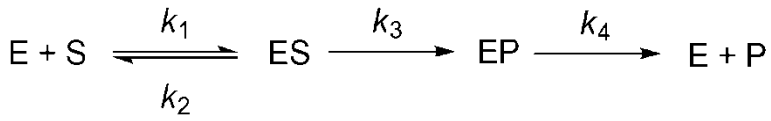

Scheme 4.6. A simple form of enzyme kinetic scheme

This simple enzymatic mechanism presents three fundamental steps: 1) substrate binding step governed by k_1 and k_2, 2) the catalytic step (which is considered to be irreversible) governed by k_3, and 3) the product release step (which is also considered to be irreversible) governed by k_4. Since the focus of the current work is on the measurement of KIE through competitive method, the kinetic parameter of interest is *V*/*K* (k_{cat}/K_m) which as discussed earlier is an apparent first-order rate constant encompassing steps "up to and including the first irreversible step". *V*/*K* related to scheme 4.6 is expressed as shown in Eq 4.11.[14]

$$\frac{V}{K} = \frac{k_1 k_3 E_t}{k_2 + k_3} \qquad \text{(Eq 4.11)}$$

As discussed earlier, the measurement of KIE by competitive methods involves a comparison of the rate constants (*V*/*K*s) for two isotopologues. Therefore, assuming a primary deuterium kinetic isotope effect, $^{D}(V/K)$ can be expressed as Eq 4.12 which is

obtained by dividing Eq 4.11 (representing a reaction with a substrate containing protium) by an analogues equation representing a reaction with a substrate containing deuterium.[14]

$$\frac{(V/K)_H}{(V/K)_D} = \frac{k_{3H}/k_{3D} + k_{3H}/k_2}{1 + k_{3H}/k_2} \quad \text{(Eq 4.12)}$$

This equation shows the relationship between apparent isotope effect $^{D}(V/K)$ shown in the left hand side of the equation and the intrinsic isotope effect (k_{3H}/k_{3D} *or* ^{D}k) shown as the first term of the numerator on the right hand side of the equation. It can be seen from Eq 4.12 that the magnitude of apparent isotope effect relative to intrinsic isotope effect is inversely dependent upon the ratio k_{3H}/k_2 (rate of catalysis to rate of substrate release).

Eq 4.12 can be rewritten in the general form as shown in Eq 4.13:[14]

$$^{D}(V/K) = \frac{^{D}k + C}{1 + C} \quad \text{(Eq 4.13)}$$

The new term *C* stands for ″commitment to catalysis″ which is the ratio of the rate of the catalytic step to the rate of the reverse step during which substrate is released (k_{3H}/k_2). The commitment to catalysis is defined as the tendency of the substrate-enzyme complex (ES) to proceed forward toward the product (through catalysis) versus its tendency to go backward through the reverse reaction resulting in the breakdown of ES to free substrate. This definition of commitment to catalysis is applicable to kinetic scheme 4.6 and for more complex kinetic mechanisms where there are more equilibrium steps during the reaction and the catalytic step is reversible, the *C* term will consist of two parts: *Cf* (the forward commitment to catalysis) which is an indication of partitioning

of reactant toward the product and C_r (the reverse commitment to catalysis) which is an indication of partitioning of product toward substrate.[14]

An example of such a complex mechanism is the sialidase-catalyzed hydrolysis of sialosides, the focus of the current study. As discussed earlier, in the current study, multiple kinetic isotope effects are measured for *M. viridifaciens* sialidase-catalyzed hydrolysis of a series of synthesized ^{13}C- and ^{2}H-labelled substrates (**1a-f**, Figure 4.3). As it was shown in Chapter 1 (Scheme 1.9), the proposed mechanism for this retaining sialidase goes through many steps. The kinetic scheme of this enzymatic reaction is shown in Scheme 4.7:

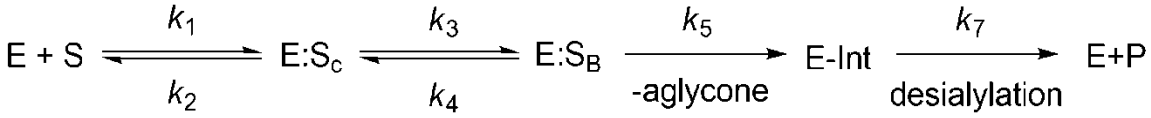

Scheme 4.7. Proposed reaction scheme for sialidase. $E:S_C$ refers to Michaelis complex in which the substrate has chair conformation whereas $E:S_B$ that presents a boat-shape conformation of substrate. E-Int is enzyme-bound intermediate whose formation is considered as the first irreversible step during the reaction. k_5 and k_7 represent the rate constants for the glycosylation (sialylation) and deglycosylation (desialylation) steps, respectively.

Step 1 represents substrate binding; step 2 involves a conformational change of the substrate from a chair to an enzyme-bound boat (or skew-boat) conformation; step 3 (the first irreversible step in sialidase-catalyzed hydrolysis) is cleavage of the glycosidic bond that occurs prior to (S_N1) or concurrent with (S_N2) formation of a sialylated enzyme intermediate; Step 4 is the desialylation step during which the glycosyl-enzyme bound intermediate (E-Int) is attacked by a water molecule to release sialic acid as the product. In this mechanism, the slow step in several cases, including the enzyme from *M. viridifaciens*[7], involves the transformation of the Michaelis complex ($E:S_B$) to the glycosyl-enzyme bound intermediate (E-Int). So, in competitive kinetic isotope effect studies on the *M. viridifaciens* sialidase-catalyzed hydrolysis, the steps from $E:S_B$ to E-

Int (the isotopically sensitive catalytic step) yields the intrinsic isotope effect (k_5) while the apparent kinetic isotope effect (*V*/*K*) includes every step between substrate binding and the first irreversible step in the reaction (k_1, k_2 and k_3, k_4, k_5) as summarized in Scheme 4.8.

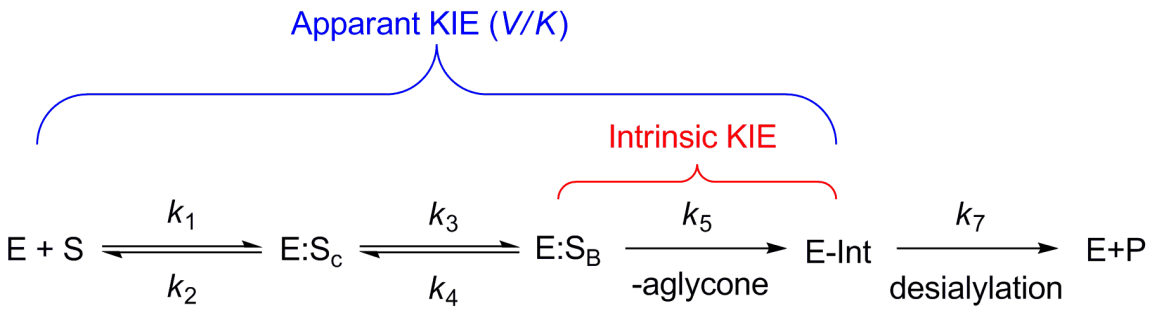

Scheme 4.8. Representation of apparent and intrinsic KIEs in a sialidase-catalyzed hydrolysis of sialosides described in Scheme 4.7.

As shown in Chapter 1 (Section 1.5.1), the *V*/*K* (k_{cat}/K_m) for this scheme takes the following form (Eq 1.14):

$$\frac{k_{cat}}{K_m} = \frac{k_1 k_3 k_5}{k_2 k_4 + k_2 k_5 + k_3 k_5} \quad \text{(Eq 4.14)}$$

In the catalytic step (k_5), the glycosidic bond between the anomeric carbon (C-2) of the sialoside and the aglycone undergoes cleavage; therefore, the primary isotope effect for this reaction is the ^{13}C kinetic isotope effect on C-2 of the sialosides (anomeric effect). Hence, the apparent *V*/*K* isotope effect with respect to substrates (**1a**, ^{13}C-2) and (**1b**, ^{12}C-2) will take the following form (Eq 4.15):

$$^{13}\left(\frac{V}{K}\right) = \frac{\dfrac{k_1 k_{3(^{12}C)} k_{5(^{12}C)}}{k_2 k_{4(^{12}C)} + k_2 k_{5(^{12}C)} + k_{3(^{12}C)} k_{5(^{12}C)}}}{\dfrac{k_1 k_{3(^{13}C)} k_{5(^{13}C)}}{k_2 k_{4(^{13}C)} + k_2 k_{5(^{13}C)} + k_{3(^{13}C)} k_{5(^{13}C)}}} \quad \text{(Eq 4.15)}$$

The Eq 4.15 can be rearranged to Eq 4.16:

$$^{13}\left(\frac{V}{K}\right)=\frac{\frac{k_{3(^{12}C)}k_{5(^{12}C)}}{k_{3(^{13}C)}k_{5(^{13}C)}}\times\frac{k_{4(^{13}C)}}{k_{4(^{12}C)}}}{1+\frac{k_{5(^{12}C)}}{k_{4(^{12}C)}}+\frac{k_{3(^{12}C)}k_{5(^{12}C)}}{k_2k_{4(^{12}C)}}}+\frac{\frac{k_{3(^{12}C)}}{k_{3(^{13}C)}}}{1+\frac{k_{4(^{12}C)}}{k_{5(^{12}C)}}+\frac{k_{3(^{12}C)}}{k_2}}+\frac{1}{1+\frac{k_2k_{4(^{12}C)}}{k_{3(^{12}C)}k_{5(^{12}C)}}+\frac{k_2}{k_{3(^{12}C)}}} \quad \text{(Eq 4.16)}$$

In this equation, the intrinsic isotope effect for step 3 involved in chemical reaction (k_5), the intrinsic isotope effect for conformational change from E:S_C to E:S_B (k_3), and the intrinsic isotope effect for conformational change from E:S_B to E:S_C (k_4) can be identified as **a**, **b**, and **c** (Eq 1.17); respectively.

$$\text{a) } ^{13}k_5=\frac{k_{5(^{12}C)}}{k_{5(^{13}C)}} \qquad \text{b)} ^{13}k_3=\frac{k_{3(^{12}C)}}{k_{3(^{13}C)}} \qquad \text{c) } ^{13}k_4=\frac{k_{4(^{12}C)}}{k_{4(^{13}C)}} \quad \text{(Eq 4.17)}$$

Therefore, the Eq 4.16 can be simplified and rearranged as Eq 4.18:

$$^{13}\left(\frac{V}{K}\right)=\frac{1}{1+\frac{k_2k_{4(^{12}C)}}{k_{3(^{12}C)}k_{5(^{12}C)}}+\frac{k_2}{k_{3(^{12}C)}}}+\frac{^{13}k_3}{1+\frac{k_{4(^{12}C)}}{k_{5(^{12}C)}}+\frac{k_{3(^{12}C)}}{k_2}}+\frac{\frac{^{13}k_3\,^{13}k_5}{^{13}k_4}}{1+\frac{k_{5(^{12}C)}}{k_{4(^{12}C)}}+\frac{k_{3(^{12}C)}k_{5(^{12}C)}}{k_2k_{4(^{12}C)}}} \quad \text{(Eq 4.18)}$$

The corresponding forward and reverse commitment factors in each term of the Eq 4.18 can be identified as follows:

$$\text{a)}\,C_{r1}=\frac{k_2}{k_{3(^{12}C)}}\left(1+\frac{k_{4(^{12}C)}}{k_{5(^{12}C)}}\right), \quad \text{b)}\,C_{f2}=\frac{k_{3(^{12}C)}}{k_2}, \quad \text{c)}\,C_{r2}=\frac{k_{4(^{12}C)}}{k_{5(^{12}C)}}$$

(Eq 4.19)

$$\text{d)}\,C_{f3}=\frac{k_{5(^{12}C)}}{k_{4(^{12}C)}}\left(1+\frac{k_{3(^{12}C)}}{k_2}\right), \quad \text{e) } ^{13}K_{E+S\rightarrow ESB}=\frac{^{13}k_3}{^{13}k_4}$$

Finally, replacing the C_r and C_f with the corresponding expressions results in the Eq 20:

$$^{13}\left(\frac{V}{K}\right)=\frac{1}{1+C_{r1}}+\frac{^{13}k_3}{1+C_{f2}+C_{r2}}+\frac{^{13}k_5\,^{13}K_{E+S\rightarrow ES_B}}{1+C_{f3}} \quad \text{(Eq 4.20)}$$

We can assume that for carbon-13 substitution there are no isotope effects on conformational changes; that is, $^{13}k_3$ = 1 and $^{13}K_{E+S\rightarrow E:SB}$ = 1; therefore, Eq 4.20 is simplified to Eq 4.21:

$$^{13}\left(\frac{V}{K}\right)=\frac{1}{1+C_{r1}}+\frac{1}{1+C_{f2}+C_{r2}}+\frac{^{13}k_5}{1+C_{f3}} \quad \text{(Eq 4.21)}$$

The same derivation can be applied for deuterium isotope effects on V/K (Eq 22); however, $^{D}k_3$ and $^{D}k_{E+S\rightarrow E:SB}$ do not necessarily equal 1 for secondary deuterium effects on *V/K* as the importance of binding isotope effects is becoming clear[15].

$$^{D}\left(\frac{V}{K}\right)=\frac{1}{1+C_{r1}}+\frac{^{D}k_3}{1+C_{f2}+C_{r2}}+\frac{^{D}k_5\,^{D}K_{E+S\rightarrow ES_B}}{1+C_{f3}} \quad \text{(Eq 4.22)}$$

In multistep enzymatic mechanisms containing ^{13}C-sensitive and deuterium-sensitive steps, it is possible to determine if these steps occur concurrently or one of them comes before the other one. In a detailed study by Cleland et al[16] on malic enzyme and glucose-6-phosphate dehydrogenase, $^{13}(V/K)$ and $^{D}(V/K)$ effects were measured. Then, by incorporation of a deuterium into the ^{13}C substrate, these authors measured the ^{13}C-isotope effect on the deuterated substrate $^{13}(V/K)_D$. The magnitude of the ^{13}C isotope effect should increase with deuterated substrates ($^{13}(V/K)_D > {}^{13}(V/K)$) if the ^{13}C- and D- sensitive steps are same. However, if the magnitude of $^{13}(V/K)_D$ is lower than

$^{13}(V/K)$, this is an indication that the two steps are different.

4.5.3 Preliminarily Interpretation of Measured KIEs

The measured KIEs on k_{cat}/K_m (V/K) for *M. viridifaciens* sialidase-catalyzed hydrolysis of natural substrate analogues (**1a-f**, Figure 4.3), which were measured by deconvolution of 1D ^{13}C NMR spectra, are tabulated in Table 4.1. The corresponding KIEs on k_{cat} (V) measured by Chan et al.[7] for the *M. viridifaciens* sialidase are also displayed in Table 4.1.

Table 4.1. Kinetic isotope effects on k_{cat}/K_m (V/K) and k_{cat} (V) for the *M. viridifaciens* sialidase-catalyzed hydrolysis of natural substrate analogues.

KIE	V/K[a]	V[b]
Anomeric (2-^{13}C)	1.029 ± 0.001	1.021 ± 0.006
Equatorial (3S)-^{2}H	0.986 ± 0.001	0.891 ± 0.008
Axial (3R)-^{2}H	0.984 ± 0.001	1.029 ± 0.007
Anomeric (2-^{13}C) on deuterated substrates-(3S)-^{2}H	1.000 ± 0.001	–
Anomeric (2-^{13}C) on deuterated substrates -(3R)-^{2}H	1.029 ± 0.001	–

[a]Reported values represent weighted averages (n = 3). [b]KIE values taken from ref 7.

Based on the large KIE value measured for the anomeric centre ($^{13}(V/K)$ = 1.029, Table 4.1), a value that is likely close to the intrinsic effect for the formation of an oxacarbenium ion-like TS during glycolysis[1], the first two terms in Eq 4.21 are likely negligible. Hence, we can approximate Eq 4.21 by shortening it to give Eq 4.23.

$$^{13}\left(\frac{V}{K}\right) \approx {}^{13}k_5 \quad \text{(Eq 4.23)}$$

In addition, as the commitment factors in Eqs 4.20 and 4.22 are the same, then

Eq 4.22 can be simplified to Eq 4.24 from which we can estimate values of equilibrium binding isotope effects (BIEs) during the *M. viridifaciens* sialidase-catalyzed hydrolyses.

$$^{D}\left(\frac{V}{K}\right) \approx {}^{D}k_5\,{}^{D}K_{E+S\rightarrow ES_B} \quad \text{(Eq 4.24)}$$

With regard to deuterium effect, values of βSDKIE lower than 1.0 were observed, indicating there is inverse β-secondary deuterium isotope effects for the C-3 equatorial position ($^{D}V_S$ = 0.891 and $^{D}(V/K)_S$ = 0.986, Table 4.1). However, the observed βSDKIE values for axial H/D (Table 4.1) show opposite effects for V (normal KIE) and V/K (inverse KIE). The inverse βSDKIE measured on V/K for axial H/D ($^{D}(V/K)_{3\text{-}R}$ = 0.984) indicates that there must be an equilibrium binding isotope effect (BIE); that is BIEs are not a component of the measured KIEs on k_{cat} (V) because k_{cat} only includes the steps from E:S_B (the accumulating Michaelis complex)[7] to free product (Scheme 4.9).

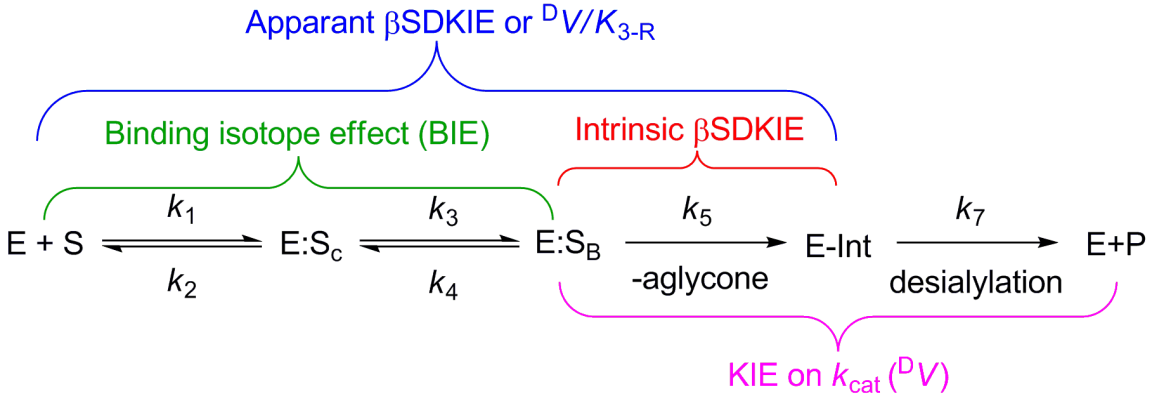

Scheme 4.9. The relationship between equilibrium binding isotope effect (BIE), the intrinsic β-secondary deuterium isotope effect (βSDKIE), and apparent βSDKIE measured by competition between isotopologues in the sialidase-catalyzed hydrolysis of natural substrate analogues. Also shown is the kinetically significant terms for isotope effects on k_{cat} (^{D}V).

As shown in Figure 4.24, if we assume that the transition state structures for glycosylation (k_5) and deglycosylation (k_7) steps are similar, then we can also estimate

that the zero point energy differences from E:S_B to both TSs will be similar. Thus, the intrinsic KIE for *V/K* should be similar to the KIE on *V*; that is, we can assume that $^{D}k_5 \approx {}^{D}V$.

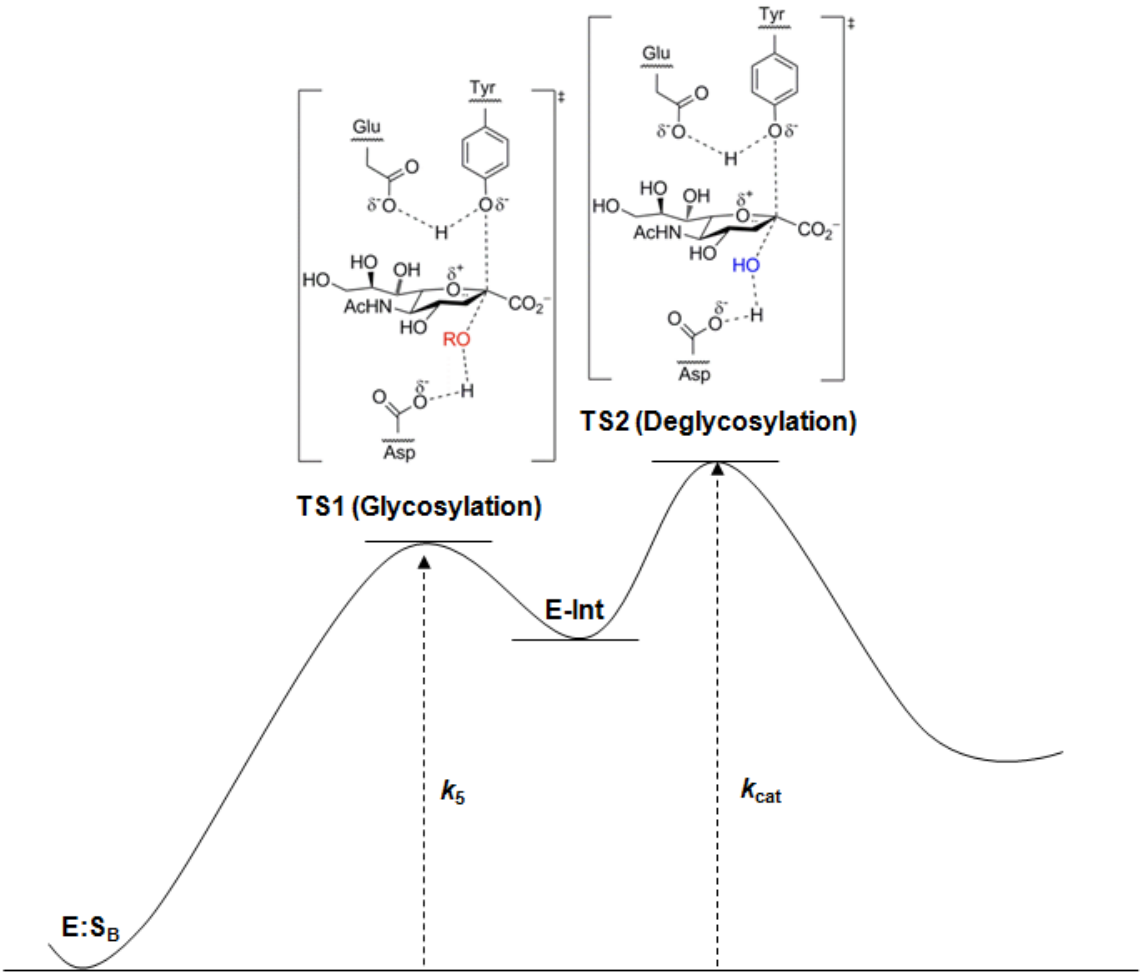

Figure 4.24. Free energy diagram related to the sialidase-catalyzed reaction shown in Scheme 4.9, highlighting the two transition state structures (**TS1** and **TS2**) of the glycosylation (k_5) and deglycosylation (k_7) steps.

Therefore, binding isotope effects (BIEs) for equatorial and axial protons at C-3 can be estimated using Eq 4.24 (these values are listed in Table 4.2).

Table 4.2. The tabulated binding isotope effects (BIEs) for equatorial and axial protons at C-3, during *M.viridifaciens* sialidase-catalyzed hydrolysis of natural substrate analogues.

KIE	V/K[a]	V[b]	BIE[c]
Equatorial (3S)-^{2}H	0.986 ± 0.001	0.891 ± 0.008	1.106
Axial (3R)-^{2}H	0.984 ± 0.001	1.029 ± 0.007	0.956

[a]Reported values represent weighted averages (n = 3). [b]KIE values taken from ref 7. [c]Binding isotope effects (BIEs) are estimated by using Eq 4.24

A detailed analysis of ^{13}C KIEs measured on deuterated isotopologues ($^{13}(V/K)_{D\text{-}3S}$ = 1.000; $^{13}(V/K)_{D\text{-}3}$ = 1.029) and ($^{13}(V/K)_{D\text{-}3R}$ = $^{13}(V/K)$ = 1.029) would currently be premature until we can confirm these differences by the use of 2D NMR spectroscopy..

4.5.4 Conclusion and Future Work

The main objective of this project is to develop both one dimensional (^{13}C-NMR) and two dimensional (HETCOR and HSQC) NMR spectroscopic methods to measure multiple kinetic isotope effects simultaneously on an enzyme-catalyzed reaction. This methodology offers many potential advantages such as: i) direct monitoring of the reaction mixture, ii) milligram quantities of the labelled substrates, iii) reducing systematic errors as all isotopologues are in the same NMR tube under the same conditions.

Measurement of KIEs using 1D-NMR spectroscopy has been successfully performed; however, peak overlap reduces the accuracy with which the KIE values can be measured. 2D-NMR spectroscopy methods potentially have advantages compared to 1D ^{13}C-NMR because of the reduced peak overlap, and our initial 2D-NMR experimental results are very promising. However optimization is still ongoing to resolve the peak phase problems in the 2D-NMR spectra.

In future work, the KIE measurements could be done using non-natural substrates carrying very good leaving groups in order to accelerate glycosylation (k_5, scheme 4.9). In such cases, it would be expected that the value of the ^{13}C kinetic isotope effects will decrease smoothly as it approaches a value of 1; while the secondary deuterium KIEs will increase, thereby permitting a deconvolution of the binding and intrinsic deuterium effects.

Finally, accurate measurements of KIEs will aid in modelling transition state structures, and thus this will improve our understanding of the mechanism of sialidase-catalyzed hydrolysis reactions.

4.6 Appendices

4.6.1 NMR Spectra

Phenyl 4-O-(β-d-glucopyranosyl)-1-thio-β-d-glucopyranose (4)

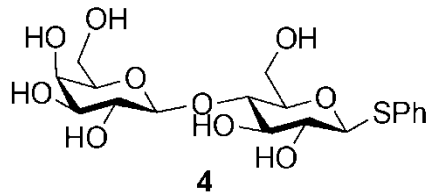

4

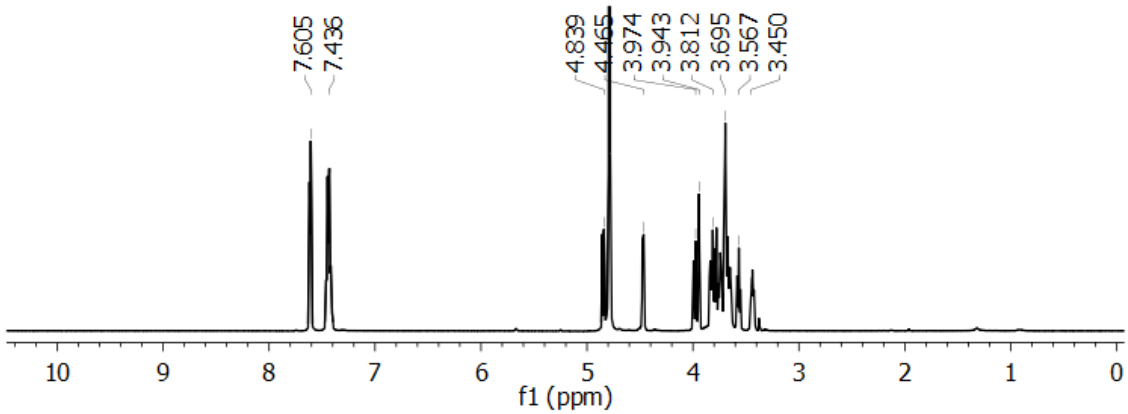

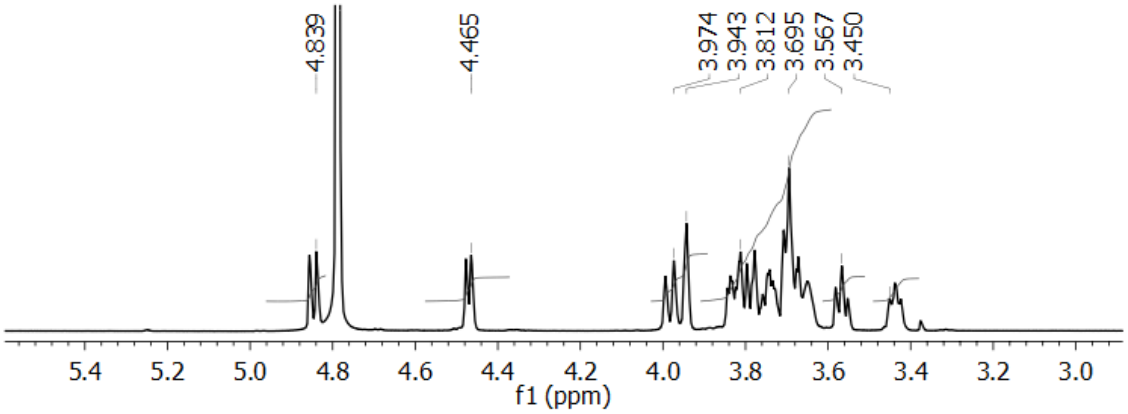

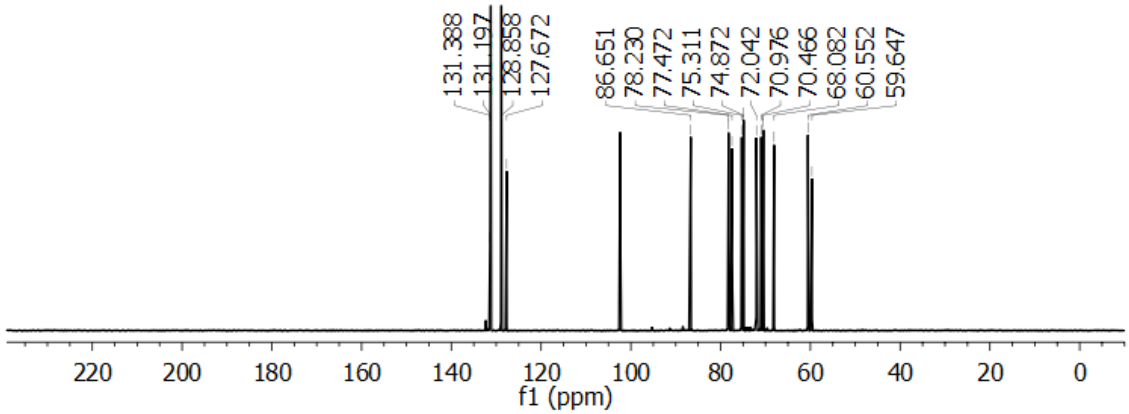

3-^{13}C β-Neu5Ac (6a) (containing 5% of α-anomer):

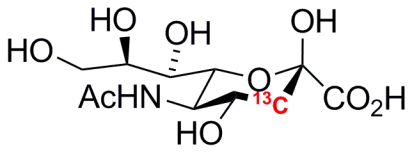

6a

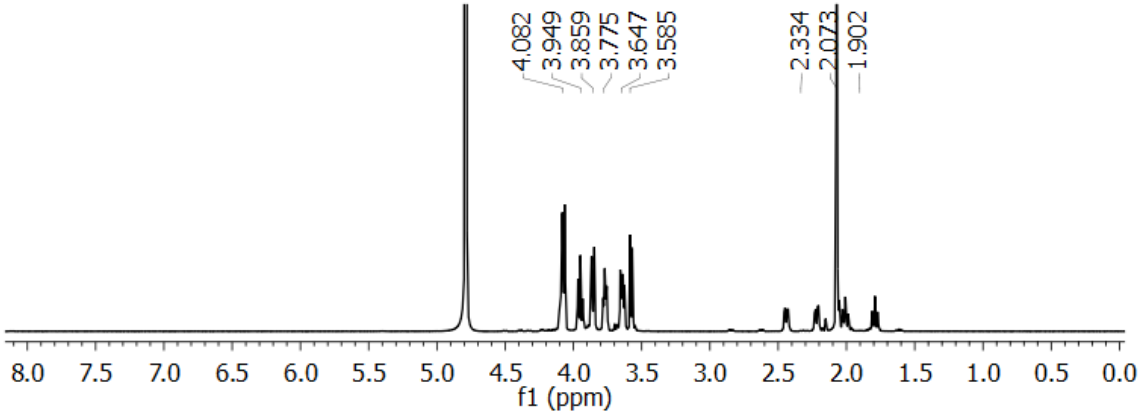

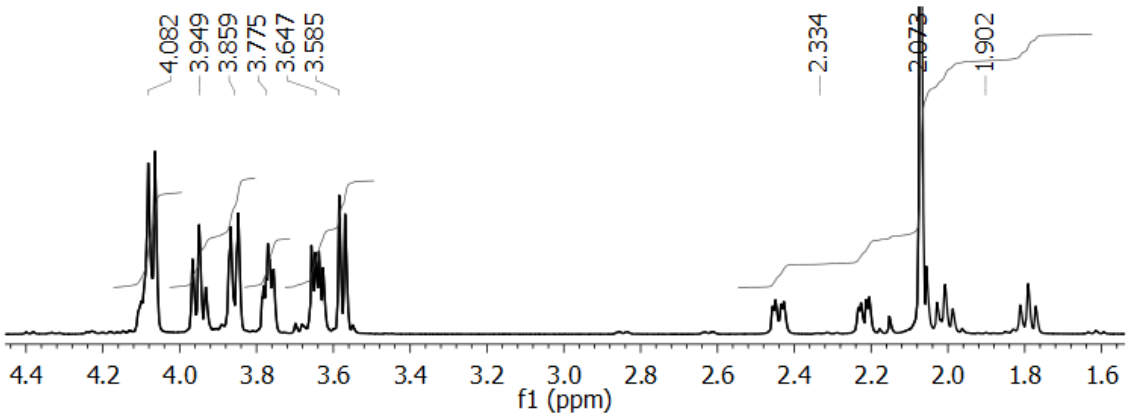

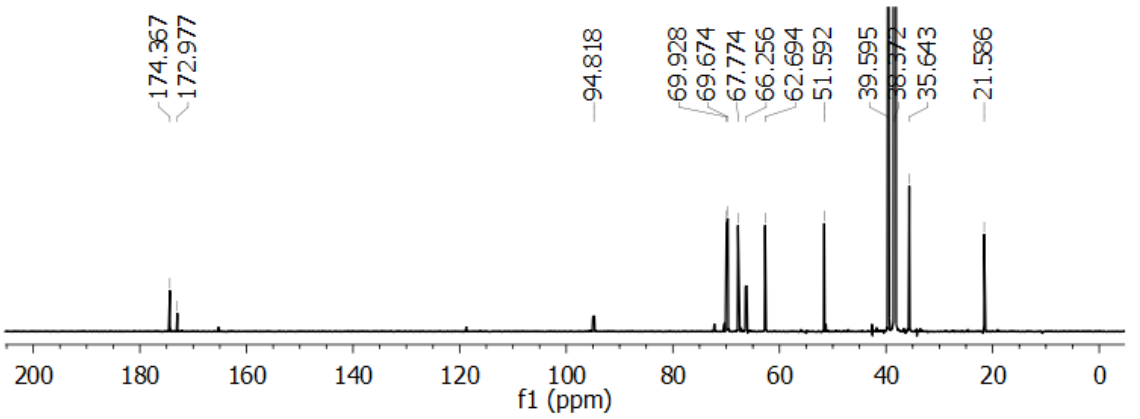

[3-^{13}C] Neu5Acα2,6LacβSPh (1a)

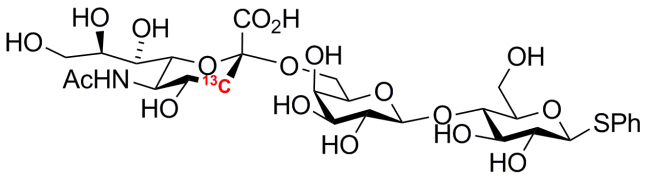

1a

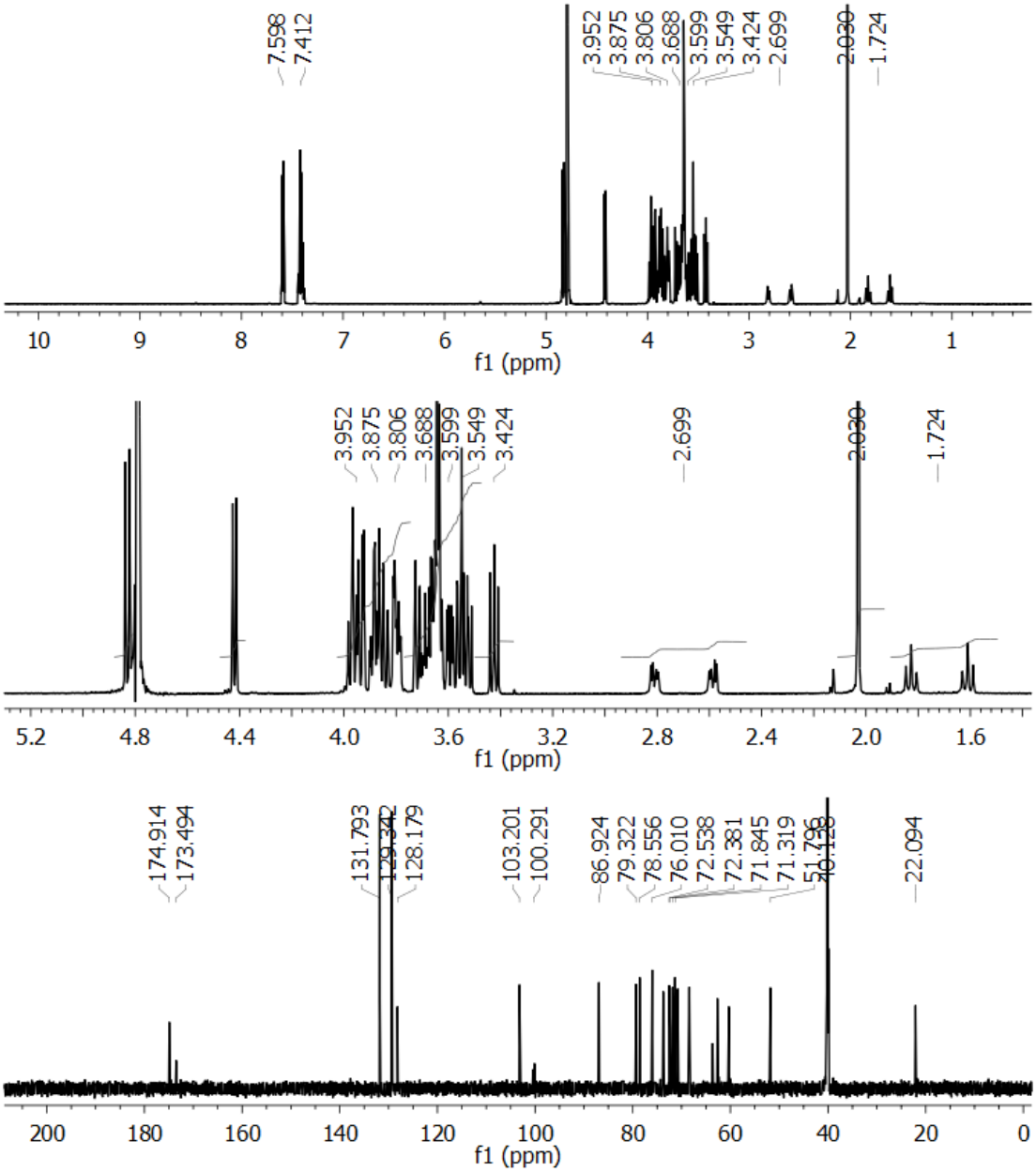

4.6.2 Hardware, Procedures and Pulse Sequences (by Dr. Andrew J. Lewis)

4.6.2.1 Hardware and Procedures Used

All NMR spectra were acquired on Bruker AVANCE II NMR spectrometers equipped with either a 5 mm Bruker TCI cryoprobe or a 5 mm Bruker QNP cryoprobe operating at 14 Tesla (600 MHz for ^{1}H, 150 MHz for ^{13}C and 92 MHz for ^{2}H). The TCI probe has the ^{1}H and ^{2}H channels on the (double-tuned) inner coil (i.e. closest to the sample for highest ^{1}H sensitivity) and ^{13}C channel on the outer coil, while the QNP probe has the ^{13}C channel on the inner coil (i.e. highest ^{13}C sensitivity) and ^{1}H and ^{2}H on the double-tuned outer coil. Both probes have the radio frequency (r.f) coils maintained at ca. 20 K and the preamplifiers at 77 K for all channels which provided excellent suppression of spurious noise arising from electronic components in the probes. For optimal r.f. performance the ^{1}H and ^{13}C probe channels were tuned and matched for each sample once the desired temperature had been achieved, and the observe and decoupler channels' offsets were set to be as close as possible to the corresponding resonances of interest (or centered if there were several). GARP4 composite pulse decoupling was used in order to reduce sample heating (these sequences require the lowest r.f power for the highest quality decoupling).

The high sensitivity of the cryogenic ^{2}H lock channel meant that stable field-locking was obtainable using as little as 1 µL of D_2O in the NMR sample (typically 500 µL of solvent in total for 5 mm NMR tube, or 200 µL for the D_2O susceptibility-matched 5 mm Shigemi tube), but more D_2O than this was usually present. Note that this low concentration of D_2O was highly desirable because it reduced to a negligible amount any potential solvent-induced isotope effects on the enzymatic reaction's kinetics. Once the ^{2}H channel tuning and matching had been adjusted for a sample containing ca. 3% D_2O

in H_2O containing a few milligrams of substrate in buffer, it did not show any noticeable sample-to-sample variation for the typical samples run, and so the ^2H matching and tuning were usually not changed. However, both the phase and the r.f. power used for the ^2H (lock) channel in field-lock mode were optimized after shimming of the sample because non-optimal lock phase can adversely affect peak shapes and peak widths, especially with repeated field unlocking and locking. The digital ^2H lock system also permitted repeated switching between the usual field-lock mode and a pulse mode (used for composite pulse decoupling of ^2H nuclei) at any point during the pulse sequence execution. Coupled with the real-time automated temperature control of the NMR sample (e.g. to compensate for r.f. heating of the samples during the extended decoupling delays necessitated by the high digital resolution and long (up to 3.5 s) FID acquisition time required), this active ^2H pulse-lock mode switching ensured that very high good magnetic field stability could be maintained during the extended acquisition (typically 1-4 hours per spectrum), which translated directly into very stable peak shapes and chemical shifts throughout the entire course of an enzymatic reaction (2-6 days). The latter two features are crucial for obtaining spectral data with the attributes needed for reliable and accurate deconvolution.

Manual shimming was performed on each sample prior to starting the automated acquisition of a consecutive series of spectra (sufficiently many as required to cover the time course of an enzymatic reaction to ca. 80-90 % completion, often 50-200 spectra). It was observed that if the ^1H peak shapes were optimized, the ^{13}C spectra usually also had similarly good (optimal) peak shapes. Shimming was therefore carried out by observing a single-transient ^1H NMR spectrum (Fourier transformed in real-time with the spectrometer operating in a single-scan or “gs” mode), as this was far more sensitive than observing the $^1H,^2H$-decoupled ^{13}C spectrum directly (even though the observed

compounds had almost 100% ^{13}C isotopic enrichment and data were acquired with cryogenically-cooled probes). As many of the (34 available) room temperature shim coils' currents as needed were adjusted in order to obtain an optimal ^{1}H NMR spectrum with peaks exhibiting close to (symmetrically) Lorentzian peak shape, whilst maintaining optimal spectral resolution and the best possible signal to noise ratio. It was vital that the final peak shapes were as symmetric as possible because although the deconvolution method used could cope with imperfect Lorenztian shapes (using a mixed Lorentzian-Gaussian (L-G) shape), it was not able to fit asymmetric peaks well, and this would greatly impact the quality, precision, and accuracy of the peak areas derived from the spectral fitting procedure.

The symmetry and closeness to Lorenztian peak shape could be easily checked at any point during the course of the shimming procedure (or spectral acquisition) using the Bruker Topspin feature "dcon" (deconvolute) to fit synthetic (i.e. calculated) purely Lorenztian or mixed L-G peak(s) to the displayed region of the ^{1}H or $^{13}C\{^{1}H,^{2}H\}$ spectrum. The result of this command is a display showing an overlay of the experimental spectrum, the synthetic peaks "best" fitting the experimental spectrum, and difference spectrum (experimental – calculated).

4.6.2.2 Pulse Sequences

Several new pulse sequences were programmed and compiled for the Bruker *Topspin* 2.x software (*Note:* as written these may not run in Topspin versions 1.x or 3.x without appropriate modifications). Invaluable assistance in coding the appropriate commands was provided by Drs. Rainer Kümmerle, Helena Kovacs, Wolfgang Bermel and Robin Stein in the NMR Application Group at Bruker and this is gratefully acknowledged. In most cases they were based on pulse sequences distributed in the

standard *Topspin* pulse program library with sequence-appropriate modifications including: i) addition of ^{2}H or ^{13}C decoupling, ii), incorporation of the ^{2}H field-lock and pulse mode switching commands, and iii) changes to the specific periods during which any decoupling was applied. Among the large variety of sequences tested for the 2-dimensional HSQC and HETCOR sequences, the best performing sequences in terms of signal-to-noise, (symmetric) peak shape, minimal baseline distortions, and good resolution are those presented below. A number of the 2-D sequences that incorporated a variety of appropriately shaped r.f. pulses (including adiabatic ones in some cases, particularly for the ^{13}C channel) were also tested, but short ca. 9-12 μs duration "hard" r.f. pulses gave superior performance and so were used for acquiring all of the data presented in this thesis.

Pulse sequence for 1-D ^{13}C Spectrum with Inverse Gated ^{1}H and ^{2}H Decoupling

For acquiring 1-dimensional ^{13}C spectra with simultaneous ^{1}H and ^{2}H inverse gated (i.e. during FID acquisition only). Uses GARP4 composite pulse decoupling and ^{2}H field-locking activated only during recycle delay.

```
;zgig1h2hf4.v2.arl
;A. Lewis SFU Nov 27 2012 modified

;from zgig1h2hf4.arl from Rainer Kuemmerle zgig1h2hf4.rak
;1D 13C sequence with simultaneous inverse gated 1H and 2H decoupling
;and 2H field-locking during recycle delay (D1)
;copied 2H decoupling coding from hncacogp2h3d
;avance-version
;using 2H lockswitch unit or BSMS 2H-TX board
;$CLASS=HighRes
;$DIM=1D
;$TYPE=
;$SUBTYPE=
;$COMMENT=
;$OWNER=Administrator

#include <Avance.incl>

"acqt0=-p1*2/3.1416"
"d11=30m"
"d12=20u"
```

```
1 ze
  d11 pl12:f2 pl17:f4
  d11 LOCKDEC_ON
  50u LOCKH_ON
  d11 H2_PULSE

2 d11 do:f2 do:f4
  d11 H2_LOCK
  6m LOCKH_OFF
  d1
  50u LOCKH_ON
  d12 H2_PULSE
  p1 ph1
  go=2 ph31 cpd2:f2 cpd4:f4
  d11 do:f2 do:f4 mc #0 to 2 F0(zd)
  d11 H2_LOCK
  d11 LOCKH_OFF
  d11 LOCKDEC_OFF
exit

ph1=0 2 2 0 1 3 3 1
ph31=0 2 2 0 1 3 3 1

;pl1 : f1 channel - power level for pulse (default)
;pl12: f2 channel - power level for CPD/BB decoupling
;pl17: f4 channel - power level for CPD/BB decoupling
;p1 : f1 channel -  high power pulse
;d1 : relaxation delay; 1-5 * T1
;d11: delay for disk I/O                  [30 msec]
;d12: delay for power switching                [20 usec]
;cpd4: decoupling according to sequence defined by cpdprg4
;pcpd4: f4 channel - 90 degree pulse for decoupling sequence
;after locking run lock.3 macro if desired
```

Pulse sequence for 2-D ^{13}C-^{1}H HETCOR Spectrum with ^{1}H and ^{2}H Decoupling

For acquiring phase sensitive, 2-dimensional, carbon-detected ^{13}C-^{1}H{^{1}H,^{2}H} heteronuclear correlation (HETCOR) spectra with refocusing of chemical shifts, simultaneous ^{1}H and ^{2}H (CPD) decoupling during the FID acquisition, and switching of the ^{2}H channel to active field-lock mode during the recycle delay. The ^{13}C-^{1}H correlation is accomplished via an INEPT transfer and phase sensitivity is achieved using the States-TPPI method. CNST11 is set to 6 for CH, CH_2 and CH_3 resonances to have the same phase.

```
;hxineptph_1H2H_lk.2.arl
;A. Lewis 27 Nov 2012 SFU from hxineptph_1H2Hdec_lock.arl
;edited Bruker std. hxineptph
;avance-version (07/04/04)
```

```
;2D heteronuclear shift correlation (HETCOR) with INEPT transfer
;X-detected, phase sensitive with refocussing of chem. shifts
;decoupling of 1H and 2H during acquisition only (Inv. Gated)
;Keeps sample locked (2H) during D1
;requires 2H lockswitch unit of BSMS 2H-TX board
;A. Bax & G.A. Morris, J. Magn. Reson. 42, 501 (1981)
;
;$CLASS=HighRes
;$DIM=2D
;$TYPE=
;$SUBTYPE=
;$COMMENT=

#include <Avance.incl>
#include <Delay.incl>

"p2=p1*2"
"p4=p3*2"
"d3=1s/(cnst2*cnst11)"
"d4=1s/(cnst2*4)"
"d5=d3-de"
"d11=30m"
"d12=20u"


"d0=3u"

"in0=inf1/2"

"DELTA=d0*2+p2"

"acqt0=-p3*2/3.1416"
1 ze
  d11 pl17:f4      ; set power for 2H(f4) decoupler pulses
  d11 pl2:f2       ; set power for 1H(f2) regular pulses
  d11 LOCKDEC_ON   ; enable use of 2H lockswitch
  50u LOCKH_ON     ; lock hold on (lock inactive)
  d11 H2_PULSE     ; set 2H to PULSE mode (for CPD decoupling)
2 d11 do:f2 do:f4  ; turn off 1H(f2) and 2H(f4) decouplers
  d11 H2_LOCK      ; set 2H to LOCK mode (for locking)
  6m LOCKH_OFF     ; lock hold off (lock active)
  d1
  d11 pl2:f2       ; set power for 1H(f2) regular pulses
  50u LOCKH_ON     ; lock hold on (lock inactive)
  d12 H2_PULSE     ; set 2H to PULSE mode (for CPD decoupling)
  (p3 ph1):f2
  d0
  p2 ph4
  d0
  d4
  (center (p4 ph2):f2 (p2 ph4) )
  d4
  DELTA
  (p3 ph3):f2 (p1 ph5)
  d3
  (center (p4 ph2):f2 (p2 ph6) )
  d5 pl12:f2       ; set power for 1H(f2) decoupler pulses
  go=2 ph31 cpd2:f2 cpd4:f4  ; start 1H and 2H decoupling
  d11 do:f2 do:f4 mc #0 to 2 F1PH(ip3, id0)
  d11 H2_LOCK      ; set 2H to LOCK mode (for locking)
```

```
  d11 LOCKH_OFF     ; lock hold off (lock active)
  d11 LOCKDEC_OFF   ; disable use of 2H lockswitch
exit

ph1=0
ph2=0 0 2 2
ph3=1 3
ph4=0 0 2 2
ph5=0 0 0 0 1 1 1 1 2 2 2 2 3 3 3 3
ph6=0 0 2 2 1 1 3 3
ph31=0 2 0 2 1 3 1 3 2 0 2 0 3 1 3 1

;pl1 : f1 channel - power for 13C pulse (default)
;pl2 : f2 channel - power for 1H pulse (default)
;pl12: f2 channel - power for 1H CPD decoupling
;pl17: f4 channel - power for 2H CPD decoupling
;p1 : f1 channel -  90 degree high power pulse
;p2 : f1 channel - 180 degree high power pulse
;p3 : f2 channel -  90 degree high power pulse
;p4 : f2 channel - 180 degree high power pulse
;d0 : incremented delay (2D)                    [3 usec]
;d1 : relaxation delay; 1-5 * T1
;d3 : 1/(6J(XH))  XH, XH2, XH3 positive
;     1/(4J(XH))  XH only
;     1/(3J(XH))  XH, XH3 positive, XH2 negative
;d4 : 1/(4J(XH))
;d5 : det equal to DE to balance echo
;d11: delay for disk I/O                        [30 msec]
;d12: delay for power switching                 [20 usec]
;cnst2: = J(XH)
;cnst11: = 6  XH, XH2, XH3 positive
;         4  XH only
;         3  XH, XH3 positive, XH2 negative
;inf1: 1/SW(H) = 2 * DW(H)
;in0: 1/(2 * SW(H)) = DW(H)
;nd0: 2
;NS: 2 * n
;DS: 16
;td1: number of experiments
;FnMODE: States-TPPI, TPPI, States or QSEQ
;cpd2: 1H(f2) dec. seq. cpdprg2 (GARP4)
;pcpd2: 1H(f2) channel  - 90 pulse for dec. sequence
;cpd4: 2H(f4) dec. seq. cpdprg4 (GARP4)
;pcpd4: 2H(f4) channel - 90 pulse for dec. sequence

;$Id: hxinepph,v 1.6 2007/04/11 13:34:30 ber Exp $
```

Pulse sequence for 2-D ^{1}H-^{13}C HSQC Spectrum with ^{13}C and ^{2}H Decoupling

For acquiring phase sensitive, 2-dimensional, proton-detected ^{1}H-$^{13}C\{^{2}H,^{13}C\}$ heteronuclear single quantum correlation (HSQC) spectra with ^{2}H and ^{13}C (CPD) decoupling during the FID acquisition and ^{2}H decoupling throughout the remainder of the pulse sequence except during the recycle delay when the ^{2}H channel is switched to

active field-lock mode. The ^{1}H-^{13}C correlation is accomplished via a double INEPT transfer using sensitivity improvement. Phase sensitivity is achieved using Echo/Antiecho-TPPI gradient selection. Trim pulses are used in the initial INEPT transfer, and gradients are used in the back-INEPT transfer.

```
;hsqcetgpsi2_dec13C2H.arl
;A. Lewis SFU 23 Feb 2013 from Bruker TS2.1 hsqcetgpsi2
;new commands suggested by Helena Kovacs
;UNBLKGRAMP replaces UNBLKGRAD, BLKGRAMP replaces BLKGRAD
;UNBLKGRAMP after acquisition starts as per noesygppr1d to keep phase correct
;avance-version (07/04/04)
;1H-13C{2H,13C} HSQC with 13C and 2H decoupling during acquisition
;and 2H decoupling during expt but not recycle delay (locked)
;2D H-1/X correlation via double inept transfer
;using sensitivity improvement
;phase sensitive using Echo/Antiecho-TPPI gradient selection
;with decoupling during acquisition
;using trim pulses in inept transfer
;with gradients in back-inept
;
;A.G. Palmer III, J. Cavanagh, P.E. Wright & M. Rance, J. Magn.
;   Reson. 93, 151-170 (1991)
;L.E. Kay, P. Keifer & T. Saarinen, J. Am. Chem. Soc. 114,
;   10663-5 (1992)
;J. Schleucher, M. Schwendinger, M. Sattler, P. Schmidt, O. Schedletzky,
;   S.J. Glaser, O.W. Sorensen & C. Griesinger, J. Biomol. NMR 4,
;   301-306 (1994)
;
;$CLASS=HighRes
;$DIM=2D
;$TYPE=
;$SUBTYPE=
;$COMMENT=

#include <Avance.incl>
#include <Grad.incl>
#include <Delay.incl>

"p2=p1*2"
"p4=p3*2"
"d4=1s/(cnst2*4)"
"d24=(d4*0.5)"
"d11=30m"
"d12=20u"
"d13=4u"

#   ifdef LABEL_CN
"p22=p21*2"
#   else
#   endif /*LABEL_CN*/

"d0=3u"

"in0=inf1/2"
```

```
"DELTA1=d13+p16+d16+4u"
"DELTA2=d24-p19-d16"
"DELTA3=d4-p16-d16"

#   ifdef LABEL_CN
"DELTA=p16+d16+50u+larger(p2,p22)+d0*2"
#   else
"DELTA=p16+d16+50u+p2+d0*2"
#   endif /*LABEL_CN*/

1 ze
  d11 pl12:f2 pl17:f4
  d11 LOCKDEC_ON
  d11 LOCKH_ON
  d11 H2_PULSE
2 30m do:f2 do:f4
  30m H2_LOCK
  6m LOCKH_OFF
  d1
  50u LOCKH_ON
  d12 H2_PULSE
3 (p1 ph1)
  d4 pl2:f2 cpd4:f4
  (center (p2 ph1) (p4 ph6):f2 )
  d4
  p28 ph1
  d13
  (p1 ph2) (p3 ph3):f2
  d0

#   ifdef LABEL_CN
  (center (p2 ph7) (p22 ph1):f3 )
#   else
  (p2 ph7)
#   endif /*LABEL_CN*/

  d0
  4u UNBLKGRAMP
  p16:gp1*EA
  d16
  (p4 ph4):f2
  DELTA
  (center (p1 ph1) (p3 ph4):f2 )
  p19:gp3
  d16
  DELTA2
  (center (p2 ph1) (p4 ph1):f2 )
  DELTA2
  p19:gp3
  d16
  (center (p1 ph2) (p3 ph5):f2 )
  p16:gp4
  d16
  DELTA3
  (center (p2 ph1) (p4 ph1):f2 )
  DELTA3
  p16:gp4
  d16
  (p1 ph1)
```

```
 DELTA1
 (p2 ph1)
 d13
 p16:gp2
 d16 pl12:f2
 go=2 ph31 cpd2:f2
 30m do:f2 do:f4 mc #0 to 2
    F1EA(igrad EA & ip5*2, id0 & ip3*2 & ip6*2 & ip31*2)
 4u BLKGRAMP
 d11 H2_LOCK
 d11 LOCKH_OFF
 d11 LOCKDEC_OFF
exit

ph1=0
ph2=1
ph3=0 2
ph4=0 0 2 2
ph5=1 1 3 3
ph6=0
ph7=0 0 2 2
ph31=0 2 2 0

;pl1 : f1 channel - 1H power for 90 pulse (default)
;pl2 : f2 channel - 13C power for 90 pulse (default)
;pl3 : f3 channel - 15N power for 90 pulse (default)
;pl12: f2 channel - power for 13C decoupling
;pl17: f4 channel - power for 2H decoupling
;p1 : f1 channel - 1H 90 deg high power pulse
;p2 : f1 channel - 1H 180 deg high power pulse
;p3 : f2 channel - 13C 90 deg high power pulse
;p4 : f2 channel - 13C 180 deg high power pulse
;p16: homospoil/gradient pulse                  [1 msec]
;p19: gradient pulse 2                         [500 usec]
;p22: f3 channel - 15N 180 deg high power pulse
;p28: f1 channel - trim pulse
;d0 : incremented delay (2D)                    [3 usec]
;d1 : relaxation delay; 1-5 * T1
;d4 : 1/(4J)XH  calculated from cnst2
;d11: delay for disk I/O                       [30 msec]
;d13: short delay                              [4 usec]
;d16: delay for homospoil/gradient recovery
;d24: 1/(8J)XH for all multiplicities
;     1/(4J)XH for XH
;cnst2: = J(XH) 1-bond 1H-13C J coupling
;inf1: 1/SW(X) = 2 * DW(X)
;in0: 1/(2 * SW(X)) = DW(X)
;nd0: 2
;NS: 1 * n
;DS: >= 16
;td1: number of experiments
;FnMODE: echo-antiecho
;cpd2: 13C decoupling using sequence defined by cpdprg2
;pcpd2: 13C (f2) 90 deg. Decoupl. seq [55-80 us]
;cpd4: 2H decoupling using sequence defined by cpdprg4
;pcpd4: 2H (f4) 90 deg. pulse for decoupl. seq [300 us]

;use gradient ratio:  gp 1 : gp 2 : gp 3 : gp 4
;                     80 : 20.1 :   11 :   -5    for C-13
;                     80 :  8.1 :   11 :   -5    for N-15
```

```
;for z-only gradients:
;gpz1: 80%
;gpz2: 20.1% for C-13, 8.1% for N-15
;gpz3: 11%
;gpz4: -5%

;use gradient files:
;gpnam1: SINE.100
;gpnam2: SINE.100
;gpnam3: SINE.100
;gpnam4: SINE.100

;preprocessor-flags-start
;LABEL_CN: for C-13 and N-15 labeled samples start experiment with
;           option -DLABEL_CN (eda: ZGOPTNS)
;preprocessor-flags-end
;$Id: hsqcetgpsi2,v 1.3 2007/04/11 13:34:30 ber Exp $
```

4.7 References

[1] Chan, J.; Lewis, A. R.; Indurugalla, D.; Schur, M.; Wakarchuk, W.; Bennet, A. J. *J Am Chem Soc* **2012**, *134*, 3748.

[2] Singleton, D. A. T., Allen A *J Am Chem Soc* **1995**, *117* 9357.

[3] Melander, V. L.; Saunders, W. H. *Reaction Rates of Isotopic Molecules.*, 1980.

[4] Chan, J.; Lewis, A. R.; Gilbert, M.; Karwaski, M. F.; Bennet, A. J. *Nat Chem Biol* **2010**, *6*, 405.

[5] Karwaski, M. F.; Wakarchuk, W. W.; Gilbert, M. *Protein Expr Purif* **2002**, *25*, 237.

[6] Kakuta, Y.; Okino, N.; Kajiwara, H.; Ichikawa, M.; Takakura, Y.; Ito, M.; Yamamoto, T. *Glycobiology* **2008**, *18*, 66.

[7] Chan, J.; Lu, A.; Bennet, A. J. *J Am Chem Soc* **2011**, *133*, 2989.

[8] Mark Ashwell , X. G., Michael L. Sinnott *J Am Chem Soc* **1992**, *114*, 10158.

[9] Fyfe, C. A. B., Darren H.; Lewis, Andrew R.; Chezeau, Jean-Michel *J Am Chem Soc* **2001**, *123*, 6882.

[10] Wolfram, S. *The Mathematica Book*; Cambridge University Press: Cambridge, UK, 2003.

[11] Manning, K. A.; Sathyamoorthy, B.; Eletsky, A.; Szyperski, T.; Murkin, A. S. *J Am Chem Soc* **2012**, *134*, 20589.

[12] Karsten, W. E.; Cook, P. F. In *Isotope Effects In Chemistry and Biology*; Kohen, A., Limbach, H. H., Eds.; Taylor & Francis Group: Boca Raton, 2006, p 793.

[13] Northrop, D. B. *Biochemistry* **1975**, *14*, 2644.

[14] Northrop, D. B. In *Isotope Effects on Enzyme-Catalyzed Reactions*; Cleland, W. W., O'Leary, M. H., Northrop, D. B., Eds.; University Park Press: Baltimore, 1977, p 122.

[15] Schramm, V. L. *Curr Opin Chem Biol* **2007**, *11*, 529.

[16] Hermes, J. D.; Roeske, C. A.; O'Leary, M. H.; Cleland, W. W. *Biochemistry* **1982**, *21*, 5106.

5 Conclusion and Future Work

5.1 Summary of This Thesis

This thesis described applications of the known mechanistic tools and the development of a new technique to precisely elucidate the function and structure of sialidases which have critical roles in numerous biological systems.

Chapter 2. The first project described in Chapter 2 is a detailed mechanistic study on the critical second chemical step of sialidase-catalyzed hydrolysis, that is, breakdown of the covalently-bound enzyme intermediate (**II**, Scheme 5.1). The first chemical step (glycosylation) was relatively easy to probe by varying the leaving groups of α-sialosides (Brønsted Analysis). However deglycosylation was impossible to probe by varying the enzymatic leaving group (a tyrosine residue) because the tyrosine involved is part of the enzyme's active site. Therefore, a mutant sialidase (*M. viridifaciens* Y370G) and a series of non-natural substrates (mono- and di-fluorophenyl *β*-D-sialosides) were used as mimics of this reaction step (**I**, Scheme 5.1) in wild-type sialidase.

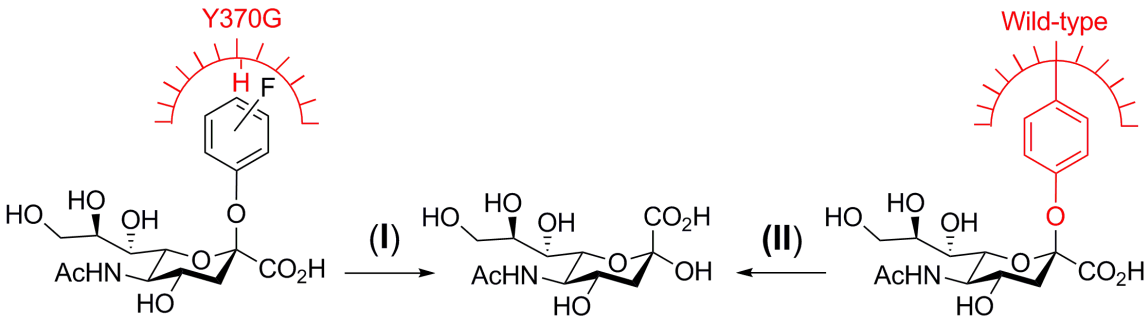

Scheme 5.1. (**II**) Breakdown of covalently-bound enzyme intermediate formed during wild-type sialidase-catalyzed hydrolysis of α-sialosides (deglycosylation step); (**I**) mimic of deglycosylation step (in wild-type sialidases) created by mutant sialidase (Y370G) and unnatural mono- and di-fluorophenyl *β*-D-sialosides

This work successfully led to the characterization of a deglycosylation transition state structure. Given that sialidases are present on the surface of the influenza virus,

and a human sialidase (NEU3) plays a role in some types of cancer, these mechanistic studies are very important.

Chapter 3. The second project described in Chapter 3 focused on a sialidase that is present on the surface of influenza virus particles. Designing a selective sialidase inhibitor that is less prone to elicit a resistance response from the influenza virus is an ongoing challenge in the development of therapeutic agents for use during pandemics. An ideal inhibitor precisely mimics the transition state for the sialidase-catalyzed hydrolysis reaction. Many inhibitors of sialidases are 4-substituted derivatives of Neu2en5Ac also known as DANA (**1**, Figure 5.1) such as Relenza (**2**, Figure 5.1), a current therapeutic agent for the treatment of influenza. However, whether Relenza and other 4-substituted derivatives of DANA are transition state analogues had never been ascertained. In the work described in Chapter 3, the mechanistic technique called transition state analogy was employed by synthesizing a series of 4-substituted derivatives of Neu2en5Ac and the corresponding 4-substituted derivatives of *p*NP-αNeu5Ac (**3**, Figure 5.1), and then binding interactions between the enzyme and inhibitors were correlated with binding interactions between the enzyme and the corresponding substrates.

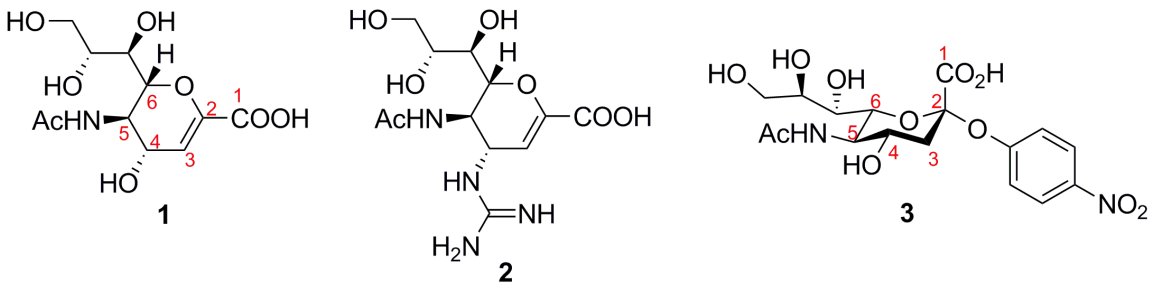

Figure 5.1. (**1**) Neu5Ac2en (DANA), (**2**) Relenza, (**3**) *p*NP-αNeu5Ac (*p*NP-αsialoside)

The linear free energy relationships (LFERs) between enzymatic catalysis and

inhibitor binding obtained in this work showed that Relenza is not a transition state analogue inhibitor of the influenza viral sialidase. This conclusion is important because the addition of a guanidino group to the DANA scaffold results serendipitously in a dramatic increase in binding potency without a concomitant increase in stabilization of the glycosylation transition state. Ultimately, this lack of transition state stabilization is the root cause for the ease with which the influenza virus generates resistant strains to Relenza.

Chapter 4. The project presented in Chapter 4 of this thesis describes the extension of one dimensional (1D) ^{13}C nuclear magnetic resonance (NMR) techniques and the development of two dimensional (2D) NMR spectroscopic methods for the simultaneous measurement of several KIEs in sialidase-catalyzed reactions. In this work, six singly- and doubly-labelled natural substrate analogues were synthesized and simultaneous KIE measurements were performed on samples containing all six isotopologues in the same NMR tube. Quantitative 1D (^{13}C) and 2D (^{1}H-^{13}C HSQC and HETCOR) NMR spectra were acquired over the course of the enzymatic (sialidase from *M. Viridifaciens*) reaction.

In any competitive measurement of KIE, as the reaction progresses, the reaction mixture becomes enriched with the slower reacting isotopologue. Since, the integrated area of a NMR signal is related to the concentration of each isotopologue present in the solution, the ratio of light to heavy isotopologues can be monitored. in this project, quantitative 2D-NMR spectra with minimal peak overlap for the six isotopologues have been acquired. This technique (2D-NMR spectroscopy) provides a couple of advantages over 1D-NMR spectroscopy: i) there is less peak overlap in 2D-NMR spectra as the added dimension leads to greater separation of the peaks, ii) data with better signal to noise ratios is attainable, especially for HSQC spectra due to proton detection. Although

there are several methods for discovering information related to the transition states during sialidases-catalyzed reactions, the highly precise measurement of KIEs possible by NMR is one of the most powerful techniques, and it provides invaluable information about the nature of the hydrolytic TS not available using other methods.

5.2 Ultimate Objective

The mechanistic studies conducted in this thesis have provided more understanding about mechanism of sialidases. As discussed in the introduction of this thesis, sialidases are widely distributed in nature such as bacteria, viruses, and mammals. Influenza, which is an infectious and viral disease, continues to cause yearly epidemics and the rarer pandemics. New reports from the Public Health Agency of Canada shows about 2000-8000 deaths per year because of influenza and its complication. Despite numerous continuing attempts to create vaccines and chemotherapeutic agents against influenza virus, the appearance of new virus strains such as H5N1 that are resistant to current antiviral drugs (Relenza and Tamiflu) can result in a major influenza pandemic. Influenza viral sialidase, is a vital target for the discovery and development of therapeutic agents against influenza. The research in this thesis has provided information about the enzymatic transition states and the mechanism of action in sialidases, including that from influenza and such information will eventually help us to design selective sialidase inhibitors with the goal of reducing the risks of future viral resistant strains.

5.3 Future Work

Following the successful analysis of 4-substituted derivatives of Ne5Ac2en as

transition state analogue inhibitor of sialidases, a similar approach can be used to examine if interactions between the other positions on inhibitor (e.g. 5-substituted derivatives of Ne5Ac2en) (**4**, Figure 5.2) are expressed at the TS for the hydrolytic corresponding modified substrates (**5**, Figure 5.2). In this way a detailed understanding of important interactions for inhibition of sialidases will be obtained. Apart from influenza neuraminidases, similar studies should be performed on the neuraminidases from different species and comparing their obtained LFER correlations. This will allow us to discover selective and specific inhibitors against these neuraminidases.

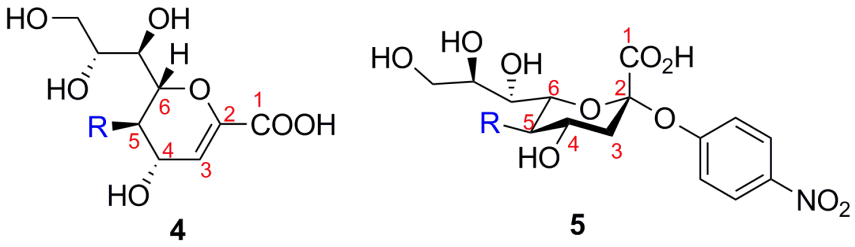

R = -NHAc, -NMe_2, -NHiPr, -guanidino, -glycolyl,
-$NHCOCH_2OH$, -N_3, -OH, -CH_2=CH_2, -CH_2CHO, CH_2CHOH

Figure 5.2. (**4**) 5-substituted derivatives of Neu5Ac2en, (**5**) 5-substituted derivatives of *p*NP-αNeu5Ac

On the other hand, based on the new developed technique described in Chapter 4, efficient measurement of KIEs can be applied to many other enzymatic systems to solve their transition state structure(s).

Eventually, the similar mechanistic studies which is combination of LFER and KIE will be done on a particular mammalian sialidase (Neu3), which is believed to be up-regulated in human prostate cancer. Such detailed mechanistic studies on Neu3 will result in designing a transition state mimic inhibitor as the best therapeutic agent against the cancer.